THE UNIVERSITY
of EDINBURGH

Investigating the differential instructive roles of WT1's isoforms

Giulia Petrovich

Thesis presented to the University of Edinburgh
for the degree of Doctor of Philosophy

2016

Declaration of Authorship

I, Giulia Petrovich, declare that this thesis titled, 'Investigating the differential instructive roles of WT1's isoforms' and the work presented in it are my own. I confirm that:

- This thesis has been entirely composed by me.
- This work has not been previously submitted for a degree or any other qualification at this University or any other institution.
- Where I have consulted the published work of others, this is always clearly attributed.
- Where I have quoted from the work of others, the source is always given.
- I have acknowledged all main sources of help.
- Where the thesis is based on work done by myself jointly with others, I have made clear what was done by others and what I have contributed myself.

Signed: _____

Date: _____

Abstract

The Wilms' tumour suppressor gene *Wt1* is a key regulator of embryonic development and tissue homeostasis. In humans, mutation in the gene may lead to childhood kidney cancer, severe glomerular kidney diseases, gonadal dysgenesis and, in rare cases, heart diseases. The importance of WT1 in embryonic development is related to its crucial function in the regulation of two cellular plasticity processes: the epithelial to mesenchymal transition (EMT) and the reverse process, the mesenchymal to epithelial transition (MET). WT1 expression persists during the waves of EMT and MET that generate certain mesodermal tissues. In fact, WT1 is a major regulator of both transitions and it is essential for the survival of mesenchyme progenitors. Furthermore, it has been proposed that WT1 is required for the derivation of progenitors from different mesothelia, possibly through an EMT. Progenitors expressing WT1 are believed to differentiate into different cell types, giving rise to coronary vasculature, adipocytes and hepatic stellate cells.

In my PhD I aimed to investigate the instructive role of different WT1 isoforms. To address this, the first goal was to generate a single plasmid that would accommodate all necessary components of an inducible system, in order to derive cellular models for the inducible expression of WT1 single isoforms. Second, I aimed to understand the processes that the single variants were sufficient to drive.

Therefore, I started with the establishment of two cellular models for the inducible expression of the main four isoforms of WT1 (with or without the exon 5 and/or the KTS, here referred as +/+, +/-, -/+ and -/-). I cloned different plasmids carrying doxycycline inducible WT1 isoforms and derived single stable clones in two epithelial kidney cell lines that do not express WT1: the MDCK and the IMCD3 cells. I then analysed the expression profiles of the clones, using either microarray or RNA sequencing, and performed cellular assays to characterize the cells after WT1 induction.

Overall, WT1 induction did not affect cell growth, cell cycle, cell migration or anchorage independent growth, suggesting that the expression of WT1 in these two cell lines does not change their oncogenic potential.

The expression analysis of the MDCK cells suggested that the induction of WT1 isoforms activates an inflammatory response, leading to the overexpression of several cytokines. Moreover, the -/+ isoform specifically caused the upregulation of fibrotic markers and the rearrangement of the actin cytoskeleton. Interestingly, the expression of the mesothelial marker *UPK3B* increased following the induction of the -/+ isoform.

Because the expression of the -/+ variant led to the most significant isoform-specific changes in both cell lines, I focused on this isoform for the validation of the transcriptomic data of the IMCD3 cells. I confirmed that the induction of WT1 -/+ in the IMCD3 cells leads to the upregulation of fibrotic markers, increases cell adhesion and activates the AKT and MAPK pathways. Moreover, there was a significant overexpression of different mesothelial markers and, importantly, of key regulators and markers of developmental processes, such as adipogenesis, skeletal and cartilage development, as well as angiogenesis. I then dissected the timing of expression of some specific markers and regulators, analysing the levels of the genes at different time points after WT1 -/+ induction. The preliminary results intimate that WT1 -/+ might induce epithelial cells in the direction of cartilage-skeletal tissue and fat, possibly through a mesothelial intermediate. The data also suggest that the induction of this isoform initiates an EMT, possibly followed by an MET, as the levels of expression of the differentiation markers and regulators increase.

To validate the proposed instructive role of WT1, it will be of crucial importance to determine both RNA and protein levels of markers and regulators at even later time points, both in IMCD3 cells and in a model of inducible embryonic stem cells, which is currently under development. In the future, it will be important to address the relevance of these findings *in vivo* and to dissect the molecular mechanisms.

Lay Summary

If you consider that your own self started from only one cell, you can easily imagine that, in order to create your fully developed body, that cell needed to multiply, giving rise to others that in turn had to divide, change their shape and move around to create and colonise all the different tissues and organs you are composed by. Thus, how does a cell know what it has to become? How does it realise that it is destined to be a part of the eye and not beating in your heart? Many of those questions are still not fully answered, but what we do know is that any cell knows how to act and when thanks to what is written in their code, the DNA, and depending on how this code is interpreted. The DNA is composed by thousands of genes, each of them coding for a specific command, which can be read, giving rise to a second form of code, called RNA, that itself is then transformed into proteins. The proteins are the actors that perform the function written in the gene, which generated them. Thus, each cell expresses a panel of RNAs and proteins that define what the cell indeed is. So, for instance, the cells composing your iris will have a different repertoire of proteins and RNAs compared to a cell of your heart. We can even say that if we know all the RNAs and proteins that are present in a cell, we can use them as a hallmark to understand what a cell is.

The proteins are not only structural components of a cells, but some of them, named transcription factors, can actually control the interpretation of the DNA, deciding which genes to read and, therefore, which RNAs will be produced and turned into other proteins. The new set of proteins will determine other changes, possibly defining a new state for the cell. During development, this dynamic process of reading and interpreting the DNA allows the cells to change states, finally leading to the acquisition of all the specific functions and different characteristics, which define the cells forming your mature body. Therefore, at the first stages of embryonic development, the cells have the potential to give rise to all the multiple kinds of cells, that will compose your tissues and organs. Those cells are known as embryonic stem cells and they multiply, generating progenitor cells, which are directed towards different cell fates. Following different pathways and passing through various intermediate stages, those cells create

completely differentiated cells, which do not have the potential to become anything else. It is of crucial importance to understand the mechanisms underlying the embryonic development, not only to know how our own body is formed, but also because it seems that some of its typical processes are aberrantly re-activated in pathological conditions, such as cancer.

During my PhD, I studied the function of a specific transcription factor, called WT1, which is involved in the development of different organs and tissues, such as heart, kidneys, bones, cartilage, adipose tissue and the mesothelium, which is a layer of cells that surrounds the embryonal body cavity and the major internal organs. Previously published data proposed that in the mesothelium there are progenitor cells that express WT1 and are able to become different cell types. In fact, they are believed to give rise to coronary vasculature, adipocytes and a particular kind of hepatic cells, called stellate cells. Moreover, it has been suggested that those progenitors express WT1 because of its key role in the control of two developmental processes: the epithelial to mesenchymal transition (EMT) and the reverse process, the mesenchymal to epithelial transition (MET). Through these transitions, the cells change their shapes and mobility, acquiring new properties: via EMT a cell, which has a cobblestone shape and is strongly attached to its neighbour cells (thus it is defined as an epithelial cell), becomes more motile, loosens the junctions that bind it to the other cells and acquires an irregular shape (therefore becoming a mesenchymal cell). Interestingly, it has been proposed that the progenitors expressing WT1 undergo an EMT to generate differentiated cells.

In my project I aimed to understand whether the expression of WT1 is sufficient to determine different cell fates. For this purpose, I needed a cell system in which I could control the expression of WT1 and study the consequences of its activation. To achieve this, I genetically modified two epithelial cell lines, creating cells in which I could switch on and off WT1 expression when I wanted. After the activation of WT1, I first checked whether the protein was affecting some cellular properties, such as cell growth, cell motility and the capacity for anchorage-independent growth, which is a sign of cells becoming tumorigenic. I concluded that WT1 was not changing these

characteristics. Then, I proceeded with the analysis of all the RNAs present in the cells after WT1 induction and I compared them with the RNAs characterising the cells in which the transcription factor was not activated. The most interesting finding was that WT1 expression activated genes that are typical of mesothelial cells and genes that are distinctive regulators and hallmarks of differentiation processes, which lead to the formation of bones, cartilage, adipose tissue and vasculature. Looking at when the expression of the genes was enhanced, I concluded that the differentiation markers increased after the mesothelial ones. Moreover, the data suggested that WT1 could drive an initial EMT, followed by the reverse process, when the cells seem to go towards the differentiation pathways. Overall, the experiments suggested that WT1 can change epithelial cells, moving them along the pathway of different fates, possibly through a mesothelial intermediate stage.

Acknowledgements

First of all, I would like to thank my supervisors, Dr Abdelkader Essafi and Prof. Nicholas Hastie, for their guidance, help and advices, which made me grow not only professionally, but also as a person.

Second, I would like to thank all my colleagues in the lab, everyone working in C3 and C4 and my office mates, because they made every day enjoyable and they have always stimulated my interest in science. Special thanks go to Selvi, for all her help, suggestions and nice chats, and to Joan and Rachel, who have always been ready to help me with my work and to teach me new techniques. A big hug goes to all the staff working in the technical services of the HGU, because they were always helpful and made my everyday work much easier. Thank you also to my graduate studies panel members for their time, advices and opinions during my progress meetings.

A big thank to my break buddies, Silvia, Sara, Raffa and Angela: you made all my lunches and coffee breaks fun and cheerful and you have always been "happy" to listen to my "occasional" complains...

Thank you to all my friends in Edinburgh, because you have always supported me, cheered me up and made me feel at home. Especially, I would like to thank my present and past flatmates, Sara, Zarko, Georgia and Paz, because you have been my great Scottish family.

Finally, my dearest thanks to my family and friends in Italy, because, even though we are far, you have always been close to me, helped me and supported me in harsh and good times.

Contents

List of Figures

List of Tables

Abbreviations

ACTA2	Alpha-actin-2 (alpha smooth muscle actin)
AKT	AKT8 virus oncogene cellular homolog
AML	acute myeloid leukaemia
Amp	Ampicillin
APS	Ammonium persulfate
BAT	Brown Adipose Tissue
BGH	Bovine Growth Hormone
bp	Base Pairs
BSA	Bovine Serum Albumin
°C	Celsius degrees
$CaCl_2$	Calcium chloride
cDNA	Complementary DNA
ChIP seq	Chromatin Immunoprecipitation Sequencing
cm	Centimetre
CMV	Cytomegalovirus
cnt	Control
Col1a1	Collagen, Type I, Alpha 1
CreERT2	Cre recombinase fused to a mutated human estrogen receptor
Ct	Threshold Cycle
D	Doxycycline
dam	Deoxyadenosine methylase
DAPI	4',6-diamidino-2-phenylindole

ddH_2O	Double distilled water
DDS	Denys-Drash syndrome
dH_2O	Distilled water
DMEM	Dulbecco's Modified Eagle Media
DNA	Deoxyribonucleic acid
dNTP	Deoxynucleotide triphosphates
Dox	Doxycycline
E	Embrionic day
E-Cadherin	Epithelial Cadherin
ECM	Extracellular matrix
EDTA	Ethylenediaminetetraacetic acid
EGFP	Enhanced green fluorescent protein
EMT	Epithelial to Mesenchymal Transition
EndMT	Endothelial to Mesenchymal Transition
ERK	Extracellular signal-regulated kinases
EV	Empty Vector
FACS	Fluorescence Activated Cell Sorting
F-actin	Filamentous actin
Fc	Fold change
FCS	Foetal Calf Serum
Flt4	Fms-related tyrosine kinase 4
FP	Fluorescent Protein
Fwd	Forward primer
g	Gram
GAPDH	Glyceraldehyde 3-phosphate dehydrogenase
GMEM	Glasgow's MEM
GO	Gene Ontology
h	Hour
hg	Housekeeping gene
HRP	Horseradish Peroxidase

HSC	Hepatic Stellate Cell
IF	Immunofluorescence
Igf	Insulin-like growth factor
IMCD3	Inner medullary collecting duct
IRES	Internal ribosome entry site
K	Lysine
Kan	Kanamycin
kb	kilobasepair
KCl	Potassium chloride
KDa	Kilodalton
KH_2PO_4	Monopotassium phosphate
KO	Knockout
l	Litre
LB	Luria-Bertani
LIF	Leukaemia Inhibitory Factor
M	Molar
MAPK	Mitogen-Activated Protein Kinase
MDCK	Madin Darby Canine Kidney
MET	Mesenchymal to Epithelial Transition
mg	Milligram
$MgCl_2$	Magnesium chloride
$MgSO_4$	Magnesium sulfate
miRNA	Micro-RNA
ml	Millilitre
mM	Millimolar
mm	Millimetre
MMP	Matrix metalloproteinases
MMT	Mesothelial to Mesenchymal Transition
mRNA	Messenger RNA
Msln	Mesothelin

μl	Microlitre
μg	Microgram
μM	Micromolar
μm	Micrometre
Na_2HPO_4	Sodium hydrogen phosphate
NaCl	Sodium chloride
NaH_2PO_4	Sodium dihydrogen phosphate
NaOH	Sodium hydroxide
Neo	Neomycin
ng	Nanogram
nM	Nanomolar
O/N	Overnight
OD	Optical Density
4-OHT	4-Hydroxytamoxifen
p-	Phosphorylated
PC	Positive Control
P/S	Penicillin/STreptomycin
PBS	Phosphate-buffered saline
PCR	Polymerase chain reaction
PFA	Paraformaldehyde
PI	Propidium Iodide
PolyA	Polyadenylation signal
Pparγ	Peroxisome proliferator-activated receptor gamma
Q-RT-PCR	Quantitative reverse transcription polymerase chain reaction
Rev	Reverse primer
RNA	Ribonucleic acid
RNA seq	RNA sequencing
rpm	Revolutions per minute
RT	Room temperature
Runx2	Runt-related transcription factor 2

S	Serine
sa	Sample
SASP	Senescence-associated secretory phenotype
SD	Standard deviation
SDS	Sodium dodecyl sulfate
Snail	Snail Family Zinc Finger 1
SV40	Simian vacuolating virus 40
T	Threonine
TAE	Tris-acetate-EDTA
TBE	Tris-borate-EDTA
TEMED	Tetramethylethylenediamine
Tet	Tetracycline-controlled transcription factor
TEV	Tobacco Etch Virus nuclear inclusion a endopeptidase
TGFβ	Transforming growth factor beta
Thbd	Thrombomodulin
TIMP	Tissue inhibitors of metalloproteinases
Tris	2-Amino-2-hydroxymethyl-propane-1,3-diol
U	Unit
Upk3B	Uroplakin 3B
UV	Ultraviolet
V	Volt
v	Volume
VCam1	Vascular cell adhesion protein 1
VegfB	Vascular endothelial growth factor B
vs	Versus
w	Weight
w/o	Without
WAGR	Wilms' tumour-aniridia-genitourinary-mental retardation syndrome
WAT	White Adipose Tissue
WB	Western Blot

wt	Wild type
WT1	Wilms' tumour 1
X-gal	5-bromo-4-chloro-3-indolyl β D-galactopyranoside
Zeb1	Zinc finger E-box binding homeobox 1
Zeo	Zeocin
ZFN	Zinc Finger nucleases
ZO-1	Zona occuldens protein 1

Symbols

+/+	WT1 +Exon 5/+KTS
+/-	WT1 +Exon 5/-KTS
-/+	WT1 -Exon5/+KTS
-/-	WT1 -Exon5/-KTS
*	P-value < 0.05
**	P-value < 0.01
**	P-value < 0.001
’	Minute
”	Second

Chapter 1

Introduction

1.1 The Wilms' tumour 1 gene and its isoforms

The *Wilms' tumour 1* (*WT1*) gene was given its name because of its crucial role in the development of the eponymous paediatric kidney tumour, where the gene was originally identified [1]. The human gene is located on chromosome 11 and consists of 10 exons, spanning about 50 kilobases (kb) of genomic sequence. Mutations in the gene were identified not only in a considerable portion of Wilms' tumours, but also in different congenital syndromes, characterised by severe kidney disease, gonadal dysgenesis, heart and diaphragm problems [2]. Thanks to the knockout (KO) of the murine orthologue, which maps on chromosome 2, *Wt1* was discovered to be essential for the development of several mesodermally derived tissues, as well as for some ectoderm derivatives. The KO mice were generated deleting the first exon of the gene and 0.5 kb of upstream sequence. The heterozygous mutants appeared normal and fertile, while none of the homozygous mice were viable, dying at embryonic day 14.5 (E14.5), probably owing to pericardial bleeding and massive oedema. Moreover, the KO mice displayed renal and gonadal agenesis, severe heart, diaphragm, lung, spleen, adrenal glands, limbs and mesothelial abnormalities [3–6]. The homozygous mutants also showed impairments in retinal development, optic nerve hypoplasia, loss of retinal ganglion cell precursor

[7] and defects in olfactory epithelia and neuron development [8]. More recently, it was shown that *Wt1* is essential for liver morphogenesis, probably because the gene disruption prevents the expansion of the progenitors of hepatic stellate cells [9].

The *WT1* gene epitomises of how a single gene can generate multiple proteins. In fact, it encodes for alternative isoforms that give rise to different proteins with four C-terminal C_2H_2 zinc fingers and an N-terminal proline/glutamine-rich regulatory region [10]. Alternative exons, start codons, splice sites and RNA editing can theoretically generate up to 36 different isoforms [2] (Figure 1.1).

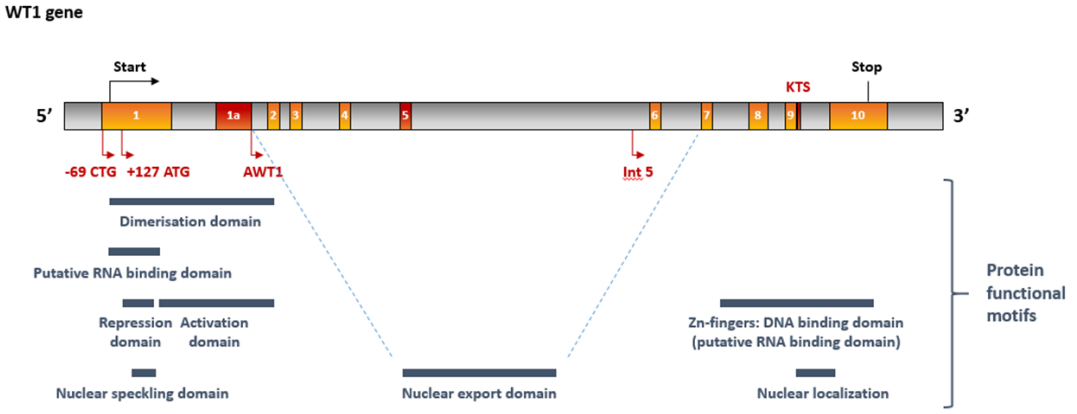

FIGURE 1.1: Diagram showing *WT1* gene and the functional motifs of the protein. The exons in the *WT1* locus are represented in yellow and red. Alternative exons, different start sites and alternative splicing sites, which can theoretically give rise to 36 isoforms, are depicted in red. The functional motifs of the protein (including the dimerisation domain, the putative RNA binding domains, the transcriptional repression and activation domains and the ones that determine WT1 localisation) with the relative positions are indicated below the diagram.

The best studied variants are the ones deriving from the alternative splicing of the exon 5 and 9, which give rise, respectively, to the insertion of 17 amino acids and to the inclusion of three residues, lysine-threonine-serine (KTS), between the third and the fourth zinc finger of the protein. These variants will be referred as +/+, +/-, -/+ and -/- (Figure 1.2). The -/+ and -/- isoforms are conserved in all the vertebrates, while the variants containing the exon 5 are present only in mammals [11]. The ratio in the levels of expression of these four transcripts is tightly controlled and maintained

temporally and spatially during kidney development, highlighting the importance of keeping the right balance between the isoforms. Specifically, the estimated ratio between the isoforms is: +/+ 8.3 : +/- 2.5 : -/+ 3.8 : -/- 1.0; therefore the +KTS isoforms are the most represented, constituting about the 60% of the transcripts [12]. The physiological role of these variants has been elucidated *in vivo* by the generation of mouse models with mutations that interfere with the production of specific isoforms. In order to generate -KTS- and +KTS-only mice, mutations were introduced into the second and first splice donor sites in intron 9, respectively. Investigating the development of these mouse mutants revealed common as well as unique functions for the KTS isoforms. Indeed, both mice had severe defects in gonad and kidney development and died soon after birth. On the other hand, while the mice expressing only the +KTS isoforms showed the most dramatic phenotype, characterised by a clear reduction in kidney size, increased stromal component, fewer glomeruli and lack of broadening of the genital ridge, the mutants lacking the +KTS variants showed impaired podocyte differentiation and male-to-female sex reversal, suggesting an essential role for these isoforms in the male sex determination programme [13]. Later on, the lack of +KTS variants has been also associated with defects in the development of the olfactory system, as the KO mutants are characterised by thinner olfactory epithelia and a reduced number of neuronal progenitors [8].

Differently from the disruption of the KTS isoforms, the KO of exon 5, which contains a protein-protein interaction domain, did not lead to any noticeable phenotypes, as the homozygous animals were viable, fertile and capable of lactation. This result indicates that the isoforms containing the exon 5 are not essential for mammal-specific functions, despite being conserved only in placental mammals [14].

Other WT1 isoforms arise from the use of two alternative start sites: a CTG start codon, located 69 bp upstream from the conventional start site, and an internal ATG codon, which resides within the exon 1 [2]. An additional truncated isoform starting at the end of intron 5 has been identified in human cancer cell lines [15]. Moreover, Dallosso et al. described another variant deriving from the use of an alternative promoter located

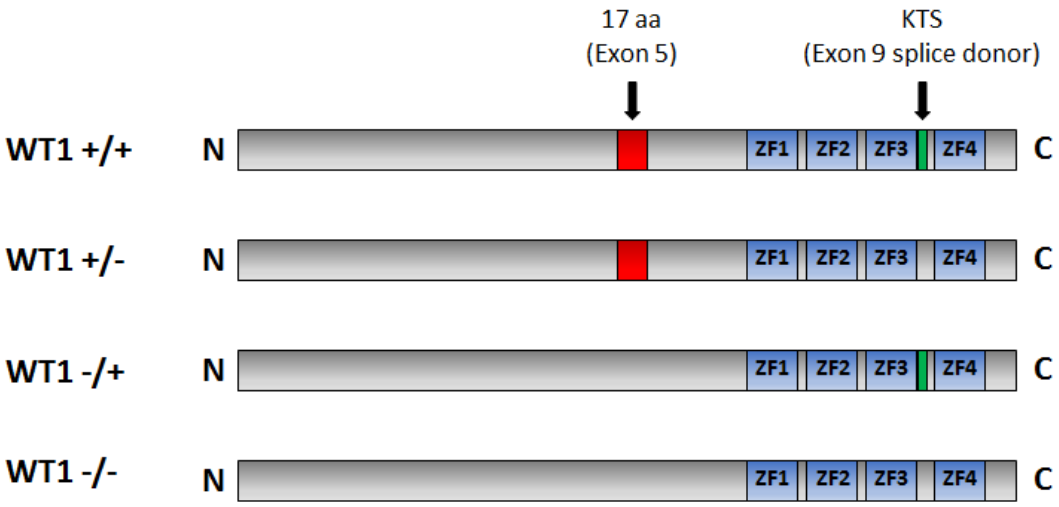

FIGURE 1.2: Diagrams representing the four main isoforms of WT1. The +/+ isoform includes both the 17 aa (amino acids), deriving from the usage of exon 5, and the KTS between the thirds and fourth zinc fingers, generated by the use of the alternative splice donor site in exon 9; the +/- variant encodes for the 17 aa, but lacks the KTS; the -/+ isoform includes only the KTS residues, while in the -/- variant both the 17 aa and the KTS are excluded.

in exon 1, whose expression is imprinted and confined to the paternal allele [16]. Last, the editing of *WT1* mRNA results in the substitution of an uracil residue in exon 6 with a cytosine, which leads to the incorporation of a proline instead of an isoleucine [17]. Among these isoforms, only the properties of the variants using the upstream alternative translation initiation have been ascertained *in vivo* with the generation of specific KO mice, by introducing a translational stop codon signal downstream the CTG initiator. Similarly to the Exon 5, the N-terminal extension is conserved only in mammals suggesting a mammalian specific function, such as embryonic implantation or lactation. However, the KO mice were viable and fertile, proving that these variants are dispensable for development and reproduction [18]. The fact that the KO animals for the exon 5 or the CTG isoforms lack clear phenotypes may indicate redundant roles of the variants; on the other hand, it neither clarified the function of these isoforms nor explained why *Wt1* gene generates so many isoforms [18].

The *WT1* gene encodes for a transcription factor, which can either activate or repress transcription (Figure 1.1). In fact, the four zinc fingers at the C-terminus of the protein are necessary for the sequence-specific nucleic acid binding of WT1, while the N-terminus of the protein contains a transcriptional repression domain (between residues 71 and 180) and an activation domain (between residues 180 and 250) [19, 20]. The N-terminal region is also characterised by the presence of two self-association domains, residing within the first 45 amino acids and at residues 157-253, respectively [21]. The physiological role for the formation of homo or heterodimers has not yet been fully understood. However, it has been shown that the association between the wild-type protein and truncated mutants results in a dominant negative activity [21, 22]. Moreover, the co-expression of both KTS isoforms in Xenopus oocytes was shown to impair the accumulation of the +KTS variants in the structures where transcription and RNA processing occur [23].

McKay et al identified a region within the repression domain that mediates the inhibition of the transcriptional activation by WT1; this region was called suppression domain and it has not been yet identified in any other transcription factor [24]. Later on, Carpenter et al. demonstrated that the co-repressor BASP1 (brain acid soluble protein 1) is required for the suppression of the transcriptional activation domain of WT1 [25]. In addition to BASP1, WT1 has been shown to recruit several transcriptional co-regulators, which determine its function as a transcriptional activator or repressor. For instance, one of the main co-activator of WT1 is the histone acetyl transferase CBP (CREB-binding protein) [26].

Other functional motifs are related to regulation of the localisation of the protein (Figure 1.1). WT1 is mainly localised in the nucleus and the nuclear localization signal has been mapped to the third zinc finger [27]. However, the protein can shuttle to the cytoplasm via direct interaction with β-actin, where it binds to active polysomes [28–30]. Moreover, it has been shown that nuclear translocation of WT1 involves importins α and β [27]. The region responsible for the nuclear export has been identified between the residues 182 and 324 [28]. Of note, differences in the localisation of the

isoforms have been reported: whereas the -KTS forms mostly display a homogeneous nuclear localisation, the +KTS variants localise predominantly to the nuclear splicing speckles, which are nuclear domains enriched in pre-mRNA splicing factors [31, 32]. The respective localisations were also confirmed *in vivo* using the isoform-specific KO models [13].

The differences in the isoforms localisation was also proposed to mirror different functions for the KTS proteins. In fact, while the -KTS isoforms are clearly involved in transcriptional regulation of multiple targets (reviewed in [33]), the +KTS variants seem to be also implicated in the regulation of the splicing process [2, 33] and they were shown to bind the DNA with reduced affinity *in vitro* [34, 35]. There is an increasing body of evidence supporting a role for the +KTS isoforms in the pre-mRNA processing. The first data suggesting a connection between the +KTS variants and the splicing process came from a study in 1995, in which Larsson et al showed that these isoforms coimmunoprecipitated with snRNPs (small nuclear ribonucleic proteins), which combine with unmodified pre-mRNA and other proteins to form a spliceosome, a large complex where splicing of pre-mRNA occurs [31]. Supporting these findings, Ladomery et al determined that WT1 is incorporated into Poly(A)+ ribonucleoproteins [36]. Moreover, it was demonstrated that specifically the isoforms containing the KTS associated with the key splicing factor U2AF65 [37] and colocalised with another essential splice factor, p116, in nuclear speckles [36]. WT1 was also reported to interact and partially colocalise in the speckles with WTAP (Wilms' tumor 1 associated protein), a putative splicing factor [38], whose Drosophila homologue is interestingly involved in the alternative splicing sex determination pathway [39]. Of note, unpublished data from out lab suggest that WT1 interacts with the RISC complex (RNA-induced silencing complex), advocating a role in the RNA interference process (Dr Selvi Bharathavikru, unpublished).

The first mRNA bound by WT1 *in vitro* was identified by Caricasole et al, who showed that WT1 interacted with the insulin-like growth factor 2 (*Igf2*) transcript and that the zinc finger 1 was particularly important in RNA binding [40]. Furthermore, both KTS

isoforms were found to bind to transcripts *in vivo* using Xenopus oocytes, but only the +KTS variants were shown to accumulate in B-snurposomes, sites for the machinery required for transcription and RNA processing. These results were consistent with an interaction of the +KTS isoforms with endogenous splice factors [23]. Later on, WT1 +KTS was also reported to bind to the alpha-actinin 1 (*Actn1*) mRNA [41]. Moreover, Wagner et al proposed that the KTS including variants can post-transcriptionally regulate the levels of ASCL1 (Achaete-scute homolog 1), a crucial gene for the proliferation and neuronal specification of progenitor cells [8]. Later on, Dudnakova et al showed that polymerised filamentous actin facilitated WT1 RNA binding [30].

Although many data suggest a post-transcriptional role for the +KTS isoforms, different evidence have also highlighted the fact that these variants can directly regulate transcription. For instance, it was shown that the +/+ isoform is the most powerful repressor of its own gene [42]. Later on, a study in 2010 demonstrated that the same isoform directly regulates the Scribbled planar cell polarity (*Scrib*) gene in kidney podocytes [43]. Intriguingly, an *in vivo* ChIP Seq (Chromatin immunoprecipitation sequencing) analysis on E18.5 kidneys identified a WT1 binding motif, which was strikingly similar to the +KTS binding sequence originally described by Bickmore et al [44, 45].

A role for WT1 in the regulation of translation has also been proposed. Indeed, both + and -KTS isoforms associate with actively translating polysomes bound to the cytoskeleton. Intact actin filaments were shown to be required for WT1 polysome loading [29]. Moreover, Bor et al demonstrated that the +KTS variants are able to regulate the translation of target mRNAs, by promoting the polysome association of mRNAs containing a specific viral element, which facilitates the export of mRNAs with retained introns [46].

Interestingly, recent findings have implicated WT1 also in the regulation of the mitotic process and chromosomal stability. In fact, during mitosis, WT1 was shown to directly interact with C-MAD2 (Mitotic Arrest Deficient 2, closed conformation), which is a component of the mitotic checkpoint complex. This association leads to a prolonged

inhibition of the anaphase-promoting complex/cyclosome (APC/C) and to a delayed degradation of its substrates, thus preventing chromosomal segregation defects and early anaphase entry [47].

1.2 WT1 expression in development and adult tissues

The expression of WT1 during mouse development was first studied by in situ hybridisation [48] and then by creating transgenic mice carrying a lacZ reporter gene inserted into the first exon of *WT1* gene on two yeast artificial chromosomes (YACs) [4, 5]. WT1 is first expressed at E8.5 in the intermediate mesoderm and in the lateral plate mesoderm. WT1-expressing cells of the intermediate mesoderm will contribute to the formation of kidneys and gonads. The lateral plate mesoderm gives rise to the coelomic epithelium, from which arise WT1 positive mesenchymal cells that contribute progenitors to the genital ridge, ovary, testis, adrenal gland and mesothelia lining the body cavities and the visceral organs. At E9.5 WT1 is expressed in the septum transversum, which arise from the coelom and contributes to liver mesothelium, peri- and epicardium, ventricular myocardium, gut mesenteries, skeletal muscle and diaphragm. At E10 WT1 is strongly expressed in the genital ridge, in the mesonephros and in the mesothelial lining of the intracoelomic organs, such as heart, gut and liver. One day later, the expression is found in the splanchnic mesodermal plate, which gives rise to the spleen, in the uninduced metanephric mesenchyme, in a small linear domain in the spinal cord and in limb musculature. At E12 WT1 keeps being expressed in the condensed mesenchyme and in the genital ridge; the expression in the spinal cord become clear. Between the 11^{th} and the 12^{th} day WT1 is also expressed in subepicardial mesenchymal cells. At 12.5 WT1 starts appearing in the limbs, specifically in the posterior and anterior marginal zones and at the base of the mesenchyme web between the third and the fourth digit. At E13 the mesothelial linings strongly express the transcription factor, while in the forming kidney WT1 is present in the involuting glomeruli and highly expressed in the renal vesicle. When the renal vesicle reaches the comma- and S-shape body stages, WT1 expression becomes confined to their proximal segments and finally it will be restricted

to the podocyte cells of the glomerulus. At this stage of development, WT1 expression spreads in more zones of the limbs, covering the intradigital webs and lining either sides of the condensing digits. Moreover, the developing sex cord is positive for WT1, as well as the body-wall musculature and a more diffuse area within the spinal cord. At E15 the expression is still present in mesothelia, gonads, mesorchium (a mesothelial-derived mesentery which contributes to the support of the testis), alongside each digit and in the remnants of the intradigital webs. Moreover, WT1 is expressed in a ventral horn region of the spinal cord and in a small region at the roof of the fourth ventricle of the brain [4, 5, 48, 49]. In the adult WT1 expression is confined to a few cell types, such as mesothelial cells, podocytes cells which surround the glomerular capillaries, Sertoli cells in the seminiferous tubules, granulosa cells of the ovarian follicles, hepatic and pancreatic stellate cells, 1% of cells in the bone marrow and stromal vascular component of some fat bodies [49, 50]. Of note, the pattern of WT1 expression in human embryos almost mirrors the one in the corresponding murine stages [48]. A recent study reported that in human embryos and foetuses WT1 localisation is mainly nuclear in developing urogenital tissues and mesothelial cells, but the protein was also immunodetected, using an antibody against the N-terminal of the protein, in the cytoplasm of developing skeletal and cardiac muscle cells and endothelial cells of forming blood vessels [51].

1.3 WT1 and the epithelial-mesenchymal balance in development

The pattern of expression of WT1 during development clearly indicates that the transcription factor is often, if not always, expressed in cells that are undergoing an epithelial to mesenchymal transition (EMT) or the reverse process, the mesenchymal to epithelial transition (MET). The EMT is a process by which the epithelial cells gain fibroblast-like properties, losing polarity and intercellular adhesion and becoming more motile; features and mechanisms of the EMT transition will be explained in detail in the next section of the chapter. After birth WT1 is expressed in cell types which co-express both

epithelial and mesenchymal markers, suggesting that WT1 positive cells maintain the potential to undergo either an EMT or an MET transition. Corroborating the notion that WT1 is pivotal for the control of these two key cellular plasticity processes, most of the tissues affected by the knockout of *Wt1* arise from the intermediate or lateral plate mesoderm and the defects have their origins in mesenchymal impairment [49, 52].

Waves of EMT and MET generate the embryo and WT1 expression persists throughout those cycles of transitions that characterize the formation of organs and tissues for which its expression is essential (Figure 1.3). Indeed, WT1 has been proven to be a crucial regulator of the EMT and MET, which characterize the development of certain mesodermal tissues. During embryogenesis, the primary EMT happens during gastrulation: the cells in the primitive streak region become primary mesenchymal cells by undergoing an EMT, which leads to the generation of the three germ layers: ectoderm, mesoderm and endoderm. Following this, most of the prime mesenchyme, which is the part of the mesoderm composed by progenitors of connective tissue, bone, cartilage, circulatory and lymphatic system, will undergo an MET, differentiating into secondary epithelia such as intermediate, paraxial and lateral plate mesoderm. The cells composing these mesodermal compartments then undergo a secondary EMT, generating mesenchymal progenitors that will differentiate into epithelial structures via a second round of MET. WT1 is expressed in mesenchymal progenitors deriving from intermediate and lateral plate mesoderm that differentiate into epithelial cells of kidneys and gonads, skeletal muscle, or endothelial and mesothelial cells. Moreover, it has been shown that WT1 is a major regulator of mesenchymal progenitors and it is required for their survival [49, 52].

Besides these cellular switches between epithelial and mesenchymal phenotypes that characterise the whole embryonic development, the EMT and MET processes are essential for the morphogenesis of specific organs. WT1 has been proved to play a crucial role in the control of the directionality of the transitions during organogenesis, by exerting dichotomous functions in a context dependent manner. For instance, the regulation of the EMT process in the epicardium, the inner layer of the mesothelium lining

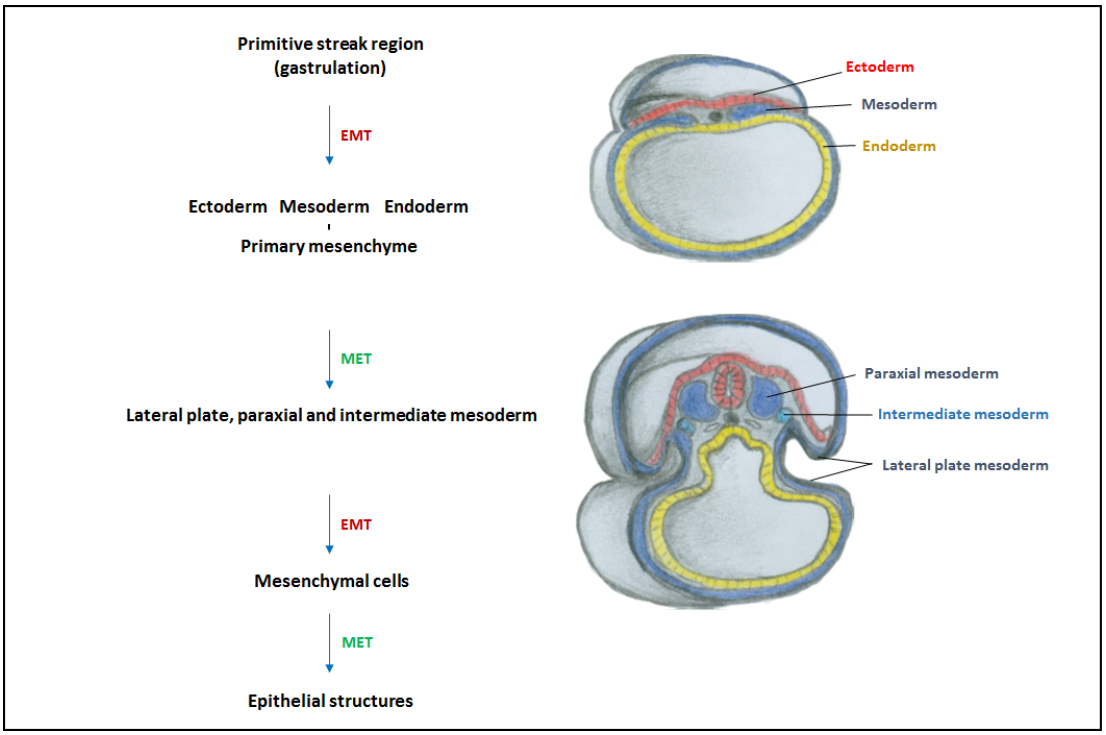

FIGURE 1.3: The alternation between EMT and MET transitions generates the embryo. During gastrulation, the cells of the primitive streak region undergo an EMT, forming the three germ layers: ectoderm, mesoderm and endoderm. Through MET, the mesodermal cells composing the primary mesenchyme generate the lateral plate, paraxial and intermediate mesoderms. By undergoing a second round of EMT, the cells of these secondary epithelia form mesenchymal cells, which will differentiate into different epithelial structures via another MET transition. Different stages of the gastrulation process are represented on the right hand side of the figure to visualise the localisation of the mentioned developmental structures.

the heart (pericardium), epitomises how the expression of WT1 in mesothelial cells controls the derivation of progenitors. Indeed, Martinez-Estrada et al demonstrated that epicardial-specific knockout of *Wt1* causes a dramatic reduction of mesenchymal cardiovascular progenitors and their derivatives, such as coronary smooth muscle and endothelial cells, interstitial fibroblasts and cadiomyocytes, leading to cardiovascular failure in the embryos between E16.5 and E18.5. WT1 was shown to directly control the expression of two of the major mediators of the EMT process: SNAIL (Snail family zinc finger 1) and E-Cadherin (Epithelial cadherin). Because disruption of *Wt1* led to increased levels of the epithelial marker E-Cadherin and to the downregulation of the mesenchymal regulator SNAIL in the epicardial cells of the mutant mice, the authors

concluded that WT1 is essential for the repression of the epithelial phenotype in epicardial progenitors [53]. On the other hand, WT1 is pivotal for the regulation of the MET process that mesenchymal cells undergo to form nephrons. Indeed, Davies et al first demonstrated that WT1 is essential for this process in organ cultures [54]; later on, Essafi at al showed that in the kidney mesenchyme WT1 directly activates *in vitro* and *in vivo* the expression of WNT4 (Wingless-Type MMTV integration site family, member 4), which is necessary and sufficient for the nephron MET, by recruiting the co-activator CBP/p300. Moreover, the authors proved that WT1 represses *Wnt4* in the epicardium by binding to the co-repressor BASP1. Therefore, the authors proposed that the activation or repression of *Wnt4* gene are mediated by the cofactors that WT1 recruits in a tissue-dependent manner. Furthermore, they determined that WT1 is required for the proper loading of CTCF (CCCTC-binding factor) and cohesin complex that delimits the *Wnt4* locus, suggesting a mechanism, named "chromatin flip-flop", by which WT1 keeps the genomic locus open in the kidney mesenchyme while closed in the epicardium [55].

Similar to the epicardium, different lineage tracing studies have suggested that the cells expressing WT1 also in other mesothelia function as progenitors of specific cell types of the organs they surround. It is likely that the differentiation happens through the modulation of the EMT transition, although this has not been proved yet for all the cases. In fact, WT1 expressing mesenchymal cells of the septum transverum were shown to generate mesothelial cells of the liver mesothelium, which then migrate into the liver primordium and differentiate into hepatic stellate cells (HSC), fibroblasts and smooth muscle cells of the portal and central veins [56]. Moreover, it was reported that WT1 positive cells of the serosal mesothelium are the major source of vasculogenic progenitors in the gut, by first undergoing an EMT transition, migrating into the gut and finally differentiating into smooth muscle cells of the main blood vessels of the gut and mesentery [57]. In a similar way, Que et al demonstrated that the cells expressing WT1 in the mesothelium lining the lungs give rise to smooth muscle cells that populate the lung vessels. The authors also suggested that WT1 positive cells could generate other cell types, as interstitial fibroblasts, alveolar myofibroblasts and some endothelial cells

[58]. Overall, these studies suggest a common and conserved mechanism for the development of blood vessels in the coelomic organs, moreover they pinpoint the embryonic mesothelia as an important source of progenitor cell population. Corroborating this function, Chau et al proved that the mesothelial cells which express WT1 contribute to some visceral white adipocyte tissue progenitors and pre-adipocytes [59].

1.4 The EMT process

The EMT transition is a process by which an epithelial cell acquires a mesenchymal phenotype. The EMT is reversible and characterised by multiple steps. In fact, epithelial cells can acquire a full or a partial mesenchymal phenotype, depending on cell type, tissue and signalling context. The cells in the intermediate stages are able to either reverse or progress to a mesenchymal state, highlighting the plastic nature of the epithelial phenotype [60]. The EMT transition is essential for normal embryonic development, but it has also been implicated in pathological conditions, such as cancer and fibrosis, which will be discussed below [61].

The epithelial cells form layers in which the cells are joined and communicate through specialised membrane structures, such as tight junctions, adherens junctions, desmosomes and gap junctions. These layers compose the epithelia, which delineate tissues and organs, forming permeability barriers. The epithelial cells are characterised by an apical-basolateral polarization, which is based on the tightly controlled distribution of adhesion molecules, such as cadherins and certain integrins. Moreover, these cells are positioned on and interact with a basement membrane that contributes to the definition of their physiology. On the other hand, mesenchymal cells do not form organised layers, they rarely contact neighbouring cells and they are not associated with a basal lamina; they can be characterised by a frontrear polarity, but typically they do not have a polarization of both cell surface molecules and actin cytoskeleton. Moreover, mesenchymal cells are more motile, at least *in vitro*, than the epithelial cells and they are characterised by enhanced invasiveness and acquisition of resistance to senescence

and apoptosis. In certain cases they also show an increased production of extracellular matrix (ECM) components. Cultured mesenchymal cells have a typical spindle-shaped fibroblast-like phenotype, while the epithelial cells are characterised by a cobblestone shape and grow in clusters [62, 63].

Although there are differences depending on the cell type, tissue context and signals that activate the process, the EMT transition is characterised by a conserved programme with typical hallmarks. In fact, in all tissues the EMT goes through key stages: the epithelial cells first lose their cell-cell contacts, causing a loss in the apical-basal polarity, they reorganise the cytoskeletal architecture, which leads to changes in cell shape, they downregulate epithelial genes and activate regulators and markers typical of the mesenchymal phenotype. As a consequence, the cells are characterised by increased cell protrusions, which facilitate their motility, and, in many cases, they have an enhanced ability to degrade ECM components, leading to a more invasive phenotype [62] (Figure 1.4).

The disruption of the intercellular epithelial junctions is one of the crucial hallmarks of the EMT. In detail, the early intermediate state of the programme involves the dissolution of tight junctions and the breakdown of the polarity complexes. The partitioning-defective (PAR) and the Crumbs complexes are associated with tight junctions and localise on the apical membrane; on the other hand, the basolateral compartment is defined by the Scribble complex. Hence, the disruption of epithelial junctions during the EMT leads to the loss of apical-basal polarity. The breakdown of the tight junctions is accompanied by decreased expression of tight junction proteins, such as claudin, occludin and zona occludens 1 (ZO-1). During the following weakening of adherens junctions and desmosomes, which characterises the late intermediate stage of the EMT, E-Cadherin, the main component of the adherens junctions and prototypical epithelial protein, is cleaved from the membrane and degraded. This allows the β-Catenin to translocate in the nucleus, where it activates genes targets of the Wnt signalling pathway, one of the central pathways involved in the EMT transition. At the

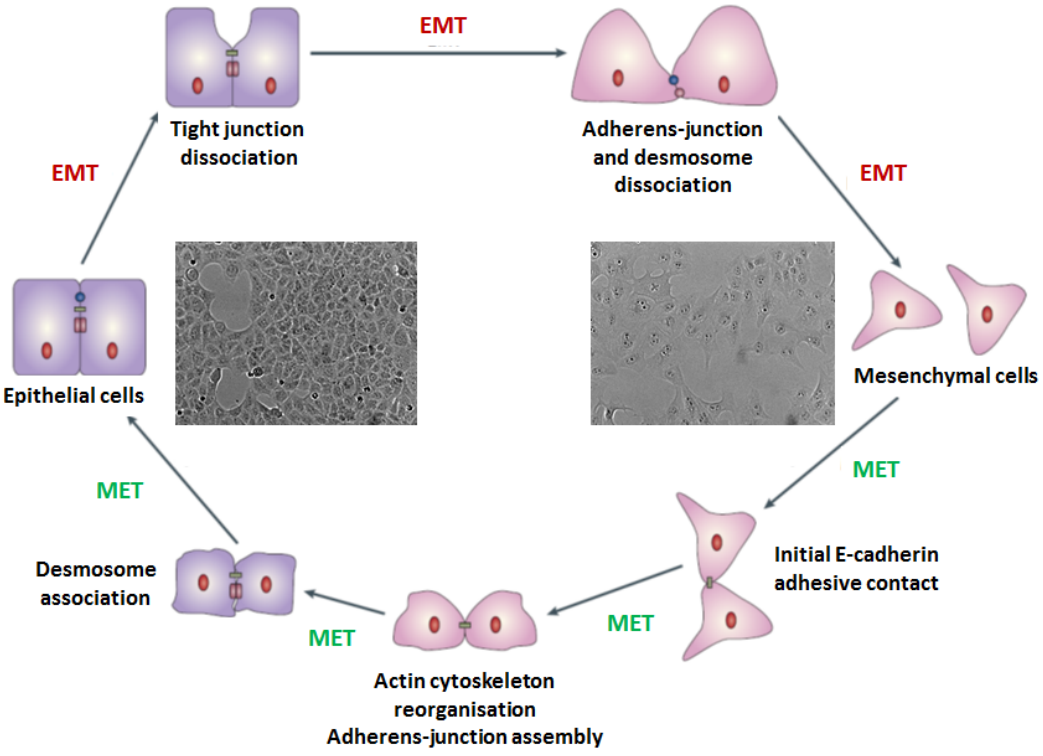

FIGURE 1.4: Schematic representation of the EMT and MET. The EMT transition is a reversible process that implies multiple steps, by which epithelial cells acquire a mesenchymal phenotype. The first stage of the EMT is characterised by the loss of tight junctions, followed by the dissociation of adherens junctions and desmosomes. The disruption of the cell-cell contacts leads to the loss of cell polarity, the reorganisation of the cytoskeleton and, finally, to the acquisition of a mesenchymal phenotype. The mesenchymal cells can revert to an epithelial phenotype, by assembling the cell-cell junctions and re-establishing an apical-basal polarity. The bright field images in the middle of the figure show the morphology of epithelial cells, represented by a monolayer of Madin Darby canine kidney (MDCK) cells, and mesenchymal cells, illustrated by the shape of MDCK cells after TGFβ treatment, a potent inducer of the EMT process.

same time, vimentin containing intermediate filaments start replacing the ones composed by cytokeratins, making the cells more motile and invasive. Also the integrity of the gap junctions is affected due to the decrease of connexin levels. Concomitant with the loss of epithelial cell junction proteins, the cells activate genes which promote mesenchymal adhesion. For example, the neural cadherin (N-cadherin) is upregulated and facilitates mesenchymal cell interactions, which are weaker than the ones mediated by the E-Cadherin. The final state of the EMT transition is achieved when the cells

have lost their epithelial junctions as well as their apical-basal polarity [60, 62].

Different extracellular signals trigger the EMT programme, including components of the ECM, soluble growth factors such as members of the FGF (fibroblast growth factor) family, EGF (epidermal growth factor), HGF (hepatocyte growth factor), VEGF (vascular endothelial growth factor) and several cytokines, including TGFβ (transforming growth factor β), TNFα (tumour necrosis factor) and the interleukins 6, 8 and 10 [63–65]. The extracellular signals activate multiple pathways, which can cooperate to induce an EMT response. For instance, TGFβ, considered one of the main triggers of the EMT programme, can induce the activation of various signalling cascades, such as Smad (mothers against decapentaplegic) signalling pathway, PI3K (phosphoinositide 3-kinase)/AKT (AKT8 virus oncogene cellular homologue), ERK (extracellular signal-regulated kinase) MAPK (mitogen-activated protein kinases), p38 MAPK and JNK (JUN N-terminal kinase) pathways. Other growth factors, including EGF, FGF, HGF and VEGF, bind to receptor tyrosine kinases (RTKs) and induce the EMT through the activation of RAS-RAF (rapidly accelerated fibrosarcoma)-MEK (Mitogen/Extracellular signal-regulated Kinase)-ERK MAPK and PI3K/AKT cascades. During inflammation, the interleukins 6 and 10 were shown to promote the transition through the Janus kinase (JAK) signal transducer, inducing SNAIL expression. Wnt, Notch and Hedgehog pathways also participate in the EMT, as well as the upregulation of the hypoxia-inducible factor 1α (HIF1α) in hypoxic conditions [62, 64, 65].

Transcriptional and post-transcriptional repression of epithelial genes and activation of mesenchymal markers drive the EMT progression. In fact, during the initial stages of the EMT master regulators of the mesenchymal phenotype, including the transcription factors SNAIL, SLUG (Snail family zinc finger 1 and 2), TWIST (Twist-related protein 1), ZEB1 and ZEB2 (zinc-finger E-box-binding 1 and 2), are activated. These transcriptional factors contribute to the EMT to different extents, depending on the cell and tissue type, as well as on the signalling pathways that initiate the EMT. Moreover, they can modulate the expression of one another and cooperate for the control of target genes. Recently, other transcription factors have been shown to regulate the EMT,

including forkhead box transcription factors, proteins belonging to the GATA family and SRY box factors [62].

In addition to the direct regulation of gene expression, mechanisms of post-transcriptional regulation contributes to the EMT transition. For example, Shapiro et al have recently shown that the induction of the EMT in mammary epithelial cells led to a global change in alternative splicing of genes that are involved in the regulation of actin cytoskeleton, cell-cell junction and cell migration. Moreover, the set of genes which showed differential splicing and the ones that changed expression levels did not always overlap, suggesting that an EMT splicing programme is parallel to the transcriptional regulation. Furthermore, they reported changes in the expression levels of RNA binding protein genes, such as the splicing factors ESRP1 and ESRP2 (Epithelial Splicing Regulatory Protein 1 and 2). Underlying the importance of the alternative splicing events for the EMT process, the authors also demonstrated that the expression of ESRP1 was sufficient to partially revert mesenchymal cells [66]. In addition to the regulation of splicing, miRNAs (microRNA) play a crucial role in the downregulation of key EMT genes. The microRNAs are 22-nucleotide RNAs that suppress their targets by mRNA destabilization and translational inhibition. Different miRNAs have been shown to target EMT transcription factors, inhibiting the transition: for example, the miR-200 family and the miR-205 regulate the expression of ZEB1 and ZEB2; SNAIL is targeted by several miRNAs, such as miR-29b and miR-30a; let-7 downregulates the HGMA2 (high-mobility group A2 protein) transcription factor, which mediates TGFβ-induced EMT response. Other miRNAs instead favour the progression of EMT. For instance, miR-9 targets E-Cadherin mRNA, while the expression of miR-155 results in the dissolution of tight junctions [67].

As mentioned above, another feature of the EMT transition is the reorganization of the actin cytoskeleton, which leads to the acquisition of an enhanced motility and enables cell elongation and directional movements. In fact, the formation of actin stress fibers, which favour cell contractility, is visible in mesenchymal cells [68]. Moreover,

the mesenchymal cells are characterised by the presence of actin-rich membrane projections, including lamellipodia, filopodia and invadopodia. The invadopodia facilitate cell invasion by degrading the ECM [69]. Importantly, the remodelling of the ECM is essential for the initiation and progression of the EMT. The epithelial cells stably adhere with the basement membrane through certain integrins, including $\alpha 3\beta 1$, $\alpha 6\beta 1$, $\alpha 9\beta 1$ and $\alpha 6\beta 4$. Integrins are transmembrane heterodimers that consist of two glycoprotein subunits, alpha and beta. They are not only important for cell-matrix and cell-cell contacts, but also regulate the transduction of different signals from the ECM, coupling cell adhesion with the remodelling of the cytoskeleton. In fact, it was reported that the integrin-fibronectin interaction induce a reorganization of the cytoskeleton and that actin stress fibers terminate at focal adhesions, which are integrin-rich cell-matrix adhesive contacts. During the EMT transition, the cells lose their interaction with the basement membrane and make contacts with the interstitial matrix. Therefore, they downregulate epithelial integrins and start expressing others which have key roles in EMT progression. For instance, $\alpha 5\beta 1$ integrin expression increases cell adhesion to fibronectin, which is upregulated during EMT, and facilitates cell migration. Moreover, the increased expression of $\alpha 1\beta 1$ or $\alpha 2\beta 1$ integrins and their interactions with type I collagen promote the breakdown of E-cadherin complexes and the nuclear translocation of β-Catenin [62, 70]. Parallel to the changes in the repertoire of integrins, the cells start also inducing the expression of proteases, such as the matrix metalloproteinases MMP2 and MMP9, which degrade the ECM and facilitate cell invasion. The degradation of the ECM might also cause the release of growth factors, which can then further contribute to the EMT progression [71].

1.5 WT1 in adult tissue maintenance

Although, as mentioned before, WT1 is expressed in very few cells in the adult, the generation of a tamoxifen inducible *Wt1* knockout model highlighted the essential role that WT1 plays in the maintenance of adult tissue homeostasis. In fact, the ubiquitous

deletion of *Wt1* in adult mice led to dramatic phenotypes, such as acute glomerulosclerosis, likely due to impairments in podocyte functions, and aberrant haematopoietic system in both bone marrow and spleen, which reflected a decrease of erythrocyte progenitors. More surprisingly, the knockout caused pancreatic atrophy and rapid and widespread loss of bone and fat [50]. It has been hypothesised that the pancreatic atrophy is caused by the activation of stellate cells, which start producing chemokines, leading to extensive cell death. Because stellate cells activation is characterised by an EMT transition, it is possible that deletion of *Wt1* leads to an unbalance in the expression of epithelial/mesenchymal genes, which switches the stellate cells from a quiescence to an active state [52]. The mutant bones were characterised by an increased number of osteoclasts; moreover, KO osteoblasts showed reduced bone differentiation ability *in vitro*, suggesting that WT1 plays a crucial role in osteoclast and osteoblast differentiation. Furthermore, the zone of proliferating cartilage of the bones of the mutant mice were irregular, indicating that WT1 might also affect chondrocyte differentiation [50]. The reduction in the size of fat pads resulted from a decrease in size of lipid vacuoles and it is believed that the fat loss was caused by both changes in systemic factors, such as the insulin growth factor 1 (IGF1) which was dramatically reduced in the mutants, and intrinsic defects to the fat lineages. In fact, following *Wt1* disruption, the population of stromal mesenchymal cells in the bone marrow, which generate both adipocytes and osteoblasts, significantly increased, suggesting impairment in their differentiation [50, 52].

Therefore, investigating the causes of these phenotypes raised the hypothesis that WT1 continues to function in mesenchymal stromal stem and/or progenitor cells in adults. Moreover, the study highlights the fact that adult tissue maintenance requires different and additional regulators compared to embryonic development, since no issues in the formation of red blood cells, bone and fat were found in the analysis of *Wt1* knockout embryos and foetuses [50, 52]. Although it is not yet sure whether WT1 in the adult life keeps regulating the EMT process in physiological conditions, contributing to the production of progenitor cells, evidence is emerging. In fact, it has been shown that WT1 expressing mesothelial cells give rise to a subset of adipocytes in the visceral

white adipose tissue (WAT) also in three months old mice [59]. On the other hand, as discussed below, a role for WT1 has been proposed in different pathological conditions, such as cancer and fibrosis, which may arise from an impairment in EMT regulation.

1.5.1 Insights on the development of tissues affected by *Wt1* KO in the adult: the bone, cartilage and fat formation

Bone and cartilage development

The skeleton and cartilage develop from cells deriving from the cranial neural crest, the somites and the lateral plate mesoderm. Initially, mesenchymal cells condense at the sites of the future bones. In membranous ossification these cells differentiate directly into osteoblasts, whereas in endochondral ossification, which is the most common process for bone formation, the condensed mesenchymal cells first become chondrocytes. Then, the chondrocytes in the centre of the condensation stop proliferating and become hypertrophic, while the ones surrounding them differentiate into osteoblasts, generating the bone collar. The hypertrophic chondrocytes remodel the extracellular matrix, by expressing different MMPs (especially 9, 13 and 14), and form mineralised matrix; they also induce angiogenesis by expressing high levels of VEGF. Finally, the hypertrophic cartilage is replaced by bone and marrow and the growth plates are formed [72, 73].

Hence, the differentiation of osteoblasts and chondrocytes follows initial common steps. In fact both cell types derive from mesenchymal progenitors, which can also give rise to adipocytes, myoblasts, stromal cells of the marrow and fibroblasts of tendons and ligaments [74, 75], highlighting possible interconnections between the tissues these cells form. The differentiation along the osteoblast lineage depends on two master transcription factors: RUNX2 (Runt-related transcription factor 2) and Osterix, which acts downstream of RUNX2. Underlying the fact that RUNX2 is essential for bone formation, disruption of *Runx2* results in the complete absence of bone formation [76] and its expression is sufficient to induce osteoblast differentiation *in vitro*, by activating osteoblast-specific genes in fibroblasts [77], and *in vivo*, as its continuous expression

leads to endochondral ossification in ectopic sites [78]. On the other hand, Osterix is also required for skeleton formation, indeed KO mutants do not develop bones, but it is essential for the late stages of osteoblastogenesis, as it is believed to induce osteoblastic differentiation in bipotential osteochondro-progenitor cells [79].

Specific markers characterise the three main stages of osteoblastogenesis, namely proliferation, matrix maturation and mineralization. Generally, the early stages are defined by the expression of alkaline phosphatase (ALP), type I collagen (COL1A1) and bone sialoprotein (BSP), while the mature osteoblasts are positive for osteocalcin (OCN) and PPR (parathyroid hormone-related protein receptor). An array of external signals orchestrates the osteoblast differentiation, including bone matrix-derived TGFβ, bone morphogenic protein 2, 4 and 7 (BMP2, BMP4, BMP7), IGF1, IGF2 and PTH (parathyroid hormone). Interestingly, the BMPs seem to be the only molecules which are involved in the specification of both osteoblasts and chondrocytes. The external signals activate a wide range of signalling pathway, such as Wnt, Hedgehog, FGF and TGFβ, which transmits signals through either SMAD (mothers against decapentaplegic)-dependent or SMAD-independent pathways, such as ERK, JNK, and p38 MAPK pathways.

As in osteoblastogenesis, chondrogenesis starts with the condensation of mesenchymal cells, which express collagens I, III and V. The chondroprogenitors then differentiate and express the cartilage-specific collagens II, IX and XI. Finally, the chondrocytes either form the articular cartilage or proliferate, terminally differentiate into hypertrophic chondrocyte and undergo apoptosis, leading to the replacement of cartilage with bone [80]. The proliferating chondrocytes are marked by the expression of collagen VI, while the hypertrophic ones express collagen X. RUNX2 and SOX9 (Sry-box transcription factor 9) are the main regulators of the chondrocyte differentiation. In fact, while RUNX2 is essential for chondrocyte maturation, SOX9 is required for chondrocyte hypertrophy and necessary to prevent osteoblastic differentiation, by inhibiting RUNX2 expression and lowering β-Catenin signalling [73, 81].

Fat development

Even though there has been much progress in the field, several aspects of the origin of fat still remain obscured. Two different types of adipose tissue coexist in mammals: the white adipose tissue (WAT) and the brown adipose tissue (BAT). Both are involved in regulating the energy balance and homeostasis, but while the WAT is the main energy storage site, the BAT is a thermogenic organ, since the brown adipocytes can convert nutrients into heat. WAT and BAT are distributed in various sites of the body, forming several depots. In particular, the WAT is present in several pads, with the largest amounts found at subcutaneous and visceral locations. There are six visceral fat depots: epicardial, perirenal, gonadal, retroperitoneal, omental and mesenteric.

During development, the fat pads do not appear simultaneously and differences in their origins have been suggested. Nowadays, lots of studies have focused on understanding the functions and development of the WAT, as its excessive expansion is associated with obesity and all the related metabolic disorders. Specifically, increased visceral fat is associated with metabolic dysfunctions, whereas increased subcutaneous WAT seems to be protective [59, 82]. Several genome-wide studies have proposed heterogeneous developmental origins not only for WAT and BAT, but also for different WAT depots, such as the visceral and the subcutaneous pads. Moreover, heterogeneity between visceral fat depots, for instance the mesenteric and omental pads, was reported. Taken together, the results highlighted the complexity of the generation of fat and suggested that the adipose depots develop from distinct developmental processes and constitute separate organs, which are not functionally equivalent [82].

Adipogenesis consists of two main steps: first mesenchymal stem cells are committed to the adipocyte lineage becoming adipocyte progenitors, second the progenitors terminally differentiate into mature adipocytes. While the differentiation step has been largely studied in vitro, the mechanisms leading to the formation of the progenitors, as well as their embryonic origin, remain enigmatic in many aspects. So far, it is believed that the progenitors of white adipocytes in the trunk derive from lateral mesoderm-derived mesenchymal precursors, while the head white depots are supposed to originate

from the neural crest. In contrast, it seems that the BAT shares a common origin with the skeletal muscles, deriving from paraxial mesoderm-derived precursors [82]. Shedding new light on the development of WAT and confirming differences between the origins of visceral and subcutaneous pads, a recent work from our lab has pinpointed the lateral plate mesoderm as the major source of visceral WAT; moreover, the authors showed that all the visceral depots are surrounded by a mesothelium and defined WT1 expressing mesothelial cells as a subset of WAT progenitors [59].

Different transcription factors, cofactors and signalling pathways contribute to the commitment of mesenchymal stem cells to the adipocyte lineage. Among the identified transcription factors, the peroxisome proliferator-activated receptor gamma (PPARγ) is the only one that is both necessary and sufficient for the adipogenesis process, as well as being required for the maintenance of the differentiate state [83]. In fact, *Ppar*γ null mice die because they do not develop any kind of adipose tissue [84]; moreover, Rosen at al proved that PPARγ is sufficient to differentiate fibroblasts into adipocytes *in vitro* and that it is essential for the development of fat *in vivo* [85]. PPARγ was also shown to downregulate RUNX2 expression, therefore inhibiting osteogenesis, while inducing the commitment of mesenchymal cells toward the adipocyte lineage [86]. On the other hand, other factors favour the differentiation towards bone and cartilage cells, for instance the transcriptional cofactor TAZ (transcriptional co-activator with PDZ binding motif) activates RUNX2 and represses PPARγ-dependent gene transcription [87]. Other transcription factors, which are crucial for adipogenesis, are several C/EBP (CCAAT-enhancer binding protein) family members, including C/EBPα, C/EBPβ and C/EBPδ. The timing of expression of these important regulators is finely tuned during adipocyte differentiation. Indeed, C/EBPβ and C/EBPδ are detected first, then PPARγ starts being expressed and activates C/EBPα, which exerts a positive feedback loop on PPARγ. Another family of transcription factors, whose importance in adipogenesis has been well documented, is the Krppel-like factor (KLF) family. It has been proposed that a cascade of KLFs characterises adipocyte differentiation, with anti-adipogenic KLFs, such as KLF2 and KLF7, being sequentially replaced by pro-adipogenic KLF, including KLF15, KLF5 and KLF6. Presumably, one of the main

functions of the KLFs is the recruitment of either co-activators or co-repressors to the Pparγ promoter [83].

Different signalling pathways are involved in the activation or inhibition of adipogenesis. One of the most important stimuli for the process is the insulin, which in the early stages functions mainly through IGF1 receptor signalling. In fact, it has been shown that the loss of insulin-receptor substrate (IRS) proteins, as well as of PI3K and AKT, inhibits adipogenesis. On the other hand, ligands of the TGFβ superfamily exert divergent effects on the process. Indeed, while TGFβ inhibits adipocyte differentiation, BMP4 seems to commit mesenchymal cells to the adipose lineage. BMP2 also promotes adipogenesis by interacting with other factors, such as insulin; moreover, it seems to stimulate the process via other additional mechanisms, for example by inducing the nuclear localization of C/EBPα. By contrast, the activation of the WNT and hedgehog pathways block adipocyte differentiation, favouring osteogenesis. On the other hand, studies on the contribution of MAPK family members on adipogenesis led to conflicting results. Nonetheless, it looks likely that the activation of ERK1 and p38 favours the adipocyte differentiation. For instance, ERK1 activity seems to be required for the proliferative phase, but it has to be reduced during the terminal differentiation phase [83].

1.6 WT1 in disease

1.6.1 Congenital syndromes

Besides tumours, mutations in *WT1* have been identified in different developmental syndromes, which generally result in renal and genitourinary abnormalities, as well as being associated with an increased risk of Wilms' tumour.

Among the renal diseases, the Denys-Drash syndrome (DDS) is characterised by severe glomerular nephropathy, often Wilms' tumour and, while the female gonads are normal, the males show ambiguous genitalia or mild hermaphroditism. The DDS is caused

by heterozygous missense mutations within the exons 8 and 9, which encode for the second and third zinc finger. Hence, the mutations affect the DNA binding properties of WT1; moreover, the dimerization of mutant and the wild-type proteins seems to prevent WT1 DNA binding, thus suggesting that the mutant proteins act in a dominant-negative manner. In addition to the diffuse mesangial sclerosis which characterises the glomerular lesion in DDS, abnormalities in the podocytes have also been detected. In fact, the DDS podocytes express low levels of WT1 and overexpress TGFβ and PDGFα (platelet-derived growth factor alpha), potent EMT inducers, as well as maintaining a fibroblast-like morphology in culture. Moreover, studies have proposed that DDS podocytes resemble a developmental form and suggested that in DDS there is a delay in the maturation of the glomeruli, characterised by the failure in completing the MET process, which is necessary for the generation of matured adult glomeruli. Missense mutations in exon 8, exon 9 and intron 9 of *WT1* have also been identified in isolated cases of FSGS (focal segmental glomerulosclerosis), where the podocyte injury was suggested to be induced via EMT, caused by excessive levels of TGFβ. Taken together, these data corroborate the assumption that physiological levels of WT1 are essential for the maintenance of a correct epithelial-mesenchymal balance and crucial for the control of EMT and MET transitions [52, 88].

Another renal syndrome caused by *WT1* mutations is Frasier syndrome. Mutations occur within the exon 9 or at the splice donor site in intron 9, leading to an unbalance in the ratio between WT1 -KTS and +KTS isoforms, with the +KTS isoforms being reduced of about 50%. Frasier patients show glomerular sclerosis, male to female reversal and frequently gonadoblastoma. The fact that the reduction of the +KTS isoforms is crucial for the occurrence of this human disease has been confirmed by the generation of mice lacking the expression of these isoforms, as they develop phenotypes that mirror the Frasier syndrome [13, 52].

The WAGR syndrome (Wilms' tumour-aniridia-genitourinary-mental retardation syndrome) is instead caused by heterozygous deletion of the 11p13 locus, which encompasses several genes, including *WT1* and *PAX6*. The disruption of one copy of *WT1*

leads to less severe renal defects, milder genitourinary abnormalities and reduced risk of Wilms' tumour compared to the DDS patients. FSGS is the most common pathology in WAGR patients and renal failure occurs in about the 40% of the cases. Interestingly, the heterozygous *Wt1* KO mice develop glomerulosclerosis and renal failure, resembling the WAGR symptoms [52, 88].

The Meacham syndrome is a rare congenital syndrome which is characterised by male pseudo-hermaphroditism, abnormalities in female genitalia, heart and diaphragm defects and, in some individuals, by adrenal and spleen anomalies. Point mutations in the zinc-finger region of *WT1* have been identified and the features of the syndrome clearly overlap with the phenotypes observed in the *Wt1* KO mice. It has been suggested that the Meacham syndrome symptoms derive from abnormalities in the EMT occurring in the coelomic epithelium and the septum transversum, in which WT1 plays a crucial role [52].

1.6.2 WT1 in cancer

The EMT and MET transitions are not only essential for normal development, but they have also been implicated in cancer progression and invasion. Specifically, the EMT process seems to be crucial for tumour dissemination, allowing epithelial cells to lose contacts with the basement membrane, become more motile and able to intravasate into lymph or blood vessels, through which they are transported to different organs. Once at the secondary site, the invasive cells can form metastases, by extravasating and undergoing an MET [89]. Furthermore, a link between the EMT and the generation of cancer stem cells has also been proposed [90]. Given the importance of EMT and MET for cancer progression and the fact that WT1 might regulate the ability to transit in either direction, it is likely that in tumours there is a strong selective pressure to promote its expression [52]. In fact, WT1 has been shown to control the EMT/MET processes through the regulation of different genes essential for the transitions, such as *E-Cadherin*, *Snail* and *Slug* [53, 91].

The role of WT1 in oncogenesis is controversial, as the data collected so far have either advocated its oncogenic role or supported a tumour suppressor function for WT1. Indeed, WT1 was originally identified as a classic tumour suppressor in the Wilms' tumour, as loss of function mutations in *WT1* gene can lead to the occurrence of this malignancy in about the 15% of the cases. The Wilms' tumour is a childhood renal cancer that affects 1 in 10,000 children [92]. As mentioned above, this cancer is also associated with congenital disorders, such as DDS and Frasier syndromes, which are caused by mutations in *WT1* gene. Although the mechanisms behind the Wilms' tumour development are still unclear, it has been shown that ablation of *Wt1* and constitutive *Igf2* overexpression in mice resulted in early onset and high frequency of Wilms' tumour, probably due to a block in mesenchyme differentiation caused by *Wt1* disruption [93]. The tumour suppressor role of WT1 was reinforced by different studies *in vitro*, which demonstrated that the overexpression of the transcription factor in multiple cancer cell lines lowered the colony formation rates, blocked proliferation and increased apoptosis [94–101]. For instance, Morrison et al showed that WT1 downregulates the Ras/MAPK pathway by activating MKP3 (mitogen-activated protein kinase phosphatase 3), inducing growth arrest and enhancing apoptosis in an osteosarcoma cell line [102]. Moreover, WT1 can induce the apoptotic process by regulating pro-apoptotic genes, such as BAK (BCL2-Antagonist/Killer 1), or alter the balance of survival signals by downregulating the receptor for EGF and insulin [103, 104]. Studies *in vivo* have also suggested a tumour suppressor role for WT1. For instance, the stable transfection of WT1, and specifically of the -/+ isoform, in a Wilms' tumour cell line reduced the tumour formation in nude mice [105]; moreover, the constitutive expression of WT1 in a malignant breast cancer cell line strongly suppressed the estrogen-stimulated tumorigenesis in nude mice [106].

Despite data supporting the tumour suppressor function of WT1, several lines of evidence suggest an opposite, oncogenic role for the transcription factor. Indeed, WT1 seems to be either over- or re-expressed in several adult tumours, including leukaemia [107], colorectal [108], breast [109], lung [110], desmoid [111], prostate [112], brain [113], ovarian [114], uterine [115] cancers and in soft tissue sarcomas [116]. Since none of these

tumours arise from tissues that normally express WT1, with the only exception of the haematopoietic system, and no mutations in *WT1* gene have been so far identified in solid tumours, it has been proposed that WT1 plays an oncogenic role in these contexts. Moreover, different studies have identified that WT1 expression correlates with poor prognosis in leukaemia [117], breast [109] and uterine [115] cancers. Of note, although many data support an oncogenic role for WT1 in leukaemogenesis [92], mutations in *WT1* gene were found in a considerable proportion of acute myeloid leukaemia (AML), indicating WT1 as an oncosuppressor, rather than an oncogene [118]. For instance, two papers have recently demonstrated that WT1 interacts with TET2 (Tet methylcytosine dioxygenase 2), an enzyme that regulates DNA hydroxymethylation, by mediating the conversion of 5-methylcytosine to 5-hydroxymethylcytosine. WT1 was shown to recruit TET2 to its target genes, activating their expression. It was demonstrated that mutations in *WT1* and *TET2* are mutually exclusive in AML patients and that AML-derived mutations in these genes disrupt their protein interaction, resulting in the deregulation of DNA hydroxymethylation, altered gene expression and aberrant hematopoietic differentiation phenotype [119, 120].

Interestingly, while in normal development and adult tissues WT1 expression is mainly restricted to the nuclear compartment [121], its cytoplasmic localization has been reported in several cancers, including tumours of the urinary tract, genital organs, breast, lung, brain, skin, bone, gastrointestinal and pancreato-biliary systems [122]. These data have raised the intriguing question whether the cytoplasmic localization of WT1 could be implicated in cancer progression or even be oncogenic itself.

The oncogenic role of WT1 has been reinforced by different studies *in vitro* and *in vivo*. For instance, Hartkamp at al showed that WT1 mediates anti-apoptotic signaling downstream of cytotoxic drugs, an effect that is negated when WT1 is cleaved by the serine protease HtrA2 (high temperature requirement protein A2) [123]. Moreover, the silencing of WT1 in cells expressing an endogenous allele of activated KRAS (Kirsten rat sarcoma viral oncogene homolog) triggered senescence in vitro and inhibited tumor progression *in vivo* [124]. Also several other studies in vitro have shown that the

inhibition of WT1 expression decreases the proliferation and induces apoptosis in cancer cell lines, including myeloid leukaemia, nerve sheath tumour and melanoma cells [125–127]. Corroborating its oncogenic function, the expression of WT1 can be stimulated in hypoxic conditions, which are similar to the tumour environment [128]. Moreover, different papers have implicated WT1 in tumour angiogenesis and vascularization. For instance, Wagner et al demonstrated that WT1 is expressed in the endothelial cells of a high proportion of different tumours and assessed that WT1 is required for endothelial cell proliferation, migration and in vitro angiogenesis [129]. In addition, Katuri and colleagues have recently shown, using xenografts models, that WT1 positively regulates angiogenesis in Ewing sarcoma [130].

Some studies have also tried to identify specific roles of single WT1 isoforms in cancer, although they did not reach unanimous results. In fact, it has been suggested that the isoforms including the exon 5 have an anti-apoptotic function on the intrinsic apoptosis pathway [131, 132] and that they might be involved in leukemia relapse [133]. Congruent with these data, the expression of the variants containing the exon 5 was shown to prevent mitochondrial damage and inhibit apoptosis in a panel of cancer cell lines [134]. In contrast, it was reported that these isoforms act as onco-suppressors, by downregulating the oncogenes C-MYC (avian myelocytomatosis virus oncogene cellular homolog) and BCL2 (B cell leukaemia 2) in Hela cells (Hewitt 1995). Mayo et al then showed that the -KTS variants upregulate BCL2 when transiently transfected in an osteosarcoma cell line, regardless of the presence of the exon 5 [135]. In 2013 two studies pointed out that the -/+ isoform is the most overexpressed WT1 variant in leukemia cell lines and in lung cancer specimens [136, 137], suggesting a selective pressure for tumours to activate its expression.

Taken together, the data highlight the complexity of the role of WT1 in cancer and indicate that it is not possible to label WT1 either as an oncogene or a tumour suppressor. Nonetheless, WT1 surely plays an important role in cancer, which possibly can be linked to its role in the regulation of the EMT transition [52].

1.6.3 WT1 in fibrosis

Although the role of WT1 in fibrosis has not been extensively investigated, some studies have found that WT1 is re-expressed in different fibrotic tissues, suggesting that the transcription factor may play a role in the disease. For instance, following ischemic injury in mice, WT1 is expressed in subepicardial mesenchymal cells and in areas of interstitial fibrosis. Similar to mice, WT1 positive cells were identified in human diseased hearts within epicardial and interstitial fibrotic areas [138]. Wagner at al also found WT1 expression in the coronary vascular endothelium after myocardial infarction in rats [7]. Moreover, WT1 expression is induced following nephrectomy in rats [139]. Interestingly, WT1 is expressed in HSCs, which are considered crucial for liver fibrosis [140], and current studies in Dr Tim Kendall lab aim to pinpoint the function of WT1 in this context (unpublished). Of note, as discussed below, several data have highlighted the importance of the EMT process during tissue fibrosis, therefore hinting at a possible involvement of WT1 in this condition.

The wound healing is a process which involves sequential phases: injury, inflammation, ECM deposition and proliferation and, finally, tissue remodelling. During the initial inflammatory phase, the neutrophils are recruited first, followed by monocytes, which differentiate in macrophages. These two types of white blood cells start releasing inflammatory and fibrogenic chemokines, which leads to the chemoattraction of T and B leukocytes. On the other hand, the proliferative phase is characterised by angiogenesis, fibroblast expansion and re-epithelialization. If the tissue injury becomes chronic, excessive ECM deposition may occur, resulting in fibrosis, scarring and loss of tissue function. The myofibroblasts are the main cell type that contributes to the synthesis and deposition of ECM and, therefore, to the fibrotic process. These cells promote wound contraction and are marked by the expression of alpha-smooth muscle actin (ACTA2), collagen type 1, MMPs and tissue inhibitors of metalloproteinases (TIMPs) [141, 142]. Whereas in physiological conditions they proliferate and favour the wound healing, in fibrosis they produce ECM components in a chronic and uncontrolled manner [142]. Moreover, the myofibroblasts together with the resident epithelial cells release an array

of cytokines, growth factors, proteases and ECM proteins, which amplify the inflammatory infiltrate. Also the angiogenesis process is believed to be associated with chronic injury. In fact, myofibroblasts in response to hypoxia produce angiogenic factors, such as FGF, VEGF and angiopoietins [141].

Different sources have been proposed to generate myofibroblasts: they can be derived from differentiation of resident mesenchymal cells and recruited fibrocytes, from perivascular smooth muscle cells, or from epithelial, endothelial and mesothelial cells undergoing EMT, EndMT (endothelial to mesenchymal transition) or MMT (mesothelial to mesenchymal transition), respectively [142, 143]. For instance, it has been shown that in mouse models of renal fibrosis, although some bone marrow mesenchymal cells contribute to fibrotic cells, the majority of myofibroblasts derive from the kidney epithelium [144]. It has also been suggested that kidney tubular epithelial cells and podocytes can undergo EMT in response to injury, participating to the scarring process [139, 145]. However, another study *in vivo* did not find any epithelial-derived myofibroblasts and identified the pericytes as the main source of fibrotic cells in kidney fibrosis [146]. Interestingly, the podocytes, which express WT1, can be considered as a specialized type of pericytes [147]. The EMT transition has been involved in the generation of scar-producing cells also in other tissues, such as liver [148] and lung [149, 150]. Another cellular plasticity process involved in the formation of myofibroblasts seems to be the EndMT. In fact, endothelial cells were suggested to be an alternative source of activated fibroblasts in kidney and cardiac fibrosis [151]. Besides epithelial and endothelial cells, also mesothelial cells can acquire a mesenchymal phenotype thought the MMT transition, a process which is crucial for normal development and wound healing, as well as being involved in the generation of myofibroblasts in different fibrotic tissues [143]. For instance, it was shown that renal dialysis injures the mesothelial lining, causing the mesothelial cells to undergo an MMT and finally resulting in fibrosis [63]. The MMT seems to be a crucial event in liver fibrosis. Indeed, Li et al demonstrated that in fibrogenesis mesothelial cells give rise to myofibroblasts and HSCs [152], which are the main contributors to liver fibrosis [140]. Importantly, the authors suggested that mesothelial cells negative for the expression of WT1 were not able to undergo the MMT

transition [152]. Two recent studies have highlighted the importance of the MMT in lung fibrosis [153, 154]. In fact, pleural mesothelial cells were shown to migrate into the lung parenchyma and differentiate into myofibroblasts. Interestingly, WT1 positive cells were aberrantly present in the fibrotic regions of the lungs of patients with idiopathic pulmonary fibrosis [153] and WT1 positive pleural mesothelial cells were found in the lung parenchyma of mice after TGFβ stimulation [154].

Regardless of the source, the myofibroblasts are activated by multiple mechanisms, such as paracrine signals from leukocytes, autocrine factors secreted by the myofibroblasts and exogenous antigens. Different molecules that induce the activation of myofibroblasts and regulate the fibrotic process have been identified. Among them, the most extensively studied is TGFβ, which is produced mainly by circulating monocytes and tissue macrophages. TGFβ is thought to directly activate the resident mesenchymal cells and to induce the EMT process in epithelial cells, differentiating them into myofibroblasts. Other cytokines, especially chemokines, and their receptors have been identified as crucial regulators of fibrosis, as they are involved in trafficking, activation and proliferation of leukocytes and their interaction with resident cells; moreover, some chemokines also exhibit potent angiogenic properties. The rich panel of cytokines that promotes the fibrosis process includes the interleukins IL1, IL4, IL5, IL13, IL6 and the chemokines CCL2, CCL3, CCL5 and CXCL1, CXCL8, CXCL9 and CXCL10. Other factors with angiogenic activity, which are important for the fibrotic process are VEGF, PDGF and FGF. Moreover, components of the renin-angiotensin-aldosterone system show pro-fibrotic properties; in particular, angiotensin II (ANG II), a hormone produced by macrophages and fibroblasts, appears to be involved in cardiac, renal and hepatic fibrosis [141, 142].

1.7 Objectives

The functions of WT1 and its isoforms have been so far addressed *in vivo* using KO models, which have provided pivotal insights on the role of WT1 in development and disease. Nonetheless, they did not allow the investigation of the instructive role of the transcription factor. In order to address *in vivo* which processes WT1 is able to induce, mice models for the upregulation of WT1 will be needed.

Aiming to address the instructive role of WT1 and to dissect the differences between its variants, during my PhD I wanted to create cellular systems for the inducible expression of single isoforms of the transcription factor. I derived two epithelial cell models in which is possible to induce WT1 isoforms expression and I started characterizing the effects of the induction by gene expression analysis and cellular assays. As WT1 exhibits specific functions depending on tissue and cellular context, using these cell lines disclosed interesting outcomes following WT1 induction, but came along with multiple limitations. Therefore, my final goal was to derive embryonic stem cells (ES) to generate mouse models, in which the expression of single variants could have been temporally (and spatially) controlled.

In this thesis I will first explain the cloning process to generate plasmids for the inducible expression of WT1 single isoforms, second I will describe the stable and inducible epithelial cell models and ES cells derived with these plasmids. Last, I will discuss the results obtained from the induction of single WT1 isoforms in the differentiated cell lines.

Although we are still far from understanding the instructive role of WT1, my work has aimed to provide the tools to start addressing this issue and has suggested interesting hints on the processes that WT1 might be able to drive.

Chapter 2

Materials and methods

2.1 Cloning methods

2.1.1 Polymerase chain reaction (PCR)

In order to amplify the inserts for the cloning reactions, I used the KOD hot start DNA polymerase (Novagen, Cat. No. 71086). To find the best annealing temperature, each couple of primers was initially tested using a rage of annealing temperatures, using a gradient between 60°C and 72°C.

Standard reaction set up:

1X Buffer for KOD hot start DNA polymerase

$MgSO_4$ 1.5 mM

dNTPs 0.2 mM (each)

Forward primer (Fwd) 0.3 μM

Reverse primer (Rev) 0.3 μM

Template DNA 10 ng

KOD hot start polymerase 0.02 U/μl

PCR grade water to a final volume of 15 μl

Cycling conditions:

Polymerase activation: 95°C for 2'

Denature: 95°C for 20"

Annealing: 10" at the best tested temperature

Extension: 70°C for 15"/kb

Repeat steps 2-4 for 35 times

To check the specificity of the reactions, the PCR products were separated by electrophoresis through an agarose gel. 1μl of 6X Orange loading dye was added to 5μl of reaction. The mixture was then loaded and run on 1% or 2% TBE (Tris-borate-EDTA) agarose gels, depending on the size of the amplicons. For every 100 ml of gel, I added 2 μl of ethidium bromide to visualise the DNA using an UV (ultraviolet) transilluminator. The gels were run using a voltage between 70 V and 120 V for the time needed to separate the bands at the expected size.

TBE 10X: 1M Tris base, 1M Boric acid, 0.02 EDTA.

6X Orange loading dye: 15% Ficoll, Orange G dye in dH_2O (distilled water)

DNA ladders used:

1 kb: 1 Kb Plus DNA Ladder (ThermoFisher Scientific, Cat. No. 10787-018)

100 bp : 100 bp DNA Ladder (Promega, Cat. No. G2101)

Table 2.1: List of restriction enzymes

Enzyme	**Supplier**	**Cat. No.**
AgeI	Thermo Fisher Scientific	FD1464
BamHI	Thermo Fisher Scientific	FD0054
BglII	Thermo Fisher Scientific	FD0083
BsiWI	Thermo Fisher Scientific	FD0854
BsrGI	Thermo Fisher Scientific	ER0931
BstBI	Thermo Fisher Scientific	FD0121
BstZ17I	Thermo Fisher Scientific	FD0704
ClaI	Thermo Fisher Scientific	FD0143
EagI	Thermo Fisher Scientific	ER0331
EcoRI	Thermo Fisher Scientific	FD0274
EcoRV	Roche	10667145001
FseI	Thermo Fisher Scientific	R0588
KpnI	Thermo Fisher Scientific	FD0524
MluI	Thermo Fisher Scientific	FD0564
NcoI	Roche	10835323001
NheI	Thermo Fisher Scientific	ER0971
PaeI	Thermo Fisher Scientific	FD0604
PvuI	Roche	10650129001
SacI	Roche	10669792001
SalI	Thermo Fisher Scientific	FD0644
SnaBI	Thermo Fisher Scientific	ER0401
SwaI	Thermo Fisher Scientific	ER1241
XhoI	Thermo Fisher Scientific	ER0691

2.1.2 Enzymatic digestion

Double stranded DNA was digested at specific sites using different restriction enzymes. All the single or double enzymatic digestions were carried on using the buffer, temperature and incubation time suggested by the manufacturer. Table 2.1 shows all the enzymes and the respective catalogue numbers used for the cloning. The digestions were checked by electrophoresis, loading on 1% or 2% TBE agarose gel 50 to 200 ng of plasmid, depending on the size of the fragments.

2.1.3 Clean-up of enzymatic reactions

To purify PCR products, bands extracted from agarose gel, as well as any enzymatic reaction, I used the NucleoSpin® Gel and PCR Clean-up kit (Macherey-Nagel, Cat. No. 740609). The PCR reactions or enzymatic digestions, that had to be excise and purified from gel, were loaded on 1% TAE (Tris-acetate-EDTA) agarose gel (+ 2 μl of ethidium bromide per 100 ml of gel) and run at 70 V. When the bands at the expected size were well separated, the DNA was visualised by an UV transilluminator and the desired band was quickly cut, to avoid mutations caused by the UV light. I determined the weight of the excise band and diluted it in 200 μl of Binding Buffer NTI per 100 mg of gel, the gel was then dissolved at 50°C for 5-10'. For PCR clean-up, the PCR reactions or enzymatic digestions were diluted in 2 volumes of Binding Buffer NTI. The mix was loaded on a NucleoSpin® Gel and PCR Clean-up column, which was spin at 11,000 X g for 30" to bind the DNA to the silica membrane. The membrane was then washed twice with 700 μl of NT3 buffer, by spinning the column for 30" at 11,000 X g. The column was then dried with an additional spin of 1'. The DNA was eluted adding 15 μl of Elution Buffer to the membrane, centrifuging for 1 min and repeating the procedure for three times. The yield and quality of the eluted DNA fragment was quantified using a spectrophotometer (NanoDrop).

50X TAE: 2.0 M Tris acetate, 0.05 M EDTA, 1 M Acetic acid in dH_2O

2.1.4 In-Fusion HD cloning

The plasmids were cloned using the In-Fusion® HD Cloning Kit (Clontech, Cat. No. 639649).

To amplify the inserts for the In-Fusion reactions, I designed and used the primers listed in Table 2.2 . All the primers contain 15 bp at the 5' end that are homologous to 15 bp at one end of the DNA fragment, to which they will be joined; the sequence at the 3' end of the primer is, instead, specific to the target gene. The melting temperature of each primer is between 58 and 65°C. The inserts were amplified using the KOD hot

start DNA polymerase and the PCR reactions were purified by NucleoSpin® Gel and PCR Clean-up kit.

Table 2.2: In-Fusion Primers

Name	**Sequence**
pAmCyan1-N1 Wt1 plasmid	
Fwd Wt1 STOP	gtgcccttctgaagcatgggttccgacgtgcgggacctgaa
Fwd Wt1 w/o STOP	tccgtggtgcccttcatgggttccgacgtgcgggacctgaa
Rev Wt1	tctagagtcgcggccctaaagcgccagctggagtttggtcatgtttc
pCMV-Tet3G-Hygromycin plasmid	
Fwd Hygro	ttggtcggtcattttcagttagcctcccccat
Rev Hygro	gatcaagatctgatcatgaaaaagcctgaactcaccgcg
pTRE3G-AmCyan1-Wt1 plasmid	
Fwd pTRE3G	attaccgccatgcattttactccctatcagtga
Rev pTRE3G	gtccggtagcgctaggtcgactttacgagggta
pTRE3G-mCherry-Wt1 plasmid	
Fwd Wt1	gacgagctgtacaagatgggttccgacgtgcggga
Rev Wt1 mCherry	catatgacgcgtgatctaaagcgccagctggagtt
pSV40-Tet3G-TRE3G-mCherry plasmid	
Fwd pSV40 Kan/Neo	gtcttcaagaattcctcagaagaactcgtcaag
Rev pSV40 Kan/Neo	tgatagggagtaaacgaggtgcactctcagtac
Fwd IRES	cctttcgtcttcaaggatatccggcccggttgtggccata
Rev IRES	cgagttcttctgacggccggcccctctccct
Fwd PolyA Tet-ON 3G	cgagttcttctgacggccggcccctctccct
Rev PolyA Tet-ON 3G	acaaccgggccggatatgtctagactggacaagag
pSV40-Tet3G-TRE3G-AmCyan1 plasmid	
Fwd for Wt1 and EV	cctaccctcgtaaagtcgacctagcgctac
Rev EV	aggctagccatatgacgcgtgctagggcaccac
Rev Wt1 AmCyan1	aggctagccatatgacgcgtctaaagcgccagctg
pGoldi Lox plasmid	
LoxP T2A(A)	ctcttgtccagtctagacatggtaccataacttcgtataatgtatgctatacgaagttatatcgatagg tccaggattctc
LoxP T2A(B)	aggtccaggattctcctcgacgtcaccgcatgttagcagacttcctctgccctctccgcttccaacgtt
FWD GFP	tccgcttccaacgttcttgtacagctcgtccatg
Rev GFP	gtgatttttttgtagatttaaatatggtgagcaagggcgaggag

Fwd IRES PS3	ctacaaaaaaatcacgcaaaattacagttaacggcatgtacagtttgtcacgatcgtcagtcctg ctcctc
Rev IRES PS3	gaggagcaggactgacgatcgtgacaaactgtacatgccgttaactgtaattttgcgtgattttt ttgtag
Fwd Zeo	tcagtcctgctcctcggccacgaagtgcacgcagttgc
Rev Zeo	gtgaggaactaaaccctcgagatggccaagttgaccagtgc
Fwd EM7	ggtttagttcctcaccttgtc
Rev EM7	aagttatggcgcgcctgttgacaattaatcatc
Fwd LoxP(2)	ggcgcgccataacttcgtataatgtatgctatacgaagttatttcgaagaattctttgccaaaatg
Rev LoxP(2)	cattttggcaaagaattcttcgaaataacttcgtatagcatacattatacgaagttatggcgcgcc
Fwd CAG	gaattctttgccaaaatgatgagacagc
Rev CAG	gccgcatagttaagccagtatacattgattattgactag
Fwd Wt1 pGoldi	acgagctgtacaagagcgatcgcatgggttccgacgtgcggga
Rev Wt1 pGoldi	ctagccatatgacgcgtctaaagcgccagctggagtttg
Fwd left arm	ctccatttataaactgccgcggtggtatacagttaacggcagccggagt
Rev left arm	catagttaagccagtagatatctctagaaagactggagttgcaga
Fwd right arm	tagtcaataatcaatgtagatatcgcggccgcagatgggcgggagtc
Rev right arm	ccgttaactgtataccaccgcggcagtttataaatggag
CAG-Tet3G-TRE3G-mCherry plasmid	
Fwd ZeoEM7	agggagaggggccggtgatcatcagtcctgctcctcggccac
Rev ZeoEM7	ccgatcgtgttgacaattaatcatcggcatagtatatcggcatagtataatacgacaaggtgagg aactaaaccatcgatatggccaagttgaccagtgc
Fwd CAG 2	tgtcaacacgatcggaattctttgccaaaatgatgagac
Rev CAG 2	atagttaagccagtatacattgattattgactagttattaatag
Fwd left arm	ctccatttataaactgccgcggtggtatacagttaacggcagccggagt
Rev left arm 2	atagttaagccagtactcgagtctagaaagactggagttgcaga
Fwd right arm	tagtcaataatcaatgtagatatcgcggccgcagatgggcgggagtc
Rev right arm	ccgttaactgtataccaccgcggcagtttataaatggag
Fwd 1 P2A Tag Wt1	ccgcagttcgaaaaagaaaatttatacttccaaggcgcatgcatgggttccgacgtgcggga
Fwd 2 P2A Tag Wt1	gagaaccctggacctcgtacgtggagccacccgcagttcgagaaaggtggaggttccggaggt ggatcgggaggtggatcgtggagccacccgcagttcgaaaaa
Fwd 3 P2A Tag Wt1	gacgagctgtacaagggaagcggagctactaacttcagcctgctgaagcaggctggagacg tggaggagaaccctggacctcgtacgtggag
Rev Wt1 P2A Tag	tagccatatgacgcgtctaaagcgccagctggagtttggtc
pGoldiLoxS plasmid	
Fwd P2A	gtccagtctagacatggtaccaggtccagggttctcctccacgtctccagcctgcttcagcaggc tgaagttagtagctccgcttccagatctc

Fwd Venus	gtagctccgcttccagatctcttgtacagctcgtccatgccgagagtgatc
Rev Venus	cgaagttataccggtatggtgagcaagggcgaggagctgttc
Fwd LoxP	gcccttgctcaccataccggtataacttcgtataatgtatgctatacgaagttatatcgatatagag cccaccgcatccc
Fwd SV40polyA	atagagcccaccgcatccccagcatg
Rev SV40polyA	catggacgagctgtacaagtaaaacgttctgtgccttctagttgccag
Fwd rsEGFP	ctggcaactagaaggcacagaacgttttacttgtacagctcgtccatg
Rev rsEGFP	gtgatttttttgtagatttaaatatggtgagcaagggcgaggagc
Fwd Venus 2	cctaccctcgtaaagtcgacatggtgagcaagggcgag
Rev Venus 2	tagccatatgacgcgtttacttgtacagctcgtccatg
Fwd Cherry 2	gtagctccgcttccagatctcttgtacagctcgtccatg
Rev Cherry 2	acgaagttataccggtatggtgagcaagggcgaggag
Fwd pTRE3GS	gtcaataatcaatgtatactttactccctatcagtgatag
Rev pTRE3GS	cttgctcaccatgtcgactttacgagggtaggaagtggta
Fwd left arm	ctccatttataaactgccgcggtggtatacagttaacggcagccggagt
Rev left arm 3	gatagggagtaaagtagatatctctagaaagactggagttgcaga
Fwd right arm	tagtcaataatcaatgtagatatcgcggccgcagatgggcgggagtc
Rev right arm	ccgttaactgtataccaccgcggcagtttataaatggag
Fwd polyBGH	acgaagttatgagctcatagagcccaccgcatccccagcatg
Rev polyBGH	cttatcatgtctggatcgtgatcaggtaaatataaaattttgtataatgtgttaaactactgattct aattgtttgtgtattttagatctgtgccttctagttgccagcc

The backbones were prepared by digesting the vectors with specific restriction enzymes. Once the digestion was checked by electrophoresis, the enzymatic reaction was purified by NucleoSpin® Gel and PCR Clean-up kit.

Once I purified the insert(s) and the linearised backbone, I proceeded with the cloning reaction: In-Fusion cloning mix (Table 2.3):

TABLE 2.3: In Fusion reaction

Component	**Cloning reaction**	**Negative control**	**Positive control**
Purified insert	200 ng	/	2 μl of 2 kb control insert
Linearised backbone	50 ng	50 ng	1 μl of pUC19 control vector
5X In-Fusion HD enzyme premix	2 μl	2 μl	2 μl
dH_2O	to 10 μl	to 10 μl	to 10 μl

The reaction was incubated for 15' at 50°C. 2.5μl of the mixture were used to transform Stellar Competent cells, as described below. After transformation, the bacteria were seeded, grown O/N (over night) and up to 24 colonies were picked and grown. The plasmid DNA was then purified and screened by PCR or by restriction enzyme digestion. To confirm the correct cloning, the plasmids were sequenced by the HGU sequencing service.

2.1.5 QuikChange lightning site-directed mutagenesis

The mutagenesis of plasmids was carried on using the QuikChange® lightning site-directed mutagenesis kit (Stratagene, Cat. No. 210519).

The mutagenic primers used are listed in Table 2.4. The forward and reverse primers contain the desired mutation in the middle of the sequence and anneal to the same sequence on opposite strands of the plasmid, their melting temperature is higher or equal to 78°C.

The mutagenic reaction to synthesise the mutant strand was prepared as indicated below:

5 μl of 10X reaction buffer

10 ng of plasmid

125 ng of forward primer

125 ng of reverse primer

1 μl of dNTPs mix

1.5 μl of QuikSolution reagent

dH_2O to 50 μl

1 μl QuikChange® Lighting Enzyme

and amplified using the following Cycling parameters:

1: 95°C for 2'

2: 95°C for 20"

3: 60°C for 10"

4: 68°C for 30"/kb of plasmid length

Repeat from 2 to 4 for 18 cycles

5: 68°C for 5'

To digest the parental methylated and hemimethylated dsDNA, the amplification product was treated with 2 μl of DpnI restriction enzyme for 5' at 37°C. 2 μl of DpnI-treated DNA was then transformed in XL10-Gold ultracompetent cells. The plasmids containing the correct mutation were screened by restriction enzyme digestion and sequenced by the HGU sequencing service.

TABLE 2.4: Primers for mutagenesis

Name	**Sequence**
Mut AatII Fwd	ccatagttgcctgacgtcccgtcgtgtagataac
Mut AatII Rev	gttatctacacgacgggacgtcaggcaactatgg
Mut BglII Fwd	cttgtccagtctagatctatccggcccggttg
Mut BglII Rev	caaccgggccggatagatctagactggacaag

2.1.6 DNA blunting

T4 DNA polymerase (Roche, Cat. No. 11004786001) was used to create blunt ended DNA: 100 ng of plasmids were mixed with 100 μM of each dNTP, 0.2 units of T4 DNA polymerase, 1X Buffer and dH_2O to a final volume of 50 μl. The mixture was incubated at room temperature (RT) for 10' and inactivated at 80°C for 15'.

2.1.7 DNA ligation

Ligation of blunt or sticky ends was performed using the T4 DNA ligase enzyme (Roche, Cat. No. 10481220001). 50 ng of template were incubated at RT with 1X Buffer, 1 unit of T4 DNA ligase and dH_2O to a final volume of 30 μl. To ligate blunt ends, the reaction was incubated O/N, to ligate sticky ends, the incubation time was of 10'.

2.1.8 Bacteria transformation

The competent cells were thawed on ice; 5 ng of plasmid or the indicated amounts of In-Fusion or mutagenesis reactions were added to transform 50 μl of bacteria. The bacteria were incubated on ice for 30' and then heat-shocked for 1' at 42°C. The tubes were then placed on ice for 2'. SOC medium was added to reach a final volume of 200 μl and the transformed bacteria were incubated by shaking (250 rpm) at 37°C for 1 hour. 1/10 and 9/10 of each culture were plated on LB (Luria-Bertani) agar plates with the selective antibiotic and grown O/N at 37°C.

Competent cells: Stellar Competent cells (Clontech, Cat. No. 636766); XL10-Gold Ultracompetent cells (Stratagene, Cat. No. 200314).

SOC medium: 2% (w/v) Tryptone, 0.5% (w/v) Yeast extract, 10 mM NaCl, 2.5 mM KCl, 10 mM $MgCl_2$, 20 mM Glucose. The medium was autoclaved before adding $MgCl_2$ and glucose.

LB agar: 5g NaCl, 5g Tryptone, 2.5g Yeast Extract, 7.5g Agar, dH_2O to 500 ml. Adjust the pH to 7.0 with 5 N NaOH. Autoclave.

Concentrations of antibiotics to select bacteria:

Ampicillin (Amp): 100 μg/ml

Kanamycin (Kan): 50 μg/ml

Zeocin (Zeo): 50 μg/ml

2.1.9 Colony screening by PCR

To select the colonies transformed with the expected plasmid, each colony was picked with a sterile tip. The tip was dipped into the KOD hot start DNA polymerase PCR reaction, containing the forward and reverse In-Fusion primers flanking the insert(s). The tip was then dropped in 500 μl of SOC medium supplemented with the appropriate antibiotic to grow the bacteria O/N by shaking (250 rpm) at 37°C. The PCR reaction was carried on as described above and the product was checked by electrophoresis.

2.1.10 Plasmid DNA purification

The plasmids were purified using Qiagen Plasmid Mini (Cat. No. 12123) or plus Maxi (Cat. No. 12963) kit. The bacteria were grown in LB medium (5 ml for Mini prep and 250 ml for Maxi prep) with the appropriate antibiotic O/N at 37°C, by shaking at 250 rpm. The bacteria were harvested by centrifugation at 6000 x g for 15' at 4°C. The

pellet was resuspended in P1 Buffer + RNase A by vortexing. An equal volume of Buffer P2 was added to lysate the cells and the mixture was incubated for 5' at RT. After the incubation, the same volume of Buffer P3 was added to neutralise the lysis buffer and to precipitate genomic DNA, proteins, cell debris and SDS (sodium dodecyl sulfate). In order to remove the precipitated materials, the lysate was centrifuged at maximum speed for 10' and the supernatant, containing the plasmid DNA, was transferred into a column. To bind the plasmid DNA to the resin, the column was centrifuged at 10,000 x g for 1'. The column was then washed twice by adding the washing buffer P3 (containing 70% ethanol) and spinning at 10,000 x g for 1'. The column was subsequently dried through another centrifugation of 1' at 10,000 x g. The plasmids DNA was then eluted by adding an appropriate volume of elution buffer to the centre of the membrane and by centrifuging for 1' at 10,000 x g. The yield and quality of the plasmid DNA was quantified using the NanoDrop.

LB medium: 10 g Tryptone, 5 g Yeast Extract, 10 g NaCl in 950 mL dH_2O. Adjust the pH of the medium to 7.0 using 1N NaOH and bring volume up to 1 liter.

2.2 Mammalian tissue culture and cell-based assays

2.2.1 Cell culture

All the cell lines were cultured in a humidified atmosphere at 37°C and 5% CO_2. MDCK (Madin Darby Canine Kidney, MDCK.2) cells and IMCD3 (Inner Medullary Collecting Duct) were kindly provided by the Ian Jackson lab. These cells were maintained in Dulbecco's Modified Eagle Media with 1 mM sodium pyruvate (DMEM - Gibco), supplemented with 10% (v/v) foetal calf serum (FCS), 1000 U/ml penicillin and 650 μg/ml streptomycin (P/S) (made by the HGU technical services). The E14, E14 *Wt1* knockout [3] and CreERT2 E14 cells (kind gift of Ian Chambers lab) were grown in GMEM (Glasgow's MEM) BHK-21 with L-Glutamine (Gibco), with the addition of 10% (v/v) FCS, 1% (v/v) non-essential amino acids (Sigma-Aldrich), 1 mM sodium

pyruvate (Sigma-Aldrich), 0.00001% (v/v) β-mercaptoethanol and LIF (leukemia inhibitory factor) (10^6 units for 1 litre of medium - made in the lab). The medium for the E14 *Wt1* knockout cells was supplemented with 250 μg/ml of G418 (Gibco).

The cells were split on average every two days, before reaching full confluence. The medium was aspirated and the cells rinsed in pre-warmed PBS (phosphate-buffered saline). After removing the PBS, the cells were detached by adding a small volume of Versene solution (containing 0.2 g/l trypsin and 0.4 g/l Sodium EDTA in a buffered salt solution with phenol red; made by HGU technical services); the cells were then incubated at 37°C for the time needed to detach the monolayer. Subsequently, an appropriate volume of medium was added to inactivate the trypsin, collect the cells and allow a single cell suspension. The cells were then seeded on cell culture grade flasks or dishes (Corning). The flasks for the culture of all the E14 cell lines were pre-coated with 0.1% gelatin (Sigma-Aldrich) in PBS. The number of passages was kept as low as possible and aliquots of cells were stored in liquid nitrogen in 1 ml FCS supplemented with 10% (v/v) dimethyl sulfoxide (DMSO). To recover cells from liquid nitrogen, they were thawed quickly in a 37°C water bath; 5 ml of medium were then added and the cell suspension was centrifuged for 5' at 1,200 rpm to remove the DMSO. The pellet of cells was then resuspended in fresh medium and seeded.

The cells were manually counted using a Neubauer haemocytometer (0.1 mm depth, 1/400 mm^2).

All the cell lines were regularly monitored for mycoplasma contamination by the HGU technical service.

PBS: Phosphate-Buffered Saline (pH 7.3): 8 g NaCl, 0.2 g KCl, 1.15 g Na_2HPO_4, 0.2 g KH_2PO_4 made up in 1 litre of dH_2O

2.2.2 Cell treatments

Doxycycline (Dox) treatment: Dox powder (Clontech, Cat. No. 631311) was diluted to 1 mg/ml in double distilled H_2O (ddH_2O) and store in the dark in aliquots at -20°C.

The cells were treated with the concentrations of Dox stated in the next chapters; the cell culture medium supplemented with Dox was changed every other day.

4-hydroxy-tamoxifen (4-OHT) treatment: The CreERT2 E14 cells were treated with 1 μM OHT (Sigma-Aldrich, Cat. No. H79904, powder diluted in methanol) for 48 hours.

Retinoic acid treatment: E14 and E14 *Wt1* KO cells were grown in monolayer in medium without LIF and supplemented with 1 μM Retinoic acid (Sigma-Aldrich, Cat. No. R2625, powder resuspended in DMSO) for 5 days.

2.2.3 XFect transfection

One day prior to the transfection, the cells were plated in 6 well plates in order to have a confluence of 70-80% at the time of transfection with Xfect^{TM} (Clontech, Cat. No. 631318). For the transfection, two mixes were prepared in microcentrifuge tubes:

Mix 1 (per well): 0.5 - 1 μg of linearised plasmid DNA + XFect Reaction Buffer to a final volume of 100 μl.

Mix 2 (per well): 0.3 μl of XFect Polymer per 1 μg of plasmid DNA + XFect Reaction BUffer to a final volume of 100 μl.

Mix 2 was gently added to Mix 1 and, after vortexing at medium speed for a few seconds, the solution was incubated for 10' at RT. 200 μl of nanoparticle complex solution were added dropwise in each well containing 2 ml of fresh medium. The cells were then incubated at 37°C in a CO_2 incubator. After 4 hours incubation, the medium containing the transfection solution was replaced with fresh medium.

2.2.4 Lipofectamine transfection

The day before transfection the cells were seeded in 6 well plates in order to get a confluence of 70-80% the following day. For the transfection with Lipofectamine® 2000 (Invitrogen, Cat. No. 11668), two mixes were prepared:

Mix 1 (per well): 1 μg of linearised plasmid DNA + Opti-MEM® I Reduced Serum Medium (Invitrogen, Cat. No. 31985) (Opti-MEM) to 100 μl.

Mix 2 (per well): 5 μl of Lipofectamine + Opti-MEM to 100 μl.

Both the mixes were incubated for 5' at RT. Mix 2 was then added dropwise to Mix 1. Following 20' incubation at RT, the transfection solution was added dropwise to the cultured cells growing in 2 ml of fresh medium. After an O/N incubation, the medium was replaced with 2 ml of fresh medium.

2.2.5 Establishment of stable cell lines

The day following cell transfection by either XFect™ or Lipofectamine®, the cells were split in 10 cm diameter culture dishes. A day later, I started the selection with the appropriate concentration of antibiotic. The concentration of each antibiotic was determined through a kill curve, which is a dose-response assay where the cells are subjected to increasing amounts of antibiotic to find the minimum concentration needed to kill all the cells over the course of one week.

Antibiotic concentration used to select eukaryotic cells:

G418 for MDCK cells: 500 μg/ml

Zeocin for IMCD3 and E14 *Wt1* KO cells: 400 μg/ml

The cells were selected for about 2 weeks, changing the medium containing the antibiotic every other day, until the appearance of clear single clones. To select the stable individual clones, I used two different approaches: the stable MDCK cells transfected with the pSV40-Tet3G-TRE3G-AmCyan1 or mCherry plasmids were induced O/N with 0.5 μg/ml of Dox, the day after the AmCyan1 or mCherry positive cells were sorted by Fluorescence Activated Cell Sorting (FACS), as explained below, and seeded in 96 well plates containing fresh medium; on the other hand, the single clones derived from MDCK cells transfected with the pSV40-Tet3G-TRE3G plasmids and from IMCD3 and E14 *Wt1* KO cells were manually picked and expanded. I made frozen stocks for each

clone. Once the single clones were established, I kept them growing in media containing half of the concentration of antibiotic initially used for the selection.

2.2.6 Flow Cytometry: Fluorescence Activated Cell Sorting (FACS)

The FACS was carried out by Elisabeth Freyer at MRC HGU using a BD FACSAria™ II System (BD Biosciences), equipped with 5 lasers and fluorescence detectors. The analysis was carried out using the FlowJO Software Version 7.6.5 (http://www.flowjo.com).

2.2.6.1 Sorting of single fluorescent cells

Pools of clones of MDCK cells stably transfected with pSV40-Tet3G-TRE3G-AmCyan1 or mCherry plasmids were trypsinised after 2 weeks of selection, washed twice in PBS and resuspended in 2 ml of PBS. Single fluorescent MDCK cells were then sorted by FACS and each cell was seeded in one well of a 96 well plate filled up with medium containing the selective antibiotic.

2.2.6.2 Cell cycle analysis

Cells were collected by tripsynisation and washed twice in PBS. The pellet was then resuspended in 300 μl of ice-cold PBS and the cells were fixed by adding 700 μl of cold pure ethanol dropwise, while vortexing. The samples were stored at 4°C until the time of analysis. After washing the cells with 1 ml of cold PBS with 1% (w/v) BSA (Bovine Serum Albumin), the pellet was resuspended in 1 ml Propidium Iodide (PI) solution (20 μg/ml PI, Sigma-Aldrich Cat. No. P4864 + 10 μg/ml RNase A in PBS). The samples were incubated for at least 30' at RT, light protected. If necessary to get a single cell suspension, the cells were resuspended using a 1 ml syringe before FACS analysis.

2.2.7 Growth curve analysis

I seeded 10,000 cells in each well of 6 well plates; the number of plates was equal to the number of time points assessed in every experiment. I considered the initial time point (day 0) as the morning after the seeding of the cells. At every time point, the cells were washed in PBS and fixed with 0.5% (v/v) glutaraldehyde in PBS for 20' at RT, under gentle shaking. After removing the fixing solution, the cells were washed twice with PBS and kept at 4°C, covered by PBS, until the time of analysis. When the cells of all the different time points were fixed, I stained them with a solution containing 0.1% (w/v) Crystal violet in PBS. The cells were stained for 30' at RT, while gently shaking. The staining solution was then removed and the wells washed three times with H_2O. The plates were dried O/N. The Crystal violet dye was then dissolved by adding in each well 1 ml of 10% (v/v) Acetic acid in dH_2O and by incubating at RT for 30', while gentle shaking. 100 μl from each well were transferred in a 96 well plate and the absorbance was read at 595 nm, using a microplate reader (BMG Labtech, FLUOstar Omega).

2.2.8 Wound healing assay

Culture inserts with a cellfree gap width of 500 μm (Ibidi, Cat. No. 80209) were transferred in 24 well plates with glass bottom (GE Healthcare Whatman, Cat. No. 7706-2370). 60 μl of cell suspension, containing enough cells to be 100% confluent the following day, were added at each side of the insert. The day after, the insert was carefully removed and each well was filled up with 1 ml of medium. The migration of the cells was live-imaged using a Zeiss live cell imaging system (Zeiss Axiovert 200), taking brightfield images every hour for 48 hours. The images were analysed by ImageJ 1.x, an open source image processing program.

2.2.9 Colony formation in soft agar

Each well of a 6 well plate was coated with 1 ml of base agar, made mixing equal volumes of 1% (w/v) agar dissolved in sterile ddH_2O and 2X DMEM (Biochrom, Cat. No. T043-01), supplemented with 20% (v/v) FCS, P/S and 4 mM L-glutamine. 7,500 cells per well were mixed with 1 ml of top agar solution, composed by equal volumes of 0.7% (w/v) agar in sterile ddH_2O and 2X DMEM with 20% (v/v) FCS, P/S, 4 mM L-glutamine and, if needed, the selective antibiotic. The cell suspension was quickly added on the top of the base agar. When the top agar solidified, I added 1 ml of fresh medium in each well. The cells were grown for 3 weeks, changing the medium every other day. The cells were then washed twice with PBS and stained with 0.005% (w/v) Crystal violet in methanol for 3 hours at RT, under gentle shaking. The wells were then washed with H_2O and dried O/N at RT. Pictures of the plates were taken and the colonies were counted using ImageJ 1.x.

2.2.10 Senescence associated beta-galactosidase staining

The cells were washed in PBS and fixed for 5' with 3% (w/v) paraformaldehyde (PFA) at RT, while gently shaking. After two washes in PBS, the cells were stained with the X-gal (5-bromo-4-chloro-3-indolyl β D-galactopyranoside) staining solution (1 ml per well of a 6 well plate). The cells were then incubated at 37°C in the dark for up to 48 hours. The staining solution was then aspirated and the cells washed with H_2O. Images were taken using an inverted microscope (Nikon Eclipse TiS).

The assay is based on the accumulation of the endogenous lysosomal β-galactosidase enzyme specifically in senescent cells. The enzyme cleaves the chromogenic substrate X-gal, producing a blue-dyed precipitate.

X-gal staining solution:

1 mg/ml X-gal (Promega, Cat. No. V394A)

5 mM Potassium ferrocyanide

5 mM Potassium ferricyanide

150 mM NaCl

2 mM $MgCl_2$

in Sodium phosphate buffer pH 6. The solution was warmed up to 37°C prior incubation to avoid the formation of crystals.

Sodium phosphate buffer pH 6:

94 mM NaH_2PO_4 * H_2O

6 mM Na_2HPO_4

2 mM $MgCl_2$

in dH_2O.

2.2.11 Cell adhesion assay

The cell adhesion assay was carried out using the CytoSelect^{TM} 48-Well Extracellular Matrix Protein (ECM) Cell Adhesion Assays (Cambridge Biosciences, Cat. No. CBA-070). The plate was allowed to warmed up to RT for a few minutes. I prepared a cell suspension of 500,000 cells per ml in serum-free medium, supplemented with 0.5% (w/v) BSA, 2 mM $CaCl_2$ and 2 mM $MgCl_2$, and seeded 150 μl in each well. The plate was then incubated for 60' in a cell culture incubator. After incubation, I carefully aspirated the medium, which contained the cells that did not attach, and gently washed for 4 times the wells with 250 μl of PBS, containing 2 mM $CaCl_2$ and 2 mM $MgCl_2$. After the last wash, I aspirated the PBS and added 200 μl of Cell Staining Solution, which stained the attached cells. The plate was incubated for 10' at RT and, subsequently, the staining solution was discarded. I gently washed the wells 4 times with 500 μl of dH_2O and then let the wells to air dry. Afterwards, I added 200 μl of Extraction solution per well and incubated the plate for 10' on an orbital shaker. Finally, I transferred 150

μl of solution in a 96 well plate and read the absorbance at 560 nm in the microplate reader (BMG Labtech, FLUOstar Omega).

2.3 Gene expression analysis

2.3.1 RNA extraction

Total RNA was extracted using the TRIzol Reagent® (Invitrogen, Cat. No. 15596-026). The cells were washed in PBS and lysed directly on the culture dish, by adding 1 ml of TRI Reagent per 10 cm diameter dish. The cell lysate was collected in a 1.5 ml tube and homogenised by repeated pipetting or using a 1 ml syringe. 0.2 ml of Chloroform per ml of TRIzol Reagent used were added to the lysate. After vortexing, the mixture was centrifuged for 15' at 4°C at maximum speed. The aqueous phase, containing the RNA, was then transferred in a new tube and 0.5 ml of isopropanol per ml of reagent used were added to allow the precipitation of the RNA. The sample was then mixed by vortexing and centrifuged for 10' at 4°C at full speed. Afterwards, the supernatant was carefully removed, the pellet was washed with 1 ml of 75% ethanol and centrifuged for 5' at 4°C at 7,500 x g. The RNA pellet was then air dried for 5-10' and resuspended in nuclease-free ddH_2O. The yield and quality of the RNA was measured by NanoDrop and 500 ng were run on a 1% TAE agarose gel to check the integrity of the RNA.

The RNA concentration and integrity number (RIN) of the samples sent for microarray analysis and RNA sequencing were measured by Agnes Gallacher (HGU technical service), using an Agilent 2100 bioanalyser.

2.3.2 cDNA synthesis

The complementary DNA (cDNA) was synthesised using the QuantiTect® Reverse Transcription Kit (Qiagen, Cat. No. 205311). First, in order to remove any contamination of genomic DNA, 2 μg of total RNA were mixed with 2 μl of gDNA Wipeout

Buffer and RNase-free water to a final volume of 14 μl. The mixture was then incubated for 2' at 42°C and subsequently placed on ice. I then added to each reaction the following reverse-transcription mix:

1 μl of Reverse-transcription master mix (containing the Quantiscript Reverse Transcriptase and RNase inhibitors)

4 μl of Quantiscript RT Buffer 5X

1 μl of RT Primer mix

The reverse-transcription reaction was incubated for 15' at 42°C. The Quantiscript Reverse Transcriptase was then inactivated by incubating for 3' at 95°C.

2.3.3 Quantitative reverse transcription polymerase chain reaction (Q-RT-PCR)

The analysis of expression of single genes was carried out using a SYBR Green-based quantitative reverse transcription polymerase chain reaction (Q-RT-PCR). The following Q-RT-PCR mix was prepared for the amplification of each sample:

5 μl of LightCycler® 480 SYBR Green I Master Mix (Roche, Cat. No. 04707516001)

0.5 μM Fwd primer

0.5 μM Rev primer

10 ng cDNA

dH_2O to 10 μl

Each sample was loaded on a LightCycler® 480 multiwell plate with 384 wells and the LightCycler® 480 Instrument II was used to amplify the cDNA, for which the primers were specific, and detect the levels of expression. The following program was used for the amplification and detection:

- Pre-incubation: 95°C for 10'

- Amplification: 95°C for 10"; Annealing temperature for 10"; 72°C for 15" (Acquisition mode = single). Repeat for 45 cycles.

- Melting curve: 95°C for 5'; 65°C for 1'; 97°C (Acquisition mode = continuous)

- Cooling: 40°C for 10"

The primers were designed using Primer3 (v.0.4.0) (http://bioinfo.ut.ee/primer3-0.4.0/) and OligoAnalyzer 3.1 (http://www.idtdna.com/calc/analyzer). Their specificity was checked with NCBI/Primer-BLAST (http://www.ncbi.nlm.nih.gov/tools/primer-blast/). Each couple of primers was tested at different annealing temperatures using three serial dilutions of template, in order to determine the best temperature for the highest efficiency and specificity of the primers.

Table 2.5 lists the primers used for Q-RT-PCR.

The levels of expression of every gene were normalised for the Ct (threshold cycle) of the housekeeping gene (hg). The Ct is the intersection between an amplification curve and a threshold line, therefore it is a relative measure of the concentration of the target in a PCR reaction.

The fold change, indicating the relative levels of expression between a sample (sa) and a control (cnt), was calculated using the formula below:

ΔCt (sa) = Ct (sa) - Ct (hg)

ΔCt (cnt) = Ct (cnt) - Ct (hg)

$\Delta\Delta$Ct = ΔCt (cnt) - ΔCt (sa)

$Fc = 2^{\Delta\Delta\ Ct}$

Table 2.5: Q-RT-PCR primers.

Gene	Fwd	Rev
Primers for canine genes		
GAPDH	CATCACTGCCACCCAGAAG	CAGTGAGCTTCCCGTTCAG
CXCL10	TCTGACTCTGAATGGTACTCAAGG	CATTGTGGCAATGATCTCAACATG
CXCL17	TCTGTTGCTGCCACTAATGC	GTGAAGAAAACCAGGAACCAAAGGC
CXCL8	TCTTGGCAGCTTTTGTCCTT	CTCAGCCTTCTTTAGAAATATCTGC
CCL2	TCTCCAGTCACCTGCTGCTA	CGGTCTTGAAGATCACAGCTTC
CCL5	AGGTCTCCGCAGCTACCTTTG	GGGTGACAAAGACGACTGCTG
CCL7	GGAAGCTGTGATCTTCAAGACC	GCTTGGGTTTTCTTGTCCAGG
MMP9	GAGTTATGGACTCTGGGCAAGG	TGTAGAGTTTCTCGCTGGGGC
TIMP2	TGTGAGTGCAAGATCACGCG	CGTTGATGCTCTTCTCCGTG
TIMP3	TGCAACTCTGACATCGTGATCCG	CTGTGTGGATGTACTGCACGTGG
TIMP4	ATCTCTTGACTGGTCAGGTCC	ACTCGTTAGGGGCTGAGATG
ACTA2	TGCGTGACATCAAGGAGAAG	ACTCCATGCCGATGAAGGAC
DESMIN	CTCAATGTCAAGATGGCCCTGGA	CCTCACTGACAACCTCCCCATC
COL1A1	GTGCCAAGGGTCTGACTGGAAGT	CTCCTGCTTCTCCATCTTTGCCAG
UPK3B	CCTGGACCTTACAGGGTGAA	AGGCTGGAGAAGTGCACAGT
Primers for murine genes		
Gapdh	CCCCAACACTGAGCATCTCC	ATTATGGGGGTCTGGGATGG
Col1a1	GAAACCCGAGGTATGCTTGATC	GAGTTTGGTGATACGTATTCTTCCG
Acta2	TCCGTGACATCAAGGAGAAG	GACTCCATCCCAATGAAAGATG
Mmp9	AGTTGTGGTCGCTGGGCAAA	GTGTAGAGTCTCTCACTAGGGCAGAA
Timp1	ATTCAAGGCTGTGGGAAATGCCG	CTTAGGCGGCCCGTGATGAGAAA
Timp2	TGTGAGTGCAAGATCACTCG	CCATTGATGCTCTTCTCTGTGA
Upk3b	CCAGGGCCCTTACAGTGTGAA	AGGCTGGAGAAACGCGTAGT
Msln	CTGCAGACCCAGACTACAAAGA	GAGGCCTGTGGGGAGACT
Thbd	ACTCTGCGAGCATTTTTGTGTCAGC	TCCACGCACTCTCCATCCACCAA
Runx2	TGGCCGGGAATGATGAGAACTA	CTGTCTGTGCCTTCTTGGTTCC
Zeb1	TTCAAACCCATAGTGGTTGCT	TGGGAGATACCAAACCAACTG
Igf2	AGTCGATGTTGGTGCTTCTCA	GAAGGCCTGCTGAAGTAGAAG
Flt4	ATGCTGAAAGAGGGCGCTACT	TGACACGCAAGAAGTTGGAGAG
VCam1	CAAGTCTACATCTCTCCCAGG	AACTTCCTGCCCCAGAAAAT
VegfB	AAGCCAGACAGGGTTGCCAT	GCTGGAGTGGGATGGATGATGTC
Pparγ	GTCTCACAATGCCATCAGGTT	CATACAAATGCTTTGCCAGGG
Snail	CTTGTGTCTGCACGACCTGT	CTTCACATCCGAGTGGGTTT
E-Cadherin	CCCTGTCTCTGCAAACCAAAA	TGCTTCCTGAGAAAATGCACAA
Desmin	CTCAATGTGAAGATGGCCTTGGA	CTCGCTGACAACCTCTCCAT
Vimentin	TGTACGAGGAGGAGATGCGGGA	TGTCTGAATGACTGCAGGGTGCTTT
Primers for mCherry-Wt1		
mCherry-Wt1	CCCCGTAATGCAGAAGAAGA	TCTTGGCCTTGTAGGTGGTC

2.3.4 Gene Expression Microarray

The total RNA was extracted from three independent biological replicates for every condition, using TRIzol Reagent®. The integrity and quantity of the RNAs were determined using Agilent 2100 bioanalyser. The RNAs (all having a RIN higher than 9.5) were sent to the Edinburgh Genomics facility at the Roslin Institute, where they were hybridised on the Affymetrix Canine Gene 1.1 ST microarray. The Affimetrix gene expression data were then analysed by Greame Grimes from the MRC HGU. The arrays were normalised using RMA method from the bioconductor affy package [155]. To determine correlation in expression data, Pearson correlation coefficients were calculated using Microsoft Excel (Microsoft UK), the hierarchical clustering of each subset was performed using R (Version 2.9.0). Linear model for the expression data of each gene were applied to compare the data from multiple arrays using the package limma [156]. Statistically differentially expressed genes were determined using the linear model results with an applied Bayes moderate t test. A Benjamini and Hochberg false discovery rate was used as a multiple testing control with a P-value < 0.05.

To identify enriched gene ontology terms (GO), I used the Gene Ontology Enrichment Analysis and Visualization tool (GOrilla, http://cbl-gorilla.cs.technion.ac.il/).

2.3.5 RNA sequencing

Total RNA was extracted using TRIzol Reagent® from two biological replicates per condition analysed. The quality and yield of RNA were determined by Agilent 2100 bioanalyser. The RNA sequencing (RNA seq) was carried out at the GATC Biotech AG (European Custom Sequencing Centre, Cologne, Germany). In the facility, the libraries were prepared: the poly-A containing mRNA molecules were purified and fragmented, the cDNA was then synthesised using random primers. After ligating the adapters and performing adapter-specific PCR amplification, the libraries were sequenced by Illumina sequencing (single read, read lenght: 50 bp, outcome of at least 30 million reads).

The RNA seq data were analysed by Dr Stuart Aitken at the HGU MRC. The protocol to analyse the RNA Seq data was based on the Cuffdiff2 protocol [157]. Briefly, the steps in the protocol are organised into bash shell scripts that are designed to be run at the command line. First, each replicate sequencing data set for each condition was aligned to the genome. Once all data were aligned, a merged assembly of transcripts found in all conditions was created by listing the cufflinks transcript outputs in a file called assemblies.txt, and by running cuff merge. The merged assembly and the aligned reads were used as inputs to cuffdiff, which performed the differential expression analysis. The final step of the Cuffdiff analysis was done in R (Version 2.9.0), using the Cummerbund library. Finally, the the cuffdiff database object was created and significant genes and isoforms were extracted at an adjusted P-value of 0.05.

The Database for Annotation, Visualization and Integrated Discovery (DAVID), a free online bioinformatics resource developed by the Laboratory of Immunopathogenesis and Bioinformatics (https://david.ncifcrf.gov/home.jsp), was used to identified enriched GO terms, functional-related gene groups and KEGG pathways (Kyoto Encyclopedia of Genes and Genomes, http://www.genome.jp/kegg/) in the list of differentially expressed genes.

2.4 Protein expression analysis

2.4.1 Total protein extraction and quantification

Cells were collected by trypsinization, pelleted and washed in cold PBS. The pellet was then kept on ice and resuspended by pipetting up and down in cold RIPA buffer (50 mM Tris HCl pH 8, 150 mM NaCl, 1% (v/v) NP-40, 0.5% (v/v) sodium deoxycholate, 0.1% (v/v) SDS in dH_2O), supplemented with a cocktail of proteinase inhibitors (Roche, Cat. No. 11873580001) and phosphatase inhibitors (Roche, Cat. No. 04906845001). The lysate was incubated on ice for 1 hour and vortexed every 15' to facilitate the

lysation. The extract was then centrifuged at maximum speed for 30' at 4°C and the supernatant, containing the total solubilised proteins, was transferred in a new tube.

The concentration of solubilised proteins was assessed using the Bio-Rad Protein Assay (Bio-Rad, Cat. No. 5000205), based on the Bradford dye-binding method, following the manufacturer's instruction.

2.4.2 Western blotting (WB)

Proteins were resolved by electrophoresis on polyacrylamide gel assembled on the Mini-PROTEAN Tetra system (Bio-Rad). The gels composing the polyacrylamide gel were prepared as followed:

Stacking gel:

4.5% (v/v) Acrylamide/Bis-Acrylamide solution (ratio 37.5:1)

0.126 M Tris HCl pH 6.8

0.1% (v/v) SDS

dH_2O to volume

Running gel:

10% or 16% Acrylamide/Bis-Acrylamide solution (ratio 37.5:1). The percentage depends on the molecular weight of the protein that has to be detected. For proteins smaller than 50 KDa, I used 16% gel.

0.375 Tris HCl pH 8.8

0.1% (v/v) SDS

dH_2O to volume

Polymerization of the gels was initiated by adding 0.01% (v/v) of 25% (w/v) ammonium persulfate (APS) and catalised with 0.001% (v/v) of tetramethylethylenediamine (TEMED).

The protein extracts were mixed 1:1 with 2X Laemmli loading Buffer and denaturated at 95°C for 5'. About 10 μg of proteins were loaded in each lane of the polyacrylamide gel. The proteins were run next to a protein ladder (PageRuler Plus Prestained Protein Ladder, ThermoFisher Scientific, Cat. No. 26619), composed by stained proteins of known molecular weights. The electrophoresis was carried out in 1X Running buffer at 70 V until the dye front reached the Running gel, then the voltage was increased up to 120 V. When the dye front was close to the bottom of the gel, the proteins were transferred on a nitrocellulose membrane (0.45 μm pore size for 10% Running gels, 0.2 μm pore size for 16% gels. Whatman, GE Healthcare) by electroblotting in 1X Transfer buffer for 1 hour at 100 V, RT. The transferred proteins were visualised by Ponceau S solution (Sigma-Aldrich, Cat. No. P7170), which was subsequently washed away with 1X TBS-T Buffer. The membrane was then saturated by incubating for 1 hour with Saturation Buffer. The incubation was carried out at RT under gentle shaking. Afterwards, the membrane was hybridised with the primary antibody specific to the protein to detect. The antibody was diluted in Saturation buffer and the incubation was done either O/N at 4°C or for 3 hours at RT, while gently shaking. Table 2.6 lists the primary antibodies used for WB and the dilutions used.

After hybridisation, the membrane was washed 5 times with 1X TBS-T Buffer (2 quick washes and 3 washes for 5' on a rocking plate). The membrane was then incubated for 1 hours at RT, gently shaking, with the appropriate horseradish peroxidase (HRP)-conjugated secondary antibody diluted 1:5000 in Saturation buffer. The secondary antibody has to be against the species where the primary antibody has been raised. Secondary antibodies used: HRP-conjugated anti-mouse (Cell signaling Technology, Cat. No. 7076), HRP-conjugated anti-rabbit (GE Healthcare, Cat. No. NA934V). The membrane was then washed in 1X TBS-T Buffer (2 quick washes, plus 3 for 5' each while shaking). The Pierce ECL Western Blotting Substrate (Thermo scientific,

Table 2.6: Primary antibodies for WB

Protein	**Dilution**	**Company**	**Cat. No.**
β-ACTIN	1:5000	Sigma-Aldrich	WH000060m1
AKT	1:1000	Cell signaling Technology	9272
ERK 1/2	1:1000	Cell signaling Technology	9102
GAPDH	1:5000	Aviva Systems Biology	OAEA00006
HSP90	1:5000	BD Transduction Laboratories	610418
mCherry	1:1000	Clontech	6325543
p21	1:1000	Santa Cruz Biotechnology	sc-397
pAKT Ser473	1:2000	Cell signaling Technology	9271
pERK 1/2 Thr202/Tyr204	1:1000	Cell signaling Technology	9101
WT1	1:1000	Santa Cruz Biotechnology	C19: sc-192
WT1	1:2000	Abcam	89901

Cat. No. 32106) was used to catalyse the enhanced chemiluminescence reaction of the HRP and the signal was detected by exposing x-ray films. The intensity of the bands' signal was quantified using ImageJ.

Buffers for WB:

2X Leammli Buffer:

62.5 mM Tris HCl pH 8

4% (v/v) SDS

0.1% (w/v) bromophenol blue

20% (v/v) glycerol

10% (v/v) β-mercaptoethanol

in dH_2O

10X Running Buffer:

0.25 M Tris HCl

2.5 M Glycine

in dH_2O, pH 8.3

Add 0.1% SDS (v/v) in the 1X solution.

10X Transfer Buffer:

0.24 M Tris HCl

1.86 M Glycine

in dH_2O

1X Transfer Buffer:

10% (v/v) 10X Transfer Buffer

20% (v/v) Methanol

in dH_2O

20X TBS buffer:

2.74 M NaCl

0.5 M Tris HCl

0.05 M KCl

in dH_2O, pH 7.4

1X TBS-T Buffer: 1X TBS + 0.1% (v/v) Tween-20

Saturation buffer: 5% (w/V) non-fat dry milk in 1X TBS-Tween Buffer

2.5 Immunofluorescence (IF)

The cells for IF were seeded on glass bottom plates (GE Healthcare Whatman, Cat. No. 7706-2370). The cells were washed twice in PBS before fixing, directly on the plate, with

Table 2.7: Primary antibodies for IF

Protein	**Dilution**	**Company**	**Cat. No.**
E-Cadherin	1:250	Cell signaling Technology	3195
WT1	1:250	Santa Cruz Biotechnology	C19: sc-192
ZO-1	1:250	Cell signaling Technology	5406

4% (w/v) PFA in PBS for 10' at RT, while gently shaking. The fixed cells were then washed in PBS and permeabilised in PBS + 0.1% Triton X-100 for 5 min at RT, under shaking. After one wash in PBS, the saturation was carried out by incubating the cells with PBS + 1% (w/v) BSA (PBS+) for 30' at RT, while shaking. The primary antibody was then hybridised by incubating O/N at 4°C, under gentle shaking. The primary antibody was diluted in PBS+; the list of antibodies and their dilutions are shown in Table 2.7. The morning after, the primary antibody was discarded and the cells were washed for 5 times (3' each) in PBS+. To detect the primary antibody, the cells were incubated with the appropriate Alexa Fluor® 488 or 594 dye-conjugated secondary antibody, diluted 1:1500 in PBS+, for 30', in the dark, at RT, while gently shaking (Alexa Fluor® 488 anti-rabbit, ThermoFisher Scientific, Cat. No. A-11034; Alexa Fluor® 594 anti-rabbit, ThermoFisher Scientific, Cat. No. R37119). After 5 washes in PBS (3' each), the nuclei were stained with DAPI (4',6-diamidino-2-phenylindole) (1 μg/ml in dH_2O) for 30". The cells were subsequently washed in dH_2O and imaged using a tissue culture inverted microscope (Nikon Eclipse TiS).

2.5.1 Phalloidin staining

The cells were fixed, permeabilised and saturated following the IF protocol. To fluorescently stain the cytoskeletal protein F-actin, the cells were incubated with the Alexa Fluor® 488 Phalloidin (Cell Signaling technology, Cat. No. 8878). The fluorescent dye-conjugated Phalloidin was diluted to a final concentration of 22 nM in PBS and

added to the cells. After a light-protected incubation of 15' at RT, while gently shaking, the solution was rinsed with PBS and the cells were imaged using a tissue culture inverted microscope (Nikon Eclipse TiS).

2.6 Genomic DNA extraction

The cells were pelleted, washed twice in PBS and resuspended by pipetting in Lysis Buffer (10 mM TrisHCl pH 8, 0.1 M EDTA pH 8, 0.5% SDS in dH_2O). 20 μg/ml of RNase A were added and the lysate was incubated for 1 hour at 37°C. Afterwards, the lysate was incubated with 100 μg/ml of Proteinase K O/N at 50°C. The day after, a Phenol:Chloroform:Isoamyl alcohol extraction was performed: an equal volume of Phenol:Chloroform:Isoamyl alcohol (25:24:1) was added to the lysate, the mixture was vortexed and centrifuged at maximum speed at RT for 10'. The aqueous phase was transferred in a new tube and the extraction was repeated a second time. Afterwards, an equal volume of Phenol:Chloroform was added and the mixture was vortexed and centrifuged at maximum speed at RT for 10'. The aqueous phase was then carefully moved in a new tube and the DNA was precipitated by adding 1/10 of volume of Sodium Acetate 3M pH 5.3 and 2 volumes of ice cold pure ethanol. The mixture was incubated O/N at -20°C. The following day, the tube was centrifuged at maximum speed for 30' at 4°C, the supernatant was removed and the DNA pellet washed with 75% ethanol. After spinning for 10' at maximum speed, the ethanol was discarded and the pellet was air dried for 5'. The genomic DNA was resuspended in Tris EDTA buffer (10 mM Tris-HCl pH 8, 1 mM EDTA) and quantified by NanoDrop.

2.7 Statistical analysis

The data are expressed as a mean value (± Standard Deviation, SD) with a P-value determined by an unpaired t test. Statistically significant is defined as P-value < 0.05.

Statistical analysis of Q-RT-PCR: All the column charts represent the mean of the fold change (Fc) ± SD of gene expression in the treated sample relative to the control, therefore the Fc of the control is always equal to 1. In order to establish whether the difference between the samples was statistically significant, I compared in the unpaired t test the average ΔCt (sa) (± SD) with the average ΔCt (cnt) (± SD). On the other hand, when the fold changes of two different samples were compared, the means of the Fc (± SD) were used in the unpaired t test.

Chapter 3

Establishing models to investigate the instructive role of WT1 single isoforms

3.1 Overview

So far the functions of the single isoforms of WT1 have been studied using different models, that overall failed to provide unanimous results and highlighted dichotomous roles of WT1 depending on the cell line and system used to either over-express or silence WT1 expression. These contrasting findings emphasize the need to further investigate the role of WT1 in normal development as well as in cancer. Importantly, up to now the instructive role of WT1 and its isoforms has not been fully addressed and dissected. Therefore, in order to understand which cellular processes WT1 is sufficient to drive, I established two different cell models expressing in an inducible manner the four main murine isoforms of WT1 (with or without the exon 5 and/or the KTS, here referred as: +/+, +/-, -/+ and -/-). In this chapter I explain the design and the cloning of the different plasmids and the establishment of the stable cell lines expressing inducible single isoforms of WT1.

I initially attempted to establish stable cell lines constitutively expressing single isoforms of WT1 fused to a fluorescent protein (FP). However, I was not able to derive stable clones, possibly due to the toxicity of WT1 constitutive over-expression. To overcome this issue, I decided to establish an inducible system. First, I created a classic Tet-On 3G inducible system that requires two different constructs: a regulator plasmid and a response plasmid. On the one hand the regulator plasmid expresses the Tet-On 3G transactivator gene under the control of the CMV promoter, on the other hand the response plasmid carries the gene of interest regulated by the Doxycycline inducible promoter pTRE3G. I cloned two pairs of vectors in which the inducible isoforms of WT1 are tagged with two different FPs, respectively AmCyan1 and mCherry. The plasmids were then sequenced and tested in transient transfection by western blot (WB) and immunofluorescence (IF) to confirm the expected pattern of FP-WT1 expression. Because the classic Tet-On 3G system is based on two distinct plasmids, two steps of integration are needed to derive stable cell clones. In order to simplify and make more efficient the establishment of stable cell lines, I decided to clone single vectors, called pSV40-Tet3G-pTRE3G-(FP)-Wt1, that express constitutively the Tet-On 3G transactivator and (FP)-WT1 in an inducible manner. I made three different single vectors: one carrying the single isoforms of WT1 fused to AmCyan1, one where the isoforms are fused to mCherry and one that lacks any FP (w/o FP). After the sequence of the plasmids was confirmed, the constructs were successfully tested in transient transfection, showing that there was expression of WT1 only after treatment with Dox and that the FP signals mirrored WT1 expression. Given the crucial role that WT1 plays in the EMT and MET transitions, I chose to derive stable and inducible MDCK cells because they are epithelial kidney cells that do not express endogenous WT1 and are a model widely used for EMT studies.

Although the inducible MDCK cell lines were proven to be a valuable and useful system for the study of the functions of WT1 single isoforms, they also showed different disadvantages. First, the single clones have different expression levels of WT1 that eventually led to a significant issue of clonal variability, as I will elucidate in the next chapter. Second, even if the murine and canine WT1 are supposed to bind to the

same promoter sequence [158], it is possible that the mouse WT1 would not behave physiologically in a dog cell.

Thus, I tried to build more homogeneous and less variable cell systems, aiming to avoid the integration of uncontrolled copy number of the plasmids and chromosomal position effects. The new set of plasmids I cloned, called pGoldiLox, offer several advantages compared to the pSV40-Tet3G-pTRE3G-(FP)-Wt1 plasmids. For instance, they contain ROSA26 homology arms to target the integration of the constructs; the SV40 promoter was substituted with the CAG promoter, which guarantees an optimal activity in the ROSA26 locus and is less subjected to silencing in ES cells; I cloned a constitutively expressed EGFP to facilitate the screening of stable clones. After testing the pGoldiLox-Wt1 vectors in transient transfection, I decided to derive stable single inducible clones using the murine IMCD3 cell line. The IMCD3 is an inner medullary collecting duct cell line and it is a polarized epithelial cell line; however it also expresses mesenchymal markers, similarly to the cells that express the endogenous WT1. Moreover, as in the MDCK cells, an EMT process can be induced in the IMCD3 cells by TGFβ treatment [159].

To establish stable clones and to integrate the pGoldiLox in the ROSA26 locus, the IMCD3 cells were transfected coupling each of the pGoldiLox-Wt1 plasmids with two Zinc Finger-encoding plasmids. The selected clones were then checked for the integration of the plasmid and WT1 expression was tested by WB. Surprisingly, most of the clones showed WT1 expression even without Dox treatment, raising the problem of dealing with a leaky system for the subsequent studies.

It is of crucial importance to address *in vivo* the relevance of the findings observed *in vitro* with the two inducible cell systems I established. Because of the leakiness of the pGoldiLox-Wt1 plasmids, I decided to design a smaller and simpler set of plasmids for the inducible and ubiquitous expression of single isoforms of WT1. In this chapter I will discuss the design and the testing of the CAG-Tet3G-TRE3G-Cherry plasmids, which are now currently used to derive wild type and *Wt1* knockout ES cells expressing inducible single isoforms of WT1.

Last, I will discuss the attempts to clone a plasmid designed for *in vivo* inducible and tissue specific expression of single isoforms of WT1, named pGoldiLoxS. The plasmid was made modifying the pGoldiLox construct: after the CAG promoter I added LoxP sites, which flank the prokaryotic and eukaryotic antibiotic resistance, a fluorescent reporter and a polyadenylation signal. Following recombination by an inducible CRE driven by a tissue specific promoter, the removal of the polyA signal would allow the transcription of the Tet-On 3G where and when desired. Furthermore, the activation of the Tet-On 3G could be finely tuned and timed using the Dox. The main problem I encountered was the transcription of the transactivator even in the absence of LoxP recombination. New strategies will be planned and adopted to solve this issue and build this potentially powerful system.

3.2 Cloning plasmids for the constitutive expression of WT1 single isoforms

In order to investigate the functions of single WT1 isoforms, I initially tried to establish stable cell lines constitutively expressing each of the four main isoforms of WT1. For this aim I chose to derive stable MDCK (Madin-Darby canine kidney) cells, as they are negative for WT1 and they are the cellular model of choice for EMT and MET studies [160]. The MDCK cells are epithelial cells derived from the distal tubule of a kidney of a normal adult female cocker spaniel. I also decided to fuse the isoforms to a FP in order to be able to easily trace WT1 expression and localization. WT1 was indeed cloned into the pAmCyan1-N1 vector at the C-terminus of the AmCyan1, a cyan tetrameric fluorescent protein of 25.5 KDa with excitation and emission maxima at 458 and 489 nm, respectively. Because the N-terminus of WT1 is loosely structured, the fusion of a fluorescent marker at the N-terminus is less likely to affect its function (Figure 3.1).

The coding sequences of *Wt1* single isoforms were cloned using the In-Fusion HD cloning technology into the pAmCyan1-N1 vector. The In-Fusion HD cloning kit allows directional and efficient cloning of one or multiple DNA fragments into a vector of choice,

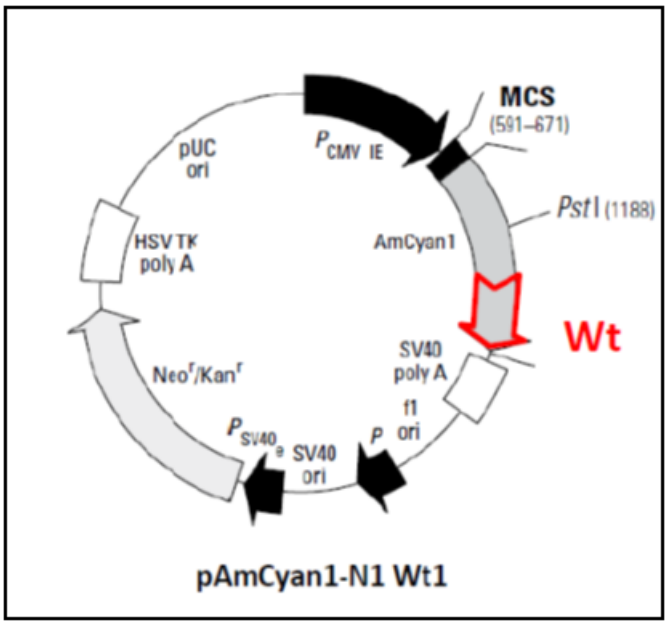

FIGURE 3.1: Diagram of pAmCyan1-N1 Wt1

thanks to the In-Fusion Enzyme that fuses PCR-generated sequences (inserts) and a linearised plasmid (backbone) by recognizing a 15 bp overlap at each end. The overlaps are engineered by designing primers for the amplification of the desired insert: the 5 end of each primer has to share 15 bp of homology with one end of the DNA fragment to which the sequence will be joined, the 3 end must contain a sequence specific for the amplification of the target insert. Because this cloning technology is based on the recombination of sequences generated by PCR, it facilitates the insertion of any desired sequences, for instance restriction enzyme sites, and the mutation of bases within the overlaps. All the cloning described in this chapter has been done using the In-Fusion technology. The sequences of the cDNA of the isoforms were amplified from the pcDNA3-EGFP-Wt1 plasmids available in the lab. The PCRs for all the cloning procedures described in this chapter were done using the high fidelity KOD Hot Start DNA Polymerase. Once I optimized the conditions for the amplification of the target sequences, the PCR products were purified. Meantime, the pAmCyan1-N1 vector was linearised with the restriction enzyme NotI and purified. I then set up the In-Fusion cloning reaction and transformed the Stellar Competent Cells, which are methyltransferase deficient chemically competent *E. coli* cells. The bacteria were grown in presence

of 50 μg/ml Kanamycin and the colonies were then PCR-screened for the insertion of Wt1 isoforms. As controls, I also cloned constructs in which the STOP codon of the AmCyan1 was not deleted, creating empty vectors (EV) of the same length of the pAmCyan1-N1-Wt1 plasmids. The main steps of the cloning procedure are shown in Figure 3.2.

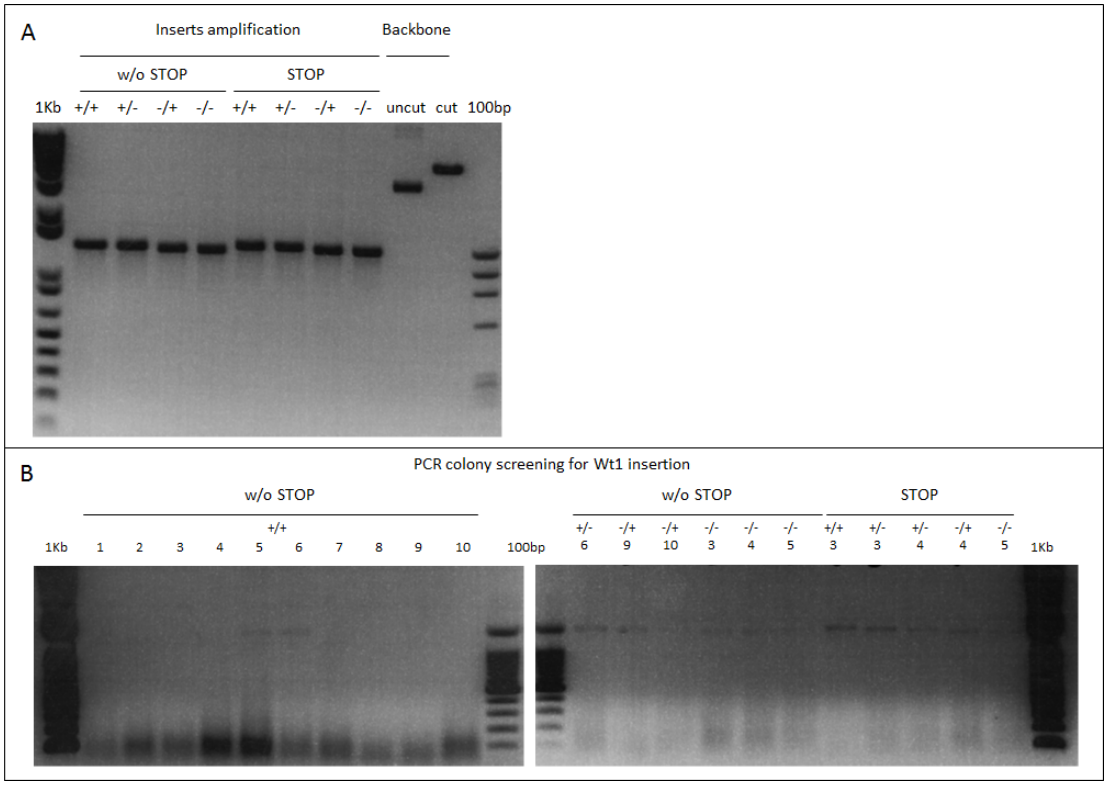

FIGURE 3.2: Step of the cloning of the pAmCyan1-N1 Wt1 plasmids. A: 1% TBE gel showing the products of the PCR amplification of the Wt1 isoforms without and with the STOP codon (inserts) and the linearization of the pAmCyan1-N1 vector (backbone). B: PCR colony screening of the plasmids to verify the insertion of Wt1 isoforms.

After the sequences of the plasmids were confirmed, the vectors were tested by transient transfection in MDCK cells. The cells transfected with 0.5 μg of the pAmCyan1-N1-Wt1 constructs seemed to show nuclear localization of the fluorescence, suggesting that the fusion of WT1 with the FP does not affect the normal localization of WT1. On the other hand, in the cells transfected with 0.5 μg of each control plasmid, the AmCyan1 signal seemed to be diffuse in the whole cell as expected (Figure 3.3). The cells were

then collected for total protein extraction and the expression of FP-WT1 was confirmed by WB.

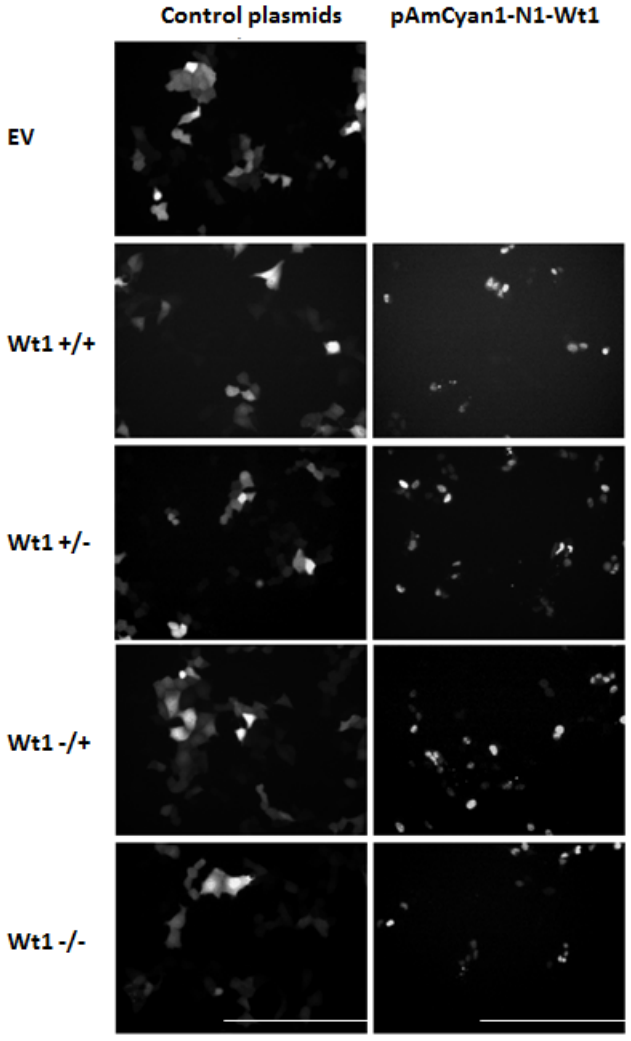

FIGURE 3.3: Transient transfection of the pAmCyan1-N1 Wt1 plasmids in MDCK cells. Images of the AmCyan1 signal in the cells transfected with the control plasmids (EV and with the STOP codon) and in the cells transfected with the plasmids that express WT1 single isforms. Scale bar = 500 μm.

In order to generate stable single clones for the expression of WT1 single isoforms, the MDCK cells were transfected with the Xfect Transfection Reagent using 1 μg of each of the pAmCyan1-N1-Wt1 linearised plasmids and selected for two weeks in 500 μg/ml G418. The pools of clones were then FACS sorted and single AmCyan1 positive cells were seeded in 96 well plates. After growing the cells for another two weeks, the single clones were analysed by WB and IF for WT1 expression. Surprisingly, none of the clones expressed WT1, suggesting the toxicity of AmCyan1-Wt1 over-expression and the lethality of the constitutive expression of those proteins. To overcome these problems I decided to establish an inducible system, which avoids the constitutive expression of the single isoforms and allows titratable and controlled levels of expression.

3.3 Creating a classic Tet-On inducible system for the inducible expression of WT1 single isoforms

The Tet-On 3G systems were developed for inducible gene expression in mammalian cells. They guarantee a tightly regulated expression of the transgene, which is reversible, quantitative and reproducible. The system is based on the constitutive expression of the Tet-On 3G transactivator in target cells that contain a gene of interest under the control of the pTRE3G promoter. Upon Dox treatment, the Tet-On 3G protein undergoes a conformational change becoming active and is able to bind to the tet operator sequences in the pTRE3G promoter. Thus, the cells will express high levels of the gene of interest only when cultured with Dox. In fact, the pTRE3G promoter is virtually silent in the absence of induction, as it lacks binding sites for any endogenous transcriptional factor. I generated two different Tet-On 3G inducible systems, creating one set in which WT1 single isoforms are tagged with the AmCyan1 reporter and one where the transgenes are fused to the mCherry gene. The mCherry is a red fluorophore with an excitation maximum at 587 nm and an emission maximum at 610 nm. While the AmCyan1 proteins form stable tetramers, the mCherry is a monomeric FP, which makes this fluorophore a more suitable fusion tag. Because WT1 proteins can dimerise [21, 161], I

chose to clone two different sets of plasmids in order to be potentially able to study the interaction between the same isoform or different ones, easily distinguishing the proteins thanks to the two fluorescent tags, whose spectra are well separated. I generated the response plasmid of the first system carrying WT1 fused to AmCyan1 by substituting the CMV promoter in the pAmCyan1-N1-Wt1 plasmids with the pTRE3G promoter. To remove the constitutive promoter, the pAmCyan1-N1-Wt1 constructs were digested with AseI and NheI, gel isolated and purified (Figure 3.4 A). The pTRE3G promoter was isolated cutting the pTRE3G-mCherry plasmid with XhoI and SalI in order to obtain a cleaner template for the PCR amplification. The primers for the cloning of the promoter were then tested at different annealing temperatures and the best condition was chosen for the gel isolation of the product (Figure 3.4 B). The obtained insert was cloned into the backbones to generate the pTRE3G-AmCyan1-(Wt1) plasmids. The colonies were screened by PCR to detect the incorporation of the pTRE3G promoter (Figure 3.4 C). The plasmid DNA was extracted from three colonies per plasmid and sequenced.

Since both the pTRE3G-AmCyan1-(Wt1) vectors and the regulator plasmid pCMV-Tet3G had a Kanamycin/Neomycin (Kan/Neo) resistance, I changed the resistance cassette of the pCMV-Tet3G plasmid with the Hygromycin gene. I removed the antibiotic resistance digesting the response vector with BstBI and BclI (Figure 3.5 A) and tested the best condition for the amplification of the Hygromycin gene from a Linear Hygromycin Marker (Figure 3.5 B). After cloning the gel isolated and purified fragment into the pCMV-Tet3G w/o Kan/Neo vector, Stellar Competent Cells were transformed and then screened for the presence of the new insert (Figure 3.5 C).

The second set of regulator and response plasmids was made by cloning in the pTRE3G-mCherry vector the four Wt1 isoforms fused to the mCherry reporter gene. In order to fuse Wt1 to the mCherry, I removed both the IRES2 sequence and the STOP codon of the reporter gene. The IRES, an internal ribosome entry site, allows the initiation of translation in the middle of an mRNA sequence, therefore creating two distinct proteins from the same mRNA. The IRES2 was removed by cutting the pTRE3G-mCherry

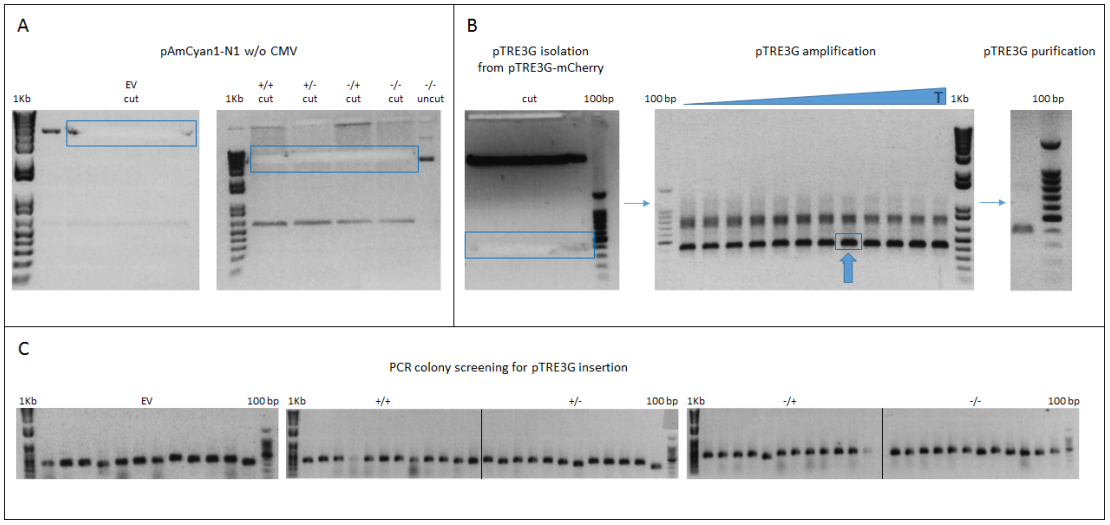

FIGURE 3.4: Cloning of the pTRE3G promoter in the pAmCyan1-N1 Wt1 plasmids. A: Removing the CMV promoter from the pAmCyan1N1 plasmids. The blue squares mark the bands cut and purified form the 1% agarose TBE gel. B: Steps to get the inserts encoding the pTRE3G promoter: the promoter was isolated from the pTRE3G-mCherry plasmid, then amplified using different temperature of annealing. The best condition and the specific band are highlighted by an arrow and a square, respectively. The band purified from the gel was run on a 2% TBE gel to confirm the purification of a single product. C: PCR colony screening to detect the plasmids that carry the pTRE3G promoter sequence.

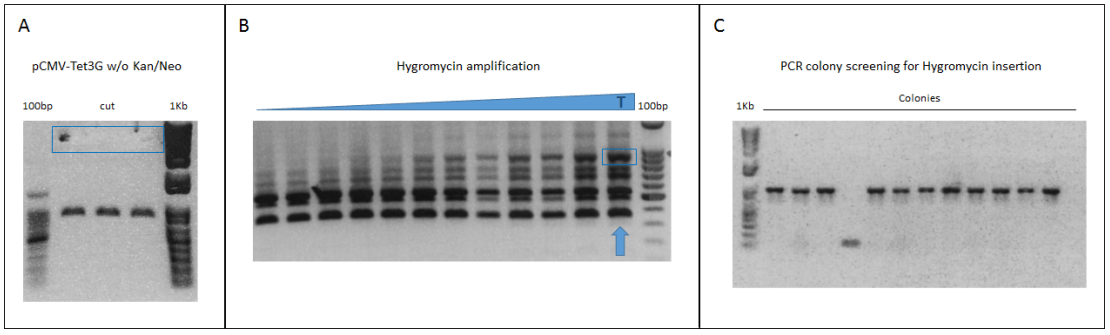

FIGURE 3.5: Cloning the Hygromycin resistance in the pCMV-Tet3G plasmid. A: Removing the Kan/Neo cassette from the pCMV-Tet3G plasmid. The cut and purified backbone is framed. B: PCR amplification of the Hygromycin sequence using a gradient of annealing temperatures. The specific amplicon is framed and the best PCR condition is marked by an arrow. C: Screening of the plasmids by PCR to detect the presence of the Hygromycin sequence. All plasmids, but the forth, are positive.

plasmid with EagI and EcoRV (Figure 3.6 A). The new backbone was gel extracted and cloned with the inserts. The isoforms were amplified from the pAmCyan1-N1 Wt1 plasmids and the PCR products were gel isolated and purified (Figure3.6 B). The transformed bacteria colonies were then checked first by PCR and then by enzymatic digestion for the successful incorporation of Wt1 in the plasmid (Figure 3.6 C). The positive colonies were then sent for sequencing.

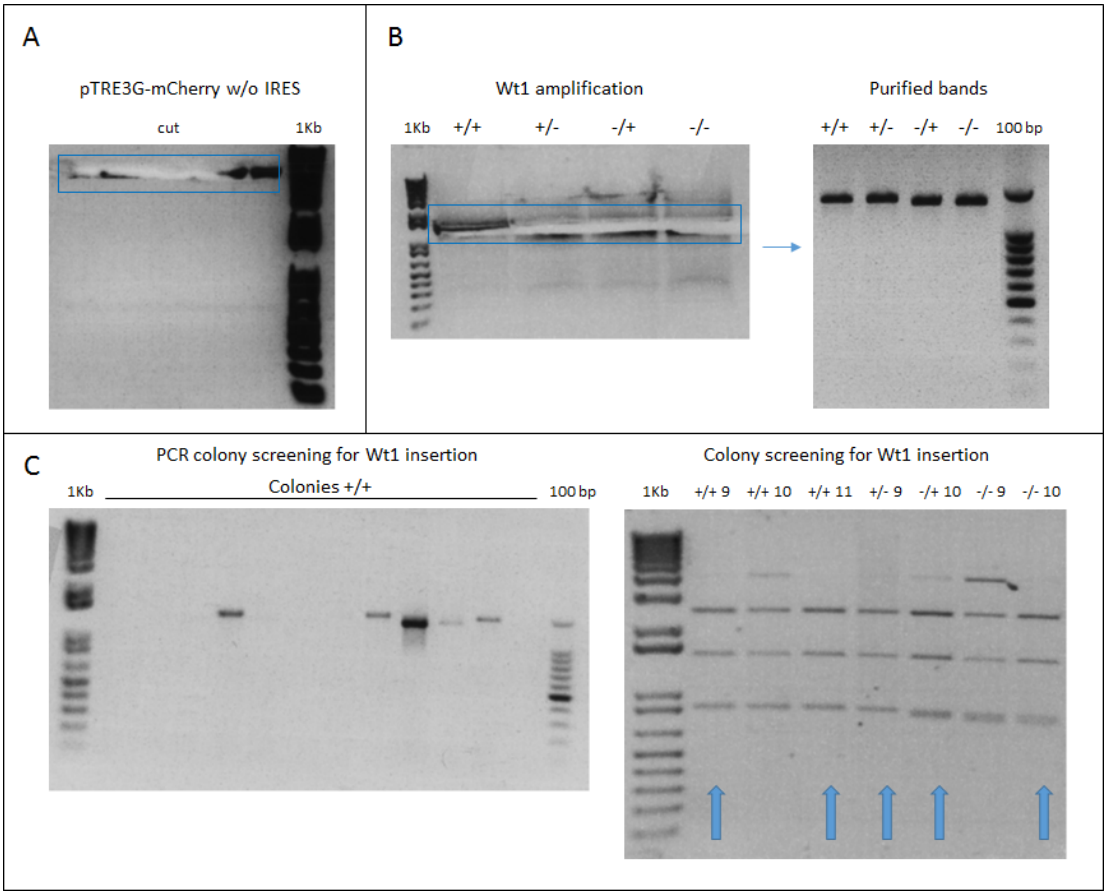

FIGURE 3.6: Cloning Wt1 single isoforms in the pTRE3G-mCherry plasmid. A: Isolation of the pTRE3G-mCherry without the IRES2 sequence (backbone). B: Gel extraction of the PCR amplified Wt1 single isoforms and resulting purified inserts run on a 1% agarose TBE gel. C: Screening to select the plasmids with the inserts: on the left hand side, example of PCR screening of the colonies transformed with pTRE3G-mCherry-Wt1 +/+; on the right hand side: 1% agarose TBE gel resolving the products of the digestion with NcoI, PvuI and BamHI. The plasmids showing the right pattern of bands are marked by an arrow.

Diagrams of the final constructs are shown in 3.7.

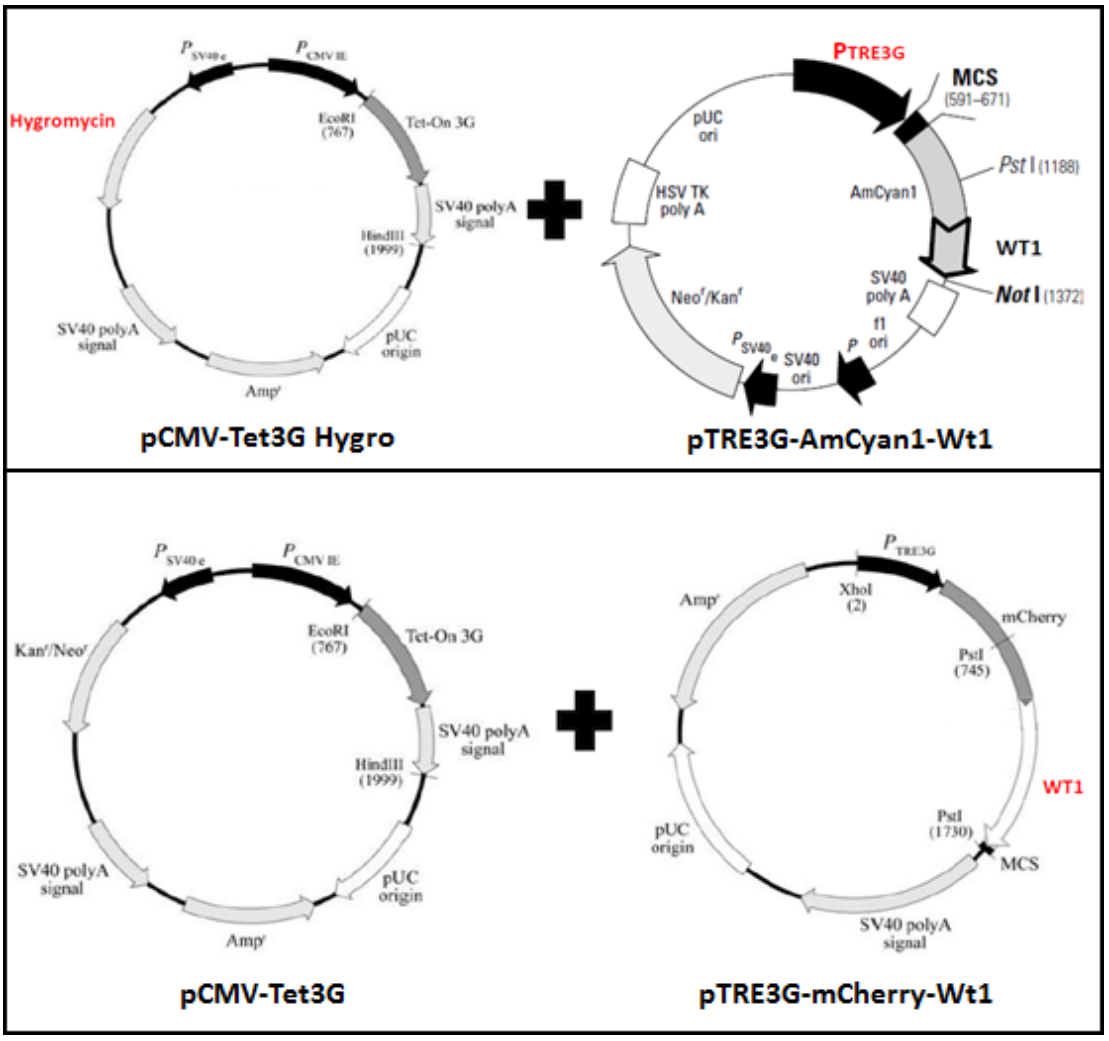

FIGURE 3.7: Diagrams of the plasmids for a classic Tet-On inducible system. The cloned sequences are highlighted in red.

The plasmids were tested by transient co-transfection in the MDCK cell line. After 24h from induction with 0.5 μg/ml of Dox, the expression of FP-WT1 was checked by both IF and WB. I also tested whether the induction was reversible by removing the Dox after 24h and growing the cells in Dox-free medium for another 24h (Figure 3.8). I confirmed that the system worked as expected: there was co-localization between WT1 and the FP, no induction without Dox and the expression was reversible. However, the main disadvantage of the classic Tet-On inducible system is the need of performing two steps of establishment of stable cell line, as the cells have to be firstly stably transfected with the regulator plasmid and secondly with the response vector. Therefore, in order to

get a more efficient system to derive stable clones, I cloned single vectors that combined the properties of both the regulator and the response plasmid.

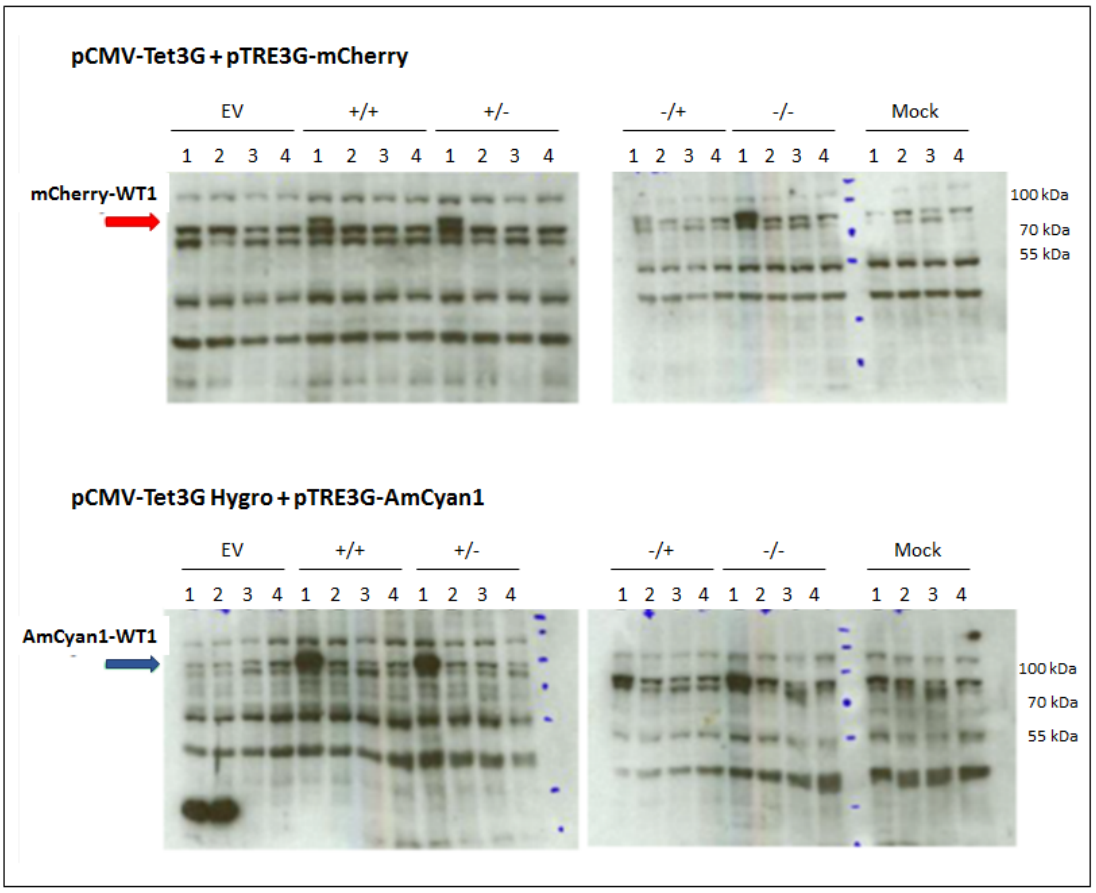

FIGURE 3.8: WB: WT1 expression in MDCK cells transiently transfected with 0.5 μg of pCMV-Tet3G and pTRE3G-FP-Wt1 plasmids. 1 = Extract of cells induced for 24h; 2 = Proteins of cells in which WT1 expression was induced for 24h and then Dox was removed for 24h; 3 = Cells without Dox induction at 24h; 4 = Cells without Dox induction at 48h. The membrane was blotted with the C19 antibody against WT1.

3.4 Establishment of the first cell model for inducible expression of WT1 single isoforms

3.4.1 Generating single vectors to induce the expression of single isoforms of WT1

Aiming to get a fast and easy system to establish cell lines expressing inducible single isoforms of WT1, I designed constructs that express the transactivator Tet-On 3G and the gene of interest under the control of the Dox inducible promoter. The vectors offer additional advantages: besides guaranteeing a titratable, reversible, traceable expression of WT1, they are easy to modify and WT1 is tagged to facilitate imaging and biochemical analysis. I cloned two vectors in which WT1 is fused to a FP, mCherry and AmCyan1 respectively, and one without tag to control that WT1 is not affected by the presence of a fused protein and to assess whether the expression of FP-WT1 is actually toxic for the cells. The vectors are called pSV40-Tet3G-TRE3G-mCherry, pSV40-Tet3G-TRE3G-AmCyan1 and pSV40-Tet3G-TRE3G respectively. I started with the generation of the pSV40-Tet3G-TRE3G-mCherry plasmid, whose cloning strategy is summarized in the diagram in Figure 3.9.

First, I linearised the pTRE3G mCherry-Wt1 and EV with XhoI in order to insert the SV40 promoter together with the resistance cassette for Kan/Neo, which were amplified from the pCMV-Tet3G plasmid (Figure 3.10). After the cloning reaction, the transformed cells were grown in the presence of 50 μg/ml Kanamycin to select for the colonies carrying the plasmids with the new resistance cassette.

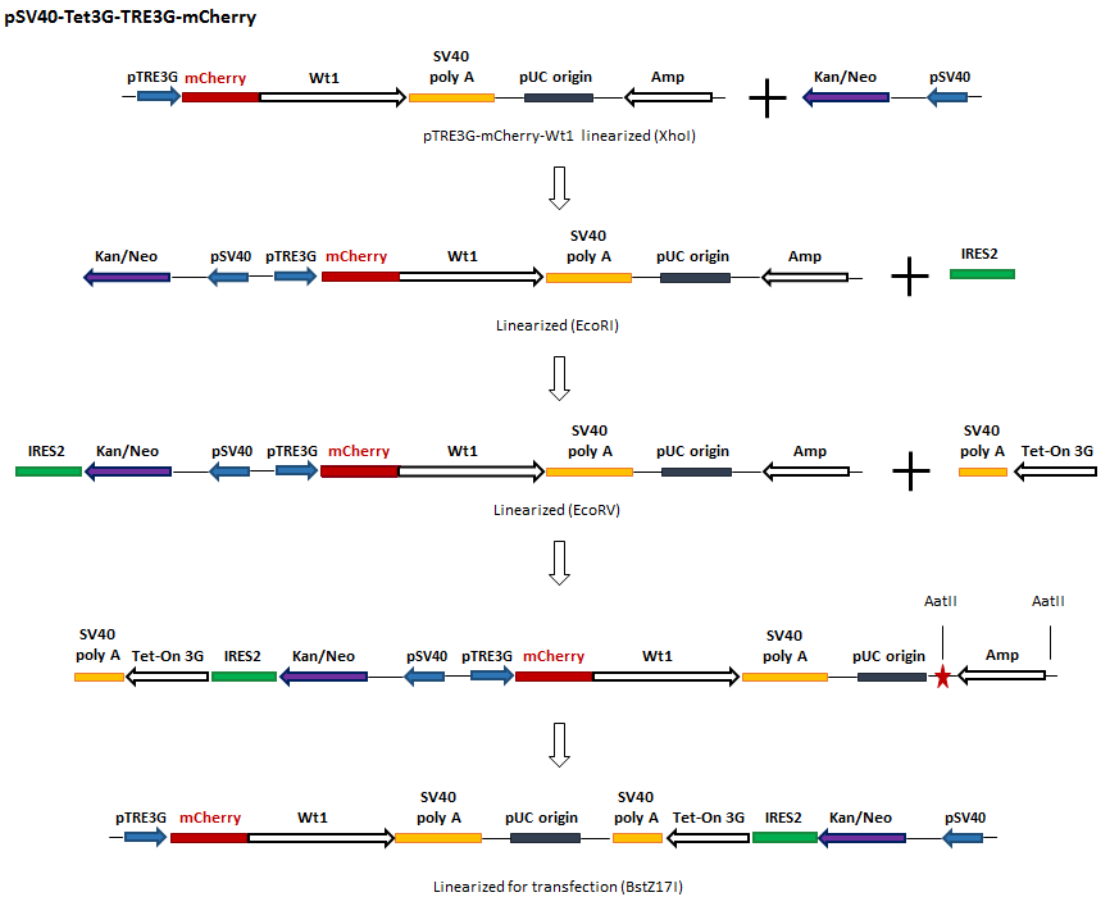

FIGURE 3.9: Schematic representation of the steps for the cloning of the pSV40-Tet3G-TRE3G-mCherry plasmids. The star represents the site of mutagenesis.

In order to place also the TetOn 3G coding sequence under the control of the SV40 promoter, I decided to insert an IRES2 sequence to create a polycistronic mRNA. Thus, the plasmid was linearised with EcoRI, which cuts after the Kan/Neo resistance gene, and the reverse-complement of the IRES2 sequence was amplified using the pTRE3G-mCherry vector as a template (Figure 3.11 A). Following the In-Fusion reaction and transformation, the colonies were screened by digestion with EcoRV, which would have cut only the plasmids with the insert (Figure 3.11 B). The positive plasmids were then linearised with EcoRV to add the reverse-complement of the TetOn 3G sequence, followed by the SV40 polyA signal to stop the transcription under the control of the

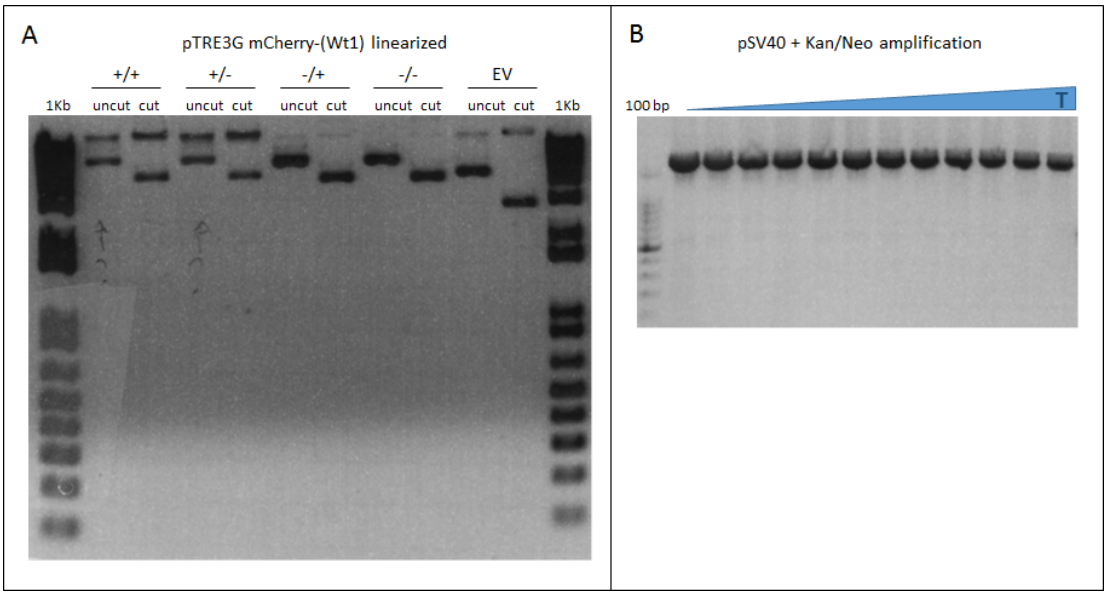

FIGURE 3.10: Cloning the pSV40-Tet3G-pTRE3G-mCherry plasmids. A: Linearization of the pTRE3G-mCherry-(Wt1) plasmids. B: Amplification of the pSV40-Kan/Neo insert using a gradient of annealing temperatures.

constitutive promoter. The insert was amplified from the pCMV-Tet3G vector (Figure 3.11 C and D). The bacterial colonies transformed with the cloning reaction were then screened by PCR to verify the insertion (Figure 3.11 E).

Because the Kan/Neo resistance works both in prokaryotic and eukaryotic cells, I decided to remove the Ampicillin cassette from the constructs. This also created shorter plasmids, removing about 1 kb from the sequence. As there were no appropriate restriction sites to remove the resistance cassette, I mutated two bp at the 5 end of the coding sequence to get a cutting site for the AatII enzyme, which had another site just after the end of the Ampicillin sequence. The plasmids were mutated with the QuikChange Lightning Site-directed mutagenesis kit. The kit uses two oligonucleotide primers containing the desired mutation that are annealed and extended during temperature cycling by the PfuUltra HF DNA polymerase, creating a mutated plasmid. The product of the mutagenic reaction is then digested with DpnI that digests specifically the parental methylated and hemimethylated DNA template. Because for the cloning I transformed a methyltransferase deficient strain of E.coli, before the mutagenesis I transformed the plasmids in a dam$^+$ strain. The mutated molecules were then

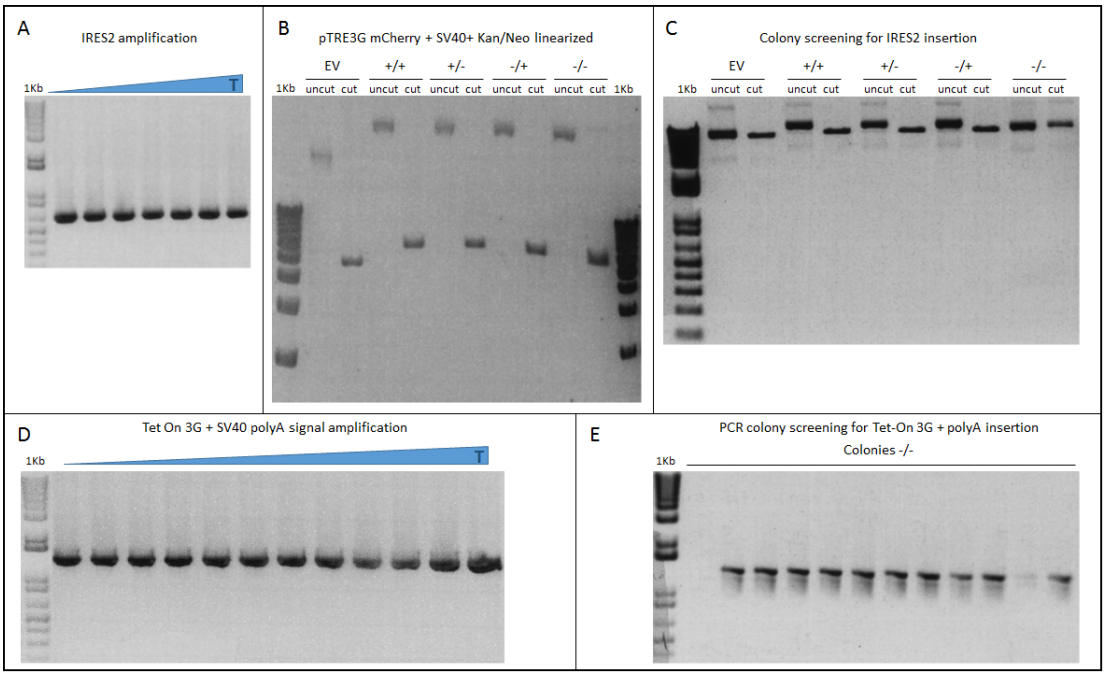

FIGURE 3.11: Cloning the pSV40-Tet3G-pTRE3G-mCherry plasmids. A: PCR gradient to amplify the IRES2 sequence. B: Linearised backbone to add the IRES2. C: Enzymatic colony screening by EcoRV digestion for the integration of the IRES2. The -/- plasmid did not show the insertion, thus different ones was screened to find a positive construct. The linearised plasmids are used as backbones for the cloning of TetOn 3G and SV40 polyA signal. D: PCR gradient to get the TetON 3G-SV40 insert. E: Example of PCR screening of the colonies transformed with the -/- construct to verify the insertion of the TetOn 3G-Sv40 polyA sequence. All plasmids are positive, but the first one.

transformed into XL10-Gold ultracompetent cells and the colonies were screened by cutting with AatII. When the plasmids were positive for the mutation, the digestion created two fragments: one of 8 kb and another one of 1 kb, corresponding to the cut out Ampicillin. I isolated from the gel the 8 kb bands, which had sticky ends that were then ligated with the T4 DNA ligase (Figure 3.12). To select the colonies transformed with the correct plasmids, I initially grew the bacteria in agar containing Kanamycin, then half of the colonies was grown in Ampicillin. The plasmid DNA of the colonies that died when cultured with Ampicillin was extracted and sequenced.

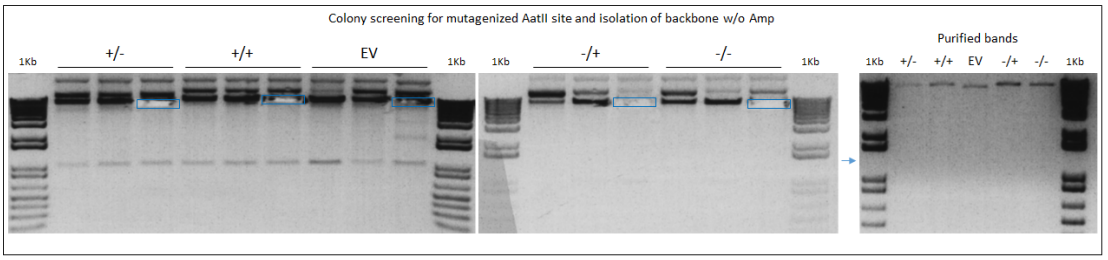

FIGURE 3.12: Cloning the pSV40-Tet3G-pTRE3G-mCherry plasmids: creating the AatII site to cut the Ampicillin sequence.Three plasmids per construct were screened for the mutagenesis of the AatII site. After digestion with AatII, the 8 kb bands were isolated and purified from one plasmid each (framed by the squares). The two bigger bands are probably due to the incomplete digestion of the plasmid. The purification of the linear and mutagenized vectors was confirmed running the plasmid DNAs on a 1% agarose TBE gel.

To clone the pSV40-Tet3G-TRE3G-AmCyan1 vectors, I cut from the pSV40-Tet3G-TRE3G-mCherry-Wt1 plasmids the mCherry-Wt1 and from the EV the mCherry, using SalI and MluI restriction enzymes. The bands corresponding to the new backbones were extracted from the gel and purified. The AmCyan1-Wt1 and the AmCyan1 sequences were amplified using for templates the pTRE3G-AmCyan1-(Wt1) plasmids. The In-Fusion reaction was then transformed into Stellar Competent Cells and the presence of the inserts in the colonies was checked by PCR (Figure 3.13). The plasmid DNAs of the colonies showing amplification were sent for sequencing.

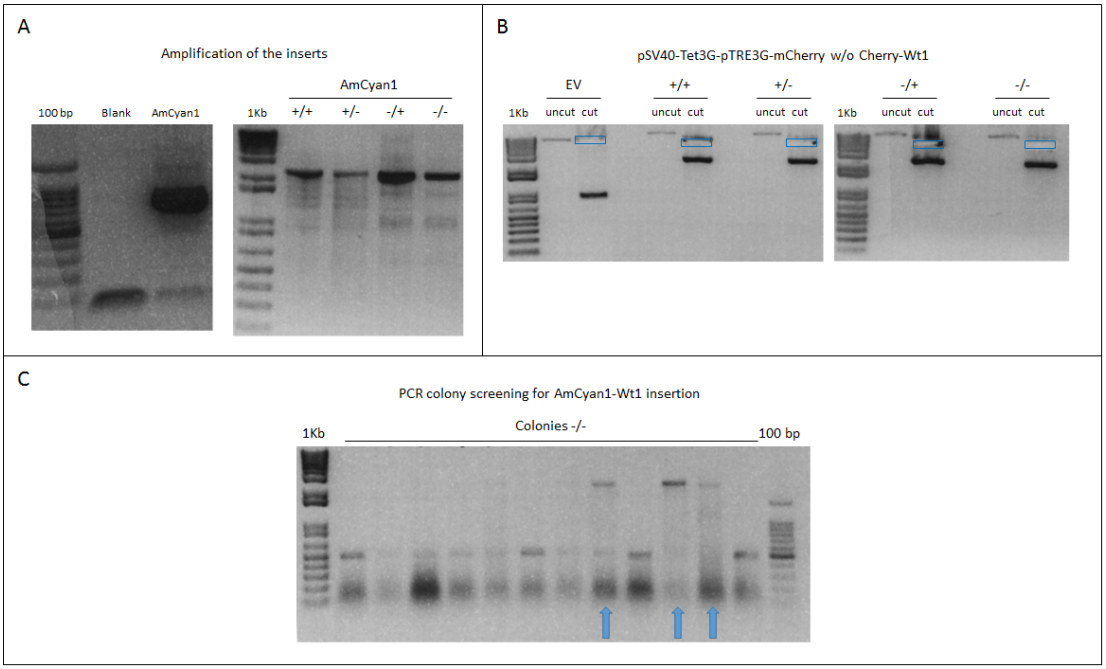

FIGURE 3.13: Cloning the pSV40-Tet3G-pTRE3G-AmCyan1 plasmids.A: PCR amplification of AmCyan1 and AmCyan1 fused to Wt1 isoforms. B: Creating the backbones by removal of mCherry-(Wt1) sequences. The gel isolated bands are indicated by blue squares. C: Example of PRC screening for AmCyan-(Wt1) integration in the AmCyan1-Wt1 -/- plasmids.

Last, I generated the plasmids that do not contain a FP fused to the single isoforms of WT1. I started removing the mCherry from the pSV40-Tet3G-TRE3G-mCherry-(Wt1) plasmids digesting with SalI and BsrGI, then I isolated the bands corresponding to the plasmids lacking the reporter gene, finally I created blunt ends with the T4 DNA polymerase and ligated by T4 DNA ligase (Figure 3.14 A). I screened the colonies double digesting the plasmid DNAs with SalI, that was not supposed to cut, and MluI, single cutter in the vector sequences (Figure 3.14 B). The correct sequence was confirmed in one plasmid for each isoform and EV.

After confirming the sequences of the constructs, all the plasmids were tested in transient transfection in the MDCK cell lines. The cells were induced with 0.5 μg/ml of Dox and after 24h the expression and localization of WT1 was detected by IF. As expected, the induced cells showed nuclear WT1, which co-localized with the FP signal in the cells transfected with the mCherry or AmCyan1 constructs. The mCherry and

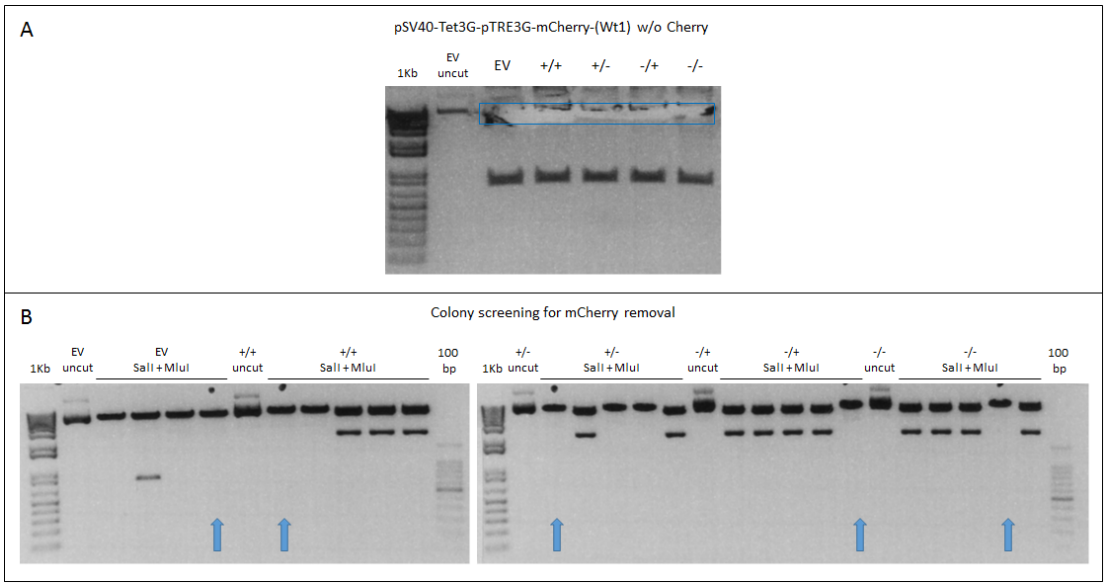

FIGURE 3.14: Cloning the pSV40-Tet3G-pTRE3G plasmids. A: Gel purification of the backbones without the mCherry gene. The cut bands are framed in the blue square. B: Screening of the plasmids that do not contain the mCherry sequence. The plasmid DNAs that were positive and sequenced are pointed out by the arrows.

AmCyan1 EV vectors instead gave a FP signal diffused in the whole cell. Moreover, there was not expression of (FP)-WT1 without induction, indicating that the SV40 promoter does not leak. Examples of the IF in the transient transfected MDCK cells with two mCherry constructs are shown in Figure 3.15.

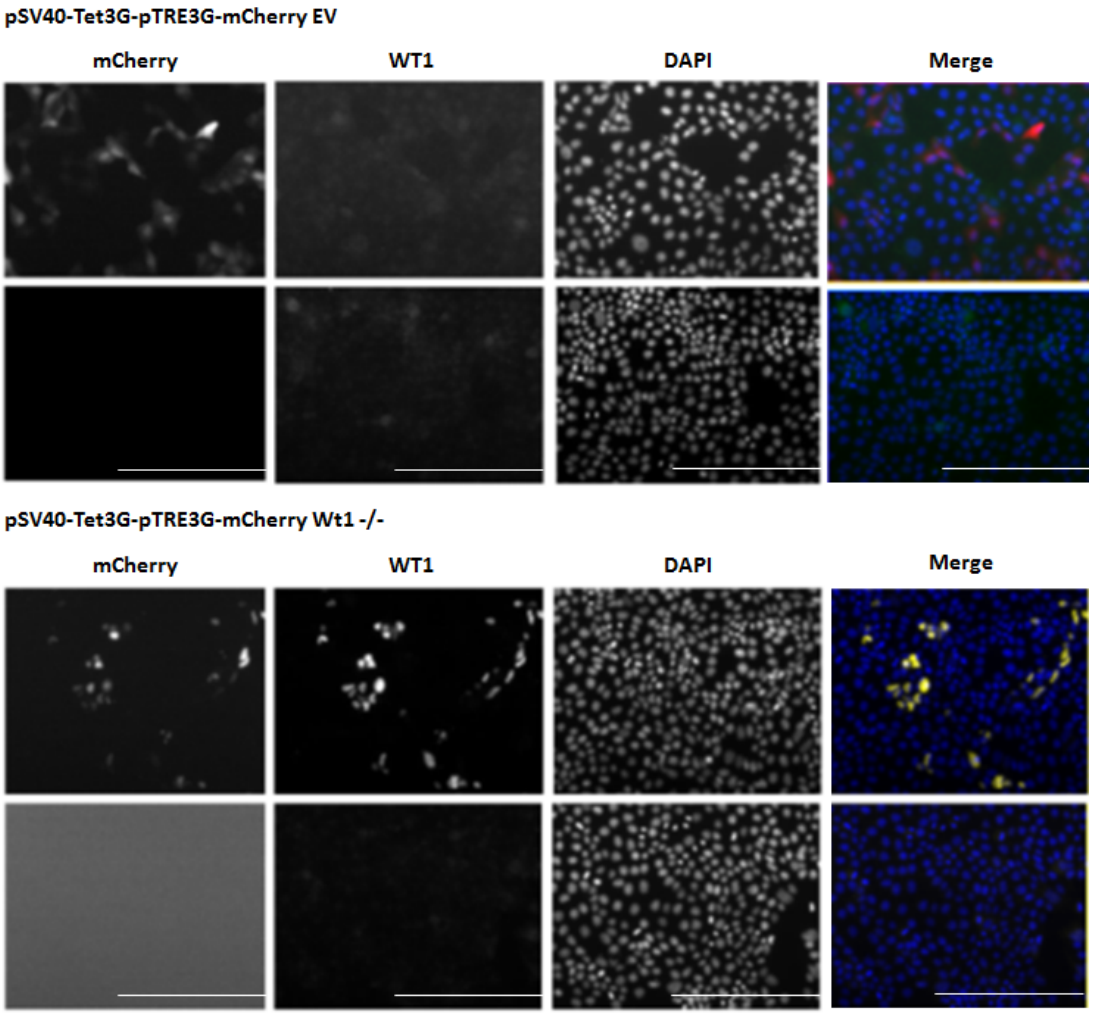

FIGURE 3.15: IF on transient transfected MDCK cells with pSV40-Tet3G-pTRE3G-mCherry EV and pSV40-Tet3G-pTRE3G-mCherry Wt1 -/- (0.5 μg per well). The IF was performed on 24h induced and non induced cells. From the left hand side: mCherry signal, WT1 (detected by the C19 antibody), DAPI staining and merge of the three signals. Scale bar = 500 μm.

3.4.2 Establishment of stable MDCK cells expressing inducible single isoforms of WT1 and characterization of WT1 levels of expression in the single clones

I decided to derive single clones stably transfected with each of the pSV40-Tet3G-TRE3G-(FP)-Wt1 plasmids. For this purpose I chose the MDCK cell line, because it is a well-known in vitro model to study the EMT and MET processes, in which WT1 plays a crucial role. The MDCK cells are kidney epithelial cells, which can easily transit to a mesenchymal phenotype if treated with factors as TGFβ [160]. To establish stable cell lines, the MDCK cells were transfected by Lipofectamine with 1 μg of each BstZ17I linearised plasmid and selected for two weeks in 500 μg/ml of G418. The pools of clones transfected with the mCherry and AmCyan1 constructs were induced overnight (O/N) with 0.5 μg/ml Dox, single fluorescent cells were then sorted by FACS, seeded in single wells of 96 well plates and grown in Dox-free medium for another two weeks. Instead, for the cells transfected with the vectors without the FP, I picked manually single clones and grew them in 96 well plates. I then analysed WT1 expression in each clone after 24h induction with 1 μg/ml Dox by IF and WB. I was able to derive at least two positive clones for each construct; examples are shown in Figure 3.16. As expected, the clones did not express WT1 in the absence of Dox and the FP signal co-localizes with WT1 expression.

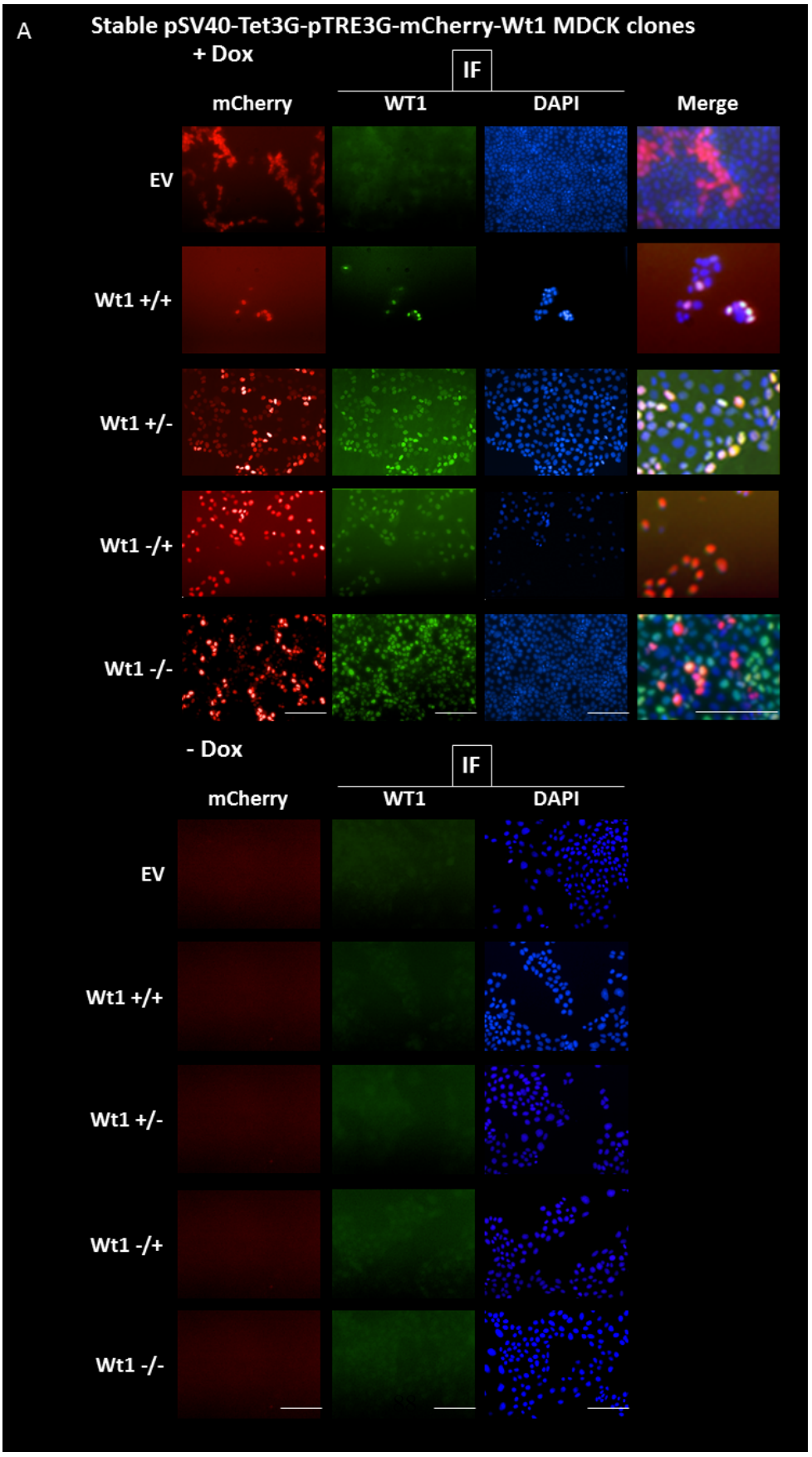
A
Stable pSV40-Tet3G-pTRE3G-mCherry-Wt1 MDCK clones
+ Dox
IF
mCherry
WT1
DAPI
Merge
EV
Wt1 +/+
Wt1 +/-
Wt1 -/+
Wt1 -/-
- Dox
IF
mCherry
WT1
DAPI
EV
Wt1 +/+
Wt1 +/-
Wt1 -/+
Wt1 -/-

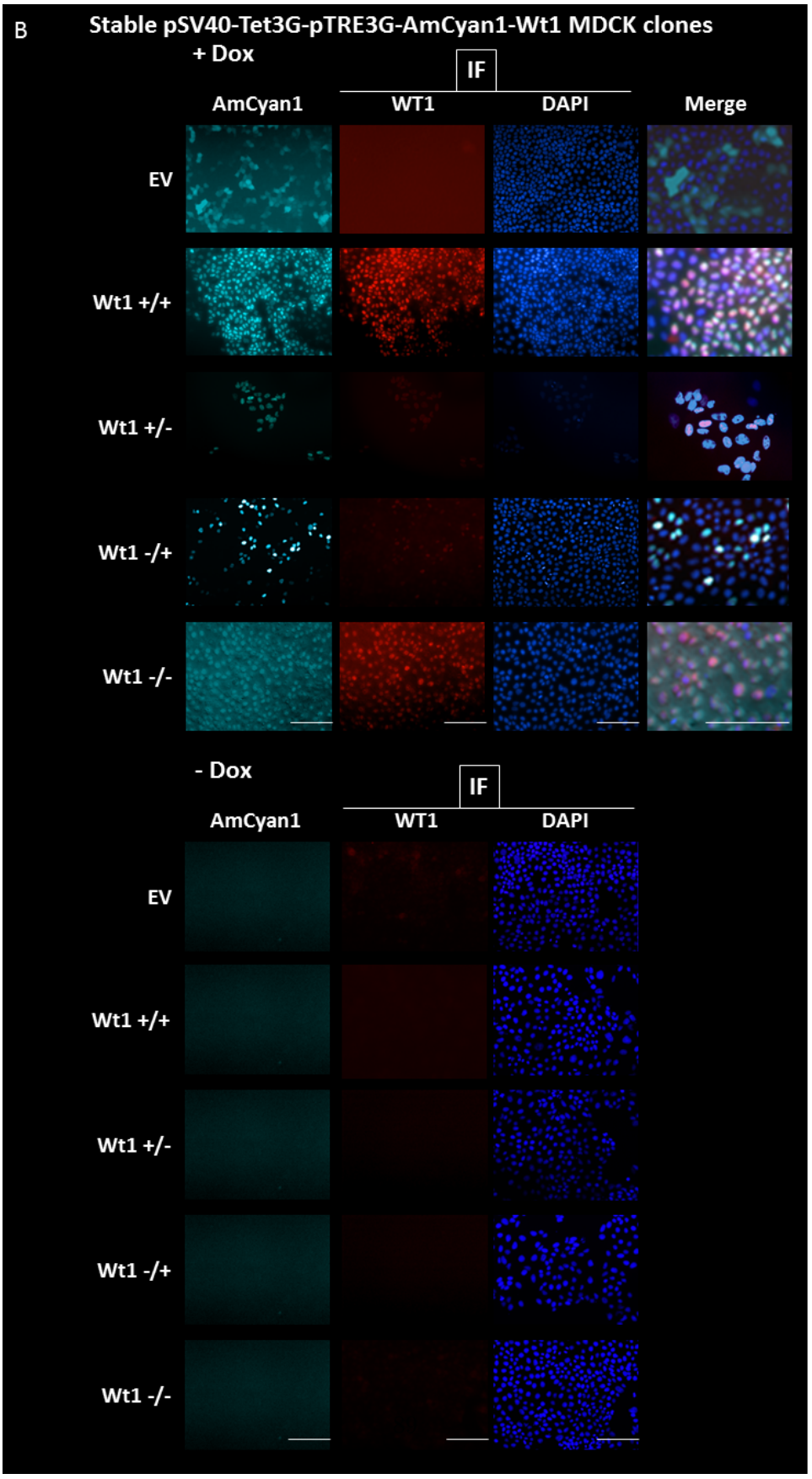
B
Stable pSV40-Tet3G-pTRE3G-AmCyan1-Wt1 MDCK clones
+ Dox
IF
AmCyan1
WT1
DAPI
Merge
EV
Wt1 +/+
Wt1 +/-
Wt1 -/+
Wt1 -/-
- Dox
IF
AmCyan1
WT1
DAPI
EV
Wt1 +/+
Wt1 +/-
Wt1 -/+
Wt1 -/-

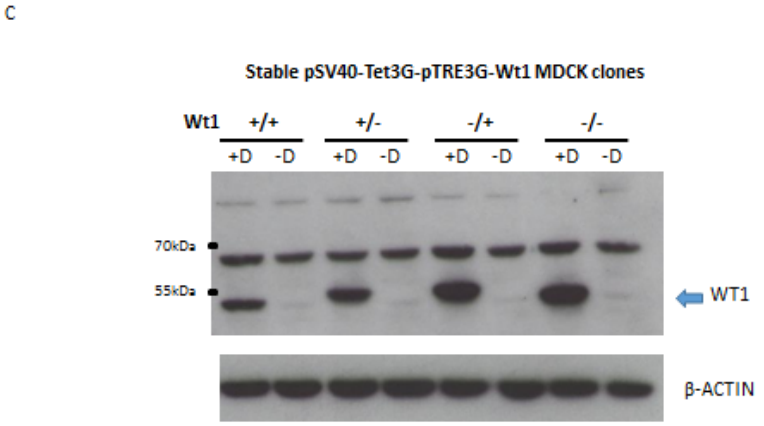

FIGURE 3.16: MDCK stable clones. A: IF: examples of stable mCherry-(WT1) MDCK clones induced with 1 μg/ml Dox and non-induced. Scale bar = 500 μm. B: IF: representative stable AmCyan1-(WT1) MDCK clones induced with 1 μg/ml of Dox and non-induced. Scale bar = 500 μm. In A and B starting from the left hand side: mCherry or AmCyan1 FP signal, WT1 expression, DAPI fluorescence and merge of the three signals. C: WB: WT1 expression in induced and non-induced MDCK clones stably transfected with the w/o FP constructs. The arrow indicates the specific molecular weight of WT1 proteins. Antibody used for WT1 detection: C19.

However, the clones showed different levels of WT1 expression, probably due to the heterogeneous integration sites and the uncontrolled copy number of plasmids that integrated. In order to test whether it was possible to balance the levels of WT1 expression among the clones, I tried to equalize the expression levels in two cherry clones per isoform. I decided to balance their levels using as reference WT1 expression in the AmCyan1 +/- 1 clone, as it expresses an amount of WT1 comparable with the endogenous WT1 in the M15 cell line. To address the issue, I treated the cells with 0, 0.25, 0.5, 1 and 2 μg/ml of Dox. After an O/N induction, I collected total proteins and detected by WB the levels of WT1 (Figure 3.17).

I concluded that the protein levels were titratable and that 0.25 μg/ml of Dox was enough to induce the expression in all the clones. I then quantified by ImageJ the intensity of the bands, I normalised them with the levels of the Actin and I defined the concentrations of Dox to use in order to theoretically balance the levels of expression (Table 3.1).

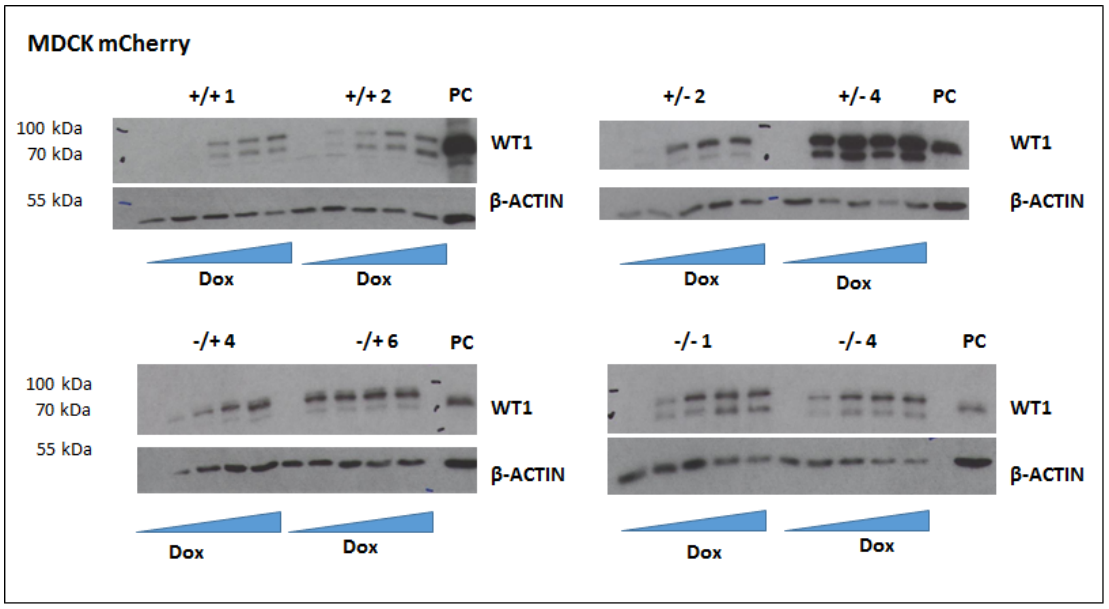

FIGURE 3.17: WB: WT1 expression in two mCherry MDCK clones per isoform after induction with increasing concentrations of Dox. PC = positive control: WT1 expression in the AmCyan1 +/- 1 clone. WT1 was detected with the C19 antibody.

TABLE 3.1: Dox concentrations used to induced the mCherry MDCK clones

Clone	**Dox (μg/ml)**
+/+ 1	7.7
+/+ 2	6
+/- 2	1
+/- 4	0.25
-/+ 4	1
-/+ 6	1
-/- 1	0.25
-/- 4	0.25

An example of quantification and determination of the concentration of Dox is shown in Figure 3.18.

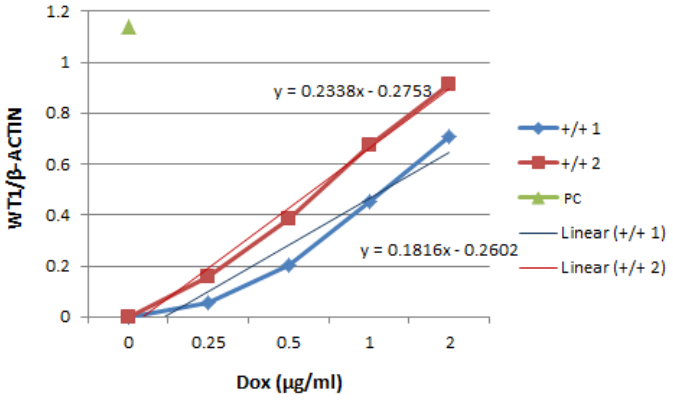

FIGURE 3.18: Relative quantification of WT1 +/+ protein expression in two mCherry clones induced with increasing amounts of Dox. The intensity of WT1 signal was normalized over the Actin and plot in a graph to calculate the interpolation lines. The equations of the lines were then used to derive the concentration of Dox required to reach the PC levels (AmCyan1 +/- 1 clone).

3.5 Second cell model to induce single isoforms of WT1

3.5.1 Cloning the pGoldiLox plasmids

The pGoldiLox constructs were designed and cloned to overcome some of the issues encountered with the pSV40-Tet3G-TRE3G-(FP) vectors. Particularly, I regarded of primary importance having plasmids that ensured a targeted integration of the transgenes and that allowed the inducible expression of WT1 also in embryonic stem cells (ES). In fact, when I tried to stably transfect ES cells with the pSV40-Tet3G-TRE3G-mCherry-Wt1 constructs, I failed to get inducible clones, most likely because of the silencing of the SV40 promoter. The pGoldiLox plasmid has several advantages compared with the previous constructs:

- It contains ROSA26 homology arms that allow the targeting of the plasmid into the ROSA26 locus, guaranteeing a uniform expression of the transgene.

- I exchanged the SV40 promoter with the CAG promoter, which has the best activity over other promoters when integrated in the ROSA26 locus [162] and it is less subjected to silencing in ES cells [163].
- Especially because the *Wt1* KO ES cells are Neomycin resistant, I substituted the Kan/Neo resistance with the less commonly used Zeocin to avoid co-transfection with other resistance markers.
- I cloned under the control of the CAG promoter the EGFP coding sequence that is thus constitutively expressed for an easy selection of the positive clones.
- To create polycistronic expression, I used either a minimal IRES, called PS3 [164], or the self-cleaving T2A peptide, which ensures a stoichiometric expression of the proteins flanking the peptide [165].
- Thanks to Cre-Lox recombination, it is possible to remove the bacterial EM7 promoter, the Zeocin and the EGFP sequences. This way there will not be overlapping FP signals under induction, the integrated piece of DNA will be shorter and I will not add any other drug resistance gene especially into ES cells. The absence of EGFP signal can be used to select the recombination events.

The steps of the cloning to build the pGoldiLox plasmids are represented and summarised in Figure 3.19

In order to eliminate from the pSV40-Tet3G-TRE3G-mCherry EV plasmid the SV40 promoter, the Kan/Neo resistance gene and the IRES2 sequences, I had to create a new restriction site to cut between the IRES2 and the TetOn 3G. I therefore decided to mutate two bp to create a second cutting site for the enzyme BglII. The mutagenesis of the plasmid was carried on with the QuikChange Lightning Site-directed mutagenesis kit and the success of the process was confirmed cutting different transformed colonies with BglII. The enzyme cut between the IRES2 and the TetOn 3G sequences, as well as between the SV40 and the Kan/Neo cassette, therefore giving rise to two bands in the successfully mutated vectors (Figure 3.20).

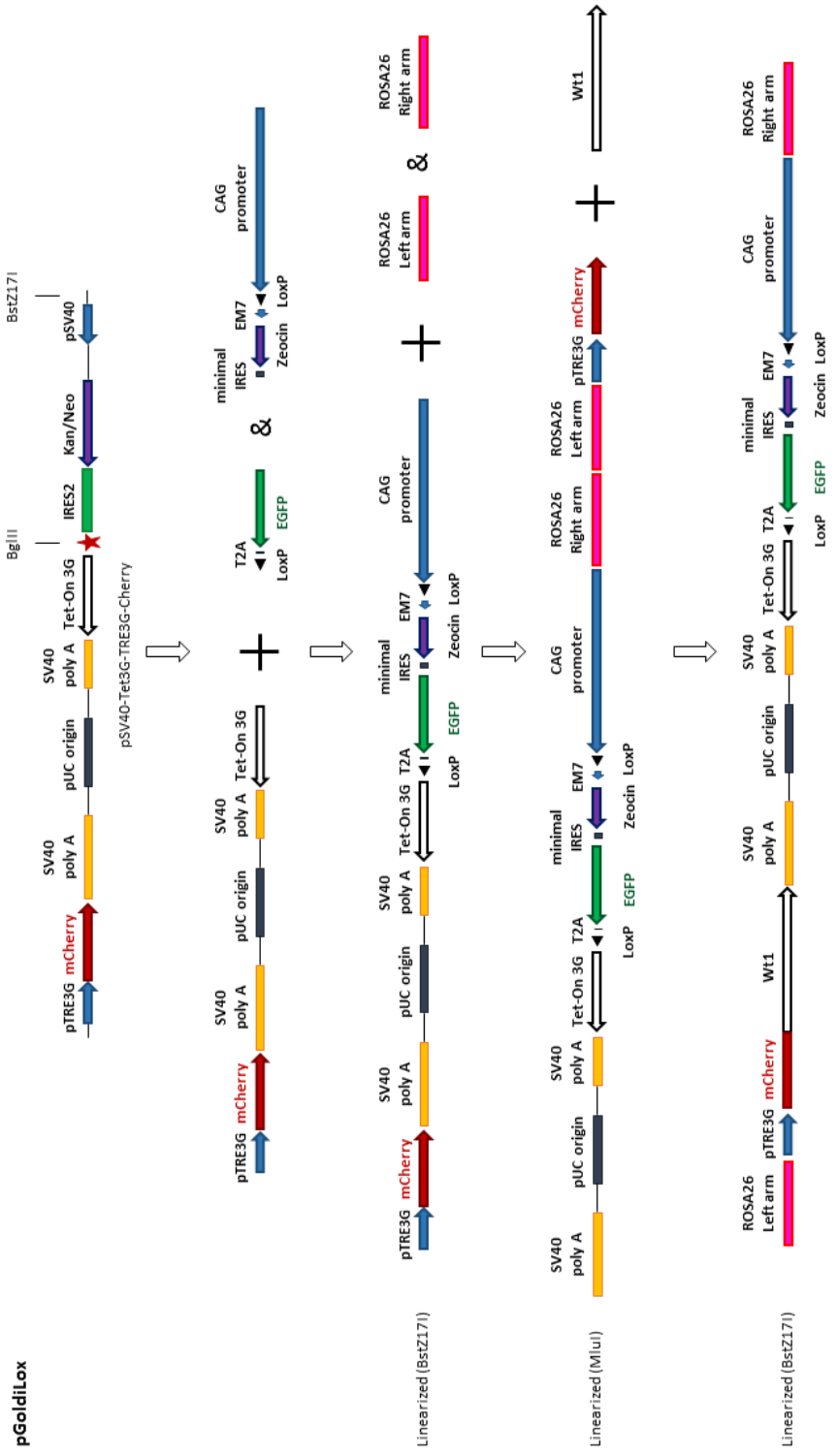

FIGURE 3.19: Diagram of the steps for the cloning of the pGoldiLox plasmids. The star represents the mutagenised site.

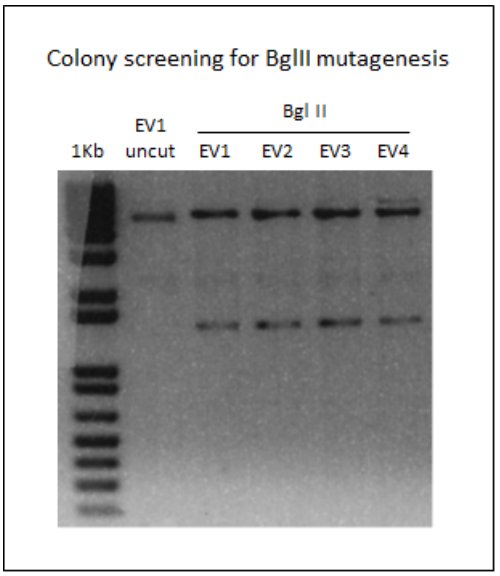

FIGURE 3.20: Cloning the pGoldiLox plasmids: screening for the mutagenized pSV40-Tet3G-TRE3G-mCherry EV plasmids. All the vector seem carrying the mutagenised site.

One of the mutated plasmid was then cut with BglII and Bstz17I to isolate the new backbone without the viral promoter, the resistance and the IRES2. Initially, I tried to "In-Fuse" the backbone and single short inserts: namely the CAG promoter, the first LoxP site, the EM7 promoter, the Zeocin cassette, the minimal IRES, the EGFP, the T2A and the second LoxP (Figure 3.21 A). However, no correct plasmids were obtained with this strategy. Therefore, I decided to create two inserts: one containing the minimal IRES, the resistance gene, the bacterial promoter, the second LoxP site and the CAG promoter; the second carrying the sequences for the first LoxP site, the T2A and the EGFP. To do that, I took advantage of the overlaps at each end of the single PCR products. At first, I tried to fuse by the In-Fusion Enzyme the components of the first insert. The In-Fusion reaction was then amplified by KOD Hot Start DNA Polymerase, using as forward primer the one used to amplify the minimal IRES and as reverse the one used for the amplification of the CAG. To get the right amplicon, the PCR reaction was performed at different annealing temperatures and the in presence or absence of 5% DMSO, which lowers the melting temperature and enhances the amplification of CG rich templates as the CAG promoter. The PCR

products were resolved on a 1% agarose gel that showed the presence of a band at the desired size when the templates were amplified using low annealing temperature and adding DMSO. The assay also showed that there was no band of the expected size in the In-Fusion reaction, letting me think that the fusion of the small inserts was indeed reached by PCR amplification and not by the In-Fusion reaction. Thus, I generated the second inserts using as template the EGFP, which was amplified initially with the forward primer coding for the first half of the LoxP-T2A sequence and the reverse primer specific for the EGFP; the PCR product obtained was then amplified with the forward primer carrying the sequence of the second half of the LoxP-T2A and with the reverse primer previously used. The amplicons were run on a 2% agarose gel and the band at the right size was cut and purified from the gel (Figure 3.21).

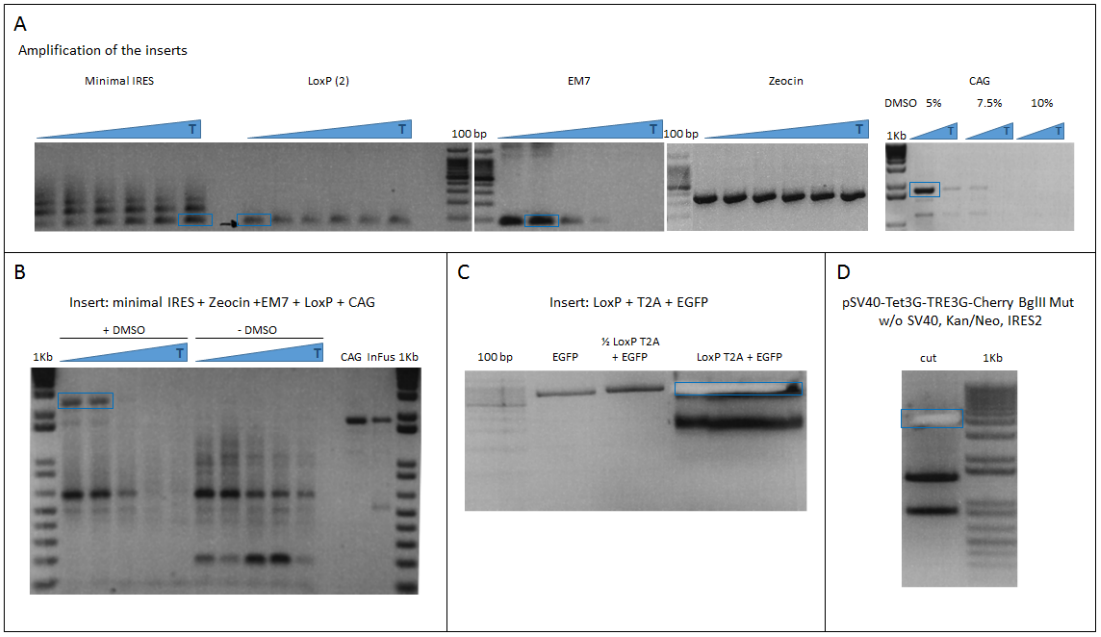

FIGURE 3.21: Cloning the pGoldiLox plasmids. A: PCR amplification of the single inserts using different temperature and/or DMSO concentrations. B: Generation by PCR of the insert containing the minimal IRES, the Zeocin, the EM7, the LoxP and the CAG. The specific products and amplification conditions are framed in a blue square. C: Steps of PCR amplifications to create the insert encoding for the LoxP, the T2A and the EGFP. The square highlights the band cut for purification. D: The new backbone, lacking the SV40 promoter, the Kan/Neo and the IRES2 sequences, was extracted from the gel.

The two inserts were then "In-Fused" with the backbone and Stellar Competent Cells

were transformed with the cloning reaction. The colonies were then screened cutting with BglII, which should not have restriction sites, and double digesting with SnaBI and KpnI, which cut in the CAG promoter sequence and in the TetOn 3G LoxP junction respectively (Figure 3.22). Even if it looked like BglII cut some of the plasmids, I sequenced the plasmid number 9 and I confirmed the correct sequence.

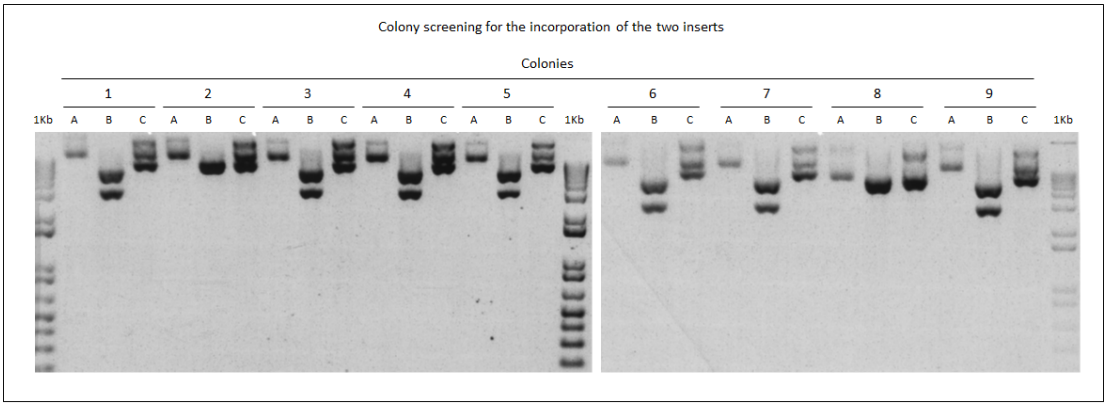

FIGURE 3.22: Cloning the pGoldiLox plasmids: enzymatic screening for plasmids correctly cloned. A: uncut plasmid, B: SnaBI + KpnI digestion, C: BglII digestion.

Next, I cloned the ROSA26 homology arms into the backbone. The plasmid was linearised with BstZ17I and the arms were amplified using as template the pDonor MCS ROSA26 plasmid [166]. The bacteria colonies transformed with the In-Fusion reaction were screened first by PCR and then by enzymatic digestion, cutting with EcoRV, whose sites flank both the arms (Figure 3.23).

FIGURE 3.23: Cloning the pGoldiLox plasmids: enzymatic screening to identify the plasmids in which the ROSA26 homology arms have integrated. The plasmid showing the correct pattern of bands is pointed out by the arrow.

The plasmid showing the correct insertion was cut with MluI in order to allow the cloning of the four main Wt1 isoforms. Wt1 inserts were amplified from the pcDNA3-EGFP-Wt1 plasmids, using primers that would have deleted the mCherry STOP codon through In-Fusion mediated recombination into the backbone. After the single isoforms were cloned into the pGoldiLox EV, the colonies were screened by PCR (Figure 3.24) and sent for sequencing.

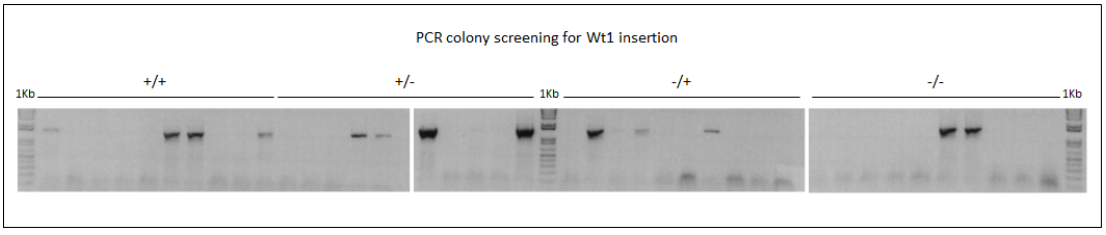

FIGURE 3.24: Cloning the pGoldiLox plasmids: PCR colony screening to identify the plasmids with Wt1 single isoforms integration.

I started testing the plasmid by transiently transfecting the pGoldiLox EV into the CreERT2 E14 cell line (kind gift of Ian Chambers lab). The cells were transfected

by Lipofectamine and the plasmids were tested under four different conditions: with medium either containing 1 μg/ml Dox, or 1 μM 4-hydroxy-tamoxifen (4-OHT) to activate the CreERT2 recombinase, or with the combination of the two drugs, last with fresh medium. As shown in Figure 3.25, after 48h the levels of the EGFP dropped in the presence of OHT and the mCherry signal was visible only under Dox treatment.

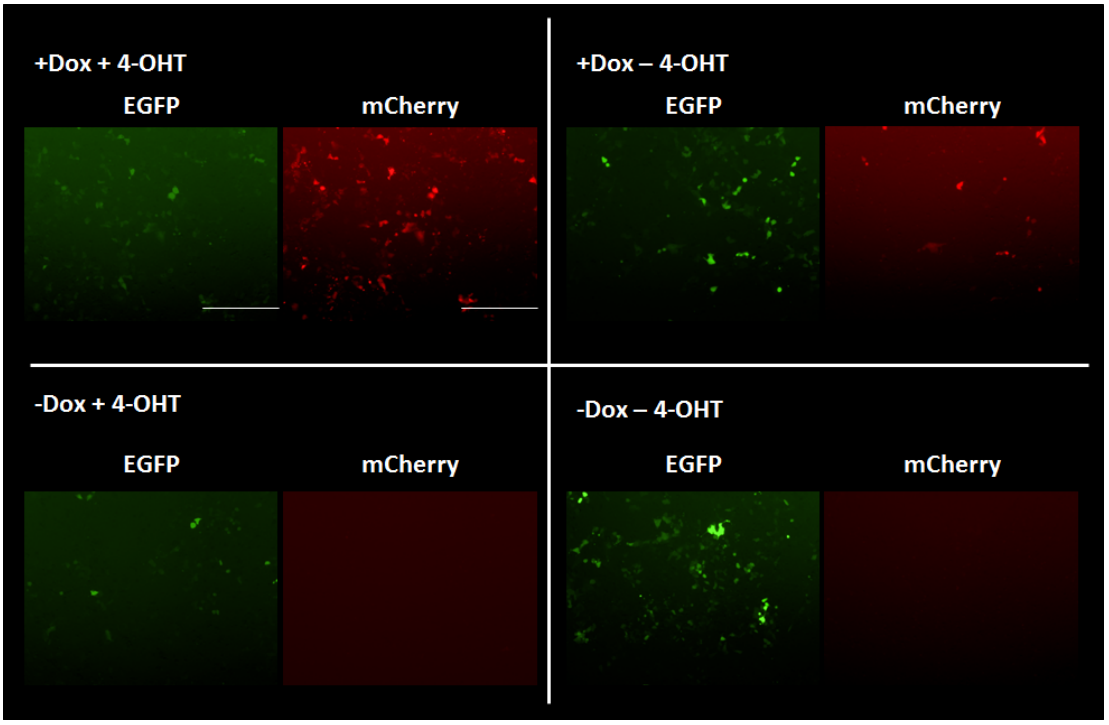

FIGURE 3.25: Transient transfection of the pGoldiLox Ev plasmid (0.5 μg per well) in CreERT2 E14 cells. FPs' signals after 48h treatment with the indicated four different condition. Scale bar = 500 μm.

To further confirm that the pGoldiLox plasmids were working as expected, I transfected into Hela cells two plasmids per isoform and collected the total protein after 24h of induction with 1 μg/ml Dox. I then visualized the mCherry-WT1 levels of expression by WB and chose the plasmids that gave the higher expression to establish stable cell lines (Figure 3.26).

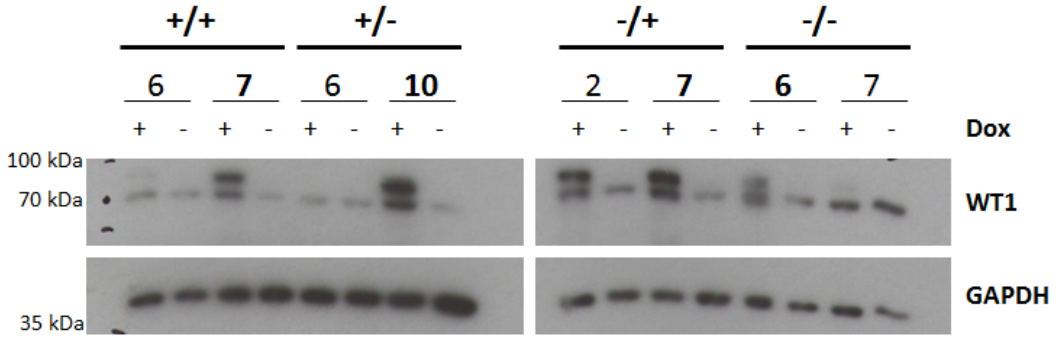

FIGURE 3.26: WB: mCherry-WT1 protein levels in Hela cells transiently transfected with 0.5 μg of two plasmids per isoform and either induced or not induced. The numbers of the plasmids that gave the best expression levels are written with bold font.

3.5.2 Deriving IMCD3 stable clones expressing single isoforms of WT1 and assessing the levels of expression of WT1

In order to create a second model to study the function of single isoforms of WT1, I chose to stably transfect the murine IMCD3 cell line with the different pGoldiLox plasmids. The IMCD3 cells were derived from the kidney inner medullary collecting duct of an SV40 transgenic mouse. Those cells, although considered epithelial, express also mesenchymal markers, resembling WT1 expressing cells. It has been shown that the balance of the expression of the epithelial and mesenchymal markers is influenced by the confluence of the cells and that an EMT can be induced under TGF and IGF1 treatment [159]. The IMCD3 cells do not express WT1, thus they are a useful model to discern the role of the single isoforms of WT1.

In order to integrate the pGoldiLox plasmids in the ROSA26 locus, the IMCD3 cells were co-transfected by Lipofectamine, coupling each of the vectors with two Zinc Finger nucleases (ZFN) encoding plasmids: the pCMV-RosaL6 ELD mutations (carrying FokI fused to RosaL6 ZFN) and the pCMV-RosaR4 KKR mutations (carrying FokI fused to RosaR4 ZFN) [166]. The ZFNs are a class of engineered DNA-binding proteins, composed by a DNA binding domain and a nuclease domain from the FokI restriction

enzyme. They facilitate genome editing by creating a double-stranded break in the defined location that induces DNA-repair processes, as the homologous recombination and the non-homologous end joining. Through the homologous recombination, it is therefore possible to target the sequences of the plasmid that are flanked by the homologous arms to the desired locus. The ZFN-encoding plasmids were a kind gift of the Ian Jackson lab. After transfection with 1 μg of total linearised plasmid DNA (I used a ratio between the amount of pGoldiLox plasmid and the ZFN encoding plasmids of 4:1:1), the cells were selected with 400 μg/ml of Zeocin for two weeks. When the single clones were clearly visible and distinguishable, I picked and expanded EGFP positive clones. To have an initial indication of whether the plasmids were integrated into the ROSA26 locus, I extracted genomic DNA from the clones and I performed a PCR screening using a forward primer which binds to a region of the ROSA26 locus beyond the 5' homology arm and a reverse primer designed inside the plasmid. Although the amplification gave rise to multiple products, the expected amplicon of 2543 bp was detected in at least one clone per isoform (examples are shown in Figure 3.27). In order to confirm the integration of a single copy of the plasmid into the ROSA26 locus, it will be necessary to perform a Southern blot assay.

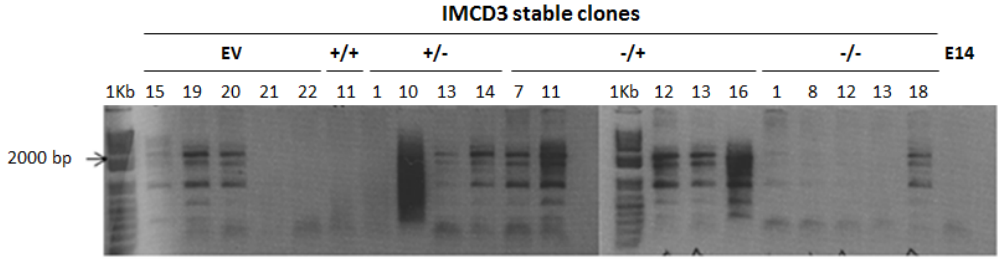

FIGURE 3.27: IMCD3 stable clones: examples of PCR amplification of the ROSA26 locus to test the integration of the plasmid. The genomic DNA of the E14 cells was used as a negative control.

I then assessed the levels of expression of WT1 in the single clones. I induced the cells O/N with 1 μg/ml of Dox, extracted total proteins and visualized by WB the expression of mCherry-WT1. As shown in Figure 3.28, some of the clones, even though positive for EGFP expression, did not express the fusion protein after induction. Moreover, most

of the clones proved to be leaky, showing high levels of expression of mCherry-WT1 even without Dox treatment. Those findings intimate that the integration of the whole and intact plasmid was problematic, or that multiple copies have integrated interfering with the expected activity of the plasmid.

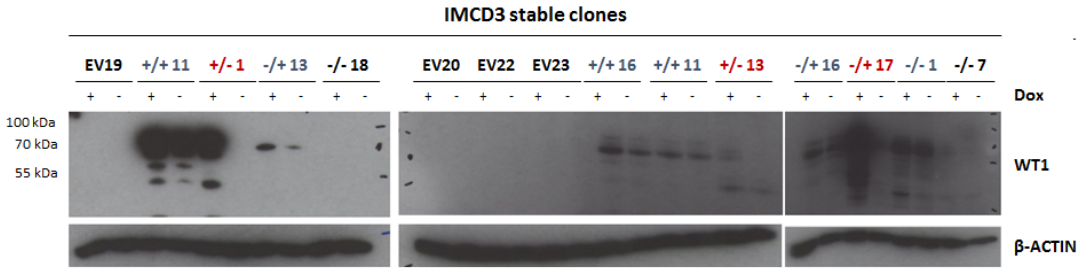

FIGURE 3.28: WB: mCherry-WT1 levels of expression in multiple IMCD3 stable clones with and without Dox. The clones that express the protein only in the presence of Dox are marked in red, the leaky clones are marked in blue, while the black clones are the EGFP positive, but mCherry-WT1 negative ones. Antibody to visualize WT1 = Abcam 89901.

Nonetheless, based on the best mCherry signal, I chose for the next experiments two clones per isoform, including non-leaky clones when possible. Figure 3.29 shows the images of the mCherry and EGFP signals in the selected clones and Figure 3.30 the protein levels of mCherry-WT1 visualized by WB. As revealed by the WB, I did not derive clones with comparable levels of expression of the single isoforms. This might be due to the fact that the plasmids are not indeed integrated in the ROSA26 locus, or to the reasons that cause the leakiness of expression, as the integration of multiple copies, or to different stability and degradation rates of the isoforms themselves.

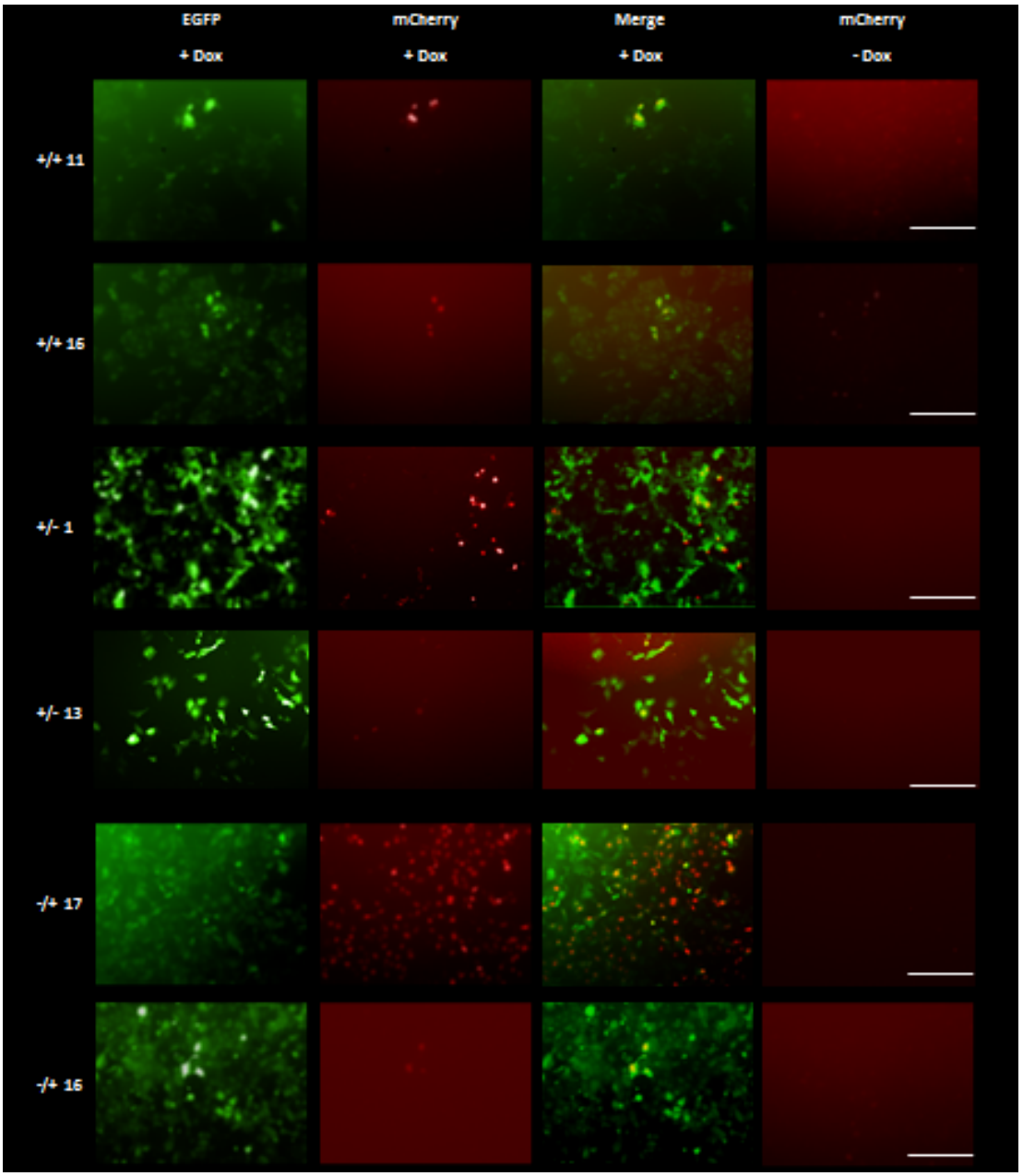
EGFP
+ Dox
mCherry
+ Dox
Merge
+ Dox
mCherry
- Dox
+/+ 11
+/+ 16
+/- 1
+/- 13
-/+ 17
-/+ 16

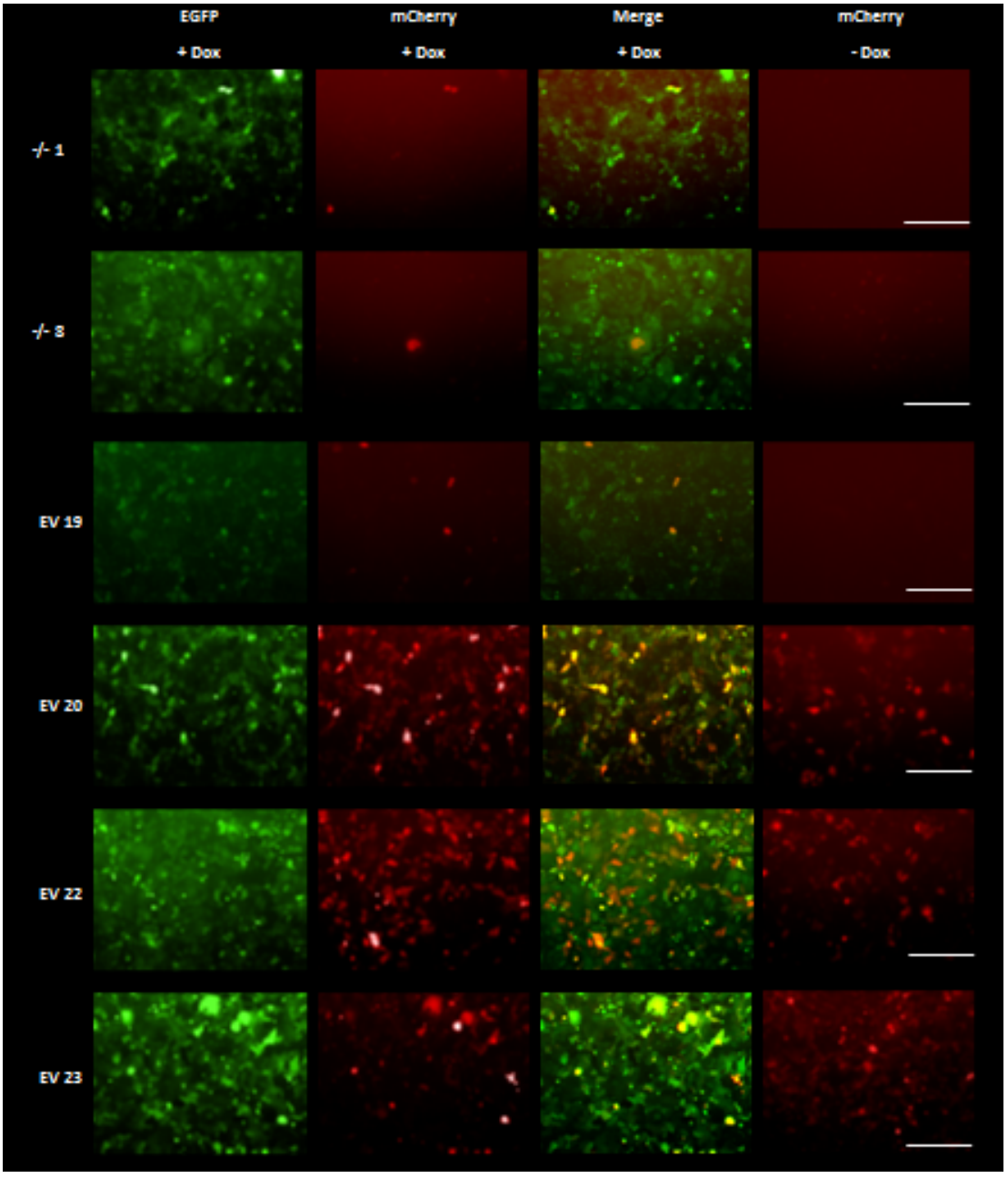

FIGURE 3.29: EGFP, mCherry and merge of the signals in selected clones after 24h of Dox treatment (1 μg/ml). The last panels on the right show the mCherry signal in the untreated clones. Scale bar = 500 μm.

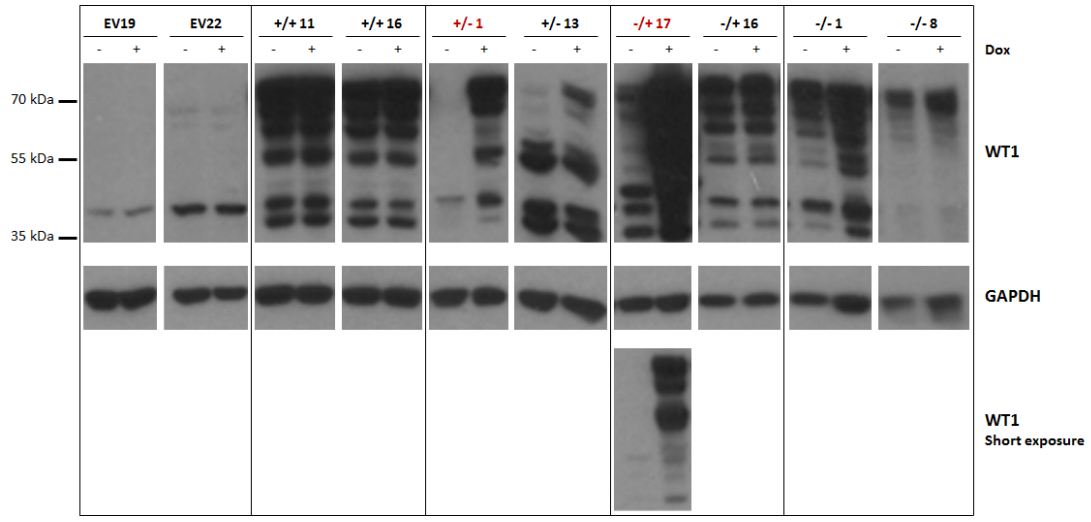

FIGURE 3.30: WB: mCherry-WT1 levels of expression in the chosen IMCD3 stable clones with and without 1 μg/ml Dox treatment at 96h. The non-leaky clones are highlighted in red. Antibody to visualize WT1 = Abcam 89901.

3.6 Cloning the CAG-Tet3G-TRE3G-mCherry vector for ubiquitous and inducible expression of WT1 isoforms

I cloned another system aiming to overcome either the issue of leakiness of the pGoldiLox plasmids and the silencing of the pSV40-Tet3G-TRE3G vectors, aiming to derive stable ES cells that express inducible single isoforms of WT1. To address this, I modified the pSV40-Tet3G-TRE3G mCherry EV, changing the SV40 promoter with the CAG promoter and the Kan/Neo resistance with the Zeocin. Moreover, I added the ROSA26 arms to target the plasmid in the ROSA26 locus. I also decided to tag WT1 isoforms with the Twin-Strep-tag®, followed by a TEV protease recognition site for the complete removal of the tag for biochemical analysis. I chose the Twin-Strep-tag® because it is a small tag of 3 kDa that does not affect the protein activity, it has a high affinity to the Strep-Tactin, an engineered streptavidin, moreover it binds reversibly and it can be efficiently eluted under gentle competitive conditions [167]. In order to be able to easily detect the transcription under the pTRE3G promoter, I cloned a P2A sequence between the mCherry FP and the tagged Wt1. The cloning process is schematised in Figure 3.31.

To clone the new set of plasmids, named CAG-Tet3G-TRE3G-mCherry-(Wt1), I first removed from the pSV40-Tet3G-TRE3G mCherry EV plasmid the Kan/Neo resistance and the SV40 by double digestion with FseI and BstZ17I. I then cloned in the backbone two inserts obtained by PCR amplification: the first encoding for the CAG promoter, the second for the prokaryotic promoter EM7 and the Zeocin. The plasmids correctly cloned were selected by looking at the pattern of bands produced by the double digestion with the KpnI and the SnaBI enzymes, which cut in the IRES2 and in the new inserted CAG sequence, respectively (Figure 3.32).

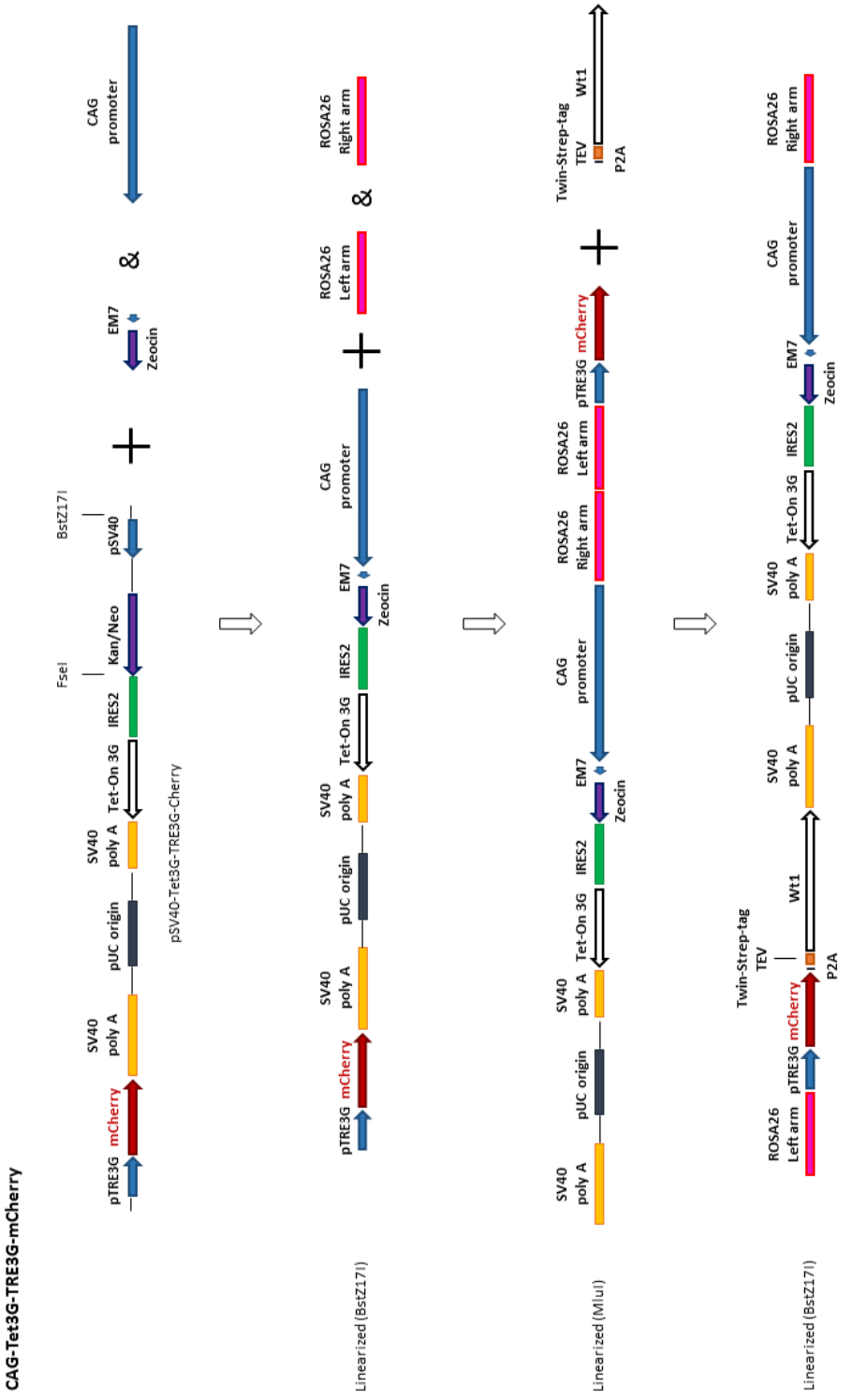

FIGURE 3.31: Diagram of the cloning process to create the CAG-Tet3G-TRE3G-mCherry plasmids

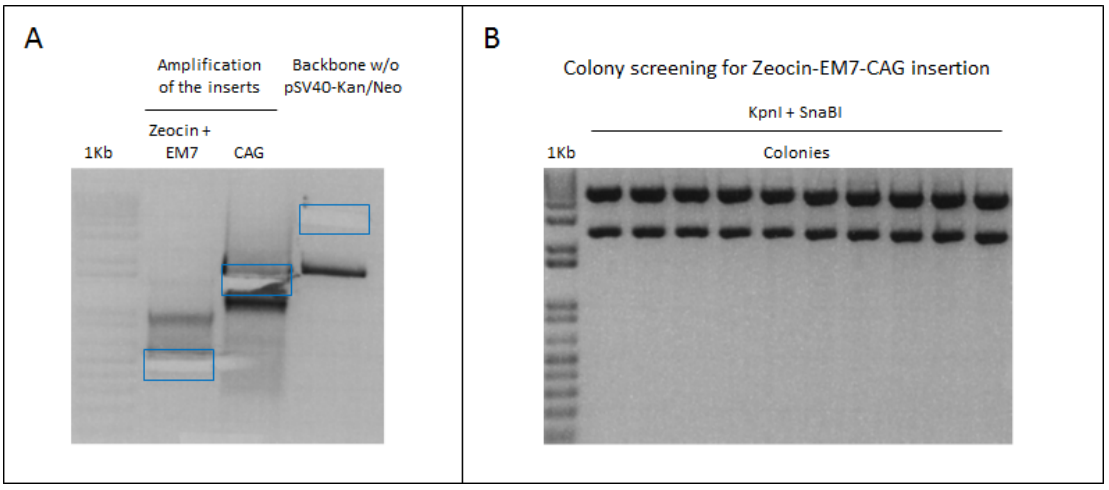

FIGURE 3.32: Cloning CAG-Tet3G-TRE3G-mCherry. A: PCR amplification of the Zeocin-EM7 and CAG inserts. The specific bands extracted from the gel and purified are framed. On the right hand side of the gel, isolation of the backbone after removal of the pSV40 and the Kan/Neo sequences. B: Identification of the correctly cloned plasmids by enzymatic digestion. All the clones are positive.

One of the positive plasmids was then linearised with BstZ17I for the insertion of the ROSA26 homologous arms. The plasmids that transformed the Stellar Competent Cells were checked for the presence of the arms by digestion with EcoRV and BrsGI, whose restriction sites flank the arms (Figure 3.33).

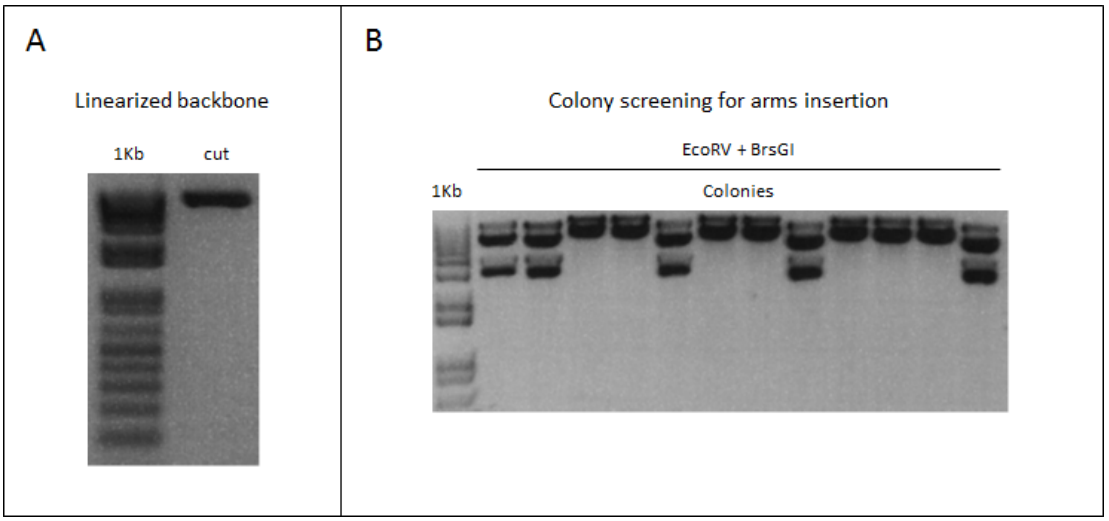

FIGURE 3.33: Cloning CAG-Tet3G-TRE3G-mCherry. A: Backbone linearised to add the arms. B: Enzymatic screening to verify the presence of the arms in the plasmids.The positive vectors showed two bands when run on the 1% agarose TBE gel.

I linearised with MluI one positive vector and "In-Fused" the Wt1 single isoforms, to which I added by PCR the Twin-Strep-tag®, the TEV recognition site and the P2A sequence at the 5' end. Because the nucleotide sequence of the Twin-Strep-tag® is not published, I derived it from the amino acid sequence (WSHPQFEK-GGGSGGGSGG-GSWSHPQFEK) using the EMBOSS Backtranseq tool. The insertion of the tagged isoforms of Wt1 in the plasmids was assessed by PCR (Figure 3.34). The constructs that showed the expected PCR products were then sequenced to confirm the correct cloning. To clone the CAG-Tet3G-TRE3G-mCherry EV, I cut one of the constructs containing Wt1 with MluI and PaeI in order to keep the Twin-Strep-tag® and the TEV sequences and get rid of Wt1 coding sequence. The plasmid without the gene of interest was then isolated from the gel, purified, blunt ended with the T4 DNA polymerase and finally ligated by T4 DNA ligase. The plasmids cloned correctly were screened by MluI and PaeI digestion.

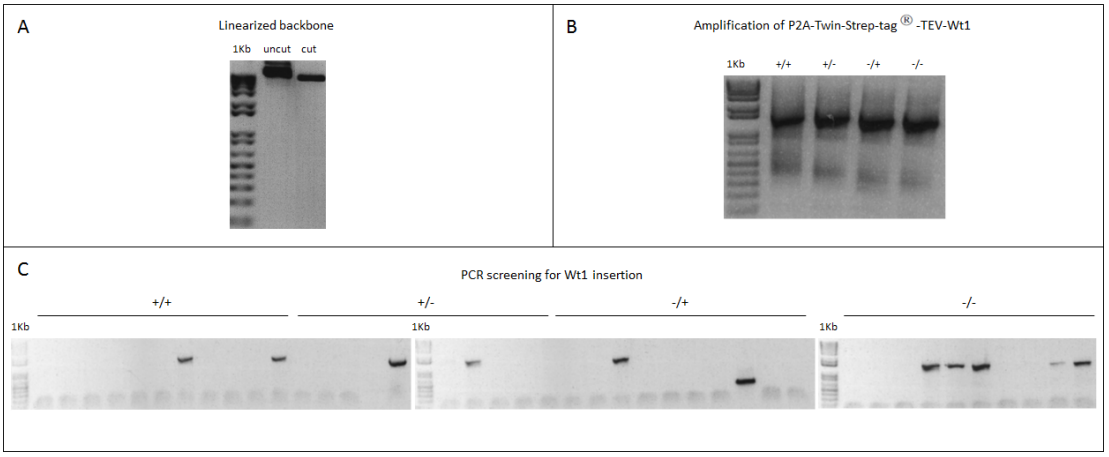

FIGURE 3.34: Cloning CAG-Tet3G-TRE3G-mCherry-Wt1. A: Backbone linearised by MluI to add Wt1 inserts. B: Final inserts, obtained with several amplifications, encoding for P2A-Twin-Strep-tag®-TEV-Wt1 isoform. C: PCR to identify the plasmids which contain the inserts.

I checked that the plasmids were working as planned by transient transfection in Hela cells. After 24h of induction with 1 μg/ml Dox, I performed an IF to see the localization and expression of the FP and WT1. As expected, only when the Dox was added, the antibody against WT1 gave a nuclear signal, while the mCherry fluorescence was distributed in the whole cell (Figure 3.35).

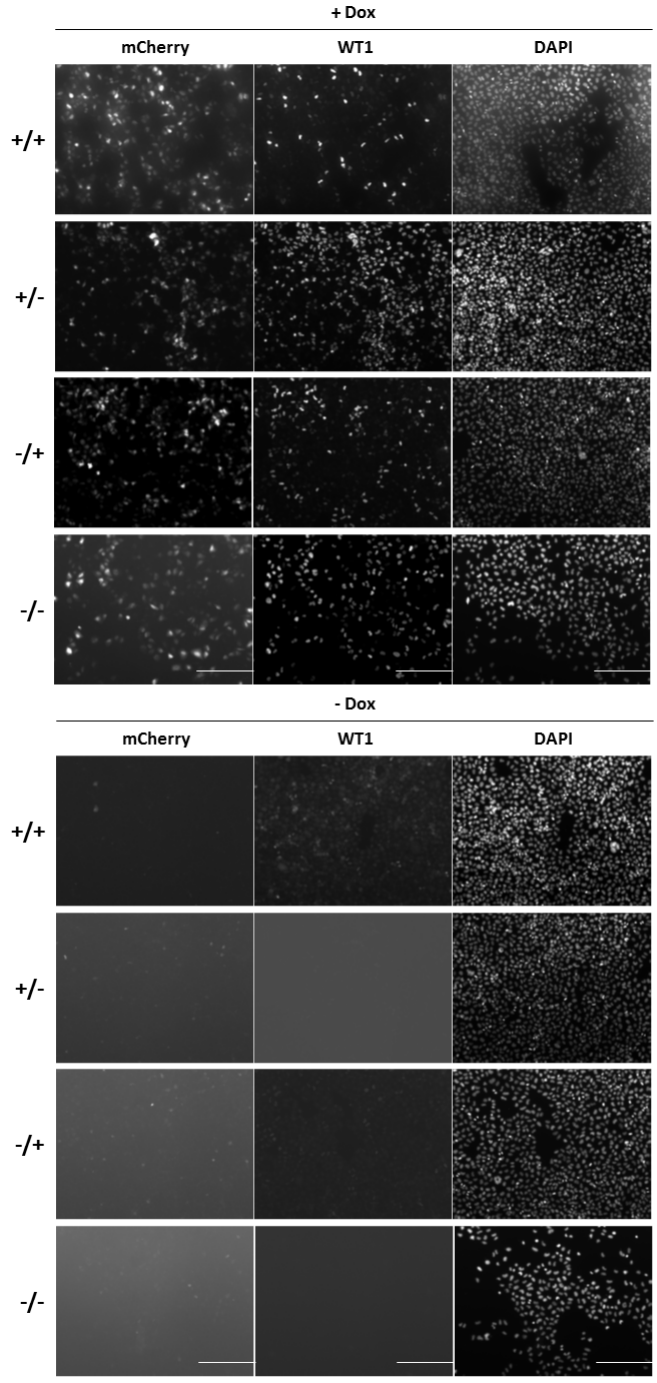

FIGURE 3.35: IF: Hela transiently transfected with 0.5 μg of CAG-Tet3G-TRE3G-mCherry-Wt1s. The pictures show the mCherry signal, the staining with WT1 antibody (Abcam 89901) and the DAPI fluorescence in cells either treated (top panels) or not (bottom panels) with Dox. Scal bar = 500 μm.

I also assessed WT1 and mCherry protein levels by WB, confirming that the expression of WT1 is not leaky and that the isoforms are cleaved from the mCherry protein (Figure 3.36). However, when I probed the blot with an antibody to the Twin-Strep-tag®, I did not detect any signal, raising the doubt that the sequence of the tag might be not correct.

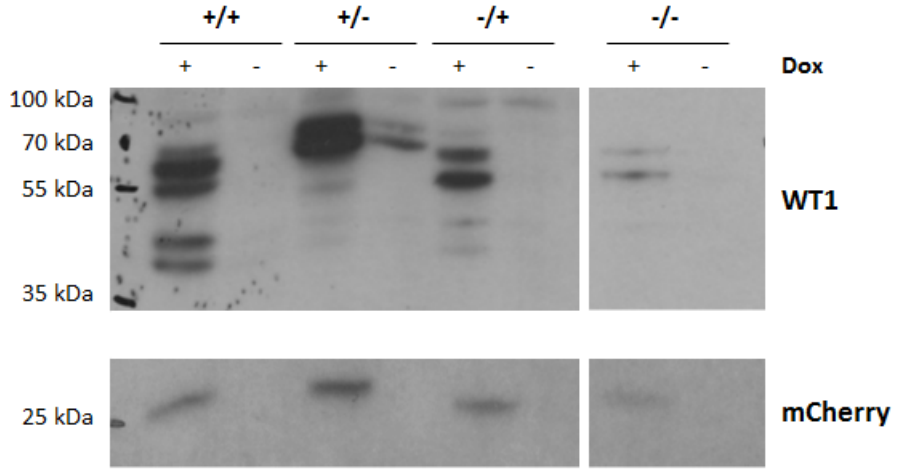

FIGURE 3.36: WB: WT1 (visualized by Abcam 89901 antibody) and mCherry protein levels in Hela cells induced and non-induced after transient transfection with 0.5 μg of the CAG-Tet3G-TRE3G-mCherry-Wt1 constructs.

As the plasmids were expressing WT1 isoforms as expected, Dr Selvi Bharathavikru and Joan Slight started deriving stable E14 *Wt1* KO cells. After selecting with 400 μg/ml of Zeocin, the single clones were picked and grown. WT1 expression after induction was tested and confirmed by IF and WB, an example of WB is show in Figure 3.37. The establishment of single clones for each isoform is still ongoing, but I am confident that with this new expression vectors we will be able to derive ES KO cells, in which we can induce single isoforms of WT1. Those cells will be extremely useful not only for rescuing studies, but also to understand the instructive role of WT1 single isoforms. Moreover, the cells can be used to create mouse models to assess *in vivo* the importance and the role of the isoforms.

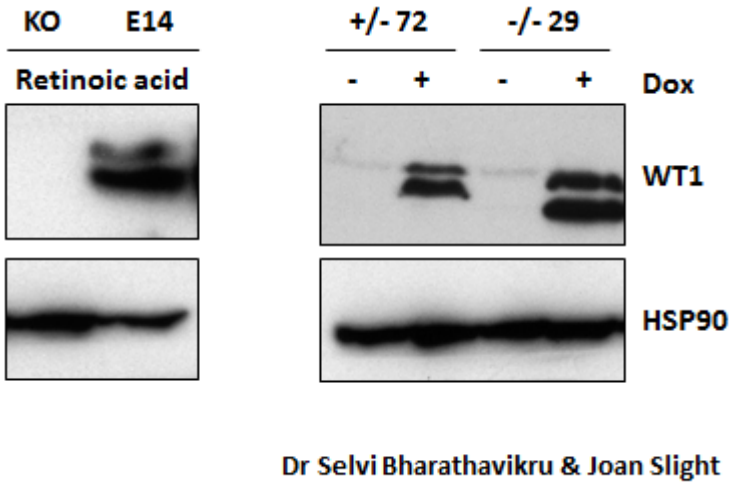

FIGURE 3.37: WB: WT1 levels in two induced (1 μg/ml Dox, 24h) and untreated E14 *Wt1* KO clones stably transfected with the CAG-Tet3G-TRE3G-mCherry-Wt1 +/- (clone 72) and -/- (clone 29) constructs. E14 *Wt1* KO cells and E14 cells were treated for 5 days with 1 μM retinoic acid and used as negative and positive control, respectively. Antibody for Wt1: Abcam 89901.

3.7 Cloning the pGoldiLoxS plasmid for inducible and tissue specific expression of WT1 single isoforms

I started to build a system that would allow the inducible expression of WT1 in a tissue specific manner. Such a system could be very valuable for either studying the function of the re-expression or over-expression of the isoforms in specific tissues and cell types, or for rescue experiments both in adult mice and embryos. Briefly, the system is based on the presence of a PolyA sequence between LoxP sites that stops the transcription before the Tet-On 3G sequence, unless Cre-mediated recombination occurs. Thus, coupling the system with a Cre recombinase driven by a tissue specific promoter will allow the expression of the transactivator in a tissue specific fashion. The induction of the isoforms can be even further regulated defining the time points when to add the Dox. Moreover, the levels of expression can be titrated by modulating the concentrations of Dox. Thus, it will also be possible to define the minimum levels

of WT1 required for rescuing KO phenotypes. The pGoldiLoxS plasmid has others distinguishing characteristics compared with the pGoldiLox plasmid:

- Before the recombination, the positive clones can be selected by the presence of the rsEGFP2 signal, a photoswitchable FP [168]. After recombination, the absence of the fluorescence can be used as a way to select the recombination events. Because the rsEGFP2 is photoswitchable, its signal does not interfere with the one of other FPs in the plasmid. This feature has been remarkably useful to test how the plasmid worked.
- The mCherry, which reports the expression levels of the Tet-On 3G transactivator following recombination, is a positive selector for the recombination events. Furthermore, it can function as a lineage tracer in combination with a Cre driven by the *Wt1* promoter.
- I exchanged the pTRE3G promoter with the pTRE3GS one, which is supposed to guarantee a 10,000 fold of up-regulation after stable transfection, performing ten times better than the original promoter.

The cloning steps are schematised in Figure 3.38.

I started modifying the pGoldiLox plasmid without the ROSA26 arms cutting out the LoxP, T2A and EGFP sequences by double digestion with SwaI and KpnI, in order to insert the sequences for the rsEGFP2 followed by the SV40 polyA, the LoxP site, the Venus gene and the P2A sequence. To efficiently clone all the pieces, I created by PCR two inserts: one containing the P2A and the Venus reporter, one encoding for the LoxP, the polyA signal and the rsEGFP2 gene. The Venus amplicon was obtained amplifying from the pCAGFucci2 plasmid, kindly provided by Dr Richard Mort, while I used the pQE 31-rsEGFP2 vector as a template for the rsEGFP2 amplification. The plasmid was a kind gift from the Jakobs lab. I fused the inserts into the backbone by In-Fusion cloning reaction and I screened the transformed colonies by PCR, looking for the incorporation of both Venus and rsEGFP2 (Figure 3.39).

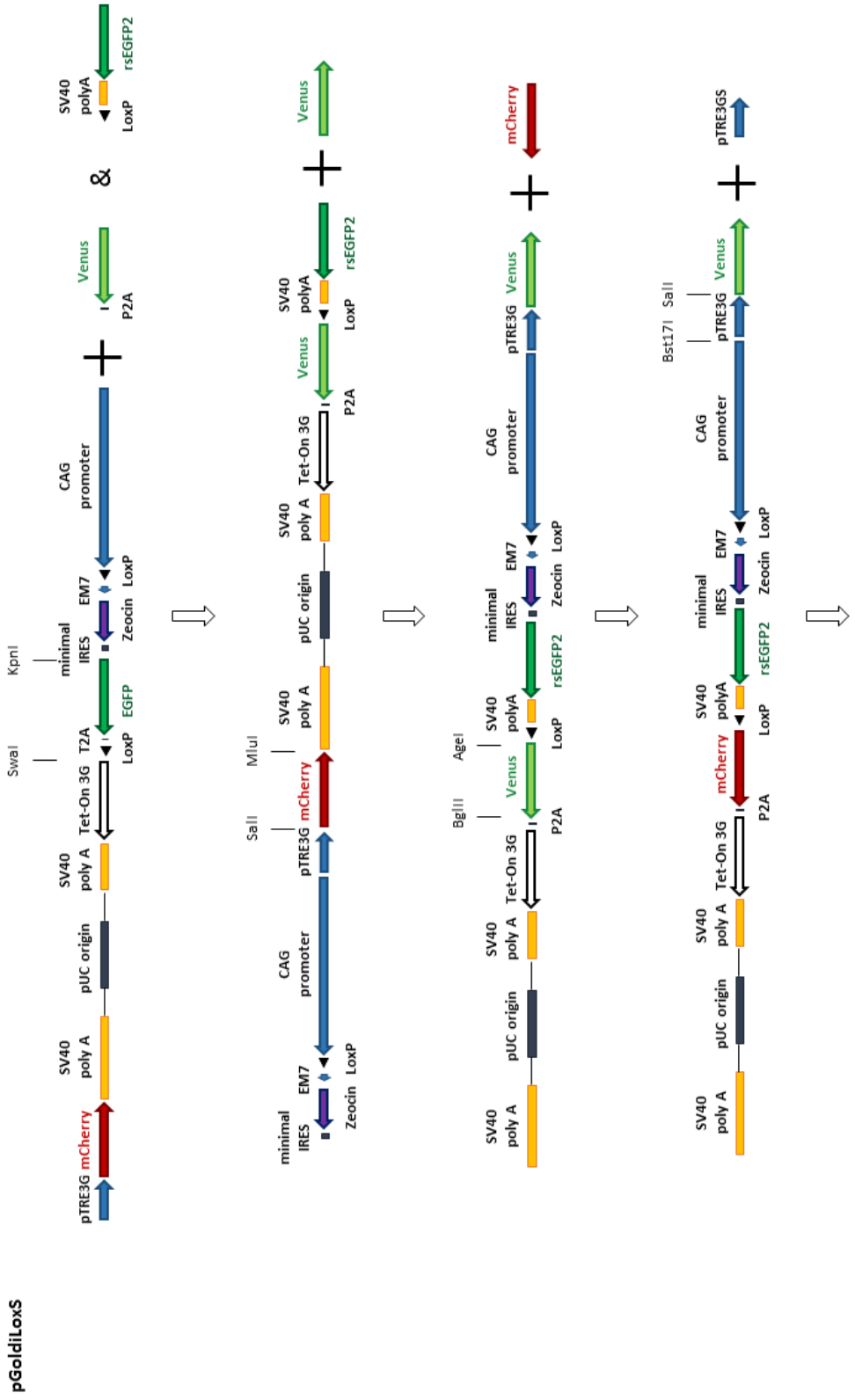
pGoldiLoxS
pTRE3G
mCherry
SV40 poly A
pUC origin
SV40 poly A
Tet-On 3G
T2A
LoxP
EGFP
SwaI
KpnI
minimal IRES
EM7
Zeocin
LoxP
CAG promoter
Venus
P2A
&
SV40 polyA
rsEGFP2
LoxP
SalI
MluI
pTRE3G
mCherry
SV40 poly A
CAG promoter
minimal IRES
EM7
Zeocin
LoxP
SV40 poly A
pUC origin
SV40 poly A
Tet-On 3G
Venus
P2A
SV40 polyA
rsEGFP2
LoxP
BglII
AgeI
SV40 poly A
pUC origin
SV40 poly A
Tet-On 3G
Venus
P2A
SV40 polyA
rsEGFP2
LoxP
minimal IRES
EM7
Zeocin
LoxP
CAG promoter
pTRE3G
Venus
mCherry
Bst17I
SalI
SV40 poly A
pUC origin
SV40 poly A
Tet-On 3G
mCherry
P2A
SV40 polyA
LoxP
rsEGFP2
minimal IRES
EM7
Zeocin
LoxP
CAG promoter
pTRE3G
Venus
pTRE3GS

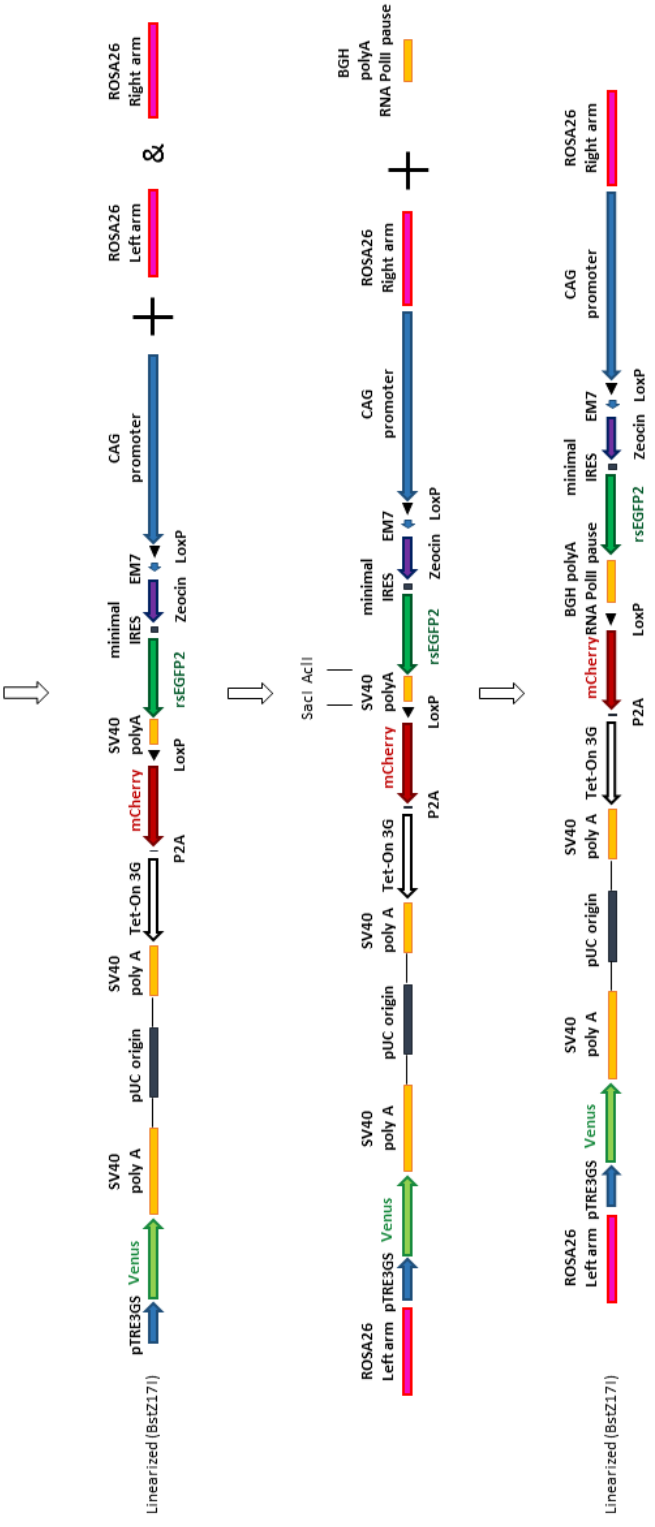

FIGURE 3.38: Diagram of the cloning of the pGoldiLoxS plasmids.

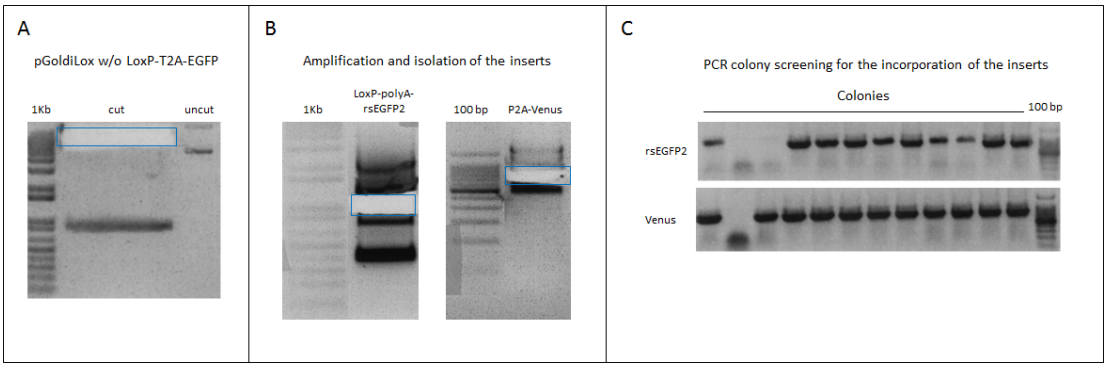

FIGURE 3.39: Cloning the pGoldiLoxS plasmids. A: Isolation of the backbone. B: Isolation of the final inserts obtained by a series of PCR reactions. The bands at the expected size were cut and isolated from the gel (framed in the blue squares). C: PCR colony screening for the incorporation of the two inserts, verified amplifying the rsEFGP2 and the Venus sequences. The second colony does not show any integration, the third one seem to have integrated the Venus insert only, while all the other are positive for the cloning of both inserts.

I tested the double positive plasmids by transient transfection in Hela cells. In this way, I confirmed the expression of the rsEGFP2 eliciting the fluorescence with a light wavelength of around 405 nm. However, when I looked at the fluorescence using the 488 nm wavelength light, which should switch off the rsEGFP2 signal, it looked like the cells were expressing the Venus protein even without Cre recombination. I was not sure whether the green fluorescence was due to the incomplete bleaching of the rsEGFP2 signal or to the Venus expression, so I decided to swap the mCherry and the Venus sequences to avoid any interference between FP signals. I therefore first cut the mCherry using the SalI and MluI enzymes, I cloned the Venus coding sequence under the control of the pTRE3G promoter and screened for positive plasmids by enzymatic digestion. Second, I cut the Venus by BglII and AgeI digestion and cloned the mCherry after the LoxP site. The colonies were screened by cutting with the same enzymes used to create the backbone (Figure 3.40).

I then decided to substitute the pTRE3G promoter with the more powerful new version of the promoter, called pTRE3GS. I amplified the promoter from the pLVX Tet One plasmid (Clontech). The original promoter was eliminated cutting with BstZ17I and SalI and the new promoter was cloned in its place. After transformation, the plasmids were screened by enzymatic digestion. I selected one of the vectors that showed the

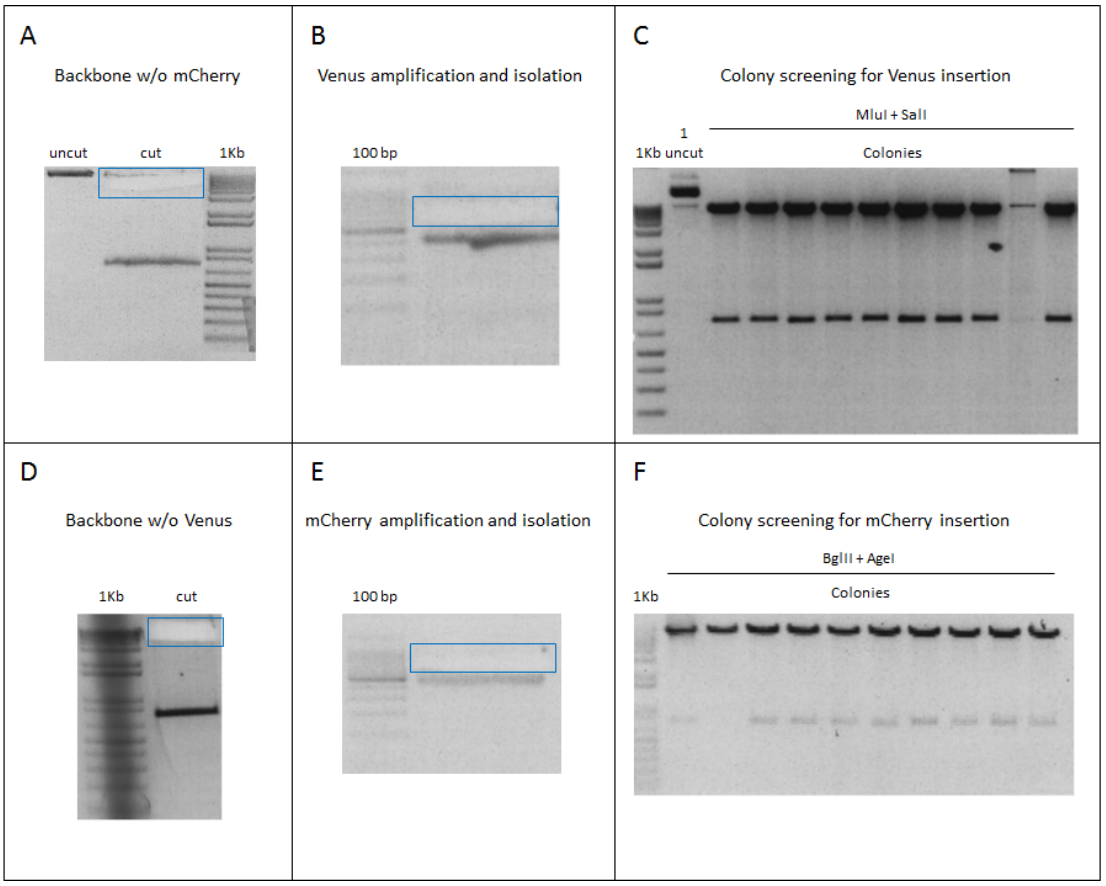

FIGURE 3.40: Cloning the pGoldiLoxS plasmids: swapping mCherry with Venus. A: Creating the backbone to insert Venus. B: Amplification of the Venus insert. The band of the right size, which is highlighted by the blue square, was extracted and purified. C: Screening the plasmids for Venus insertion by enzymatic digestion. All the constructs seem to be positive. D: Preparation of the backbone for cloning mCherry. E: Amplification of the insert coding for the mCherry FP. The specific amplicon was isolated from the gel. F: Screening the plasmids that have integrated the mCherry sequence. All the colonies, but the first two, seem to be positive.

right size of the promoter to continue the cloning with the insertion of the ROSA26 homologous arms. The correct cloning of the arms in the plasmids was assessed by PCR (Figure 3.42). Three plasmids were then sequenced and the expected sequence was confirmed.

I tested the pGoldiLoxS vector by transient transfection in the Hela cells to exclude any possible recombination of the LoxP sites. The cells were grown for 24h with or without Dox and then I looked at the expression of the FPs. The cells expressed the

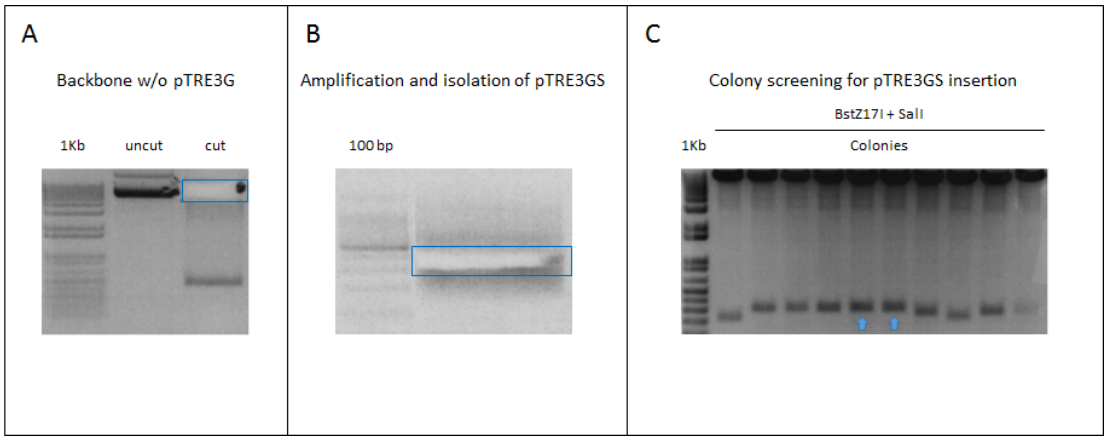

FIGURE 3.41: Cloning the pGoldiLoxS plasmids. A: Cutting the pTRE3G promoter to substitute it with the pTRE3GS promoter. B: Isolation of the PCR product encoding for the pTRE3GS promoter. C: Digestion of the plasmids to select the ones where pTRE3GS has integrated. The plasmids showing the expected pattern of bands are marked with arrows.

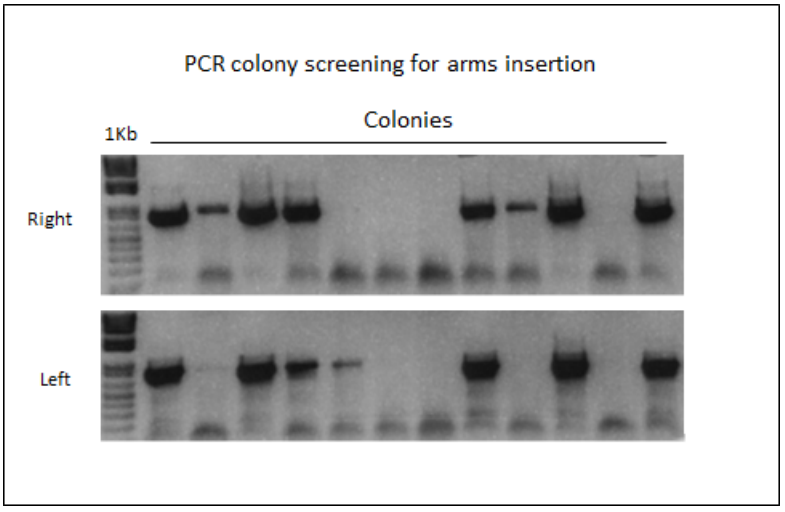

FIGURE 3.42: Cloning the pGoldiLoxS plasmids: PCR to select the plasmids in which both arms have integrated. Each arm was amplified by PCR, the plasmids that amplified both amplicons were considered positive.

rsEGFP2, however they also expressed the mCherry and therefore the Venus when the Dox was added. I concluded that somehow the SV40 polyA signal was not sufficient to stop the transcription after the rsEGFP2. I thus decided to change the SV40 polyA with the BGH polyA signal followed by a RNA polymerase II pause signal from the human α-2 globin gene, whose sequence was copied from the pLentiX tet One plasmid (Clontech). The pause site is supposed to enhance the utilization of an upstream polyA signal [169]. The backbone was made cutting out the SV40 polyA with SacI and AclI, while the insert was created by two steps of PCR: I started attaching the first half of the pausing site sequence to the BGH polyA signal and the resulting product was then used as a template to add the second half of the sequence. After the cloning and the transformation, the plasmids were screened, digesting with the enzymes used to cut the backbone (Figure 3.43).

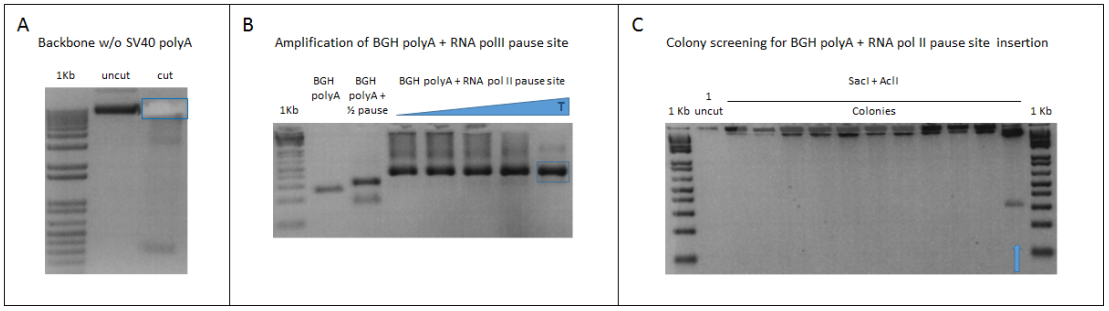

FIGURE 3.43: Cloning the pGoldiLoxS plasmid: swapping the SV40 polyA with the BGH polyA and the RNA polII pausing site. A: Cutting the SV40 polyA to generate the backbone. B: Amplicons resulting from the PCR reactions to create the insert encoding the BHG polyA and the RNA polII pausing site. The best condition for the last step of amplification is highlighted by a blue square. C: Colony screening by enzymatic digestion to detect the inclusion of the insert. The only positive colony is pointed out by the arrow.

I confirmed the cloning by sequencing and I investigated how the new pGoldiLoxS EV worked after transfecting the CreERT2 E14 cell line. The cells were treated for 48h with four different conditions: combining the Dox (1 μg/ml) and the 4-OHT (1 μM) and using either the Dox or the 4-OHT or fresh medium. I checked the pattern of expression of the FPs and noticed that in the presence of 4-OHT the rsEGFP2 fluorescence was significantly reduced, meaning that the LoxP recombination happened; however, even

in the absence of 4-OHT, the cells were still expressing a small amount of mCherry as well as Venus if the Dox had been added in the medium (Figure 3.44).

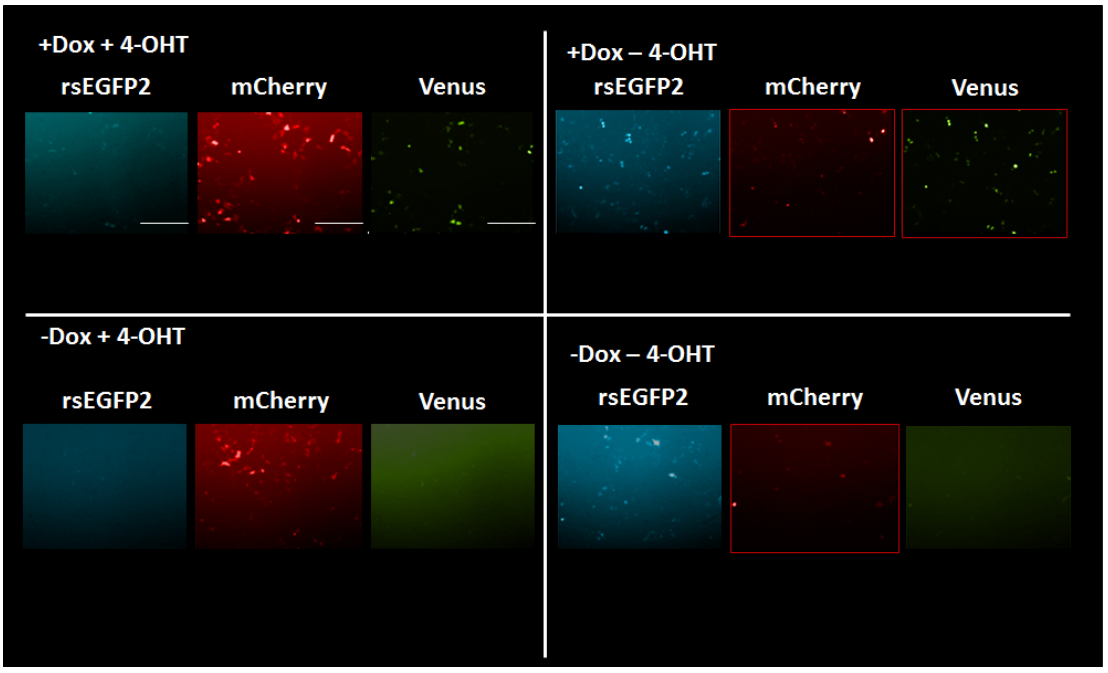

FIGURE 3.44: CreERT2 E14 cells transiently transfected with the pGoldiLoxS plamid (0.5 μg per well): FPs's fluorescence after 48h of treatment with the indicated conditions. The unexpected signals are framed in red. Scale bar = 500 μm.

I confirmed that I had encountered the same issue I had with the previous EV transfecting the E14 cell line. Even in the absence of possible recombination events, the mCherry was still expressed.

In order to create a system for the inducible and tissue specific expression of single isoforms of WT1, it will be essential to stop the leakiness of the pGoldiLoxS plasmid, a possible strategy could be adding a LoxP-STOP-LoxP cassette after the polyA signal.

Chapter 4

Exploring the function of single WT1 isoforms in the MDCK clones

4.1 Overview

In this chapter I will discuss the effects of the induction of WT1 in the stable MDCK cells. As explained in Chapter 1, I derived MDCK stable single clones expressing four different isoforms of WT1, which were either fused or not to an FP (mCherry or AmCyan1). Because the mCherry protein is monomeric and generally considered a better fusion tag compared to the AmCyan1 protein, I decided to focus my experiments on the mCherry clones. I also validated the results in one clone w/o FP per isoform, in order to ascertain whether the fluorescent marker was affecting WT1 function. Therefore, I used for each experiment three clones per isoform: two mCherry clones and one w/o FP. Because it was not possible to balance the levels of induction of WT1 across the established cell lines, I chose the clones based on the best expression levels of the induced isoform. Figure 4.1 shows WT1 protein levels in the selected clones after 96h

of induction with the established amounts of Dox for the mCherry clones (Table 3.1) and with 1 μg/ml Dox for the w/o FP ones.

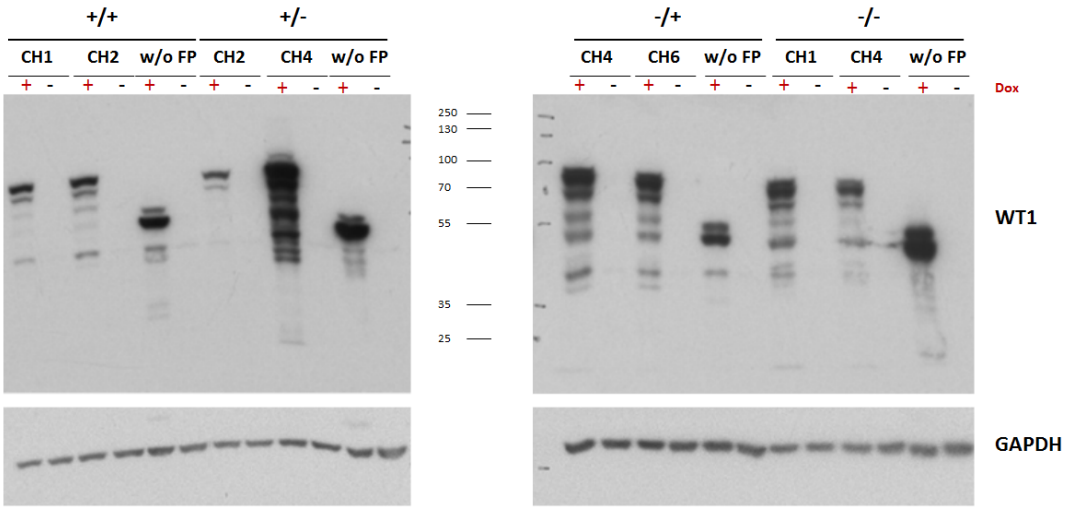

FIGURE 4.1: WT1 protein levels in the 96h induced and non-induced MDCK clones chosen for the subsequent experiments. Antibody against WT1: Abcam 8990.

Aiming to understand the consequences of the induction of the different isoforms of WT1 in the epithelial MDCK cells, I initially performed an expression analysis on 96h induced mCherry clones and non-induced clones using the Affymetrix Canine Gene 1.1 ST microarray. The profiling showed that the induction of all the isoforms upregulated the expression of different chemokines that characterised an immune and inflammatory response. Moreover, three out of four isoforms, namely +/-, -/+ and -/-, seemed to affect the regulation of the cell cycle and cell proliferation, while the isoforms lacking the exon 5 appeared to influence the cell motility and regulate the angiogenesis process. From the microarray analysis it was clear that the most significant isoform-specific changes happened with the induction of the -/+ isoform. Indeed, the expression of that isoform seemed to modify cell junctions, cell adhesion, extracellular matrix organization and the structure of the actin cytoskeleton.

I validated the upregulation of various chemokines using Q-RT-PCR (quantitative reverse transcription polymerase chain reaction), confirming that most of the investigated

cytokines were indeed over-expressed following WT1 induction in all the three clones analysed per isoform.

In order to verify whether WT1 was influencing cell proliferation and cell cycle, I followed the growth of the clones over 8 days and analysed the cycle phases at 4 and 8 days. I confirmed that the +/+ isoform did not affect the proliferation nor the cell cycle, but on the other hand it was not possible to validate the result for the other isoforms, as not all the three clones behaved in the same way. Moreover, it was difficult to attribute the inconsistencies to different expression levels of WT1 across the clones. The diverse rates in cell growth and distribution in the cell cycle phases may be caused by intrinsic clonal variability, although it cannot be excluded that the fusion with the mCherry protein was indeed affecting the function of certain isoforms. For instance, the two clones carrying the -/+ isoform fused to the mCherry showed impaired cell growth and block in G1 phase.

I decided to test the predicted changes in cell motility performing wound healing assays. I found that the clones expressing the -/+ isoform fused to the mCherry had a reduced motility. The +/- and -/- expressing cells did not show any statistically significant changes, while, unexpectedly, one out of three +/+ clones seemed to close the wound more slowly than the control. I then challenged the cells in another assay that tests the oncogenic potential of the cells: the soft agar colony formation assay. As expected, the induction of the +/+ isoform did not affect the number or the size of the grown colonies; on the other hand the expression of the -/- isoform reduced the number of colonies in two clones and the size of the colonies in the third clone, suggesting that the -/- isoform induction does affect the ability of growing in the absence of anchorage. The induction of the +/- isoform decreased the number of forming colonies only in one clone, whereas the expression of the -/+ protein almost nullified the anchorage-independent growth only in the clones where the isoform is fused to the mCherry marker.

The data pointed out interesting, although unique, features characterising the mCherry -/+ clones. Indeed, they not only showed impaired cell growth, possibly caused by the block in the cell cycle, decreased motility and reduced anchorage-independent growth,

but also a striking change in morphology upon Dox treatment. Indeed, the cells became remarkably bigger in size than the control and many induced cells were multinucleated. The multinucleated giant cells also stained positive for the X-gal senescence marker at 96h of induction. The clones, though, did not meet all the criteria to be defined as senescent cells, because they did not completely stop growing, the phenotype was revertible after Dox removal, the senescence-associated heterochromatin foci were not visible by DAPI staining and the cells did not show signs of DNA damage when stained for γH2AX.

As predicted by the microarray analysis, the mCherry -/+ clones undergo a rearrangement of the actin cytoskeleton upon induction. In fact, the phalloidin staining that marks the filamentous actin (F-actin) network revealed the appearance of aligned stress fibers, which can affect cell migration and adhesion [170]. Last, I validated in both the mCherry -/+ clones the upregulation of genes involved in the extracellular matrix organization, as the metalloproteinase 9 (*MMP9*), different inhibitors of metalloproteinases (*TIMPs*) and type I collagen (*COL1A1*). Moreover, the induced cells showed a marked over-expression of the α smooth muscle actin (*ACTA2*) gene. As I will discuss in the chapter, taken together, the data concerning the mCherry -/+ clones suggest that the induction of the isoform induces a fibrotic phenotype.

Overall, the expression analysis and the cellular assays performed in the MDCK clones did not reach indisputable and consistent results. Thus, it was difficult to define a specific role of the single isoforms of WT1 in the different cellular aspects that I investigated. These results highlighted the difficulties of working with single clones made by random integration of the plasmids, as positioning effects cannot be excluded. To overcome these problems, more clones should be analysed in order to minimise the clonal variability and to be able to identify the clones that do not behave consistently with the majority of the clones.

TABLE 4.1: Total number of genes differentially expressed by the induction of WT1 isoforms

Isoform	**Gene number**
+/+	103
+/-	874
-/+	3032
-/-	306

4.2 Expression analysis by microarray

In order to explore the different roles of the main four isoforms of WT1, I decided to analyse the transcriptome of induced and non-induced single MDCK clones. The expression analysis was performed on one mCherry clone per isoform, namely +/+ 2, +/- 4, -/+ 6 and -/- 1. The cells were grown in the presence or absence of Dox at the concentrations stated in Table 3.1 for 96h. The time point was chosen based on preliminary results, showing changes in cell morphology occurring after 4 days of induction of certain isoforms. The mRNAs of three independent experiments were sent to the Edinburgh Genomics facility at the Roslin Institute, where the mRNAs were hybridised on the Affymetrix Canine Gene 1.1 ST microarray. The resulting data were sorted in .CEL files that were then analysed by Graeme Grimes, who determined the differently expressed genes between each induced clone and the respective control. Table 4.1 summarises the numbers of genes whose expression levels changed following the induction of each isoform. Considering that the -KTS isoforms are regarded to function efficiently as transcriptional factors, while the +KTS isoforms seem to be more implicated in post-transcriptional regulation, it was maybe unexpected to find that the induction of the -/+ isoform led to the highest number of differentially expressed genes. Nonetheless, this result highlights the importance of the -/+ isoform, which has the highest expression levels among the conserved isoforms [12].

I then looked for enriched Gene Ontology (GO) terms using the free online tool GOrilla (http://cbl-gorilla.cs.technion.ac.il/), which identifies and visualises enriched GO terms

in a given gene list [171]. The most relevant enriched GO terms per isoform and the relative P-values are summarised in Figure 4.2.

+/+	+/-	-/+	-/-	
Response to external biotic stimulus	Response to virus			P value < 10^-9
	Cholesterol biosynthetic process			
	Response to external biotic stimulus		Response to external biotic stimulus	P value 10^-7 – 10^-9
			Response to stress	
Response to molecule of bacterial origin	Regulation of lymphocyte migration	Regulation of cell motility	Regulation of leukocyte migration	P value 10^-5 – 10^-7
Positive regulation of immune system process		Cell junction organization	Chemokine mediated signalling pathway	
		Regulation of cell communication	Positive regulation of chemotaxis	
		Regulation of vasculature development	Inflammatory response	
Response to stress	Cytokine production involved in immune response	Response to cytokine	Regulation of cell motility	P value 10^-3 – 10^-5
Regulation of inflammatory response	Positive regulation of chemotaxis	Regulation of immune response	Regulation of cell cycle and proliferation	
Response to cytokines	Regulation of cell cycle and proliferation	Cell chemotaxis	Regulation of angiogenesis	
Leukocyte chemotaxis		Regulation of cell cycle and proliferation		
		Extracellular structure organization		
		Cell adhesion		
		Actin cytoskeleton organization		

FIGURE 4.2: Most relevant enriched GO terms and corresponding P-values from the microarray analysis by GOrilla.

From this analysis, it was clear that the induction of all the isoforms was leading to the activation of an immune and inflammatory response. In particular, there was a significant upregulation of various cytokines, which seemed to be mainly involved in the chemotaxis of leukocytes. All the isoforms, with the exception of the +/+, seemed to affect the expression of genes involved in cell proliferation and cell cycle, while the isoforms lacking the exon 5 appeared to influence also the levels of genes implicated in cell motility.

Quite surprisingly considering that there were only 30 common genes differentially expressed by all the isoforms, the cellular processes overall influenced by the induction of the single isoforms was not strikingly different. The Venn diagrams in Figure 4.3 represent the numbers of common and unique genes upregulated or downregulated

across the clones. The names of the genes that belongs to every section of the diagrams are listed in the Appendix section A.2.

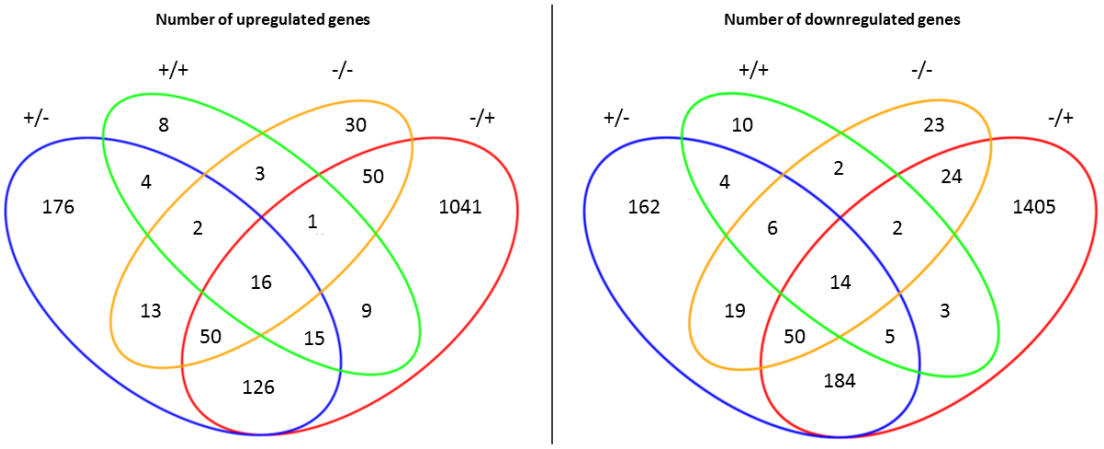

FIGURE 4.3: Venn diagrams representing the number of common and unique genes upregulated (on the left hand side) and downregulated (on the right hand side) by the induction of single WT1 isoforms in the MDCK clones according to analysis of the microarray data.

Only the induction of the -/+ isoform showed clear isoform-specific changes, as well as the highest number of genes uniquely regulated. In fact, its expression was predicted to alter components of the cell junctions, cell adhesion, the network of the actin cytoskeleton and the organization of the extracellular matrix.

I decided to validate by Q-RT-PCR the changes in expression of some key genes identified by the microarray analysis, using for each isoform two different mCherry clones, as well as a clone expressing the protein not fused to an FP. I chose to include a w/o FP clone aiming to verify whether the fusion of WT1 with a fluorescent marker was affecting its functions. In order to confirm that the changes were not due to the presence of the Dox or to the mCherry protein, I compared the levels of expression also with a mCherry EV clone. Employing the same three clones per isoform as well as the EV clone, I investigated whether WT1 isoforms were involved in the regulation of cell cycle, proliferation and motility by performing different cell-based assays.

4.3 WT1 isoforms induce the expression of different chemokines in the MDCK clones

Among the GO terms that the microarray analysis pointed out, the initiation of a pro-inflammatory response and the chemotaxis of leukocytes seemed to be common features characterising all the induced clones. I therefore decided to validate the overexpression of some genes included in the GO terms, focusing on the variation of expression of different chemokines.

The chemokines are a family of chemotactic cytokines that play a pivotal role in the regulation of leukocyte trafficking in both pathological and physiological conditions. It has become clear that the importance of various chemokines is not only limited to the development and function of the immune system, but it extends to different processes, such as angiogenesis, wound healing, tumour development and metastasis, as well as cellular senescence [172–174]. Moreover, recent studies have highlighted crucial roles of the chemokines in a variety of developmental processes, such as epicardium and mammary gland development, primordial germ cell migration, endodermal development and migration of sensory neuron progenitors [175–179]. Besides, different cell types outside the immune system produce chemokines even in the absence of an inflammatory response, for instance embryonic epicardial cells [175], primary mouse muscle cells [180] and human mesenchymal stem cells [181].

Chemokines exert their functions by binding to their cognate receptors, which belong to the G protein-coupled receptor family. Most chemokines are produced as secretory proteins, once secreted, they bind to endothelial cells and/or to the extracellular matrix via interaction with proteoglycans and glycosaminoglycans. Structurally, the chemokines are divided in two main subfamilies: the CXC group, which has an amino acid between the first two cysteine residues, and the CC subfamily, where the first cysteine residues are adjacent [172, 173].

I analysed by Q-RT-PCR the levels of expression of different chemokines in three 96h induced and non-induced single MDCK clones for each isoform (two mCherry clones and

one w/o FP clone as mentioned above) and in one 96h treated or untreated mCherry EV clone. For the statistical analysis, I decided to consider the three clones as three independent biological replicates. I reported the levels of expression of the chemokines in each single clone in Figure A.1 in the Appendix section. The gene expression levels of every sample were first normalized against the levels of the housekeeping gene *GAPDH*. I then calculated the relative fold change in the mRNA expression by comparing the levels of treated and untreated sample. If I observed differences in the expression between the +Dox mCherry EV sample and the corresponding -Dox sample, I took into account the effect of the Dox and the mCherry expression for the final calculation of the fold change value. Overall, inducing the mCherry expression in the EV clone downregulated the expression of the chemokines that I analysed, with the exception of the *CCL5* (Figure 4.4). The detailed method to estimate the fold change is written in the Materials and Methods section of the thesis.

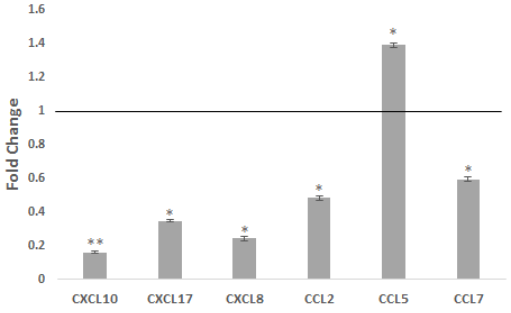

FIGURE 4.4: Q-RT-PCR to determine the levels of expression of different chemokines in the 96h induced mCherry EV MDCK clone. The gene levels were first normalized for the *GAPDH* expression levels. The chart represents the fold change of the mRNA expression in the +Dox samples relative to the levels in the -Dox samples. The fold change of the -Dox samples, which is equal to 1, is represented by the black horizontal line. SD of the mean of the fold changes of two technical replicates. *: P-value < 0.05, **: P-value < 0.01.

From the analysis of the Q-RT-PCR (Figure 4.5), I was able to validate the upregulation of three chemokines belonging to the CXC family, namely *CXCL10*, *CXCL17* and *CXCL8*. The mRNA levels of the first two molecules were consistently overexpressed in all the induced clones of every isoforms, reaching levels of expression tens or even hundreds of times higher than the controls. Although *CXCL8* expression was highly

enhanced in all the clones, the average upregulation was not statistically significant in the +/- clones, because of the high variability in the relative expression across the single clones. Besides, the different observed fold change values did not correlate with the relative WT1 +/- expression of the clones.

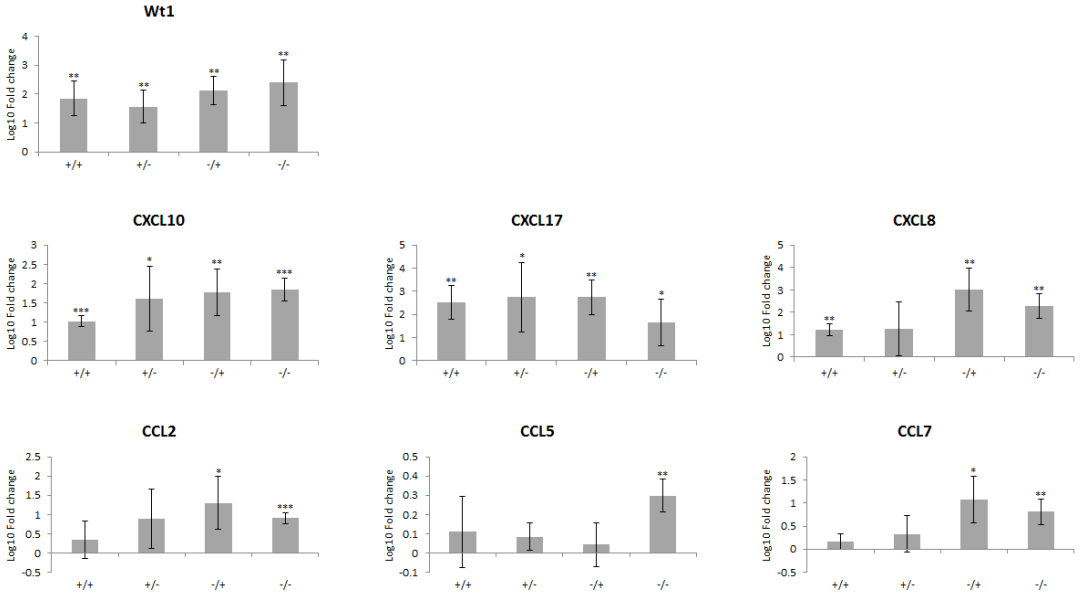

FIGURE 4.5: Q-RT-PCR to determine the levels of expression of different chemokines in 96h induced MDCK clones. The gene levels in each sample were first normalized for the *GAPDH* expression levels. The column graphs represent the Log10 fold change of the mRNA expression in the +Dox samples relative to the levels in the -Dox and EV samples. SD of the mean of the relative expression in three clones per isoform. *: P-value < 0.05, **: P-value < 0.01, ***: P-value < 0.001.

I then checked the changes in expression of three chemokines of the CC subfamily: *CCL2*, *CCL5* and *CCL7*. On average, the expression levels of the cytokines tended to increase, but there was strong variability in the fold changes across the single clones, underlying the presence of clonal differences. Nonetheless, I was able to ascertain that the induction of the -/- isoform led to the overexpression of all the investigated CC chemokines, that the induction of the -/+ isoform upregulated *CCL2* and *CCL7* mRNA levels in all the clones, whereas the expression of the isoforms lacking the exon 5 did not cause consistent changes in the gene expression levels.

Therefore, I concluded from this experiment that all WT1 isoforms are likely to promote the transcription of *CXCL10*, *CXCL17* and *CXCL8* genes, although we are measuring the mRNA steady state levels, therefore we cannot exclude post-transcriptional regulations. On the other hand, only the isoforms without the exon 5 seem to be involved in the upregulation of the expression of *CCL2* and *CCL7*. Specifically the induction of the -/- isoform consistently enhanced the transcription of all the CC chemokines analysed. Since the expression of these cytokines is a hallmark of inflammation and because all these molecules are involved in the chemotaxis of different types of leukocytes [172], I hypothesise that the expression of WT1 isoforms in the MDCK cells leads to the generation of a pro-inflammatory environment that potentially can attract leukocytes. Moreover, it would be interesting to study the possible consequences on other processes such as angiogenesis, as CXCL17 and CXCL8 are considered pro-angiogenic factor, whereas CXCL10 is supposed to be an angiostatic chemokine [172, 182].

In the past few years, different papers have suggested correlations between WT1 and some of the chemokines I found differentially regulated by the induction of WT1 isoforms. For instance, WT1 was proved to inhibit both directly and indirectly the expression of *Cxcl10* and *Ccl5* during epicardium development in mice, where they reduce epicardial cell migration and cardiomyocyte proliferation respectively [175]. The fact that in kidney cells WT1 activates both *CXCL10* and *CCL5* genes might suggests that WT1 can induce or inhibit them in a tissue- and context-dependent manner. Recently, a correlation between the expression of *WT1* and *CXCL8* has been proposed: in fact, the mRNA levels of *CXCL8* decreased upon silencing of *WT1* in a cell line of squamous cell carcinoma of the head and neck [183]. Moreover, both *CXCL8* and *CCL7* were found upregulated in a leukaemia cell line stably transfected with the +/- WT1 isoform, but not with the +/+ variant [184]. Finally, *CCL2* and *WT1* were found to be co-expressed in different human lung cancer cell lines [185].

4.4 The induction of WT1 isoforms impairs the cell proliferation and the cell cycle only in specific clones

The analysis of the enriched GO terms in the microarray pointed out a possible involvement of the +/-, -/+ and -/- isoforms in the regulation of cell proliferation and cell cycle in the MDCK clones. In the literature there are many papers that relate WT1 to the control of these two cellular processes. However, not all the studies reached concordant results. In fact, depending on the cell model used or on the method employed to overexpress or inhibit WT1 expression, WT1 was found to either impair or enhance cell proliferation. For example, in 1993 Haber et al showed that the transfection of the four main isoforms of WT1 suppressed the growth of a human Wilms tumour cell line [94]. Later on, Morrison et al proposed that the induction of WT1 -/- in an osteosarcoma cell line transactivates the mitogen-activated protein kinase phosphatase 3 (MKP3), a negative regulator of the Ras/MAPK pathway, leading to growth arrest [102]. Moreover, WT1 -KTS mediated cell cycle arrest in the same cell line has been associated with induction of the cyclin-dependent kinase inhibitor 1A gene (*CDKN1A*), also known as p21 [95]. Other evidence advocating the growth inhibitory effect of WT1 come from two studies that showed how the transduction of WT1 -/- in human hematopoietic progenitor cells and in leukemia-derived cell lines led to growth arrest and differentiation [96, 97]. Furthermore, Murata et al reported that the overexpression of the +/- isoform in myeloblastic leukaemia cells led to G1 arrest and increased apoptosis [98].

On the other hand, the exogenous expression of all WT1 isoforms in two human breast cancer cell lines, in a leukemic line and in KRAS mutant lung cancer cell lines was shown to stimulate cell proliferation by activating the c-Myc promoter [186, 187]. However, a previous study reported that both WT1 -KTS and +KTS actually repressed c-Myc promoter in transiently transfected Hela cells [188]. Supporting a pro-proliferative role of WT1, Algar et al showed that the abrogation of WT1 protein expression by antisense oligonucleotide blocked cell proliferation in myeloid leukaemia cell lines [125]. Moreover, WT1 knockdown was proved to reduce the cell growth of a malignant peripheral nerve

sheath tumour cell line, by decreasing the protein levels of cyclin D1 and inhibiting Akt phosphorylation [126]. Similarly, the silencing of WT1 in a murine melanoma cell line led to impaired cell proliferation and increased apoptosis [127].

Taken together, these results indicate that WT1 can influence cellular proliferation in a cell type-dependent manner, highlighting how this transcription factor can play dichotomous functions depending on the contexts.

4.4.1 Analysis of the proliferation of the MDCK single clones

In order to verify whether WT1 induction was influencing the cell growth of the mCherry and w/o FP MDCK inducible cells, I decided to follow the proliferation of the clones over 8 days of Dox treatment. The same number of cells was seeded in as many 6 well plates as the time points analysed. The following day I either added or not the Dox and at each time point I fixed and stained the cells with crystal violet, which binds the DNA. After dissolving the dried crystal violet, I measured its absorbance at 595 nm, which is proportional to the amount of cells in each well. With this method I determined the growth curve for each induced and non-induced clone (Figure 4.6).

I first confirmed that the presence of Dox was not affecting the proliferation of the mCherry EV clone. As predicted by the microarray analysis, the +/+ isoform did not impair the growth of any induced clone. The proliferation of the induced +/- 4 clone, which was analysed by the array, was indeed slower than the control. However, I did not see differences in the other two +/- clones analysed. The discrepancy in the outcomes is unlikely to be due to different protein expression levels of the isoform across the clones, as the mCherry +/- 4 and the w/o FP clones seem to have comparable levels of WT1 protein after 96h of induction (Figure 4.1). Therefore, I assume that the inconsistent results are due to basic clonal differences. On the other hand, the induction of both the -/+ and -/- isoforms inhibited the growth of the two mCherry clones, but not of the w/o FP clones. Once again, the results do not seem to be related to different expression levels of WT1, as the expression of the -/+ isoform was balanced across the

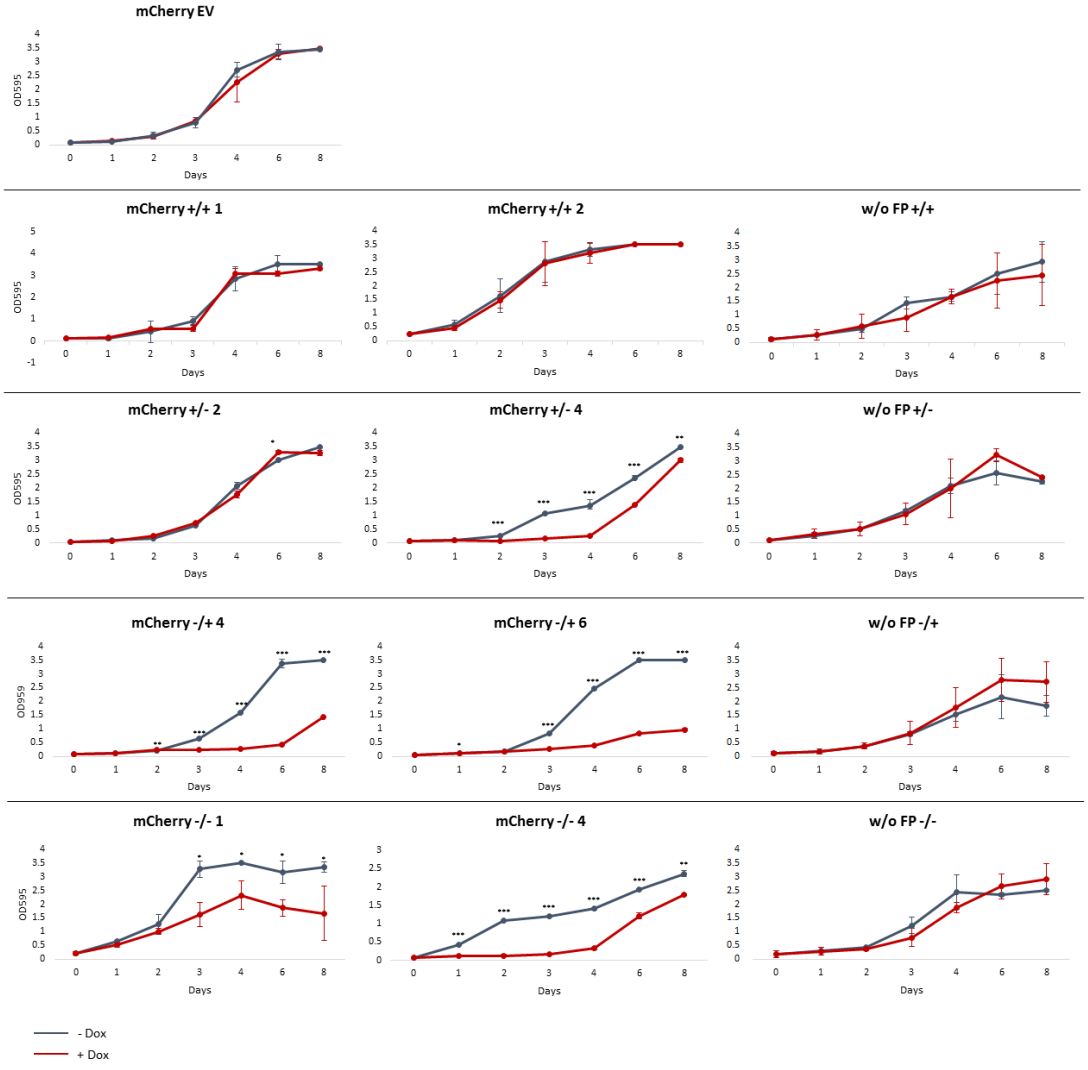

FIGURE 4.6: Growth curves of the induced and non-induced MDCK clones. SD of the mean of two independent experiments.*: P-value < 0.05, **: P-value < 0.01, ***: P-value < 0.001.

clones and the induction of the -/- w/o FP clone seems to lead to the highest expression levels (Figure 4.1). The result might suggest that the fusion of the mCherry to WT1 somehow influences its functions. However, in order to start confirming this hypothesis it will be necessary at least to test more w/o FP clones.

4.4.2 Testing whether WT1 affects the phases of the cell cycle

I investigated whether the induced MDCK clones showed impaired cell cycle compared with the Dox controls. To this aim, I stained the cells with Propidium iodide (PI) after 96h and 8 days of induction and I analysed by FACS the cells in G1, S and G2 phase. On average, the percentage of cells in each phase across the three clones per isoform was not affected by WT1 induction (Figure 4.7).

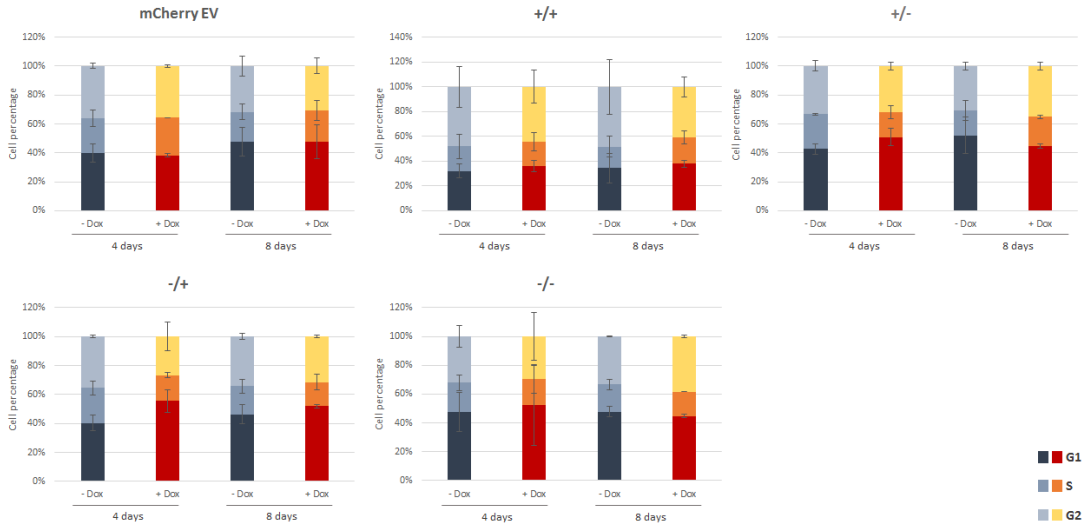

FIGURE 4.7: Percentages of cells distributed in G1,S and G2 phases of the cell cycle in induced and non-induced MDCK clones after 4 and 8 days. SD of the mean of three clones per isoform. Two independent experiments were carried on for each clone.

Thus, this result suggests that the cell cycle of the clones is not impaired by the expression of any of the isoforms. However, I noticed that the mCherry -/+ clones were behaving clearly differently. Indeed, their cell cycle was arrested in G1 phase at either 4 or 8 days of induction (Figure 4.8). This result contrasts with the previously reported

observation that the +KTS variants do not influence the cell cycle of a transiently transfected human osteosarcoma cell line [95].

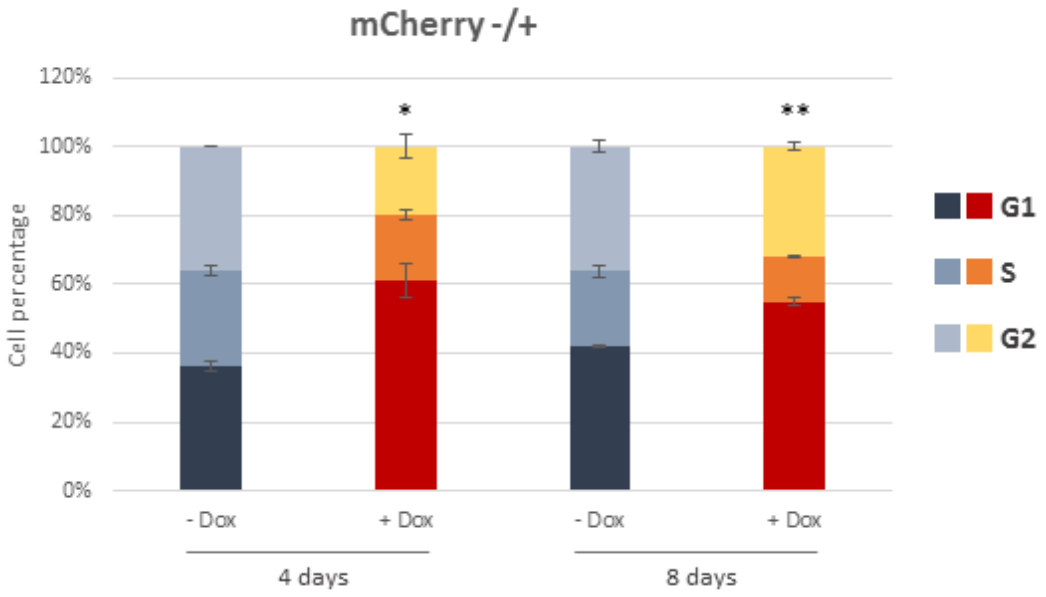

FIGURE 4.8: Percentages of cells distributed in the cell cycle phases of two induced and non-induced mCherry -/+ MDCK clones after 4 and 8 days. SD of the mean of two clones per isoform. Two biological replicates were done to analyse each clone. *: P-value < 0.05, **: P-value < 0.01.

Since none of the main genes involved in G1-S progression or arrest was found differentially expressed in the microarray analysis of the -/+ 6 mCherry clone, I thought that the block in the G1 phase might have been caused by post-transcriptional regulation of one of the regulator of the cell cycle progression. Knowing that *CDKN1A* mRNA levels are upregulated by the ectopic overexpression of a -KTS variant [95], I tested whether the induction of the -/+ isoform could induce p21 protein expression in the mCherry -/+ 6 clone. To this aim, I visualized by WB the levels of p21 after 96h of induction. Because I noticed that many antibodies did not actually work in canine cells, I decided to use as positive controls both MDCK and Hela cells treated O/N with 10 nM of Actnomycin-D, which is known to induce p21 expression. By this assay, I confirmed that p21 protein levels were upregulated upon WT1 -/+ induction in the mCherry -/+ 6 clone (Figure 4.9), providing a possible reason for the block in the cell

cycle seen by FACS. It is important to mention that a study demonstrated that the overexpression of WT1 leads to G1 phase arrest through the downregulation of CDK4- and CDK2-associated kinase activity, without affecting the levels of CDK4, CDK2 and cyclin D1 [189].

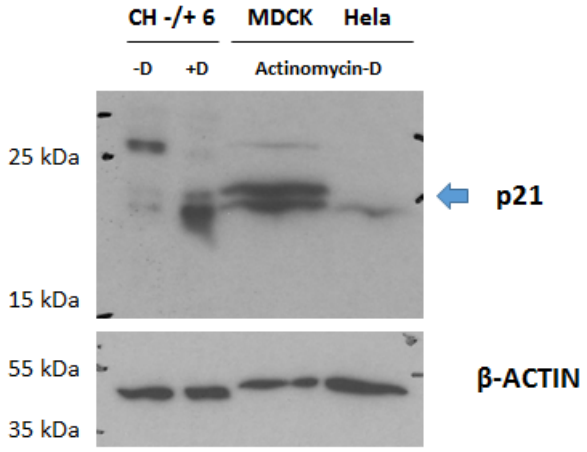

FIGURE 4.9: WB: p21 protein levels in 96h induced and non-induced -/+ 6 mCherry clone. The protein extracts of Hela and MDCK cells treated O/N with 10 nM Actinomycin-D were used as positive controls. The arrow points the specific band for p21.

From the two cell-based assays described in this section, I cannot conclude for sure that the induction of different WT1 single isoforms affects the proliferation or the cell cycle of the MDCK clones. The results highlight initial and basal differences across the single clones that could be potentially minimise testing more clones. Moreover, some data concerning the isoforms lacking the exon 5 have underlined differences between the mCherry and the w/o FP clones, indicating a possible interference of the FP with the activity of the transcriptional factor that should be further investigated. A paper published in 2015 has indeed reported a case in which the enzymatic activity and localization of the procaspase 1 was impaired by its fusion with the mCherry marker [190].

4.5 The motility of certain stable clones is influenced by WT1 induction

In order to assess whether the induction of single isoforms of WT1 affected the cell motility of the MDCK single clones, I decided to perform a wound healing assay, which is a well-established method to measure the migration of cells *in vitro*. The MDCK clones were cultured in the presence or absence of Dox. On the third day of induction an equal number of induced or non-induced cells was transferred in both sides of a culture insert, which has a 500 μm cell free gap. After 96h of induction the cells reached full confluence, the inserts were then removed and the cells were live imaged for 48h. I then calculated the speed of the cells by measuring the area covered and divided it by the time taken to fill it in (Figure4.10).

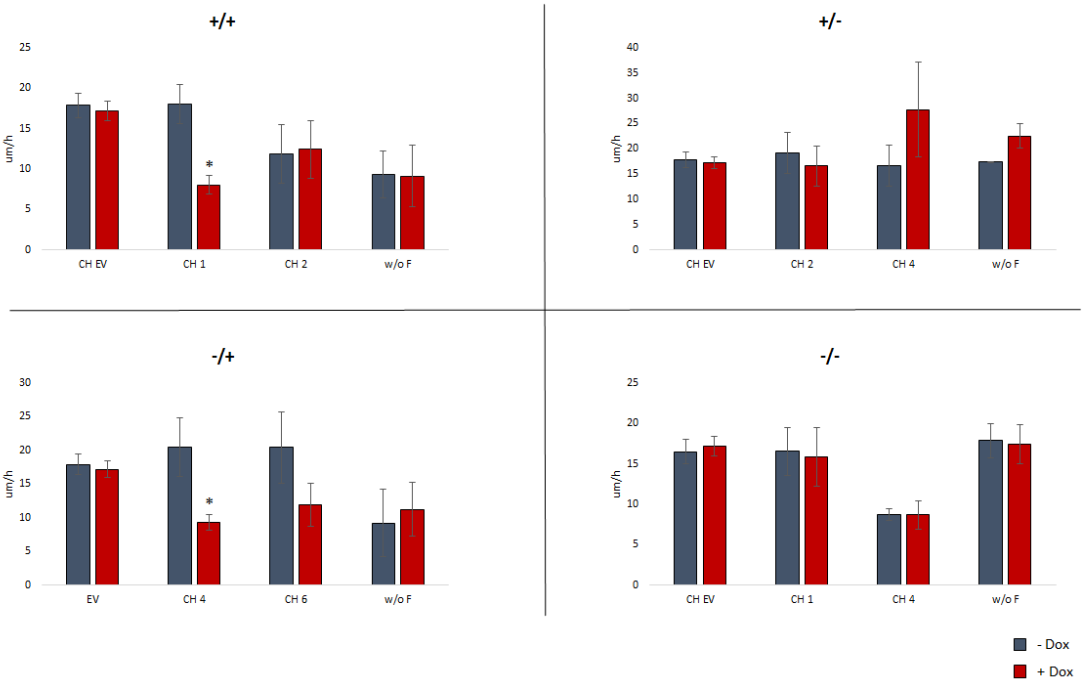

FIGURE 4.10: Wound healing assay: the column graph represents the speed (μm/h) of 96h induced or not induced MDCK clones (two mCherry clones and one w/o FP clone for each isoform, plus a mCherry EV clone). The velocity has been calculated dividing the maximum area covered within 48h for the hours taken to fill that area in. SD of the mean of two biological replicates.*: P-value < 0.05.

Importantly, I confirmed that the migratory potential of the mCherry EV clone was not affected by the Dox treatment. As the microarray analysis suggested, the induced mCherry -/+ clones showed different cell motility. In fact, they were slower than the controls in closing the wound. However, the w/o FP -/+ clone did not behave in the same way, highlighting once again the unique properties of this clone. Opposite from what expected from the expression analysis, the induction of the -/- isoform did not affect the time needed to close the wound, indicating that at least the speed of migration of the cells was not compromised. On the other hand, the expression of the +/- isoform in the clone number 4 seemed to unexpectedly lower the time to close the gap. However, the difference with the control is not statistically significant as only two replicates were performed for each clone. Surprisingly, the induction of the mCherry +/+ 1 clone led to a statistically significant reduction of the migration speed. Figure 4.11 shows representative images of the clones that showed significant differences at 24h of live imaging.

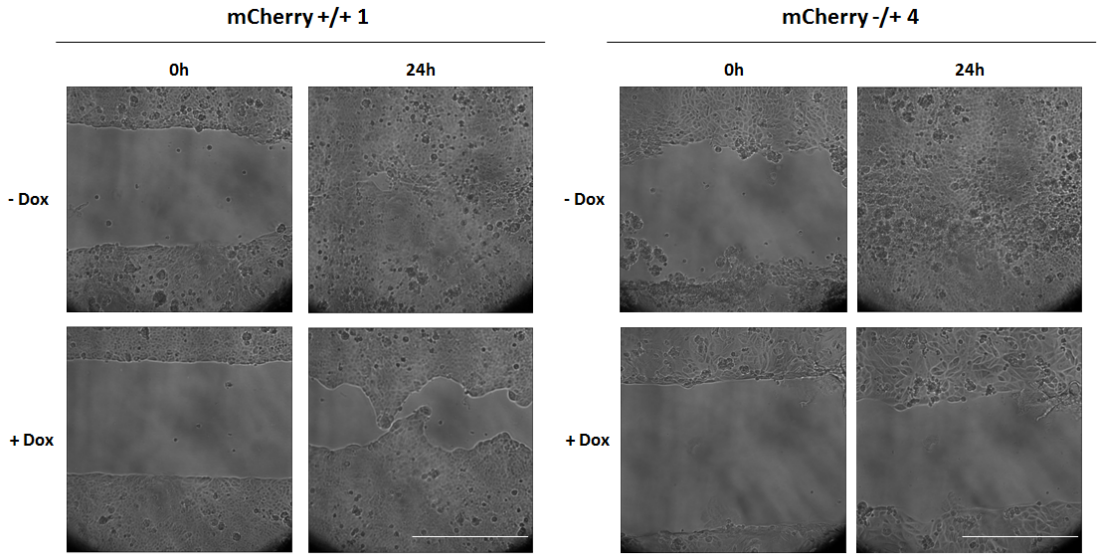

FIGURE 4.11: Wound healing assay: bright field images of the MDCK clones that showed an impaired velocity in the closure of the wound under induction. The images were taken at 0 and 24h from the start of the live imaging. Scale bar = 500 μm.

The fact that WT1 influences cell migration ability has been previously reported. For instance, the overexpression of WT1 in a non-small-cell lung cancer cell line, as well

as in prostate cancer cells, was found to promote cell motility via suppression of the E-cadherin [191, 192]. Accordingly, the downregulation of WT1 by siRNA in ovarian cancer cells led to a slower migration compared to the controls [193]. Moreover, Jomgeow et al showed that the constitutive expression of the -/- isoform in an ovarian cancer cell line promoted cell migration by modulation cytoskeletal dynamics [194]. Overall, these papers suggest that WT1 increases the cell migration ability of human cancer cell lines. However, until now there are no data reporting WT1 influence in motility of non-transformed cells.

4.6 Assessing the induced clones ability of growing without anchorage

I decided to assess whether the induction of the single isoforms of WT1 was affecting another aspect of the cell growth, which is also regarded as a sign of cell transformation: the ability of anchorage-independent growth. Over the years, the tumorigenic capacity of the MDCK cells have been a matter of debate. In 2011 a detailed analysis of the tumorigenicity of 3 different lots of unmodified MDCK cells concluded that all the batches were indeed tumorigenic in athymic nude mice, even if they showed heterogeneous tumour-forming capacity and tumor latency [195].

In order to understand whether WT1 isoforms affected the potential of anchorage-independent growth of the cells, I performed soft agar colony formation assays. I therefore compared the number (Figure 4.12) and the size of the colonies forming from induced and non-induced cells after 3 weeks.

I noticed that just adding the Dox to the mCherry EV clone led to a higher number of colonies, but the difference with the control was not statistically significant. Nor was the number or the size of the colonies forming from the MDCK +/+ clones affected by the induction of the isoform. On the other hand, the +/- isoform impaired the number and reduced the size of the colonies when induced in the clone number 4, underlying

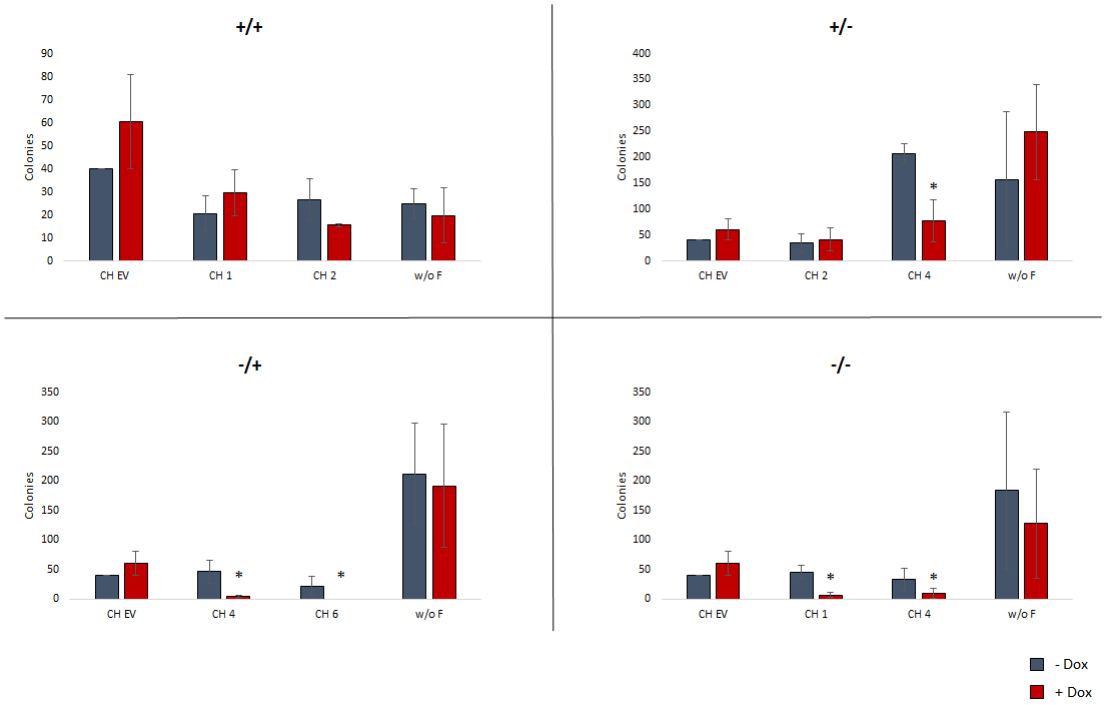

FIGURE 4.12: Soft agar colony formation assay in MDCK clones: number of forming colonies after 3 weeks of growth in media with or without Dox. SD of the mean of two biological replicates. *: P-value < 0.05.

once again the peculiar properties of this clone (Figure 4.13). Similarly, both the induced mCherry -/+ clones showed a drastic reduction in the number of colonies when compared with the respective controls (Figure 4.13). The anchorage-independent growth of the -/+ w/o FP clone, though, was not affected by the expression of WT1. Overall, it looked like all the +/- and -/+ clones that showed inhibited cell proliferation upon induction also formed fewer colonies in soft agar. Lastly, the induction of WT1 -/- in the mCherry clones was almost nullifying the cell growth in soft agar. Moreover, even if the number of forming colonies was not statistically different between the w/o FP induced and non-induced cells, the colonies formed by the induced cells were visibly smaller (Figure 4.13). Therefore, I determined that the -/- isoform was the only variant that consistently inhibited the growth in soft agar of all the clones analysed. Hence, WT1 -/- could be involved in the impairment of the oncogenic potential of the MDCK cells.

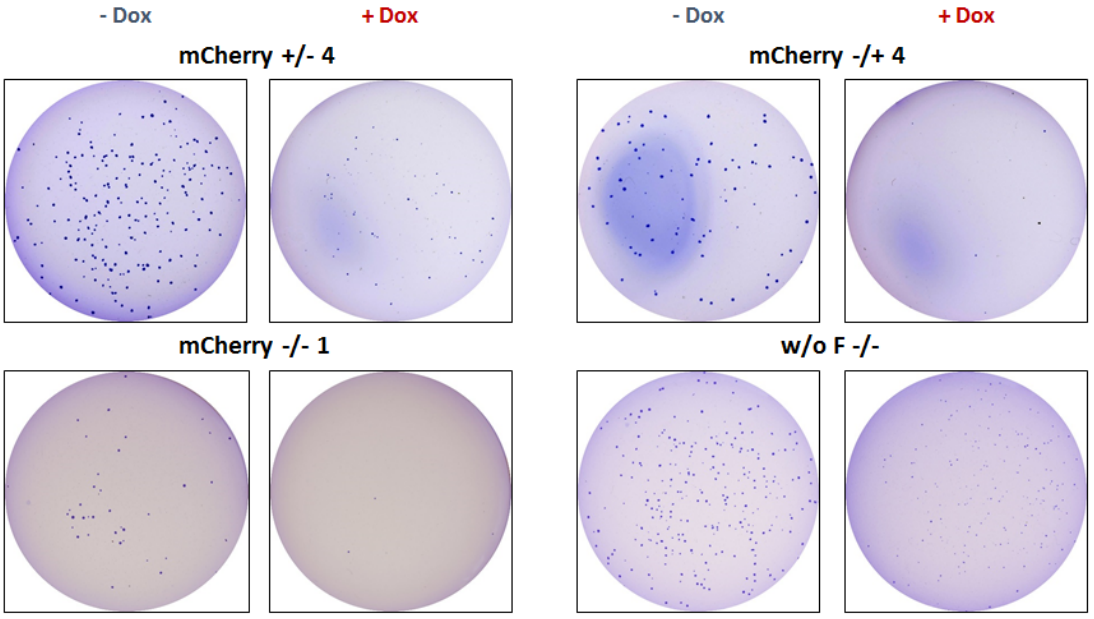

FIGURE 4.13: Soft agar colony formation assay in MDCK clones: representative images of the colonies forming from mCherry +/- 4, -/+ 4, -/- 1 and w/o FP -/- clones after 3 weeks of growth in the presence or absence of Dox.

According to the some of the data presented in this section, WT1 was reported to compromise the ability of anchorage-independent growth in certain cell lines. For instance, the stable transfection of the transcriptional factor in a cell line established from a Wilms' tumour explant reduced the number of colonies grown in soft agar [99, 105]. Furthermore, the +KTS isoforms, and in particular the -/+ variant, inhibited the clonogenicity of a murine myeloblastic leukaemia cell line [100]. On the other hand, the +/- isoform, but not the +/+, impaired the forming colony ability of another leukaemia cell line in a methylcellulose semi-solid medium [184]. WT1 was also found to suppress the clonal growth of a breast tumour cell line in soft-agar [101]. Finally, a WT1-derived peptide was shown to be an antitumor agent that suppresses both proliferation and soft agar colony formation in a melanoma cell line [196].

4.7 About the mCherry -/+ MDCK clones

I will dedicate the last section of this chapter to the explanation of some intriguing, even if unique, characteristics of the two mCherry -/+ WT1 clones. As I have shown so far, these two clones behaved differently from their w/o FP counterpart in the cell-based assays I performed. Indeed, their proliferation was inhibited upon induction, probably because of the block in G1 phase, which is possibly due to the post-transcriptional upregulation of p21. Moreover, the induced cells speed in migration was lower than the controls and they formed a strikingly reduced number of colonies in soft agar. Therefore, WT1 -/+ seems to exert anti-tumour functions when induced in the two clones. Moreover, the microarray analysis highlighted some significant isoform-specific changes, which now I can also argue to be mCherry clones-specific.

4.7.1 The induction of the -/+ isoform in the mCherry clones leads to drastic morphological changes and the appearance of multinucleated cells

After only 48h from the activation of the mCherry-WT1 -/+, it was noticeable that the morphology of the cells was different from the non-induced cells. At 96h, the morphological changes were very clear, with the induced cells being remarkably and visibly bigger in size than the controls (Figure 4.14).

I investigated whether the changes in the phenotype were associated with an alteration of the cell junction organization. I therefore decided to visualize by IF the localization of two proteins involved in cell-cell adhesion: the E-Cadherin, an adhesion molecule with central roles in epithelial cell behaviour, and ZO-1, component of the tight junctions. The staining showed that neither the E-cadherin nor ZO-1 were mislocalized in the 96h induced cells, as they were not lost from the cell-cell junctions and the antibodies clearly stained the cell-cell borders. However, the IF pointed out another characteristic of the induced cells: the presence of multinucleated cells (Figure 4.15). Interestingly,

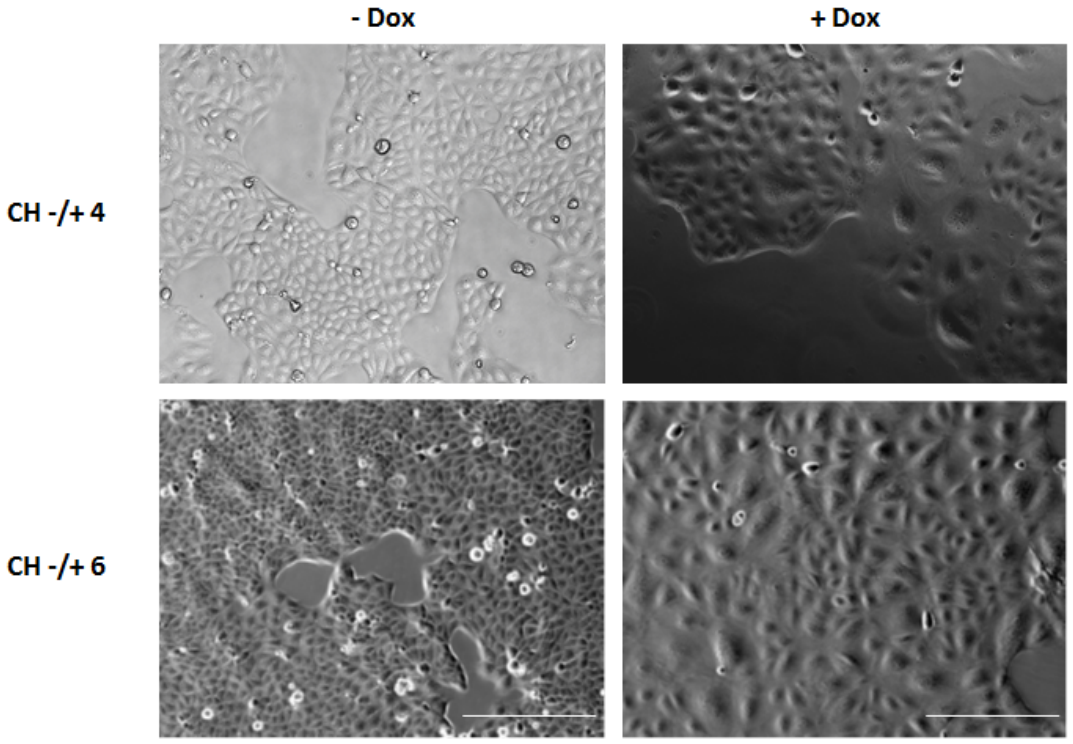

FIGURE 4.14: Bright field images of the two mCherry -/+ MDCK clones after 96h of growth in +Dox or -Dox media. Scale bar = 500 μm.

the appearance of large and multinucleated cells has been already reported in a Wilms' tumour cell line stably transfected with the -/+ isoform [105].

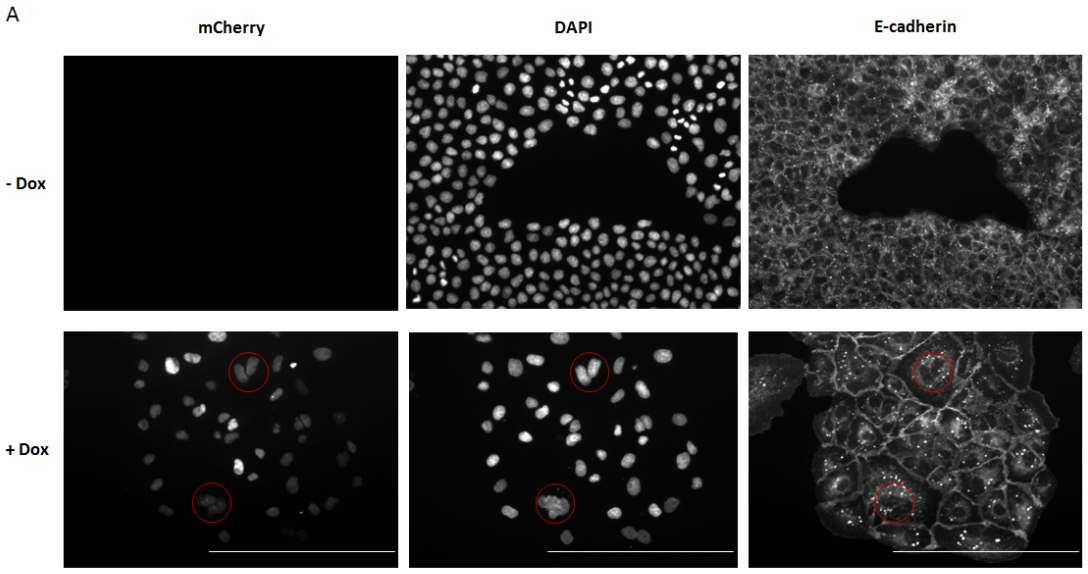
A
mCherry
DAPI
E-cadherin
- Dox
+ Dox

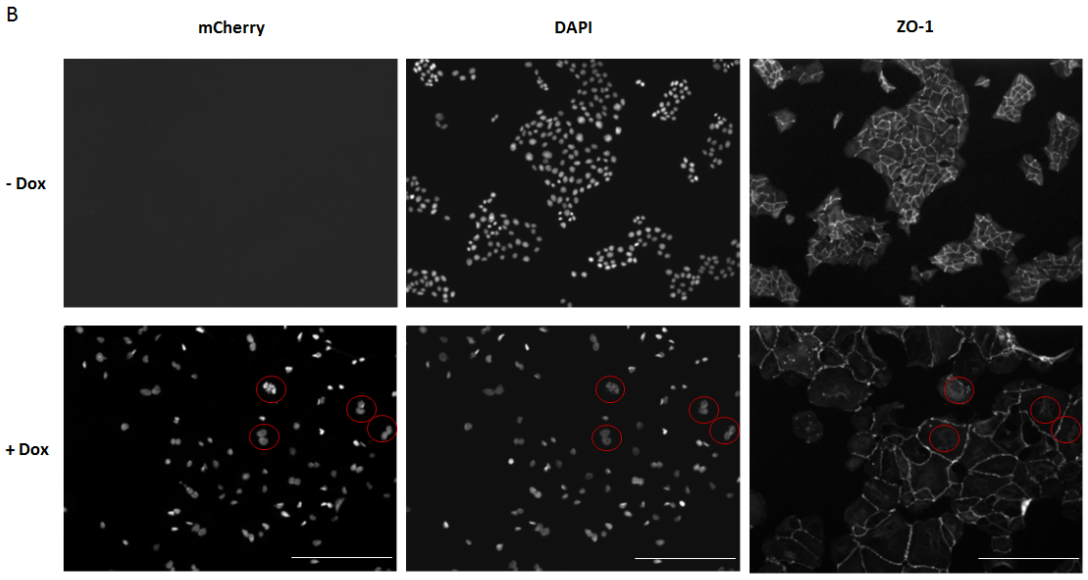
B
mCherry
DAPI
ZO-1
- Dox
+ Dox

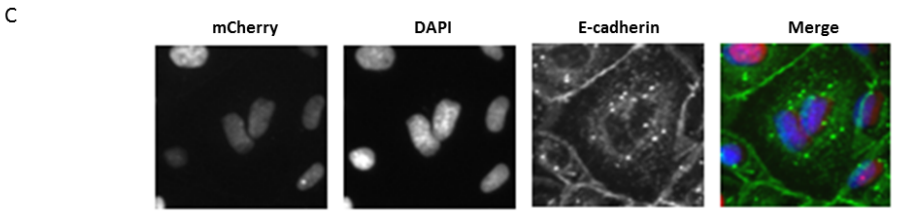

FIGURE 4.15: A: E-cadherin staining in 96h induced and non-induced mCherry -/+ 6 MDCK clone. Left panel: mCherry fluorescence, middle panel: DAPI staining, right panel: IF with the E-cadherin antibody.B: ZO-1 staining in 96h induced and non-induced mCherry -/+ 6 MDCK clone. Left panel: mCherry fluorescence, middle panel: DAPI staining, right panel: IF with the ZO-1 antibody. The red circles highlight examples of multinucleated cells. Scale bar = 500 μm. C: Magnification of a multinucleated cell among the 96h induced mCherry -/+ 6 MDCK cells. From the left hand side: mCherry signal, DAPI and E-Cadherin stainings, merge of the signals.

I noticed that the morphology of the induced cells reminded the one of the giant multinucleated cells. Multinucleated giant cells are well-known to form from macrophage origin; nonetheless, also other cell types, such as primary-derived murine fibroblasts, have been reported to form them, even in the absence of co-cultured macrophages. This phenomenon can be due to cell fusion or to nuclear division without cytokinesis. It has also been shown that these cells can arise as a response to a foreign body, as well as in fibrosis, cancer and aged tissues [197].

4.7.2 The induced clones show evidences of cell senescence

Based on the data collected so far, I decided to test whether the -/+ clones presented signs of cellular senescence after induction. In fact there were some hints suggesting that the cells were undergoing senescence upon induction: I determined that the induced cells had a block in G1 phase of the cell cycle, that they were much bigger than the controls and that they produced chemokines like CCL2 and CXCL8, which have been associated with the senescence-associated secretory phenotype (SASP) [174, 198]. Moreover, it has been shown that the multinucleated giant cells risen from primary fibroblasts have senescent-like features [197]. I therefore stained the cells with X-gal, which detects an increase in the β-galactosidase activity, a marker generally associated with cellular

senescence [199]. Both the clones stained positive at 96h of Dox treatment (Figure 4.16), indicating that the cells were possibly undergoing senescence.

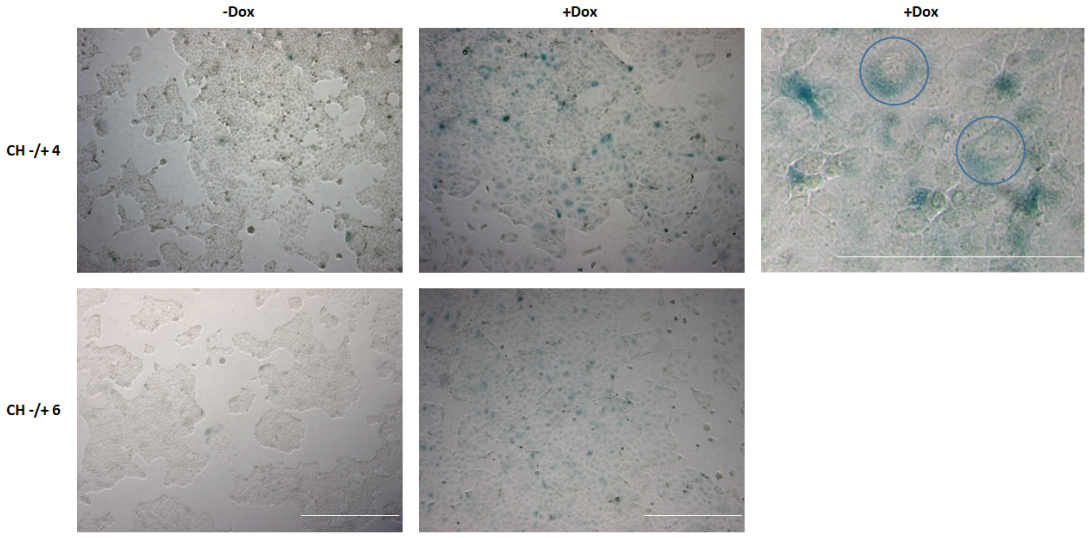

FIGURE 4.16: X-gal staining of the two mCherry -/+ MDCK clones after 96h of induction.The high magnification image on the left hand side shows x-gal positive multinucleated cells highlighted by blue circles. Scale bar = 500 μm.

One of the main hallmarks of senescence is permanent and irreversible growth arrest, indeed so far there are no physiological stimuli that are known to reverse the process [200]. However, when I removed the Dox after 8 days of induction, the MDCK -/+ cells completely reversed their phenotype after just 4 days of growth in the absence of Dox. In fact, the cells upon Dox removal became smaller, resembling the size of cells that have not been induced (Figure 4.17 shows the example of the -/+ 6 clone). The reversed cells kept growing to a rate comparable to the non-induced cells and they did not show any sign of cellular senescence.

Moreover, the nuclear DAPI staining never highlighted the presence of senescence-associated heterochromatic foci (SAHF), another typical feature of senescent cells [200]. I also checked whether the -/+ isoform was inducing a DNA damage response, which is one of the main factors that leads to senescence [200]. I thus tested the presence of γH2AX, a marker for DNA double stranded breaks [201]. However, no phosphorylation of the H2AX histone was detected (data not shown).

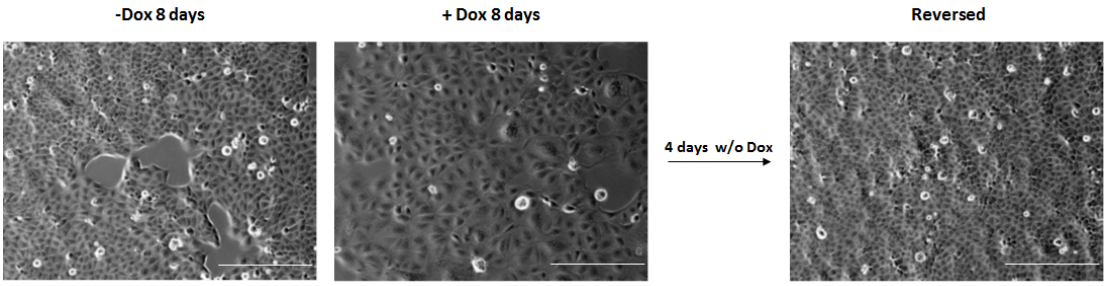

FIGURE 4.17: Reversible phenotype of the mCherry -/+ 6 MDCK clone. Bright field images of 8 days non-induced/induced cells and of 8 days induced cells after 4 days of Dox withdrawal. Scale bar = 500 μm.

Therefore, the induced MDCK mCherry -/+ clones presented some characteristics of senescent cells: increased β-galactosidase activity, enlarged size, pro-inflammatory chemokines production, block in the cell cycle and p21 overexpression. On the other hand, they could not be defined fully senescent cells, as the phenotype was reversible after Dox removal, indicating that the growth arrest was not permanent, and SAHF were never visible in the nuclei.

4.7.3 Remodelling of the actin cytoskeleton in the MDCK mCherry -/+ clones

The actin cytoskeleton has a pivotal role in various cellular processes, such as migration, morphogenesis, phagocytosis and cytokinesis. It is composed by actomyosin bundles that can form stress fibers, which are the major contractile structures of non-muscle cells and play a central role in cell adhesion and contraction. The fibers are often anchored to focal adhesions, which connect the actin cytoskeleton to the extracellular matrix (ECM). The bundles are prominent especially in certain types of cells, as fibroblast, smooth muscle and endothelial cells [202].

The microarray analysis suggested a possible involvement of the -/+ WT1 isoform in the organization of the actin cytoskeleton. In order to see whether the induction of the isoform indeed led to the remodelling of the actin cytoskeleton in the mCherry -/+ clones, I visualised the F-actin by probing 96h induced and non-induced cells with Phalloidin conjugated to a fluorescent dye. The staining showed a clear rearrangement of the F-actin organization, characterised by the clear appearance of prominent and thick stress fibers upon Dox induction (Figure 4.18).

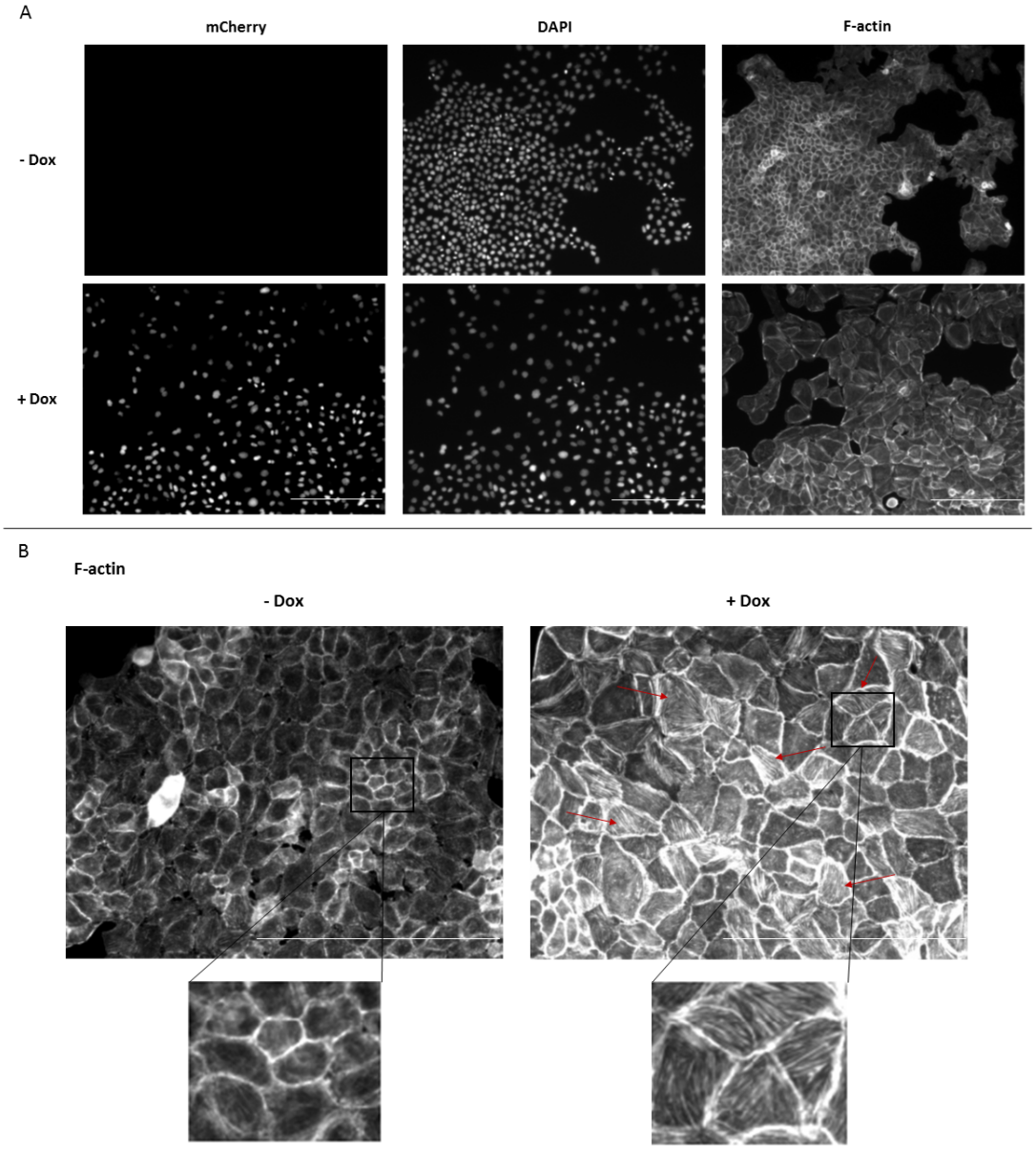

FIGURE 4.18: A: Phalloidin staining in the 96h induced and non-induced mCherry -/+ 6 MDCK clone. Left panels: mCherry fluorescence, middle panels: DAPI staining, right panels: F-actin staining. B: top panels: higher magnification images of the Phalloidin staining in 96h -Dox and +Dox mCherry -/+ 6 cells. The arrows point at the prominent and thick fibers in the Dox treated cells. Scale bar = 500 μm. Bottom panels: magnification of cells with equal F-actin staining from Dox treated and untreated cells.

The exact role of the stress fibers in cell migration has been so far elusive. Indeed, they are absent from some highly motile cells, such as leukocytes, and it has been proposed that they actually inhibit cell motility, rather than enhance it [202]. This hypothesis is corroborated by the actual compromised cell migration of the induced mCherry clones (Figure 4.10). Moreover, the stress fibers of non-motile cells are supposed to be thick and stable; by contrast, motile cells seem to contain fewer, thinner and more dynamic stress fibers [203]. Interestingly, it has been shown that the primary-derived giant multinucleated cells are characterised by prominent stress fibers [197].

It is important to mention that the second most overexpressed gene in the microarray analysis of the -/+ 6 mCherry clone was the transgelin gene (Log2 fold change: 6.28, adjusted P Value: 6.78 E-18). The name "transgelin" is due to its ability to induce gelation of the actin filaments in vitro. It has been reported that reducing the expression levels of the gene in fibroblast leads to less organized and potentially more dynamic actin cytoskeleton [204]. Importantly, high levels of transgelin have been observed also in senescent mammalian cells [205]. Thus, it would be interesting to investigate whether the actin cytoskeleton remodelling is caused by the transgelin upregulation.

4.7.4 The -/+ isoform induces changes in the organization of the ECM and fibrosis especially in the mCherry clones

To further characterise the induced mCherry MDCK clones, I decided to validate by Q-RT-PCR some of the genes grouped in another GO term that resulted enriched from the analysis of the array: the organization of the ECM. The ECM is composed by a variety of proteins and polysaccharides, which are secreted by the cells and form an organized network in association with the cell surfaces. It not only provides an essential physical scaffolding, but it also initiates crucial signals for tissue morphogenesis, differentiation and homeostasis [206].

Comparing the expression levels of the genes in the 96h induced mCherry -/+ clones with the ones in the non-induced controls and in the mCherry EV clone, I confirmed

the upregulation of the matrix metalloproteinase 9 (*MMP9*), of different inhibitors of metalloproteinases, namely *TIMP2*, *TIMP3* and *TIMP4*, and of the type I collagen gene (*COL1A1*). Moreover, the cells were characterised by the overexpression of both *DESMIN* and *ACTA2* genes (Figure 4.19). Of note, the majority of these genes had fold changes tens or even hundreds times higher than the controls.

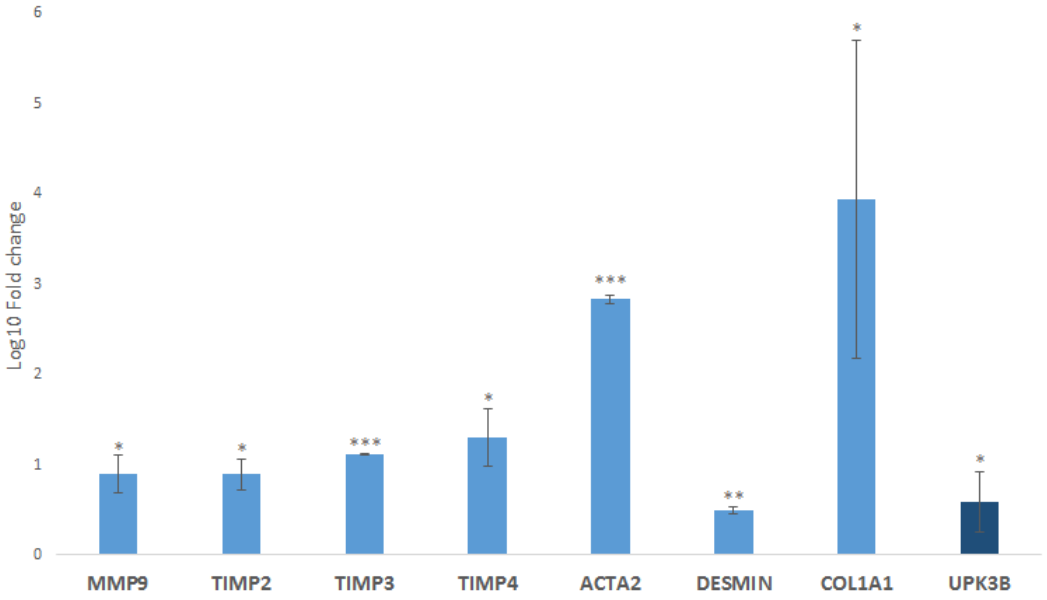

FIGURE 4.19: Q-RT-PCR of different genes highly overexpressed in the mCherry -/+ MDCK clones. Before calculating the expression fold changes, every gene level in each sample was normalized with the *GAPDH* levels. The column graph represents the Log10 fold change of the levels of expression in 96h induced clones relative to the expression in non-induced clones and in the induced EV clone. SD of the mean of the Log10 fold changes in the two clones. *: P-value < 0.05, **: P-value < 0.01, ***: P-value < 0.001.

It is important to mention that, although not to the same extent, some of these genes were overexpressed also in the induced -/+ w/o FP clone, namely *MMP9*, *TIMP3*, *TIMP4*, *ACTA2* and *DESMIN* (Figure 4.20). Hence, the data suggest that the induction of ECM remodelling genes is particularly enhanced in the mCherry clones, but also characterised the Dox treated -/+ w/o FP clone.

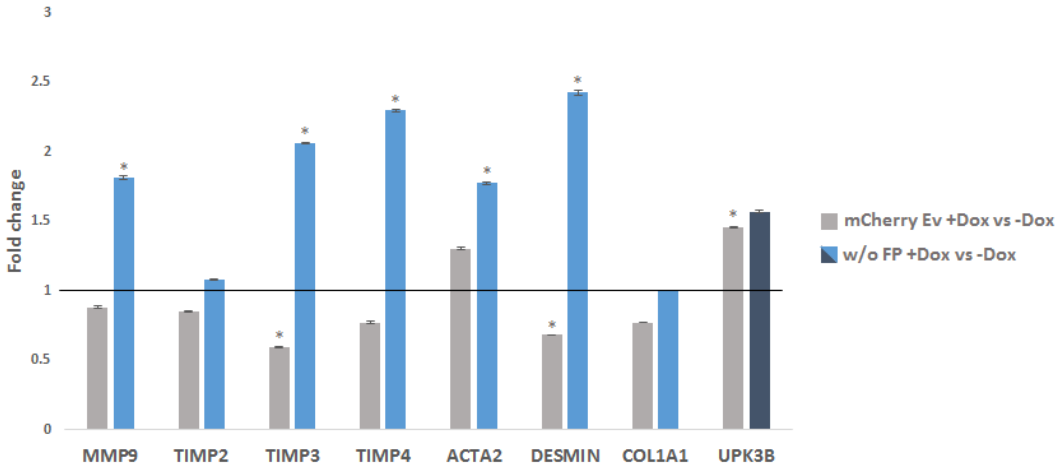

FIGURE 4.20: Q-RT-PCR to define the levels of expression of ECM remodelling genes and *UPK3B* in the induced MDCK w/o FP and mCherry EV clones. The levels of each gene were first normalized for the *GAPDH* expression. The fold changes were calculated comparing the levels in the +Dox samples versus the -Dox ones. Therefore, the reference fold change of the -Dox samples is equal to 1 and it is underlined by the black horizontal lines. SD of the mean of the fold changes of two technical duplicates. *: P-value < 0.05.

The overall upregulation of these genes suggests that the cells acquired a fibrotic phenotype after WT1 induction. Whereas the normal wound healing process is characterised by an injury, an inflammatory response, the activation of fibroblasts into myofibroblasts, and a final tissue remodelling and resolution phase, the fibrosis is a process marked by the excessive and uncontrolled deposition of ECM, which eventually leads to the loss of tissue functions. In particular, among the main constituents of the fibrotic lesions there is the interstitial type I collagen, which is highly upregulated in the mCherry -/+ induced clones. Moreover, many metalloproteinases, such as the MMP9, have been shown

to have pro-fibrotic functions. The metalloproteinases have a pivotal role in the maintenance of the ECM, being responsible of the turnover and degradation of many ECM components [207]. It has also been recognised that MMPs' functions extend to several other processes, such as cell migration, leukocyte activation and chemokine processing. Interestingly, the MMP9 processes and modulates the activation of the CXCL8 [208], which was found overexpressed in the induced -/+ MDCK clones. Several inhibitors of the MMPs have also been implied in the promotion of fibrosis, for example TIMP1 and TIMP2 were shown to mediate the activation of myofibroblasts in liver fibrosis. In contrast, TIMP3 is supposed to play anti-fibrotic functions in liver, lung and kidney fibrosis [207]. On the other hand, corroborating the hypothesis of a fibrotic-like phenotype, the *ACTA2* gene was significantly upregulated after Dox treatment. In fact, this gene encodes for one of the main markers used to identify fibrotic cells: the α smooth muscle actin. Another feature characterising the myofibroblasts, at least in liver fibrosis, is the expression of the *DESMIN* gene [140], which is overexpressed in the induced clones.

Interestingly, I also validated the overexpression of a mesothelial cell marker, the uroplakin 3B (UPK3B), in the induced mCherry -/+ cells (Figure 4.19). A link between mesothelial cells and fibrotic cells has been suggested. In fact Li et al proposed that mesothelial cells surrounding the liver are progenitor cells capable to differentiate into hepatic stellate cells (HSC), fibroblasts and smooth muscle cells. Furthermore, the authors suggested that mesothelial cells can give rise to HSCs and myofibroblasts during fibrosis, possibly through a mesothelial to mesenchymal cell transition. Although the expression of WT1 was heterogeneous in the mesothelial cell population, it seemed that WT1-negative cells were not able to undergo the transition [152].

The involvement of WT1 in fibrosis still needs to be extensively investigated. It has been shown that, following ischemic injury, epicardial fibrosis in mice is characterised by WT1 expression in subepicardial mesenchymal cells [138]. The re-expression of WT1 has also been noticed in a rat model of progressive tubulointerstitial fibrosis [139]. Moreover, WT1 positive cells were found in the fibrotic lesions in the lungs of patients

with idiopathic pulmonary fibrosis [153]. Interestingly, WT1 is expressed in the HSCs that are considered the main source of myofibroblasts in liver fibrosis and its function in this context is currently under investigation (Dr Tim Kendall, unpublished).

Chapter 5

Investigating the function of single WT1 isoforms in the IMCD3 clones with a closer view on the -/+ variant

5.1 Overview

In this chapter I will examine the outcomes of the induction of WT1 single isoforms in the second cell model I generated: the IMCD3 single clones stably transfected with the pGoldiLox-(Wt1) plasmids. The IMCD3 cells were derived form a murine inner medullary collecting duct, they do not express WT1 and they are generally considered epithelial cells, although they co-express mesenchymal markers, a property that makes them similar to the cells expressing the endogenous WT1. The stable clones constitutively express the EGFP fluorescent protein, while the transcription of the mCherry-(Wt1) coding sequence is regulated by a Dox-inducible promoter. Nonetheless, as I mentioned in the first result chapter, the majority of the single clones is leaky, in fact many clones express mCherry-(WT1) even in the absence of Dox. For the following

experiments, I selected two clones per isoform and four EV clones based on the highest expression of the fusion protein (or the fluorescence marker alone for the EV clones) after induction and, when possible, I included non-leaky clones (Figure 3.28 and Figure 3.29).

Knowing that the induction of specific WT1 isoforms was affecting the growth of some MDCK clones, I decided to test whether I could find similar effects expressing the WT1 variants in the IMCD3 clones. Because of the leakiness of expression, I compared the proliferation of the induced cells with the growth rate of two EV clones treated with Dox. I concluded that only the two -/+ clones were growing slower than the controls. To validate that the result was not due to intrinsic clone variability, I used the non-leaky -/+ clone (namely -/+ 17) to compare the proliferation of induced and non-induced cells. Because the cells grew at the same rate independently of the presence of Dox, I assumed that the growth impairment, noticed comparing with the EV clone, was not caused by the induction of the -/+ WT1 isoform, but instead depended on initial different properties of the single clones. I also verified that the distribution of the cells in the phases of the cell cycle was not affected by the overexpression of WT1 single isoforms in any of the IMCD3 clones.

I then investigated whether the induced clones showed different oncogenic potential when compared with two EV clones. To this purpose, I carried out two cell-based assays: the wound healing assay, to test the migration of the cells, and the soft agar colony formation assay, to determine the ability of anchorage-independent growth. From the wound healing assay, I concluded that the induced clones closed the wound at a comparable speed with the EV clones; therefore, the expression of WT1 single isoforms does not affect the migration potential of the cells. On the other hand, the +/+ and +/- clones tested in the soft agar colony assay formed more colonies compared with the two EV clones. The -/+ and -/- clones did not show any significant difference in the number of colonies, although the size of the colonies generating from the -/- clone was bigger than the ones forming from the EV clones. Thus, the result suggested that

the induction of the +/+, +/- and -/- isoforms facilitated the anchorage-independent growth of the cells.

In order to investigate the changes in the cell transcriptomes upon induction of the single isoforms, I decided to perform an RNA sequencing (RNA seq) at 96h of Dox treatment. I compared one induced clone per isoform against an induced EV clone. Similarly to the outcome of the microarray analysis of the MDCK clones, the clone that showed the most remarkable isoform-specific changes was the -/+ clone. I therefore decided to validate and further study the role of the -/+ isoform.

The initial analysis of the RNA seq highlighted several pathways and processes differentially regulated by the induction of the -/+ isoform, such as the extracellular matrix organization, cell adhesion, ECM-receptor interaction, the activation of the MAPK (mitogen-activated protein kinases) pathway and, interestingly, some of the developmental processes WT1 is well-known to play a pivotal role in: urogenital system, heart, mammary gland, skeletal and cartilage development and angiogenesis. Moreover, the main mesothelial markers were found upregulated, as well as one of the principal regulators of adipogenesis. In order to exclude that the changes seen in the RNA seq were simply due to the clone variability between the EV and the -/+ clone, in the validation I also compared the induced and non-induced cells of the non-leaky clone. To verify the data, I either used cell-based assays, WB or Q-RT-PCR.

In order to confirm that the induction of the -/+ isoform was modifying the cell adhesion and the ECM-receptor interaction, I performed an ECM cell adhesion assay, which suggested that the induced cells could adhere to selected ECM substrates more strongly than the non-induced cells. Moreover, I confirmed by Q-RT-PCR the upregulation of the expression of different molecules involved in the modification of the ECM. The overexpression of most of these genes was also verified in a second -/+ clone, whose expression levels were compared with the levels of different EV clones, because of its leakiness of WT1 expression.

I then validated the activation of the MAPK pathway by comparing the levels of phospho-ERK (extracellular signal-regulated kinase) 1/2 in induced and non-induced -/+ 17 and EV clones. I also noticed that, resulting from the induction of the -/+ isoform, there was an activation of the AKT pathway. Interestingly, the activation of these two pathways seems to be important for different aspects of the mesoderm development.

Last, I decided to verify the upregulation in the expression of specific regulators and markers of the development of four mesoderm derivatives: cartilage, bone, blood vessels and adipose tissue. The changes in expression have been checked in a time course, comparing the levels of the induced and non-induced -/+ 17 clone over eight days. It has been shown that the progenitors of the coronary vasculature and the white adipose tissue (WAT) derive from the mesothelia lining the heart and the visceral WAT, respectively, and that WT1 is essential for the derivation of these progenitors, likely regulating an EMT transition [53, 59]. Hence, I also investigated in the time course the variations of the expression levels of mesothelial markers and genes involved in the EMT process. The results suggest that WT1 might induce epithelial cells along the pathway to different fates, possibly through a mesothelial intermediate.

5.2 The expression of WT1 single isoforms does not affect the proliferation or the cell cycle of the IMCD3 clones

As previously discussed in Chapter 2, the influence of WT1 on cell proliferation has been a matter of debate over the past few decades. Overall, the data in the literature suggest that WT1 can either promote or inhibit cell growth depending on the cell model used and the context. Because I noticed that the induction of single isoforms affected the proliferation of specific MDCK clones, I was interested to understand whether the data could have been replicated and confirmed using the IMCD3 clones. To test the influence of WT1 single isoforms on the proliferation of the induced IMCD3 clones, I decided to compare their growth curve with the one of an induced EV clone. Indeed,

the expression of the single isoforms in most of the clones cannot be controlled or even increased by adding the Dox (Figure 3.28). It is important to point out that using the induced EV clones as controls allows to subtract the influence of the Dox or the mCherry protein on the process analysed, but it does not prove that the outcomes are due to the expression of WT1, rather than to the clonal variability.

The proliferation of the cells was monitored by staining the fixed cells with crystal violet at 0, 1, 2, 3, 4, 6 and 8 days of induction with 1 μg/ml of Dox. After drying the stained cells, the crystal violet was dissolved using the same volume of 10% acetic acid for each well and its absorbance, which is proportional to the amount of cells in the well, was measured at 595 nm. As shown in Figure 5.1 A, I compared the first set of clones with the EV clone number 19 and the second set with the EV clone 22. Overall, in both cases the +/+, +/- and -/- clones were proliferating at the same rate as the EV clones. On the other hand, the two -/+ clones, similarly to the MDCK mCherry -/+ clones, grew slower than the controls. Because one of the -/+ clones I used, namely the -/+ 17, does not show a significant leakage in the expression of the isoform, which can be highly induced by the Dox (Figure 3.28), I decided to validate the result comparing the proliferation of the induced and non-induced clone. Surprisingly, there was no difference between the growth rates of the Dox treated and untreated cells (Figure 5.1 B). Thus, I reason that the reduced rate of proliferation of the -/+ 17 clone in comparison with the EV 19 clone is actually due to the variability between the clones and not to the expression of the -/+ isoform. Nonetheless, it is important to notice that the induction of the mCherry-WT1 -/+ fusion protein does not influence the cell proliferation of the IMCD3 clone, as could be the case for the MDCK mCherry clones.

I then tested whether there were differences between one induced clone per isoform and one EV clone in the percentages of cells in the cell cycle phases. The PI staining at 4 and 8 days of induction did not highlight any relevant differences in the cell distribution in the three phases (Figure 5.2), confirming that the expression of WT1 single isoforms does not affect the cell proliferation of the IMCD3 clones.

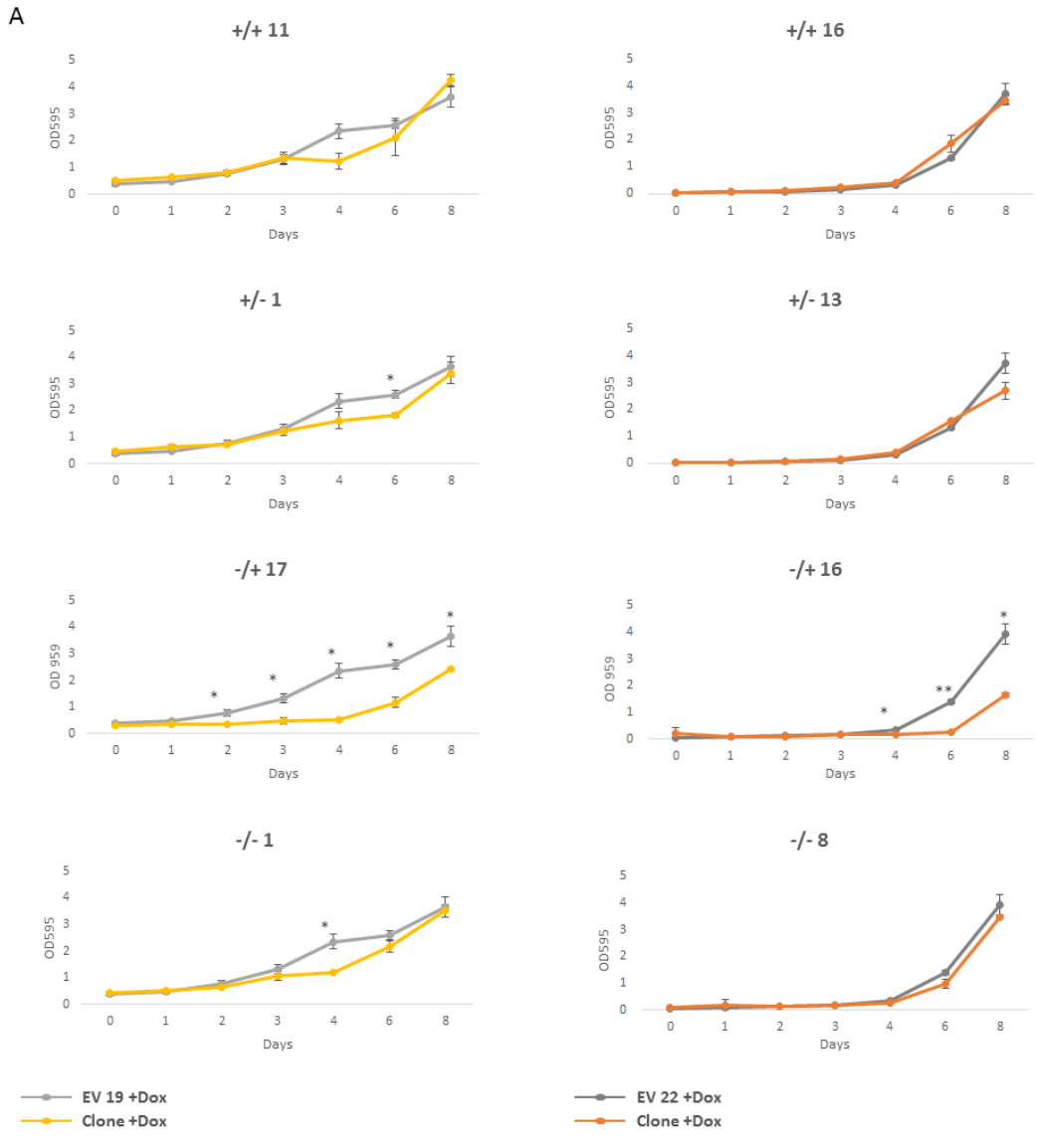
A
+/+ 11
+/+ 16
+/- 1
+/- 13
-/+ 17
-/+ 16
-/- 1
-/- 8
OD595
OD 959
Days
EV 19 +Dox
Clone +Dox
EV 22 +Dox
Clone +Dox

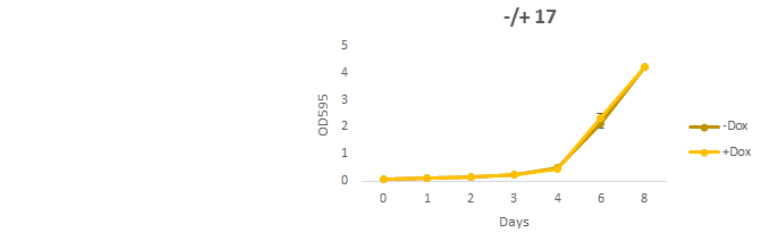
B
-/+ 17
OD595
Days
-Dox
+Dox

FIGURE 5.1: A: Growth curves of the WT1-IMCD3 clones compared with the induced EV 19 or the induced EV 22 clone. SD of the mean of two technical replicates. *: P-value < 0.05, **: P-value < 0.01. B: Growth curve of the induced and non induced IMCD3 -/+ 17 clone. SD of the mean of two technical replicates.

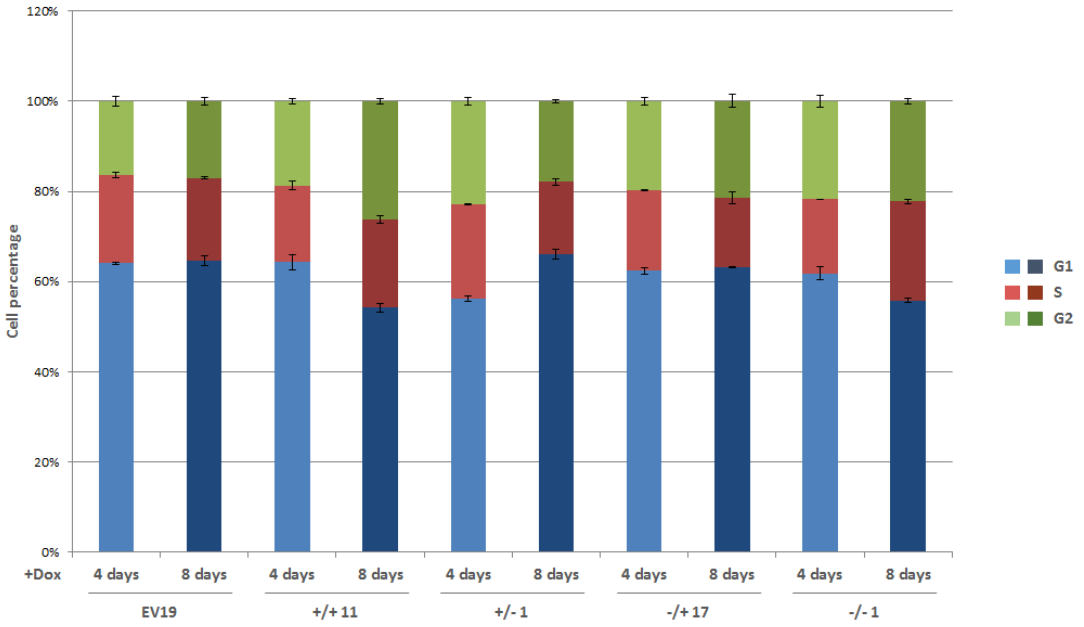

FIGURE 5.2: Percentages of distribution of the cells of the IMCD3 clones in the phases of the cell cycle after 4 and 8 days of Dox induction. SD of the mean of two technical replicates.

5.3 WT1 expression does not influence the oncogenic potential of the IMCD3 cells

Despite of the fact that WT1 was initially identified as a tumour suppressor in Wilms' tumour, there is an increasing body of evidence advocating an oncogenic function of WT1. Indeed, wild-type WT1 has been found expressed in a variety of solid tumours derived from tissues that normally do not express the transcription factor, such as soft tissue sarcoma [116], colorectal [108, 209], breast [109], lung [110], desmoid [111], prostate [112], brain [113] and ovarian [114] cancers. Many studies have strongly supported an oncogenic role for WT1 in leukaemogenesis [210]; however, *WT1* mutations

have been found in a significant proportion of acute myeloid leukaemias, suggesting a tumour suppressor role of WT1 [118].

Reinforcing an oncogenic function, several studies *in vivo* and *in vitro* have shown that the silencing of WT1 results in enhanced apoptosis, senescence, inhibition of malignant cell growth and increased mitochondrial damage [124–127, 134, 135, 186, 211]. Furthermore, Wagner et al demonstrated that WT1 is upregulated in hypoxic conditions, which resemble the tumour environment [128]. WT1 was also shown to be involved in tumour angiogenesis and vascularization [129].

On the other hand, WT1's role as a tumour suppressor is supported by other *in vitro* studies, which led to opposite conclusions. In fact, it has been demonstrated that the overexpression of WT1 in different cancer cells blocks their proliferation [94–98, 102, 188], lowers their colony formation rates [94, 99–101] and enhances the apoptosis process [103, 104, 212]. Moreover a Wilms tumour cell line, ectopically expressing the WT1 -/+ isoform, exhibited reduced tumour formation in nude mice [105].

Taken together, the data suggest that WT1 oncogenic or tumour suppressive effect might depend on the cell type and on how the cells respond to variations in *WT1* expression or mutations at specific times of development. However, WT1 importance in tumours is underlined by the fact that WT1 is not only considered a prognostic marker for different cancers, but also a target for the development of therapeutic strategies [213] [214].

In order to assess whether the expression of WT1 single isoforms was influencing the oncogenic potential of the IMCD3 cells, I decided to use two cell-based assays: the wound healing assay and the soft agar colony formation assay. If WT1 enhanced the tumorigenicity, the cells were expected to migrate faster than the controls and to form more colonies when grown in the absence of anchorage.

5.3.1 The expression of WT1 single isoform does not alter the migration rate of the IMCD3 clones

The velocity of the IMCD3 clones was measured using wound healing assays. Two clones for each isoform were treated with 1 μg/ml of Dox for 96h and compared with two induced EV clones. The cells were seeded and grown to confluence in culture inserts with a gap or 500 μm. At 96h of induction the inserts were removed and the cells were live imaged for a total time of 48h. The speed of migration was then calculated dividing the maximal covered area by the time taken to colonise it. The assay demonstrated that there were no differences in the speed of migration of the cells, suggesting that the expression of the single isoforms does not influence the motility of the clones (Figure 5.3 A). I also tested whether the induced cells of the non-leaky clone -/+ 17 closed the wound at a different speed compared to the non-induced cells. The induction of the -/+ isoform indeed decreased the time taken to fill in the gap; however, I also noticed that the Dox treatment of one of the EV clones increased the migration rate of the cells (Figure 5.3 B and C). Although the -/+ 17 clone migrates more slowly than the EV clone, I cannot decidedly conclude that the motility of the -/+ 17 clone is influenced by the induction of the WT1 isoform, as the increased speed may be due to the Dox itself. There is also no statistical difference between the velocities of the induced -/+ 17 and EV cells.

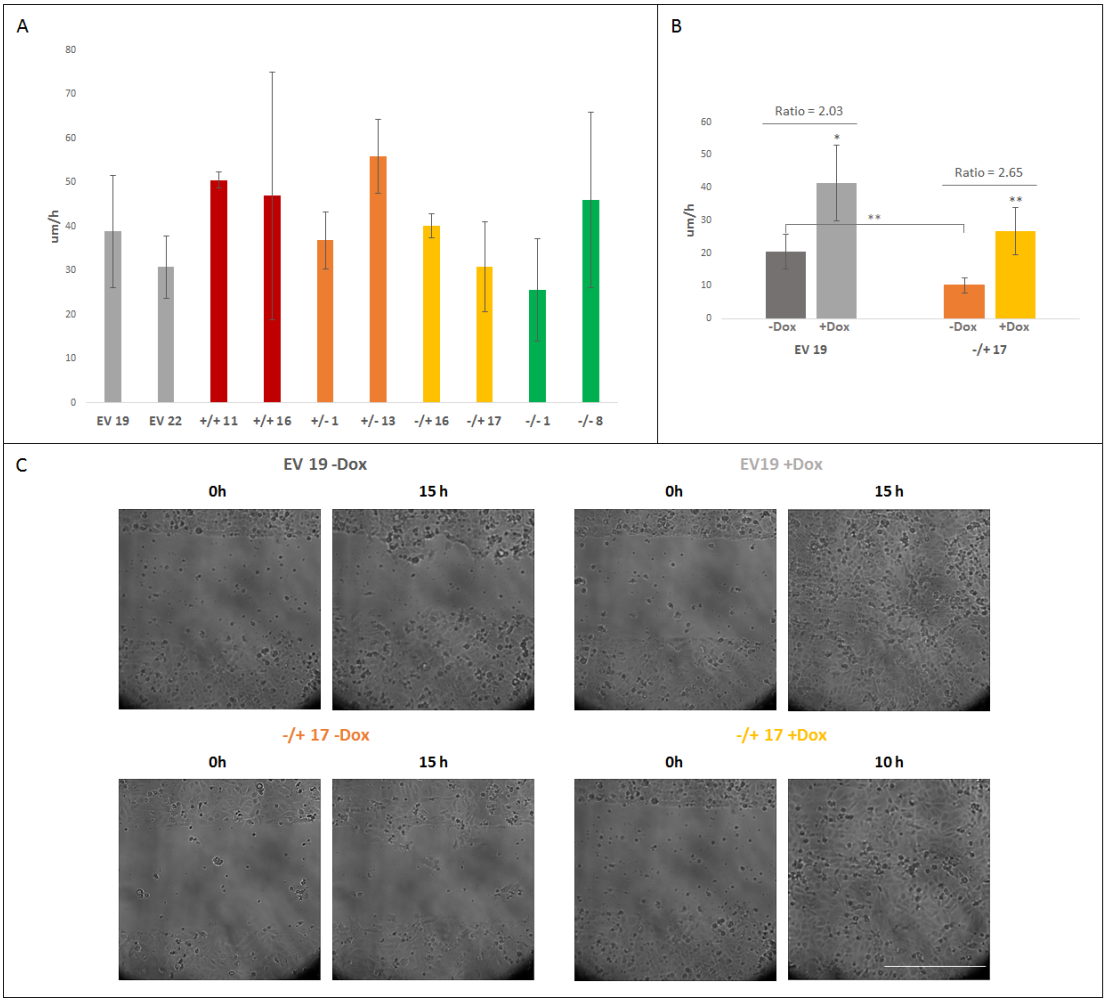

FIGURE 5.3: Testing the IMCD3 clones' speed of migration in the wound healing assay. A: Average speed of the 96h induced IMCD3 clones. SD of the mean of technical duplicates of two biological replicates. B: Velocity of the 96h Dox treated and untreated EV 19 and -/+ 17 clones. SD of the mean of two biological replicates, each carried on in duplicates. *: P-value < 0.05, **: P-value < 0.01. On the top of the graphs the ratios between the speed of induced and non induced cells are reported. C: Example images taken during the live imaging of the induced and non induced EV 19 and -/+ 17 clones while closing the wound. The pictures reflect and represent the quantification in Figure B. Scale bar = 500 μm.

5.3.2 The +/+, +/- and -/- isoforms seem to facilitate the cell growth in soft agar

In order to determine the ability of the IMCD3 clones to grow in the absence of anchorage, I initially seeded the same number of cells and grew each 1 μg/ml Dox induced clone in soft agar for 3 weeks; I then counted the colonies that formed. I decided to use as positive control for the assay a pool of IMCD3 clones stably transfected with a plasmid for the constitutive expression of HRasG12V (refer to Figure A.2 in the Appendix section to see the level of upregulation of HRasG12V in the pool of stable clones when compared to untransfected IMCD3 cells). The MSCV-HRasV12 construct was kindly provided by Dr Juan Carlos Acosta. The HRas mutant is indeed supposed to transform the cells, giving them an advantage for the growth in soft agar [215].

From this assay (Figure 5.4 A), I concluded that the +/+ and +/- clones formed more colonies compared to both the two EV clones used as controls. On the other hand, the two -/+ clones and the -/- clone did not generate a different amount of colonies. The pool of clones expressing the HRas mutant did not prove to be a perfect positive control, as the number of colonies forming from the pool did not differ from the controls; on the other hand, the size of the HRas mutant colonies was visibly bigger and comparable to the ones forming from the culture of the +/+, +/- and -/- clones, suggesting that the HRas mutant might confer an advantage to grow in the absence of anchorage (Figure 5.4 C). These data suggest that the expression of the +/+, +/- and, maybe, of the -/- isoforms facilitates the growth of the cells in absence of anchorage, indicating that these WT1 variants may increase the oncogenic potential of the cells. However, it is important to underline that the comparison with the EV clones does not take into account the intrinsic clonal variability.

Because the wound healing assay showed that the Dox itself could influence certain properties of the IMCD3 cells, I tested whether the growth in soft agar of one of the EV clones was affected by the Dox treatment. The assay demonstrated that there were no differences in the number of colonies formed by the induced and non-induced cells. Moreover, I confirmed that the expression of the -/+ isoform was not affecting the

anchorage-independent growth of the cells by comparing the amount and the size of the colonies generating from the Dox treated and untreated -/+ 17 clone (Figure 5.4 B and C).

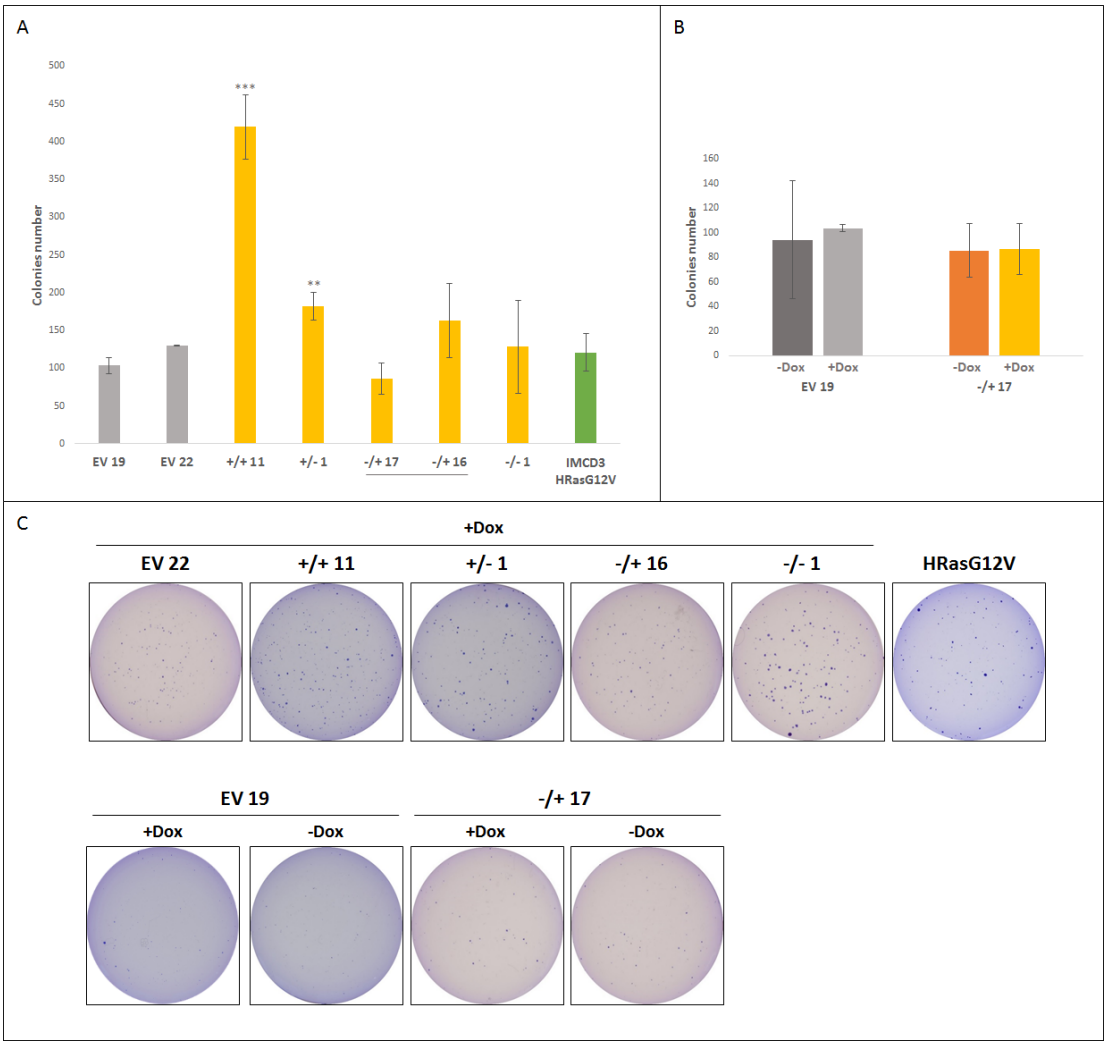

FIGURE 5.4: IMCD3 clones growing in soft agar. A: number of colonies formed by each induced clone after 3 weeks of growth in soft agar. The pool of clone of IMCD3 HRasG12V was used as positive control. SD of the mean of two biological replicates. **: P-value < 0.01, ***: P-value < 0.001. B: Comparison between the number of colonies generated by the induced and non induced EV 19 and -/+ 17 clones. SD of the mean of two biological replicates. C: Representative pictures of the colonies formed by each clone in soft agar.

TABLE 5.1: RNA seq: numbers of genes differentially regulated in each induced IMCD3 clone in comparison with the EV19 induced clone.

IMCD3 clone	**Gene number**
+/+ 11	740
+/- 1	1591
-/+ 17	1484
-/- 1	1360

5.4 The IMCD3 -/+ 17 clone shows the most remarkable isoform-specific changes in the RNA Seq analysis

In order to gain an insight into the function of the single WT1 isoforms in the IMCD3 clones, I employed a genome-wide approach to study the changes in gene expression. Thus, I decided to analyse by Illumina RNA Seq the transcriptomes of one 96h induced clone per isoform (namely +/+ 11, +/- 1, -/+ 17 and -/- 1) and of the induced EV 19 clone, which was used as control. After extracting total RNA from two biological replicates per clone, the RNA Seq was carried out at the GATC Biotech; the data were then analysed by Dr Stuart Aitken. The total number of genes that changed expression levels in comparison with the EV clone are summarised in Table 5.1. The Venn diagrams in Figure 5.5 show instead the number of commonly or uniquely upregulated and downregulated genes in the clones. The names of the genes belonging to each of the sections of the Venn diagrams are listed in the Appendix section A.2. The data show that the +/- and the -/+ clones have the highest total number of differentially expressed genes. Specifically, the expression of the -/+ and the +/- isoforms leads to the highest number of uniquely induced and repressed genes, respectively.

The analysis of the RNA seq data also allows the identification of differential usage of exons. Although this analysis is very preliminary and has not been yet validated, it highlights the presence of different transcript variants depending on the expressed WT1 isoform. One of the best examples comes from the comparison between the EV, +/+ and -/- expressing IMCD3 clones. Indeed, as shown in Figure 5.6, the +/+ clone

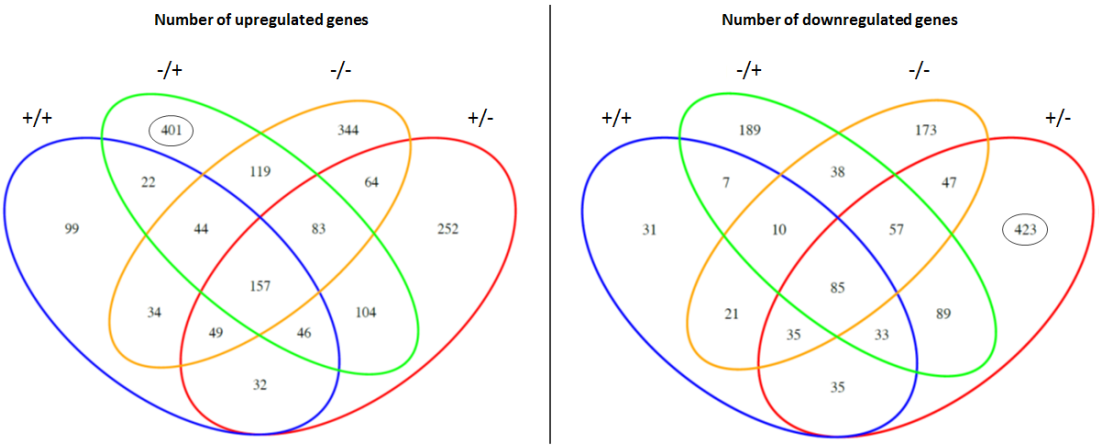

FIGURE 5.5: RNA seq analysis: Venn diagrams representing the numbers of genes uniquely or commonly upregulated (left panel) and downregulated (right panel) in the induced IMCD3 clones. The circles highlight the highest numbers of uniquely up- or down- regulated genes.

expresses isoforms of the *Cd55* gene which lacks the exon 17, while the -/- cells express transcripts that include the exon. On the other hand, the EV clone seems to express both the isoforms. The CD55 molecule is involved in the regulation of the complement cascade and it has been shown that in human cells alternative splicing generates two proteins: while the lack of splicing at the N-terminus encodes for a secreted form, the spliced mRNA generates a membrane-bound protein [216]. Interestingly, the +/+ isoform has already been reported to inhibit alternative splicing through its interaction with the splicing factor RBM4 (RNA-binding Motif Protein 4) [217]. The analysis and validation of the RNA seq data will provide new evidence about WT1 regulation of splicing events and will improve our knowledge on how the single isoforms can affect not only the levels of expression, but also the function of different genes. Thus, it would be very interesting to validate the presence of different CD55 proteins upon upregulation of specific WT1 isoforms and see whether those proteins have in murine cells the same function reported in human cell lines.

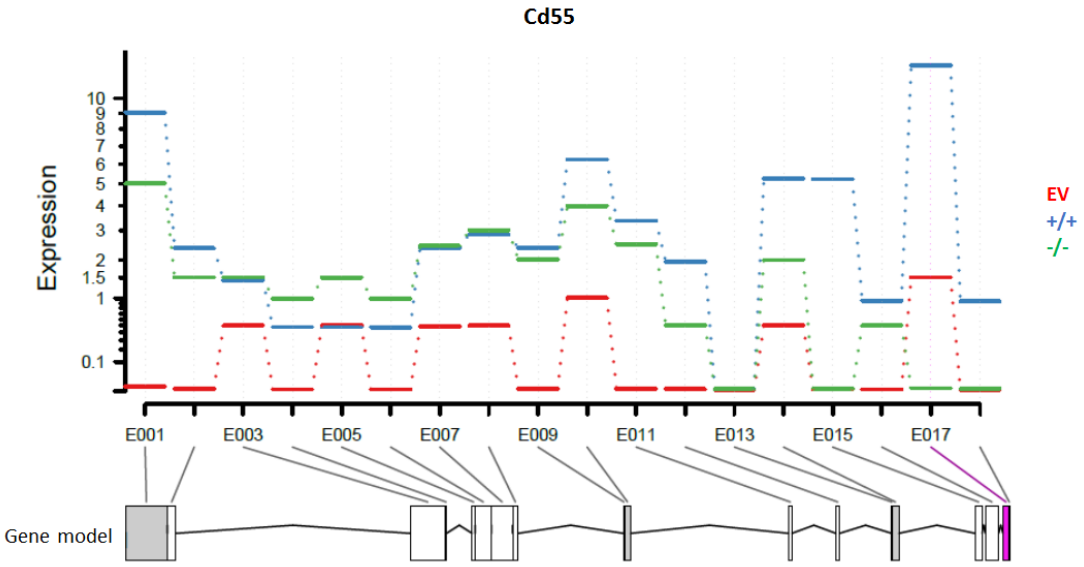

FIGURE 5.6: Differential usage of exons of the *Cd55* gene in the induced EV (red), +/+ (blue) and -/- (green) IMCD3 clones. The y-axis represents the Log2 fold change of expression, while on the x-axis there are the different exons. The diagram at the bottom represents the *Cd55* gene model and the differentially expressed exon 17 is highlighted in pink.

I then categorised in GO terms and pathways the differentially expressed genes by using the free online bioinformatics tool DAVID (https://david.ncifcrf.gov/home.jsp). Similarly to the result obtained with the microarray analysis on the MDCK clones, the expression of the -/+ isoform seemed to induce the most significant isoform-specific changes. Thus, I decided to focus the validation of the RNA Seq on this isoform.

The analysis of the genes that had different expression levels in the IMCD3 -/+ 17 clone versus the EV 19 clone indicated changes in specific processes. Table 5.2 lists the most enriched GO terms relative to the cellular physiology. I have already shown that neither the proliferation nor the cell motion were actually affected by the induction of the -/+ isoform in the non-leaky clone, leading me to the conclusion that the differences noticed between the EV and the -/+ clones are due to different intrinsic properties of the clones rather than to the expression of WT1.

Table 5.3 summarises the top pathways of the KEGG database (Kyoto Encyclopaedia

TABLE 5.2: GO terms relative to cellular physiology and associated P and Benjamini values characterising the induced IMCD3 -/+ 17 clone in the DAVID analysis .

GO term	**P-value**	**Benjamini**
Cell adhesion	1.10E-13	3.20E-10
Regulation of cell proliferation	1.70E-10	1.60E-07
Extracellular structure organization	1.80E-07	4.60E-05
Epithelial cell differentiation	6.80E-05	7.40E-03
Extracellular matrix organization	1.20E-04	1.20E-0.2
Positive regulation of cell differentiation	2.80E-04	2.40E-02
Cell motion	5.10E-04	3.70E-02

TABLE 5.3: KEGG pathways and associated P and Benjamini values resulting from the DAVID analysis of the differentially induced genes in the IMCD3 -/+ 17 clone.

KEGG pathway	**P-value**	**Benjamini**
ECM-receptor interaction	1.00E-05	1.70E-03
Pathways in cancer	1.80E-04	1.00E-02
Axon guidance	2.20E-04	9.30E-03
Focal adhesion	4.70E-04	1.60E-02
Regulation of actin cytoskeleton	3.90E-03	1.00E-01
MAPK signalling pathway	4.70E-03	1.10E-01
Complement and coagulation cascade	4.90E-03	9.90E-02
Gap junction	1.50E-02	1.90E-01
Cell adhesion molecules	1.90E-02	2.20E-01
Tight junction	4.50E-02	4.00E-01
Cytokine-cytokine interaction	4.90E-02	4.10E-01
Wnt signalling pathway	5.10E-02	4.10E-01
Chondroitin sulfate biosynthesis	6.10E-02	4.50E-01
Leukocyte transendothelial migration	6.60E-02	4.40E-01

of Genes and Genomes) that are supposed to be affected by the expression of the -/+ isoform. I decided to validate three of the processes that resulted from the analysis: the ECM organization, which interestingly was also affected in the induced MDCK -/+ clones, the cell adhesion and the activation of the MAPK pathway.

In Table 5.4 I have listed the developmental processes that resulted enriched from the analysis of the genes differentially expressed in the -/+ 17 clone. Interestingly, a crucial

TABLE 5.4: GO terms relative to developmental processes and associated P and Benjamini values characterising the induced IMCD3 -/+ 17 clone in the DAVID analysis.

GO term	**P-value**	**Benjamini**
Epithelium development	4.90E-09	2.80E-06
Blood vessel development	4.90E-09	3.50E-06
Angiogenesis	3.90E-06	1.80E-05
Urogenital system development	4.40E-06	8.30E-04
Morphogenesis of branching structure	8.80E-06	1.50E-03
Tube development	1.70E-05	2.30E-03
Kidney development	2.60E-05	3.40E-03
Skeletal system development	4.00E-05	4.80E-03
Ectoderm development	2.10E-04	1.90E-02
Heart development	4.90E-04	3.80E-02
Mammary gland development	5.70E-04	4.10E-02
Cartilage development	6.40E-04	4.30E-02
Gland development	7.40E-04	4.90E-02

role of WT1 in these processes has been already largely reported, but it is not yet known whether WT1 is actually sufficient to drive them.

5.5 WT1 -/+ and the cell-matrix interaction

The cell-matrix interaction is a key process for organ development, cell migration, invasion, tissue remodelling and wound healing. The cells bind to the ECM through specific adhesion molecules, called integrins. It has been previously reported that WT1 is able to regulate the transcription of adhesion receptors as well as components of the ECM, in particular of the basement membrane. In fact, in 1999 Hosono and colleagues reported that the stable transfection of WT1 -/- isoform in mouse fibroblasts induced the expression of the Integrin $\alpha 8$ and the Collagen IV [218]. Accordingly, more recently Chen et al demonstrated that WT1 maintains testicular cord integrity by modulating the expression of two genes encoding for type IV collagen, namely *Col4a1* and *Col4a2* [219]. Moreover, Kirshner et al showed that -KTS WT1 activates the Integrin $\alpha 4$ gene (*ITGA4*) in human embryonic kidney cells, promoting cell adhesion [220].

5.5.1 The induction of the -/+ isoform enhances cell adhesion

I decided to test whether the expression of the -/+ WT1 isoform was affecting the cell adhesion, as predicted by the RNA seq analysis. To this aim, I used an ECM Cell adhesion assay (Cambridge Bioscience), consisting of an array of wells pre-coated with five different ECM substrates, including Collagen IV, Laminin I (components of the basement membrane), Fibronectin, Collagen I and Fibrinogen (components of the interstitial matrix), plus BSA as negative control. After seeding in each well an equal number of 96h induced or non-induced IMCD3 -/+ 17 cells and induced EV 19 cells, I incubated the cells for 1 hour. The non-adherent cells were then washed away, while the remaining cells were stained. The optical density (OD) at 560 nm of the staining solution, proportional to the amount of adherent cells in each well, was then measured. Finally, I calculated the ratio between the absorbance of the wells containing the induced IMCD3 -/+ 17 cells and the one of the wells in which the controls (non-induced or EV cells) were seeded; the ratio was then expressed into percentage (Figure 5.7). The OD 560 nm of the wells pre-coated with BSA was considered as blank. From this assay, I concluded that the induced cells could adhere to the substrates more strongly than both the controls, with the exception of the interaction with the Collagen I that was not significantly increased in comparison to the EV cells. Importantly, I was able to validate the result comparing the Dox treated and untreated clone, indicating that the increased cell adhesion is likely to be due to the induction of the -/+ isoform.

Interestingly, different genes encoding for integrin subunits, such as *Itga2*, *Itga5*, *Itga7* and *Itgb3*, were differentially regulated in the RNA seq analysis. Moreover, the *Cav1* gene, which has been involved in the regulation of the fibronectin matrix turnover [221], was found significantly upregulated.

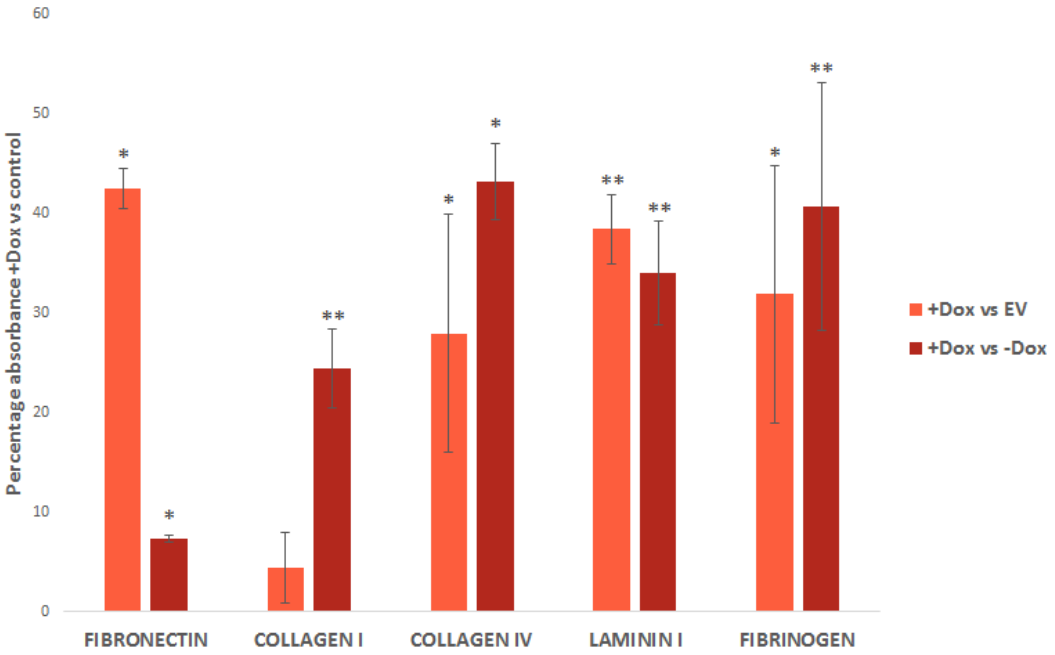

FIGURE 5.7: Adhesion assay. The column graph represents the increment in percentage of the OD 560 nm, which is proportional to the amount of adherent cells, of the 96h induced IMCD3 -/+ 17 clone versus either the induced IMCD3 EV19 clone or the non induced -/+ 17 clone. SD of the mean of duplicates of two biological replicates. The P-value was calculated comparing the average absorbance of the +Dox sample (± SD) with the average absorbance (± SD) of the control. *: P-value < 0.05, **: P-value < 0.01.

5.5.2 The expression of the -/+ isoform leads to the upregulation of genes involved in ECM remodelling and fibrosis

I then validated by Q-RT-PCR some of the genes involved in the ECM organization, which are also considered fibrotic markers. Some of these genes were strikingly found upregulated in the induced MDCK -/+ clones too. In order to confirm the data of the RNA seq, I decided to determine the changes of the expression levels in two IMCD3 -/+ clones. As shown in Figure 5.8, the -/+ 16 clone is leaky and there is no difference in the Cherry-WT1 -/+ expression between the Dox treated and untreated clone. Therefore, I reasoned to compare the mRNA levels of the induced clone with the average expression of different induced EV clones. I chose four single EV clones in order to minimise the clonal variation. On the other hand, the induced -/+ 17 clone shows a significant

upregulation of the isoform compared to the non-induced clone. Thus, I decided to validate the variation of the gene levels in the induced clone comparing both with the untreated cells and with the average expression of the four induced EV clones.

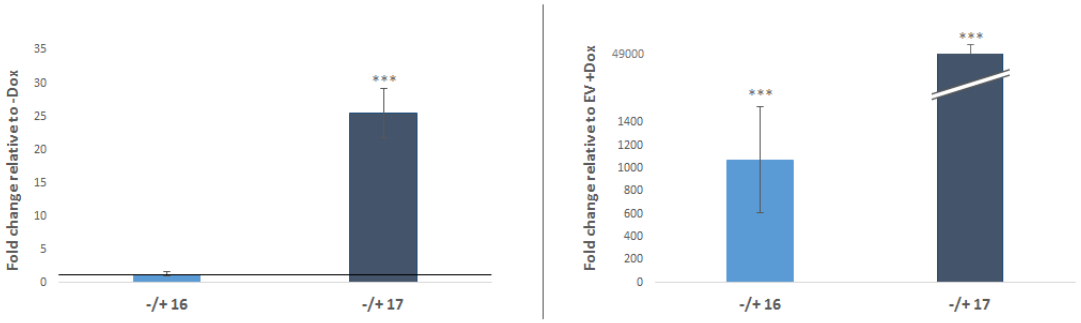

FIGURE 5.8: Q-RT-PCR: mCherry-Wt1 mRNA relative expression in -/+ 16 and 17 IMCD3 clones. After normalizing the gene expression with the *Gapdh* levels, the fold change of expression was calculated comparing the levels in the 96h induced clones with either the levels of the non induced clones (left panel) or the average of expression in four different EV clones (right panel). -/+ 16 clones: SD of the mean of two biological replicates; -/+ 17 clone : SD of the mean of three biological replicates. In the chart on the left hand side, the horizontal line underlines the fold change of the non induced clones, which is equal to 1. ***: P-value < 0.001.

As shown in Figure 5.9, the *Col1a1* gene, which encodes for the most abundant protein in the ECM and it is one of the principal components of the fibrotic lesions [206], was not significantly upregulated in the induced -/+ 16 clone, but strongly overexpressed upon induction in the -/+ 17 clone. The difference might be either due to intrinsic properties of the clones or to the different levels of expression of the isoform (Figures 3.30 and 5.8). On the other hand, the *Acta2* and *Mmp9* mRNA levels were significantly upregulated in the induced -/+ 16 and -/+ 17 clones when compared with the EV clones. Among the genes encoding for inhibitors of metalloproteinases, only the pro-fibrotic *Timp1* gene seemed to be slightly, but consistently, upregulated in the induced clones. It is important to notice that the levels of the analysed genes were not influenced by the Dox treatment in the EV clones.

Taken together, the data indicate that the -/+ WT1 isoform is involved in the cell-matrix interaction, both modulating the cell adhesion and, possibly, the deposition of ECM components. Moreover, because the overexpression of smooth muscle actin

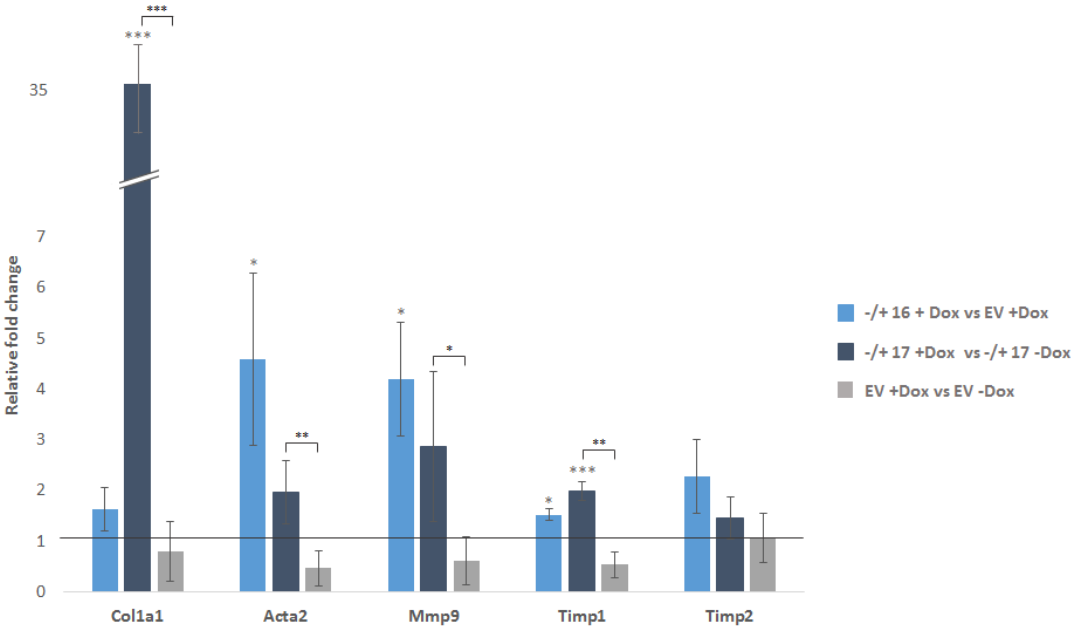

FIGURE 5.9: Q-RT-PCR: relative expression of ECM and fibrotic genes in the -/+ 16 and 17 IMCD3 clones. Before calculating the fold changes, every gene level in each sample was normalized for the *Gapdh* levels of expression. The first series of the column chart represents the fold changes of the expression in the 96h -/+ 16 induced clone over the average expression in four induced EV clones (SD of the mean of two biological replicate). The second series is the expression fold changes in the 96h induced -/+ 17 clone versus the non induced clone (SD of the mean of three biological replicates). The third series represent the fold change of the average expression in four induced EV clones versus the average levels in the non induced EV clones (SD of the mean of the fold changes in the four clones). The horizontal black line underlines the fold change of the controls, which is equal to 1. *: P-value < 0.05, **: P-value < 0.01, ***: P-value < 0.001.

and ECM constituents, as well as the upregulation of metalloproteinases and TIMPs, characterised the transformation of fibroblasts to myofibroblasts [207], the data suggest that the -/+ WT1 isoform could be involved the induction of a fibrotic process.

5.6 The induction of the -/+ isoform activates the MAPK and the AKT signalling pathways

Among the predicted KEGG pathways characterising the induced IMCD3 -/+ 17 clone there was the regulation of the MAPK signalling pathway. In order to validate its activation, I compared the levels of the phosphorylated and total MAPK ERK 1/2 of 96h induced and non-induced IMCD3 -/+ 17 and EV 19 clones. As shown by the WB and its quantification (Figure 5.10 A and B), I proved the upregulation of the phosphorylation levels upon induction of the -/+ isoform. I also noticed that the Dox treatment in the EV clone led to the activation of the pathway, even though the increment in the ratio between the levels of p-ERK 1/2 and total ERK 1/2 was lower than the ratio in the -/+ 17 clone. Therefore, I suggest that the induction of the -/+ isoform is likely able to activate the MAPK pathway, although the increased phosphorylation levels are probably boosted by the presence of Dox.

Different papers have already reported connections between the expression of WT1 and the regulation of the MAPK pathway. For instance, Li et al have recently shown that WT1 +/- can activate the MAPK pathway in leukemic cells [184]. Similarly, Kim and colleagues demonstrated that the inducible expression of WT1 -/- in a Wilms' tumour cell line directly upregulates genes implicated in the pathway [222]. In contrast, two papers have suggested that WT1 -KTS decreases the activation of the pathway in leukemic cells, through the transactivation of two Ras/MAPK inhibitors [102, 223]. Moreover, the induction of WT1 was shown to downregulate the phosphorylation levels of both ERK 1/2 and AKT in a human osteosarcoma cell line [224]. It has also been reported that the activation of the MAPK pathway can regulate WT1 expression, suggesting the possibility of a regulation loop between the two. In fact, Sarfstein et al demonstrated that Insulin-like growth factor 1 (IGF1) induces WT1 expression by activating both the MAPK and the AKT pathway in a neurally derived cell line [225].

Because WT1 expression seems to regulate, as well as being affected, by both the MAPK and the AKT pathways [224, 225], I decided to test whether also the latter was

activated in the induced IMCD3 -/+ 17 clone. I therefore visualised by WB the levels of total AKT and phosphorylated AKT in Dox treated and untreated -/+ 17 and EV 19 cells at 96h (Figure 5.10 C and D). The assay demonstrated that the induction of the -/+ isoform led to increased levels of phosphorylated and active AKT. Differently from the MAPK pathway, the induction of the EV clone seems to rather inhibit than activate the pathway.

According to the data presented, it has been shown that WT1 knockdown decreases AKT phosphorylation levels in a human peripheral nerve sheath tumour cell line [126]. Furthermore, multiple papers have reported that the inhibition of the AKT pathway reduces WT1 expression in different cancer cell lines [137, 226, 227].

Similarly to WT1, the release of the human CXCL8 can be mediated by both the MAPK and the AKT pathway [228]; at the same time, it was demonstrated that CXCL8 can activate the AKT signalling pathway in a nasopharyngeal carcinoma cell line [229]. Because, the induced MDCK clones were characterised by the overexpression of the Interleukin 8 gene, I was interested to see whether the induced IMCD3 cells shared the same feature. Because the *CXCL8* gene is absent from the mouse genome, I checked in the RNA seq analysis whether the genes of the two functionally related chemokines, *Cxcl6* and *Cxcl5*, were differentially regulated in the induced clones. Similar to the expression analysis in the canine cells, I found that the *Cxcl5* gene was upregulated in all the IMCD3 clones (Table 5.5 summarises the analysis of the data from the RNA seq). Interestingly, as shown above, the expression of the *Mmp9*, which is able to cleave and activate the Cxcl5 chemokine [230], is upregulated in the -/+ IMCD3 clones, resembling the MDCK -/+ clones. Hence, it will be very important to validate the overexpression of the *Cxcl5* gene by Q-RT-PCR.

Another intriguing parallel between the function of WT1 and both the MAPK and the AKT pathways is their involvement in mesoderm development. Indeed, WT1 is a major regulator of development and maintenance of certain mesodermally derived tissue [49]. Also the *Erk2* gene plays a crucial role in mesoderm development, as it has been shown that the knockout embryos fail to form mesoderm [231]. On the other hand,

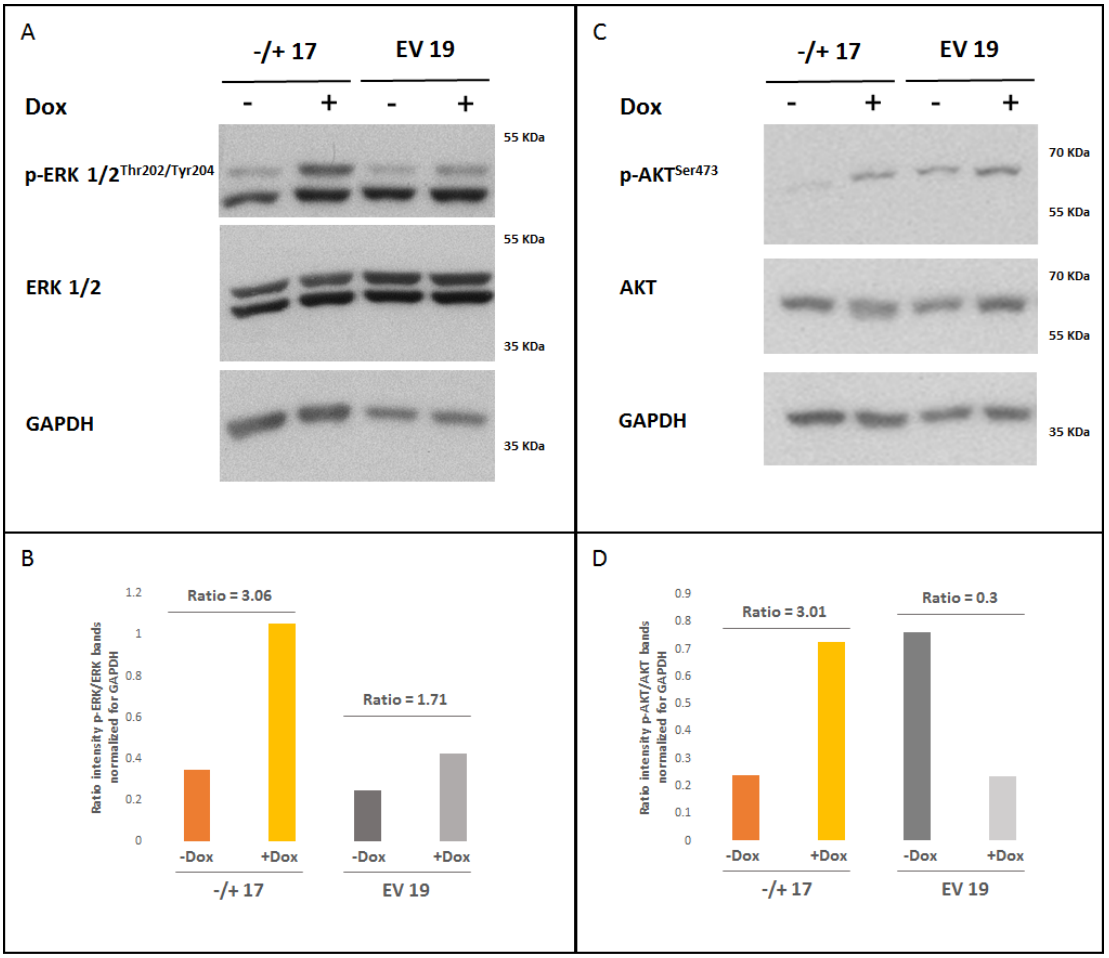

FIGURE 5.10: WB: ERK 1/2 and AKT activation in the IMCD3 -/+ 17 and EV 19 clones. A: Protein levels of p-ERK 1/2 (Thr202 and Tyr204), total ERK 1/2 and GAPDH in total protein extracts of 96h Dox treated and untreated -/+ 17 and EV 19 IMCD3 clones. B: Quantification of the protein levels in section A by ImageJ, which measures the intensity of the bands' signals. After normalising the intensity of the p-ERK 1/2 and total ERK bands for the relative GAPDH signal, the ratio between the amount of the phosphorylated form and the total protein was calculated for each sample. Then, the ratio between the pERK/tot ERK ratios of the +Dox and -Dox samples was calculated and reported at the top of the graphs. C: p-AKT (Ser473), total AKT and GAPDH protein levels in 96h induced and non induced -/+ 17 and EV 19 clones. D: Quantification of the intensity of the bands in section C by ImageJ. After normalising the intensity of each band for the respective GAPDH signal, the ratio between the phophorylated AKT and the total protein was calculated. The ratio between the pAKT/tot AKT ratios of the +Dox and -Dox samples was calculated and written at the top of the column charts.

TABLE 5.5: Data from the RNA seq analysis relative to the expression of the *Cxcl5* gene in the 96h IMCD3 induced clones.

IMCD3 clone	**Log2 fold change**	**P-value**	**Q-value**
+/+ 11	3.02	5.00E-05	0.002176
+/- 1	1.98	9.00E-04	0.014217
-/+ 17	2.30	4.00E-04	0.007725
-/- 1	3.68	5.00E-05	0.001441

although there is no direct evidence that the function of the AKT pathway is pivotal during mesoderm formation, p-AKT is abundantly expressed in the murine paraxial mesoderm [232]. Furthermore, there is increasing evidence that the activation of the pathway is important for the regulation of the EMT process, which is required for the generation of the three germ layers [233]. Moreover, an interesting correlation between the activation of the AKT pathway and the expression of the insulin-like growth factor-2 (*Igf2*) has been proposed. In fact, the *Akt1* and *Igf2* null mice have similar phenotypes [234]; furthermore, the expression of IGF2, which is encoded by an imprinted gene, and the phosphorylation of AKT show parallel expression patterns in murine ES cells [233]. Indeed, it has been shown that IGF2 can mediate the activation of the pathway [235]. Interestingly, Morali et al proposed that IGF2 is able to induce the expression of mesoderm markers during in vitro differentiation of ES cells [236], suggesting another possible correlation between IGF2 expression, AKT activation and the mesoderm formation.

Different papers have also demonstrated that the expression of *WT1* and *IGF2* are closely related. Indeed, it has been shown that inactivating mutations of *WT1* in Wilms' tumour patients result in the biallelic expression of *IGF2* [93, 237]. Confirming the involvement of both the genes in the nephroblastoma formation, Hu et al generated a mouse model of Wilms' tumour by ablating *Wt1* and constitutionally upregulating *Igf2* expression. Interestingly, they also noticed that the cancers developed by the mice were characterised by enhanced ERK 1/2 phosphorylation, proved to be specifically due to the overexpression of *Igf2* [93]. Different studies have shown that WT1 regulates *IGF2* expression: Nichols et al noticed an upregulation of the *IGF2* mRNA levels in a Wilms'

TABLE 5.6: Data from the RNA seq analysis relative to the expression of the *Igf2*, *Igf2r* and *Igf1r* genes in the 96h IMCD3 induced clones.

IMCD3 clone	**Log2 fold change**	**P-value**	**Q-value**
Igf2			
+/+ 11	5.83	5.00E-05	0.002176
+/- 1	3.33	1.00E-04	0.002253
-/+ 17	10.74	5.00E-05	0.001287
-/- 1	9.29	5.00E-05	0.001441
Igf2r			
+/+ 11	0.80	1.00E-04	0.004074
+/- 1	1.14	5.00E-05	0.001234
-/+ 17	0.97	0.00025	0.005214
-/- 1	0.9	8.00E-04	0.01473
Igf1r			
+/- 1	-0.75558	5.00E-05	0.001234

tumour cell line stably transfected with the -KTS isoform [238], while Drummond and colleagues reported that WT1 is a potent repressor of IGF2 transcription [239]. Finally, Caricasole et al identified in an exonic RNA sequence the binding site for the +KTS isoforms [40].

Interestingly, according to the RNA seq data, the expression of the *Igf2* and the *Igf2r* (insulin-like growth factor 2 receptor) genes is upregulated in all the induced WT1-IMCD3 clones, while the *Igf1r* (insulin-like growth factor 1 receptor) seems to be downregulated specifically in the +/- clone. Table 5.6 shows the data from the RNA seq analysis. It would be fascinating to investigate whether these changes in levels of expression are due to transcriptional or post-transcriptional regulation.

5.7 The induction of the -/+ WT1 isoform in the IMCD3 -/+ 17 clone induces the expression of specific markers and regulators of different mesoderm derivatives

As mentioned above, the analysis of the differentially expressed genes in the induced IMCD3 -/+ 17 clone showed enriched GO terms relative to different developmental processes (Table 5.4). A detailed analysis of the genes listed in each GO term highlighted the presence of specific markers and regulators of angiogenesis, adipogenesis, skeletal and cartilage development, as well as the regulation of mesothelial markers (Figure 5.11).

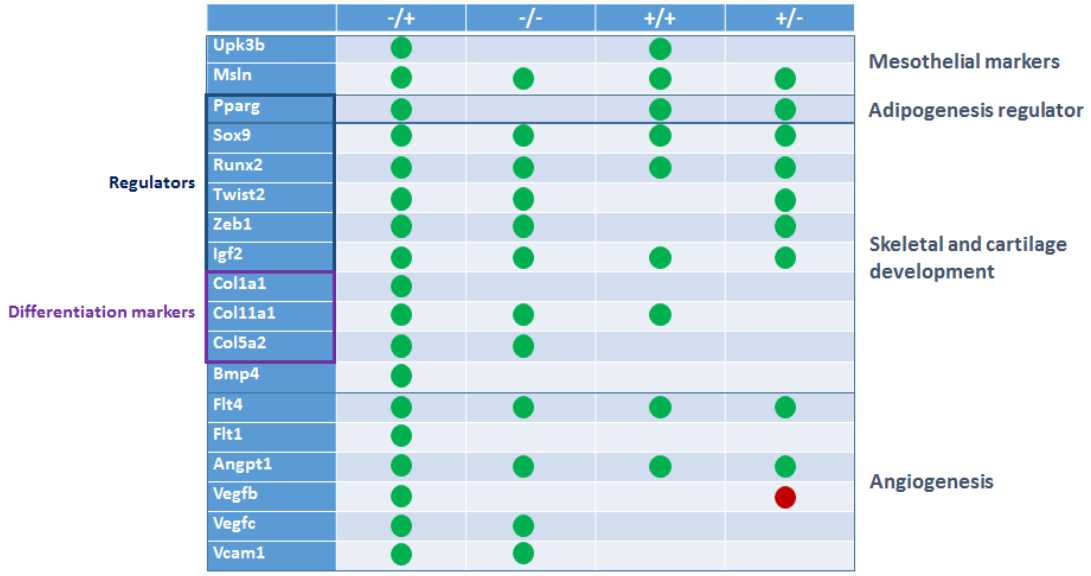

FIGURE 5.11: Regulators and markers of specific developmental processes upregulated in the induced -/+ 17 clone. The table also highlights whether the genes are upregulated (green dots) or downregulated (red dots) in the IMCD3 clones expressing the other WT1 isoforms.

A crucial role of WT1 in the formation of the mentioned mesoderm derivatives has been already observed using different mouse models. In fact, the *Wt1* homozygous knockout mice die in utero probably due to pericardial bleeding [3] and the conditional knockout in the epicardium leads to death in midgestation because of cardiovascular failure

[53]. Moreover, the tamoxifen-mediated deletion of *Wt1* in the adult mice results in a widespread loss of bone and body fat [50]. It has been proposed that the phenotypes observed in the knockout models arise from the alteration of mesenchymal cell populations and from the misregulation of the EMT and MET transitions [49]. Recently, different data have pointed out the importance of the WT1 expressing mesothelia as a source of mesenchymal progenitors during heart, lung, gut, liver and adipose tissue development [9, 50, 53, 56–58]. Moreover, Wilms' tumours carrying *WT1* mutation seem to include ectopic fat, bone, cartilage and muscle, suggesting a role for WT1 in their progenitor cells [49].

Given all these evidence, I was interested not only in validating by Q-RT-PCR the overexpression of the genes predicted by the RNA seq, but also in understanding the timing of their expression. Hence, I performed a time course analysis of the gene expression at 1, 2, 3, 4, 6 and 8 days of induction of the IMCD3 -/+ 17 cells. The levels of expression were compared with the ones of the untreated cells collected in the same day. For the experiment, I initially seeded different numbers of cells for each time point in order to obtain the same confluence of both Dox treated and untreated cells at every day of collection (around 70-80%). This was done in order to avoid variations in gene expression due to different cell confluence. To maintain a consistent cell density, the cells for the 6 and 8 day time points had to be split at 96h.

First, I looked at the changes in expression of the mesothelial markers Uroplakin 3b (*Upk3b*), Mesothelin (*Msln*), and Thrombomodulin (*Thbd*) [240, 241] (Figure 5.12). The *Upk3b* mRNA started being upregulated at 48h and further increased after 8 days of induction. The *Msln* was slightly, but consistently throughout the three independent biological replicates, overexpressed at 4 and 8 days of induction; the fact that the upregulation at 6 days was not statistically significant might be due to the differences in the expression of the mCherry-Wt1 in the replicates. Last, *Thbd* gene expression was enhanced at 72 and 96h.

I also checked whether the mesothelial genes were upregulated in the IMCD3 -/+ 16 clone at 96h of induction (Figure 5.13). The expression levels were compared to the

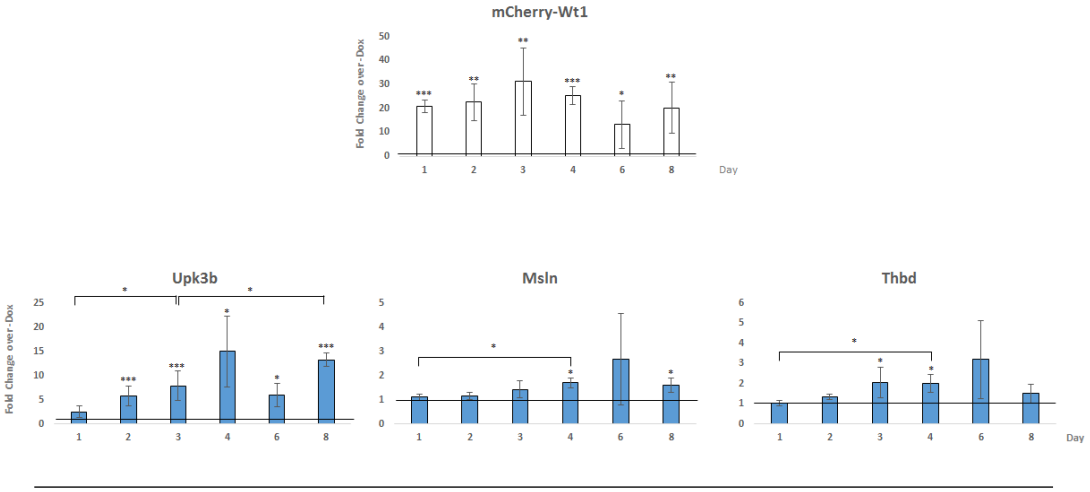

FIGURE 5.12: Q-RT-PCR: fold changes of the expression of mCherry-Wt1, *Upk3b*, *Msln* and *Thbd* in the induced IMCD3 -/+ 17 versus the non induced clone at the indicated time points. The expression of the genes was normalized for the *Gapdh* levels of expression in every sample. In each chart, the horizontal black line underlines the fold change of the non induced clone, which is equal to 1. SD of the mean of three biological replicates. *: P-value < 0.05, **: P-value < 0.01, ***: P-value < 0.001.

average expression in four induced EV clones. I could not confirm the overexpression of the *Upk3b* gene, because the variation between the levels of the two replicates did not allow to reach the statistical power. Similarly, the upregulation of the *Msln* levels was not statistically significant. Moreover, I did not notice differences in the levels of the *Thbd* gene. The inconsistencies in the extent of induction of the genes between the two clones may be due to the lower WT1 -/+ expression levels in the -/+ 16 cells. The MSLN, UPK3B and WT1 are co-expressed in normal mesothelial cells of E14.5 embryos and adults [59]; moreover, subsets of malignant mesothelioma stain positive for WT1 and MSLN or THBD [242, 243]. Although the expression of these four genes is often correlated, so far there are no evidence indicating that WT1 can regulate the mesothelial markers. Therefore, it would be very interesting to assess whether WT1 -/+ can directly regulate their gene expression at a transcriptional or post-transcriptional level.

Second, I determined the levels of expression of markers and regulators of bone and cartilage development by Q-RT-PCR during the time course (Figure 5.14, yellow charts).

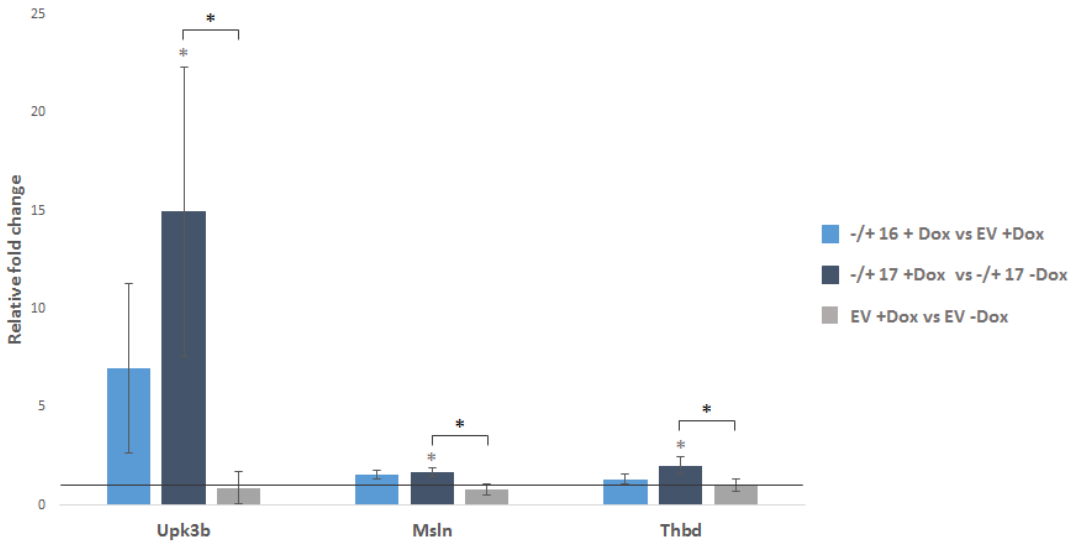

FIGURE 5.13: Q-RT-PCR: fold changes in the expression of mesothelial genes in 96h induced IMCD3 -/+ 16, -/+ 17 and four EV clones. The first series of the chart represents the fold changes of the induced -/+ 16 clone versus the average expression in four EV clones (SD of the mean of two biological replicates). The second series shows the fold changes of the expression in the induced -/+ 17 clone compared with the non induced clone (SD of the mean of three biological replicates). The third series represents the fold changes of the levels of expression in four induced EV clones over the expression levels in the non induced clones (SD of the mean of the four clones). The horizontal line highlights the fold change of the controls, which is equal to 1. *: P-value < 0.05.

The runt-related transcription factor 2 (RUNX2) is a major regulator of skeletal and cartilage development. Indeed, the *Runx2* knockout mice exhibited a complete lack of bone formation and impaired final chondrocyte differentiation [76]. Moreover, *in vitro* and *in vivo* studies have shown that the expression of RUNX2 is sufficient to induce osteoblast differentiation [79]. This transcription factor is considered an initial marker of osteogenic cell lineage, whose expression is maintained during all the differentiation process as well as in mature osteocytes. One of the genes induced by RUNX2 is *Col1a1*, an early marker of osteoblast differentiation, which is absent in the osteocytes [79]. In the time course experiment, I determined that *Runx2* levels increase after 48h of induction and further rise in the following days. On the other hand, *Col1a1* expression is upregulated at 48 and 72h, the overexpression reaches a peak at 96h and then starts decreasing at 6 and 8 days of induction. Different papers have reported a fall in the

overexpression levels of *Col1a1* at 7 days of induced osteoblastic differentiation in human mesenchymal stromal cells [244, 245].

The involvement of the Zinc Finger E-Box Binding Homeobox 1 (*Zeb1*) gene in bone and cartilage development is evident from the phenotype of the null mice, which exhibited skeletal and cartilage defects in various lineages [246]. Even though the molecular mechanisms behind the phenotype are not entirely clear, they are probably related to the ZEB1 mediated regulation of the TGFβ/BMP signalling [247]. I determined that the expression levels of this transcription factor increased significantly after 8 days of induction.

I then characterised the variations in the expression of *Igf2*, which is a known target of WT1 [33]. The gene started being upregulated at 96h of induction and then the levels further increased at the last time point. Various data have suggested a role for IGF2 in bone and cartilage development. First, the *Igf2*$^{-/-}$ mice are viable dwarfs and have delay in ossification [248]. Second, the induced chondrogenic and osteoblast differentiation of parthenogenetic murine embryonic stem cells is improved by the supplementation with IGF2 [249, 250]. Third, a study in human mesenchymal stromal cells showed that IGF2 and IGFBP2 (Insulin-Like Growth Factor Binding Protein 2) promote osteogenic differentiation [244]. In this study the authors suggest a model that connects the functions of Integrin α5 (ITGA5), IGF2 and IGFBP2 in osteoblast differentiation. Interestingly, the levels of both *Itga5* and *Igfbp2* are differentially regulated in the RNA seq analysis. According to the model, the activation of ITGA5 enhances signalling pathways, as the MAPK and the AKT pathways (which were as well found activated in the IMCD3 -/+ 17 induced clone), that activate the expression of IGF2 and IGFB2, which in turn trigger osteoblast differentiation, as shown by the induction of markers such as RUNX2 and COL1A1 [244].

I then decided to validate the overexpression of genes involved in angiogenesis (Figure 5.14 orange graphs). The Fms-related tyrosine kinase 4 (*Flt4*) gene, which plays a crucial role in the cardiovascular system development, as its disruption results in abortive blood vessel formation [251], increased at 96h of induction. On the other hand, the

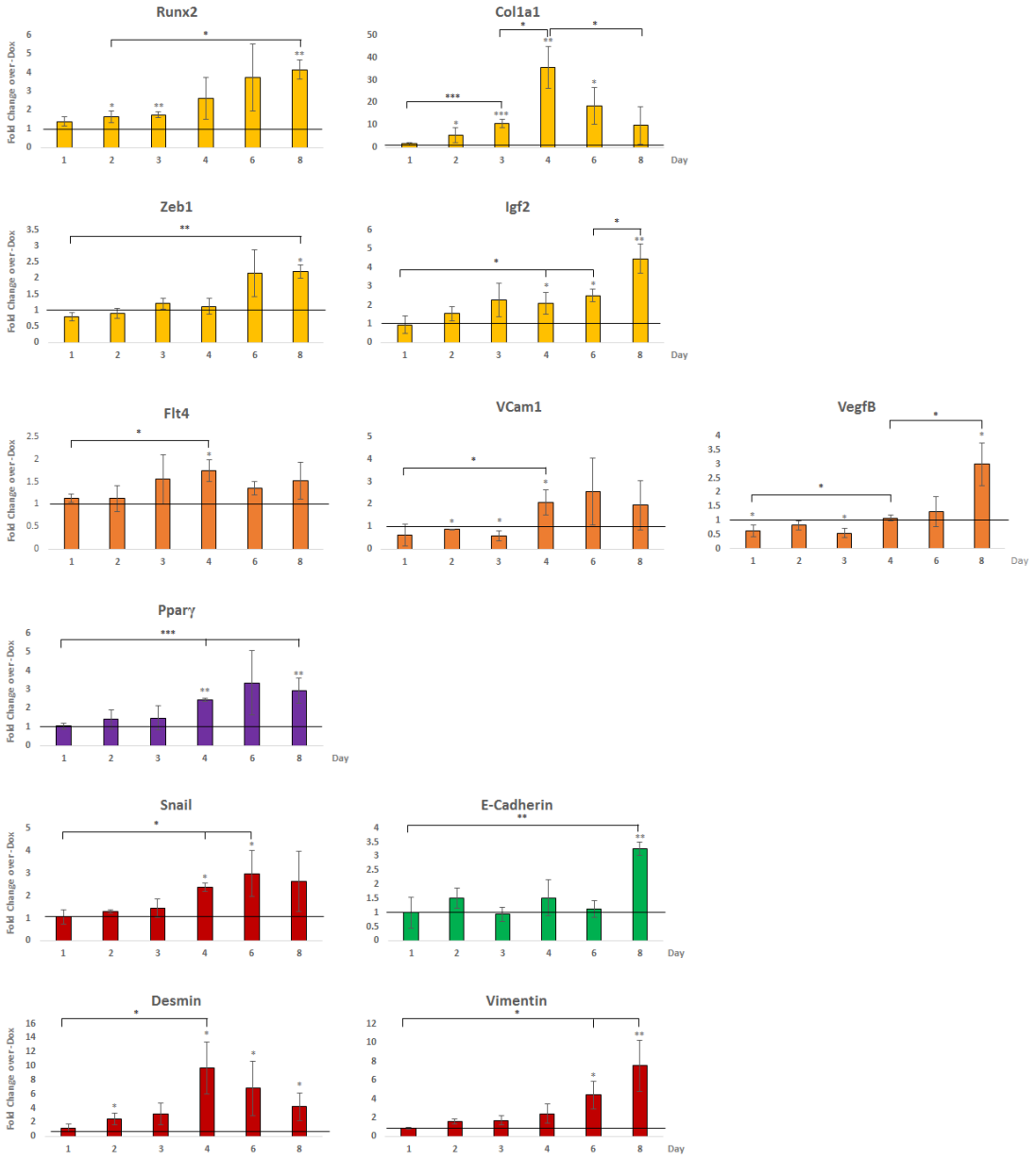

FIGURE 5.14: Q-RT-PCR: time course of the expression of developmental and EMT genes in the induced IMCD3 -/+ 17 clone. Yellow charts: regulators and markers of chondrogenic and osteoblast differentiation; orange charts: genes related to angiogenesis; purple chart: regulator of adipogenesis; red charts: mesenchymal genes; green chart: epithelial marker. Before calculating the fold changes, the expression levels of the genes were normalized for the *Gapdh* expression in each sample. Each chart represents the fold changes of the induced clone versus the untreated cells. The fold changes of the controls, equal to 1, is indicated by the horizontal line in each graph. *: P-value < 0.05, **: P-value < 0.01, ***: P-value < 0.001.

Vascular cell adhesion molecule 1 (*VCam1*) seems to be initially mildly inhibited by the induction of -/+ WT1, but at 96h the expression levels increase and the gene is upregulated. VCAM1 is a cell surface glycoprotein expressed by cytokine-activated endothelia in inflamed tissues. The knockout of the gene results in loss of coronary artery formation and absence of the epicardium [252]. Moreover, VCAM1 and its integrin receptor are required for vascularization, as they facilitate the adhesion of endothelial and mural cells in developing vessels [253]. Similarly to VCAM1, the expression of the Vascular endothelial growth factor B (*VegfB*) gene is downregulated in the first time points, at 96h its levels start increasing until they reach a peak of upregulation at 8 days of induction. The *VegfB* gene is critical for the survival of vascular progenitor cell, vascular endothelial cells, pericytes and smooth muscle cells [254].

One of the most interesting genes that came up from the RNA seq analysis was probably the Peroxisome proliferator-activated receptor gamma (*Pparγ*). PPARγ is a nuclear hormone receptor, which is critical for the apidogenesis since it promotes the differentiation process both *in vitro* and *in vivo* [85]. Moreover, one null mouse, survived until term following placental reconstitution, exhibited complete absence of all types of adipose tissue, as well as fatty liver and haemorrhages [84]. After 4 days of WT1 -/+ induction, *Pparγ* levels started being upregulated and kept being overexpressed until the last time point (Figure 5.14, purple graph). Interestingly, it has also been reported that the levels of *Zeb1* increase during induced adipogenesis in vitro; moreover *Zeb1* mRNA levels are higher in obese mice [255], suggesting a function for ZEB1 in adipogenesis.

Last, I checked the modulation of the levels of EMT and MET markers after WT1 -/+ induction (Figure 5.14, green and red charts). WT1 is a major regulator of the waves of EMT and MET that characterise the generation of certain mesodermal tissues [49]. Highlighting the importance of WT1 in both the transitions, WT1 was shown to regulate the bi-directionality of EMT, controlling epicardial EMT progression, while regulating nephron MET [53, 55]. A crucial role for WT1 has also been proposed in the derivation of progenitor cells from different mesothelia, a process which was suggested

to be characterized by an EMT transition [53, 57, 58]. Specifically, in the epicardium WT1 was proved to be required for the formation for cardiovascular progenitor through the control of the EMT process [53].

During the time course, the EMT regulator Snail family zinc finger 1 (*Snail*), which is a known transcriptional target of WT1 [53], is significantly upregulated at 4 and 6 days from the induction. The difference is expression at 8 days is not statistically significant and may indicate that the expression levels decrease from the last time point onward. On the other hand, the epithelial marker E-Cadherin, which is a direct target of both WT1 and SNAIL [33, 63], starts being upregulated at 8 days of induction, coinciding with the hypothesized downregulation of *Snail*. The *Desmin* gene, which encodes for an intermediate filament that marks mesenchymal cells, starts being upregulated at 48h, reaches a peak of expression at 96h and keeps being upregulated till the last time point. From the modulation of the expression of these three genes, I hypothesise that the induction of WT1 -/+ results in an initial EMT process, possibly followed by the reverse process starting from the latest time point. Interestingly, it has been recently demonstrated that activation of PPARγ leads to the inhibition of TGFβ-induced EMT in lung cancer cells [256]. On the other hand, in contrast to the hypothesis, the levels of the mesenchymal marker Vimentin increase at the last two time points, suggesting that the cells are not reversing the mesenchymal-like phenotype.

In summary, the data from the time course experiment reveal that the induction of the -/+ WT1 isoform in one clone of IMCD3 cells results in the overexpression of markers and regulators of specific developmental processes, suggesting that the -/+ variant might direct epithelial cells to different fates. The upregulation of many developmental markers and regulatory factors seems to reach a peak after 8 days of induction, whereas the expression of the mesothelial markers seem to be enhanced mainly in the first four days. Hence, I hypothesize that WT1 -/+ initially induces an epithelial to mesothelial transition, characterized by increased levels of mesenchymal markers and by unvaried levels of epithelial markers; the expression of WT1 in mesothelial-like cells then leads to

the upregulation of differentiation markers, which possibly coincides with the acquisition of a more epithelial phenotype.

Chapter 6

Discussion

The *Wilms' Tumour 1* (*WT1*) gene was originally identified because of its disruption in 20% of nephroblastomas, a childhood malignant renal tumour. Besides leading to the eponymous tumour, mutations in the human gene have also been found in different pathologies, such as the Denys-Drash, Frasier and Meacham syndromes. The first two conditions impair kidney and genitalia development, while the latter is characterised by male-female sex reversal as well as heart and diaphragm abnormalities [10, 257–259]. In mouse, *Wt1* is essential for the development of a variety of mesoderm derivatives, such as kidneys, gonads, heart, spleen, adrenal glands, diaphragm, limbs and coronary vasculature [3–6, 260, 261]; moreover, WT1 has been implicated in liver and retinal development [7, 9]. Besides its importance in development, it has been shown that WT1 is crucial for the maintenance of adult tissue homeostasis. Indeed, ubiquitously deleting *Wt1* in adult mice results in dramatic phenotypes, as the mutant mice develop severe glomerulosclerosis, massive spleen and exocrine pancreas atrophy, rapid loss of bone and fat volumes, and defects in erythropoiesis [50]. Such fatal consequences of *Wt1* disruption were unexpected, since in the adult tissues WT1 is expressed only in a few cells, including mesothelial cells, podocytes, Sertoli, granulosa, hepatic stellate cells and 1% of bone marrow cells. Therefore, the phenotypes might be explained with the hypothesis that WT1 continues to function in mesenchymal stromal stem and/or

progenitor cells in adults [50]. Furthermore, increasing evidence support an important role of WT1 in tissue repair and regeneration. In fact, WT1 induction in response to damage in different tissues suggests that Wt1 might be a key factor in tissue repair [49].

The *Wt1* gene can theoretically give rise up to 36 different proteins, all characterised by four C-terminal C_2H_2 zinc fingers and an N-terminal proline/glutamine-rich regulatory region. The most-studied variants are the ones encoding or skipping the exon 5 and including or excluding the three amino acids lysine-threonine-serine (KTS) between zinc fingers 3 and 4 (here referred as +/+, +/-, -/+ and -/-). The ratio between the four main isoforms, with the +KTS variants representing about the 60% of the total transcripts, is tightly regulated and kept temporally and spatially constant during kidney development [12]. While the isoforms lacking the KTS clearly regulate gene transcription, it seems that the +KTS variants are more implicated in post-transcriptional regulation, as they co-localise and interact more strongly than the -KTS variants with splicing factors [2, 10, 33]. Moreover, recent unpublished data from our lab suggest that WT1 can interact with components of the RISC complex (RNA-induced silencing complex) (Dr Selvi Bharathavikru, unpublished).

WT1 is a complex transcription factor, whose multiple isoforms have been shown to play redundant as well as distinctive roles in development and disease. Indeed, both -KTS-only and +KTS-only mice die soon after birth due to kidney defects, however the phenotypes of the two strains are different: while the mice expressing only the +KTS isoforms show the most dramatic defects in kidney and gonad formation, the mutants lacking the +KTS variants exhibit impairment in podocyte differentiation and male-to-female sex reversal [13]. On the other hand, although the variants containing the exon 5 are conserved only in mammals, suggesting a mammalian-specific function of the isoforms, the mice lacking this exon are viable and fertile [14]. In disease, unbalanced ratios in the expression of WT1 isoforms has been found in genetic disorders as well as in cancers. For instance, the Frasier syndrome is characterised by a splice site mutation in the *WT1* gene that leads to the underrepresentation of the +KTS variants [262]. Furthermore, Baudry et al detected in Wilms' tumour samples a decrease in

the expression of the isoforms which include the exon 5 [263]. A drop in the levels of the +/+ isoform was also identified in AML (acute myeloid leukaemia) patients [136]; however, the opposite observation was reported by other studies [133, 264].

Most of the phenotypes resulting from the impaired or disrupted expression of *Wt1* and its isoforms have been linked to its crucial function in the regulation of the EMT and MET transitions, two cellular plasticity processes which are essential for normal development and maintenance of adult tissues [52]. WT1 controls the transition between the mesenchymal and epithelial state in a tissue- and context-dependent manner and it is mainly expressed in cells that maintain the potential to transit in either direction of the process [53, 55]. Defects in *Wt1* expression can therefore lead to an unbalance in the mesenchymal-epithelial state of the cells and cause several diseases and developmental abnormalities [52].

Although WT1 functions in physiological and pathological conditions have been extensively studied *in vivo* especially using knockout mouse models, little is known about the instructive role of WT1 and its isoforms. In order to nail down which processes WT1 variants are sufficient to drive, it is necessary to generate a mouse model in which the single isoforms could be induced and overexpressed. In order to address this, first I aimed to clone plasmids for the inducible expression of WT1 isoforms. Because I was not able to derive stable ES cells with the first two types of constructs I made, I established stable inducible epithelial cell lines to start understanding, via expression analysis and cellular assays, how the expression of the isoforms could affect epithelial cells and which cellular processes and pathways the variants were able to induce. However, using the most recent plasmids I cloned, Dr Selvi Bharathavikru and Joan Slight were able to derive inducible and stable E14 *Wt1* KO single clones. These ES cells not only represent an essential resource to address WT1 instructive role *in vitro*, but they can be injected into mice to validate the findings *in vivo*. Moreover, they can be used to try to rescue KO phenotypes.

In this chapter I will discuss the characteristics of the cell models I created and the main findings I obtained from the induction of the single isoforms in the stable clones.

In particular, I will examine the similarities or differences in the results I found using the two epithelial cell lines. Last, I will talk about the future doors that the present work can open.

6.1 The cell models to investigate the role of single isoforms of WT1

I generated two different cell models to induce the expression of WT1 single isoforms and study their functions. I first aimed to design single plasmids that would have guaranteed an inducible, traceable and titratable expression of the gene of interest. To this purpose, I fused at the N-terminus of the cDNA of the murine WT1 isoforms the sequence of a fluorescent reporter. The fusion products were then cloned under the control of a Dox inducible promoter. All the plasmids I created require one single step of transfection and selection to derive inducible clones, reducing considerably the time needed to establish stable clones by using a classic Tet-On 3G inducible system, which requires the integration of two different constructs. Moreover, the plasmids are very easy to modify, thanks to the insertion of single cutting sites between each insert.

I used the first set of plasmids I created, called pSV40-Tet3G-TRE3G-(FP)-(Wt1), to generate stable single clone in the MDCK cell line. The MDCK cells were chosen because they are well-characterised renal epithelial cells, they do not express endogenous WT1 to detectable levels and they are the model of choice to study the EMT process [160], in which WT1 is proved to play a pivotal role. Although canine and murine WT1 proteins are conserved for the 88% (http://www.ensembl.org) and the promoter binding sites of the transcriptional factor are supposed to be highly conserved between the two species [158], I cannot exclude that there might be biases in the function of the mouse WT1 in dog cells.

I established MDCK single clones using all the pSV40-Tet3G-TRE3G constructs. Hence, I derived cells expressing inducible mCherry-WT1, AmCyan1-WT1 and w/o FP WT1.

For the subsequent experiments I decided to use the cells stably transfected with the mCherry and w/o FP plasmids. The constructs carrying the red fluorophore were chosen over the AmCyan1 ones, because the mCherry is a monomeric protein which is supposed to be a better fusion tag. However, having constructs and stable cell lines with the WT1 isoforms fused to different fluorescent proteins can be a valuable tool to study the interaction between variants. Indeed, establishing single clones expressing two isoforms marked by distinctive fluorophores can be achieved by a second round of stable transfection and selection, or it might be possible to fuse single clones to create synkaryons.

The MDCK stable single clones showed a non-leaky inducible expression of WT1 isoforms. The levels of expression were titratable by adding different concentrations of Dox and reversible upon Dox removal. Moreover, the expression and localization of WT1 in the clones established with the FP-Wt1 constructs could be traced thanks to the fused fluorescent marker. The presence of the fluorophore is not only an excellent tool for imaging purposes, but it can also facilitate biochemical analysis. However, it is important to prove that the fusion between the FP and WT1 does not compromise the functioning of the transcription factor, as hinted at some data I will discuss below. For this reason it was crucial to establish control single clones for the expression of single isoforms not fused to any tag. Another control that was employed in the experiments was an mCherry EV clone to determine possible effects due to the supplement of Dox in the medium and to the expression of the FP alone.

The MDCK clones proved to be a valuable model to study the function of WT1 isoforms, even though they presented limitations that made the validation of the results sometimes problematic. In fact, the clones showed high clonal variability and different levels of expression of the single isoforms between the single clones, which made them difficult to compare. The clonal variation was probably due to the random integration of the plasmids, which led to position effects, and to the uncontrolled number of integrated copies.

Although the variation between single clones is inevitable to a certain extent, I tried to reduce the issue when cloning the pGoldiLox plasmids, by adding homologous arms for the recombination in the ROSA26 locus. These plasmids were indeed designed to improve some of the problems encountered with the pSV40-Tet3G-TRE3G-(FP)-(Wt1) vectors. First, the integration of the vectors could have been controlled and targeted to the ROSA26 locus to gain a uniform expression of the isoforms in the clones. Second, the addition of the constitutively expressed EGFP fluorescent protein facilitated the selection of positive clones. Third, the viral SV40 promoter was exchanged with the CAG promoter to reduce the silencing of the promoter in the establishment of stable ES cells [162, 163]. Last, the plasmids encode for a rarely used antibiotic resistance in order to avoid co-transfection with any other resistance markers.

The pGoldiLox plasmids were used to derive stable inducible single clones in the IMCD3 cell line. The IMCD3 cells were chosen because they are murine kidney cells, which are negative for WT1 expression, while positive for both epithelial and mesenchymal markers, property that make then similar to the cells that express the endogenous WT1. After establishing the single clones by co-transfecting each of the pGoldiLox plasmids with two ZFN-encoding vectors, I realised that the majority of the clones expressed the mCherry-WT1 isoforms even in the absence of Dox. This issue could be explained by an interference of the CAG promoter with the sequences regulated by the Dox inducible pTRE3G promoter or might be due to a faulty integration of the whole plasmid. Moreover, the integration in the ROSA26 locus was suggested, but not confirmed, by PCR only in certain clones; as a result, the clones did not express the same levels of the isoforms upon induction. Finding clones in which the vector integrated in the expected locus was difficult and probably required the screening of many more clones. As later on confirmed by the establishment of the ES stable clones, in order to improve the efficiency of integration I should have co-transfected higher amounts of plasmids and used nucleoporation to transfect the cells, as suggested by Perez-Pinera et al [166]. The leakiness of the majority of the IMCD3 clones and the random integration of the plasmids led to two main issues: the impossibility of comparing the induced clone with the non-induced counterpart and, thus, the challenge

of finding the right control. I reasoned that the best controls were the induced EV clones, because the comparison would have taken into account the supplement of Dox as well as the mCherry expression. Moreover, I decided to use more than one EV clone in order to reduce the clonal variability. Another issue related to the interpretation of the data is the lack of control clones expressing WT1 isoforms, which are not fused to a fluorescent marker. Therefore, it will be important to confirm the data in a system in which WT1 is not tagged. Despite these limitations, the experiments using the IMCD3 clones provided interesting hints on the function of the single isoforms of WT1 that will be crucial to definitely validate also using the third system we developed.

Because of the defects of the pGoldiLox plasmids, I decided to clone shorter and simpler plasmids to generate stable ES cells for the inducible expression of WT1 single isoforms. The new constructs were called CAG-Tet3G-TRE3G-mCherry-(Wt1) and they were made by modifying the pSV40-Tet3G-TRE3G-mCherry plasmid. Differently from the original plasmid, the new vectors contain the CAG promoter, the Zeocin resistance and the ROSA26 homologous arms. Moreover, the induction can be followed with the mCherry expression, but the WT1 isoforms are not fused with the fluorescent protein. In order to facilitate the biochemical analysis, I wanted to tag WT1 with the small Twin-Strep-tag, which is predicted not to affect the protein activity [167]. However, preliminary data raised the doubt that the tag is actually not expressed. This might be due to the incorrect sequence of the tag, which I had to derive from the amino acid sequence, as it is not publicly available. The CAG-Tet3G-TRE3G-mCherry-(Wt1) plasmids coupled with the ZFN-coding vectors were anyway used to establish stable E14 *Wt1* KO cells by Dr Selvi Bharathavikru and Joan Slight. The clones so far seem to be inducible and non-leaky; moreover, PCR preliminary data sustain a correct integration of the plasmids into the ROSA26 locus. These inducible ES cells represent a great tool to further study the instructive role of WT1 *in vitro* and *in vivo*, allowing in the next future the generation of a new mouse model for the ubiquitous overexpression of each variant of WT1. Because the expression of the single isoform is titratable, it will be also possible to determine the minimal expression levels required to rescue the KO phenotypes.

6.2 The single WT1 isoforms and their effects on cell proliferation and oncogenic potential

The influence of WT1 on cell proliferation and oncogenic potential has been mainly addressed using cancer cell models, while the effect on non-transformed cells has been less investigated. Overall, the data in the literature suggest dichotomous functions of WT1 and its isoforms, depending on the cell line employed and the way used to modify WT1 expression. Hence, so far several studies have labelled WT1 either as an oncogene or a tumour suppressor.

From both the microarray and RNA seq analysis, it seemed that the induction of specific isoforms affected cell proliferation. Therefore, I decided to assay the growth rate of the MDCK and IMCD3 clones both in normal adherent culture and in the absence of anchorage, which provides an indication of cellular transformation. Overall, the proliferation of the MCDK and IMCD3 cells as monolayers on a substrate was not affected by the expression of the single isoforms. The assay underlined the presence of intrinsic variabilities either between clones expressing the same isoform or between WT1-expressing clones and EV clones, therefore coming to certain and unanimous conclusions was problematic. In particular, the behaviour of the mCherry -/+ MDCK clones stood out. In fact, only these two clones showed a clear block in G1 phase of the cell cycle, likely due to the upregulation of p21.

Similarly, the growth in soft agar gave different outcomes depending on the tested clone and the cell line used. Specifically, the +/+ isoform seemed to increase the number of colonies formed only in the IMCD3 clone. The induction of the +/- variant favoured the anchorage-independent growth of the IMCD3 clone, but lowered the colonies formed by one of the +/- MDCK clones. On the other hand, the WT1 -/+ expression drastically reduced the number of colonies generated by the two mCherry -/+ MDCK clones, but it did not influence the growth of the IMCD3 or the MDCK w/o FP clones. Last, the expression of the -/- isoform in the IMCD3 clone, although not modifying the number, increased the size of the colonies, while the induction of the variant in the MDCK

clones seemed to inhibit the cell potential to grow without anchorage. Despite the clonal differences, overall the data might suggest that the induction of WT1 in the MDCK cells, which are tumorigenic in nude mice [195], tends to inhibit the anchorage-independent growth of the cells, whereas the expression in the IMCD3 cells, whose oncogenic potential has not been investigated, leads to the opposite tendency.

Another aspect of the cellular physiology that the genome-wide analysis on certain induced clones highlighted was a change in the expression of genes related to cell motility, whose increase can also be related to the acquisition of oncogenic properties. I therefore decided to measure the speed of migration of the MDCK and IMCD3 clones using a wound healing assay. Generally, the induction of none of the isoforms influenced the velocity of the cells consistently throughout the clones. Nonetheless, the expression of the -/+ isoform in the mCherry -/+ MDCK clones led to a reduction of the migration rate, while it tended to increase the speed of the IMCD3 -/+ 17 clone, although the interpretation of this last result was complicated by the influence of the Dox itself on one of the EV clones.

In conclusion, the influence of WT1 expression on cell proliferation, both on substrate or in soft agar, and on cell migration was not consistent and varied among the single clones. Also, some of the data worryingly suggested a possible influence of the mCherry tag on WT1 activity, since in some cases only the clones expressing the fusion protein gave different outcomes in the assays. Although in order to exclude this possibility it will be necessary to analyse more clones to establish which are the outliers, the fact that the IMCD3 clones, which express WT1 fused to the FP, do not always behave according to the MDCK counterparts, might suggest that the mCherry-WT1 fusion does not have peculiar properties and specific functions itself.

6.3 The induction of the -/+ isoform changes the expression of many genes and affects processes specifically regulated by this variant

From the expression analysis of both the MDCK and IMCD3 clones, it became clear that the -/+ isoform induced the most relevant isoform-specific changes as well as a very high number of differentially regulated genes. This result highlights the importance of the most expressed variant among the conserved isoforms in all the vertebrates. Since multiple genes and processes seem to be commonly regulated by all the isoforms, it would be interesting to assess whether the expression of single isoforms can induce the expression of the endogenous *Wt1*.

Because the -/+ isoform is supposed to have both post-transcriptional and transcriptional functions, it will be important to investigate whether the changes are due to direct regulation of the genes or/and to post-transcriptional events, which might, for example, stabilise the mRNA. Moreover, it will be interesting to validate and confirm, also for the -/+ isoform, the preliminary observation that the expression of the +/+ isoform in the IMCD3 cells favours the exclusion of one of the exons in the *Cd55 gene*. Of note, Markus et al reported that the +/+ isoform interacts with the splicing factor RMB4 and inhibits its ability to regulate alternative splicing [217].

Supporting post-transcriptional functions for the +KTS variants, these isoforms localize to the nuclear speckles and directly associate with some components of the spliceosomes [31, 32]. Moreover, two studies reported that the +KTS isoforms interact with splicing factors, suggesting a role in the pre-mRNA splicing [37, 217]. In 1996, Caricasole et al described the first WT1 +KTS mRNA target, defining an exonic RNA sequence as the binding site to the *Igf2* mRNA [40]. More recent studies suggested that the variant including the three amino acids interacts with the *Actn1* (alpha-actinin 1) mRNA [41] and can upregulate post-transcriptionally the mRNA and protein of a crucial gene for the development of olfactory neurons [8]. However, the +KTS isoforms were also proved to be able to regulate the gene expression at the transcriptional level. Indeed, specific

DNA binding sequences for the +KTS isoforms have been described [45], as well as direct transcriptional targets [42, 43]. Moreover, a recent study identified by ChIP-Seq (Chromatin immunoprecipitation sequencing) on embryonic kidneys a WT1 binding motif, which is highly similar to the sequence identified as the +KTS target [44].

6.4 The -/+ isoform and the induction of a fibrotic-like phenotype

Among the processes that specifically the -/+ isoform seems to regulate both in the MDCK and the IMCD3 clones, there is the modification of the ECM organization. Indeed, I validated the upregulation of different genes involved in the ECM remodelling upon induction of the -/+ isoform, including the *Mmp9*, *Col1a1* and some metalloprotease inhibitors. One of the IMCD3 -/+ clones also showed an increased adhesion to a variety of ECM substrates, suggesting an upregulation of cell adhesion molecules. Interestingly, some genes encoding for integrin subunits were found differentially regulated in the expression analysis; moreover, the induced clone was also characterised by the phosphorylation of components of the MAPK and AKT pathways, which are both activated by integrin-mediated signalling [265].

The modulation of the ECM organization is a crucial event during development and disease. The ECM not only provides physical support to the tissues, but it is also essential for the maintenance of their homeostasis. In fact, components of the ECM constantly interact with the epithelial cells through the binding to cell receptors, such as the integrins. The interaction between cells and components of the ECM leads to the transmission of an array of signals, regulating cell shape, adhesion, migration, proliferation, survival, apoptosis as well as differentiation. Moreover, the ECM is a reserve of ligands, since it binds and locally releases numerous growth factors. The cells keep synthesizing, degrading, remodelling and reassembling the ECM. Specifically, the cleavage of ECM components is the most important process that regulates the ECM organization and its abundance. A correct ECM proteolysis is achieved by the combined

and balanced functions of proteases, such as the metalloproteinases (MMPs), and their inhibitors, called TIMPs [266].

It has been shown that ECM remodelling is essential for the development of different organs, including lungs, mammary and submandibular glands. In particular, it is crucial for the formation of branching structures, which requires the repetitive formation of epithelial structures that invade the embryonic ECM. Moreover, the ECM releases different growth factors, which favour various developmental processes, such as the vascularization of the organs [266].

On the other hand, a dysregulation in ECM remodelling is associated with different pathological conditions, such as tissue fibrosis, which is characterised by an abnormal ECM deposition and stiffness. The fibrosis is a consequence of an aberrant and chronic wound healing response, which involves the activation of local fibroblasts into myofibroblasts, the recruitment of immune cells and the accumulation of ECM, due to the altered activation of MMPs and TIMPs and to the exaggerated production of ECM components [141]. Because the induction of the WT1 -/+ isoform especially in the MDCK cells, and partially in the IMCD3 clones, causes the upregulation of pro-fibrotic genes, such as *MMP9*, *COL1a1* and different TIMPs, as well as the overexpression of the fibrotic markers *ACTA2* and *DESMIN*, I suggest that the expression of this variant might be involved in the promotion of the scarring process at least in the MDCK cells. Corroborating this hypothesis, the induction of the -/+ isoform in the MDCK clones results in the upregulation of several chemokines, which are central mediators of the initiation and progression of the tissue fibrosis, by recruiting inflammatory cells and promoting angiogenesis [141]. Specifically, the induced -/+ MDCK clones show the overexpression of the pro-fibrotic chemokines *CCL2*, *CCL7*, *CXCL8* and *CXCL10*; similarly, the Dox treatment of the -/+ IMCD3 cells seems to upregulate the *Cxcl5* gene, which encodes for a murine chemokine functionally related to the CXCL8 [230]. Of note, one of the induced -/+ IMCD3 clones is characterised by the activation of the MAPK and AKT pathways, both involved in the release of the CXCL8 [228]. The CXCL8 was also demonstrated to be able in turn to activate the AKT pathway itself

[229]. Importantly, the continuous AKT activation is pivotal for the upregulation of the *Acta2* expression and for the myofibrobalst differentiation [267]. However, the finding of the upregulation of the *Pparγ* gene in the IMCD3 -/+ 17 clone contrasts the hypothesis of the induction of a fibrotic phenotype in this cell line. In fact, PPARγ inhibits the activation of hepatic stellate cells, the proliferation of lung myofibroblasts and dermal fibrosis [267].

Interestingly, the phenotype observed in the mCherry -/+ MDCK clones after induction, characterised by the appearance of giant multinucleated cells, was noticed in fibrotic tissues [197]. Moreover, the presence of prominent stress fibers in the induced clones is also a characteristic feature of activated myofibroblasts [170]. Last, the Dox treated cells showed some features typical of cellular senescence, which is associated with significant changes in ECM and production of multiple chemokines [198]. Furthermore, senescence has been proposed as a mechanism which blocks the excessive proliferation of myofibroblasts to limit the fibrotic process [268]. Although I detected this phenotype only in the two MDCK mCherry clones, it is important to mention that the appearance of large and multinucleated cells was already observed in a Wilms' tumour cell line stably expressing the -/+ isoform [105]. This might suggest and provide an indirect piece of evidence that the phenotype is not indeed induced by the mCherry-WT1 fusion protein, but by the WT1 isoform itself.

Taken together, these data suggest that the induction of the -/+ isoform in both the MDCK and IMCD3 clones causes the upregulation of ECM remodelling genes. Moreover, at least in the MDCK clones, it promotes the upregulation of fibrotic markers and it induces an inflammatory response. This can be particularly relevant for shedding a new light on the role of WT1 in wound healing, tissue repair and fibrosis. In fact, WT1 has been found expressed in epicardial fibrosis following ischemic injury, as well as in renal and lung fibrosis [138, 139, 153]. Moreover, WT1 is expressed in the hepatic stellate cells, which activate in response to liver injury, undergoing several functional changes, such as matrix remodelling, actin reorganization, chemotaxis and contraction.

Dissecting the function of WT1 in tissue fibrosis is essential to determine whether WT1 can be considered as a therapeutic target.

6.5 The induction of the WT1 -/+ in one of the IMCD3 clones leads the cells to the middle of a junction with different paths to choose

The importance of WT1 in development and disease is paralleled with its crucial role in the control of the EMT and MET transitions. Recently, particular attention has been paid to the role of the expression of WT1 in different mesothelia, supposed to be crucial for the morphogenesis and, possibly, for the maintenance of certain organs. The mesothelium is a layer of flat cells that derives from the mesoderm and lines the coelomic cavity of the embryo; in the adult it is composed of a simple squamous epithelium that covers the peritoneum, the pericardium and the pleura.

The expression of WT1 in the embryonic mesothelium has been proved to be crucial for the development of different organs, such as liver, lungs, heart and adipose pads. For instance, two papers advocated a central role of the mesothelial expression of WT1 for liver morphogenesis. First, it has been shown that the WT1 positive mesenchymal cells, which delaminate from the coelomic epithelium that covers the liver primordium, are essential for the generation of the progenitors of the stellate cells [9]. Later on, Asahina et al demonstrated that cells from the septum transversum mesenchyme that express WT1 give rise to mesothelial cells, which migrate and generate stellate cells, fibroblasts and smooth muscle cells of the portal and central veins [56]. Different papers suggested a critical role of WT1 in a conserved mechanism for the development of blood vessels in all the coelomic organs. In fact, it was shown that a subset of serosal mesothelial cells, which line the intestinal tube and express WT1, undergo an EMT transition and migrate into the gut to differentiate into smooth muscle cells, which surround the major blood vessels in the mesentery and gut [57]. Similarly, WT1 expressing mesothelial cells were demonstrated to be a source of vascular smooth muscle cells in the developing lung [58].

In 2010, Martinez-Estrada et al determined that WT1 is essential for the generation of epicardial-derived mesenchymal cardiovascular progenitors and their derivatives, such as coronary blood vessels and cardiomyocytes, thanks to the regulation of the EMT process [53]. Later on, WT1 was proved to mark a subset of visceral white adipocyte tissue progenitors. Moreover, the WT1 expressing mesothelium, which surrounds the visceral fat depots, was shown to produce adipocytes during embryonic development as well as postnatally [59].

Given all these evidence, the upregulation of mesothelial markers, such as *Upk3b*, *Msln* and *Thbd*, within the first four days from the induction of the -/+ isoform in one of the IMCD3 clones is particularly relevant. Indeed, it may indicate that the expression of this variant of WT1 is sufficient to direct epithelial cells to a more mesothelial phenotype. This might be achieved by the induction of an epithelial to mesothelial transition, as suggested by the upregulation of different mesenchymal markers, such as *Snail*, *Desmin*, *Col1a1*, *Acta2* and *Mmp9*, coupled with the maintenance of the levels of the epithelial marker *E-Cadherin*. Following the upregulation of mesothelial and mesenchymal genes, the sustained induction of the -/+ isoform seems to lead to the upregulation of regulators and markers of different developmental processes, namely skeletal and cartilage development, angiogenesis and adipogenesis. WT1 is already known to play an essential role in the formation and maintenance of all these structures, but whether the expression of WT1 is sufficient to drive their development remains to be investigated. First, I validated the overexpression of the *Runx2*, *Col1a1*, *Zeb1* and *Igf2* genes, whose functions are pivotal for skeletal and cartilage development. Second, among the genes involved in the regulation of the vascularization process, I confirmed the upregulation of *Flt4* and *VCam1* at 96h form the induction; of particular note, is the overexpression of *VegfB* at the latest time point, as it is essential for the survival of vascular progenitor cells and their derivatives [254]. Last, I validated the upregulation of one of the main regulators of adipogenesis, *Ppar*γ, whose expression starts being enhanced from the forth day. Interestingly, I also determined the upregulation of *E-cadherin* at 8 days from the induction. The increase in expression levels of the epithelial marker was concomitant with the peak of upregulation of the majority of the differentiation

markers and regulators; moreover, it was paralleled with the downregulation of some mesenchymal genes as *Snail* and *Desmin*.

Taken together, the data might suggest that the induction of WT1 -/+ first leads the epithelial cells to the acquisition of a mesothelial phenotype, also through the modulation of mesenchymal genes; the extended expression of the isoform then directs the cells along the pathway to different fates, a process which is possibly concurrent with a mesothelial to epithelial transition. Therefore, understanding the mechanisms beneath these changes might shed a new light on the function of WT1 in development, particularly on the importance of WT1 expression in mesothelial cells. Moreover, the data emphasize the great potential of an inducible system for the expression of WT1 isoforms to address and investigate their instructive roles.

6.6 Conclusions and future directions

The first goal of my work has been establishing an inducible system for the expression of single isoform of WT1. I generated different plasmids, aiming to improve their functions to finally establish stable ES cells. In order to start addressing the instructive role of WT1, I derived two epithelial cell lines, which express in a Dox-dependent manner each of the four main isoforms of WT1. The single clones have been proved to be a good tool to investigate the processes that WT1 is able to induce. By genome-wide expression analysis and cellular assays, I was indeed able to characterise the induced cells, with a particular focus on the -/+ clones. In fact, the -/+ clones show the most remarkable changes upon induction in both the cell lines, underling a crucial role for the +KTS isoforms, which are the most expressed variants of WT1. From the study, I concluded that the main feature characterising the MDCK -/+ cells is the induction of a fibrotic-like phenotype, coupled with an inflammation response. On the other hand, the expression of WT1 -/+ in the IMCD3 clones leads to the upregulation of mesothelial markers, together with the overexpression of pivotal genes for the development of bone, cartilage, vasculature and fat; moreover, the induction of the isoform

causes the modulation of EMT genes, suggesting an initial transition of the epithelial cells toward a mesothelial phenotype, followed by the reverse process, which coincides with the peak of expression of several differentiation genes. The latter results raise the interesting hypothesis that WT1 -/+ is indeed sufficient to direct epithelial cells to different differentiation pathways, possibly through a mesothelial intermediate state.

In order to confirm the expression data obtained with the induction of the -/+ IMCD3 clones, I want to establish the protein expression levels in a time course, which will also include later time points to follow the hypothesised mesothelial to epithelial transition. It will be also necessary to validate all the expression data in a second IMCD3 -/+ clone.

Second, I want to address the mechanism behind the regulation of the genes. To this aim, I will define which genes are direct transcriptional targets of WT1, using a ChIP-seq approach. Moreover, in order to identify post-transcriptionally regulated genes, I can employ two techniques that allow the identification of ribonucleoprotein complexes: the RNA-IP (RNA immunoprecipitation), used to detect the binding of individual proteins to specific RNA molecules, and the Clash (cross-linking ligation and sequencing of hybrids), which allows high-throughput identification of sites of protein-RNA and RNA-RNA interactions.

Third, it will be very interesting to follow up and validate the data, suggested by the RNA seq analysis, regarding the preferential usage of certain exons depending on the expressed WT1 isoform. Confirming these predictions will shed a new light on WT1-mediated regulation of the splicing process and suggest another way for WT1 to influence the expression and function of genes.

Last, I want to establish the differentiation potential of the IMCD3 cells, by culturing the induced and non-induced cells in different conditioned media to assess their ability to differentiate into multiple lineages.

Crucially, I want to address the relevance of the findings *in vivo*. This is now possible thanks to the establishment of stable *Wt1* KO ES cells, in which I can induce the

expression of single isoforms of WT1 and further study their instructive roles. The stable ES cells can be assessed for their potential to differentiate into the three germ layers by embryoid body formation. Moreover, they can be used to address whether the expression of single isoforms can rescue the KO phenotypes and to establish the minimal expression required to rescue. The final crucial goal will be the generation of mouse models for the ubiquitous expression of single WT1 variants. These mouse models will be essential to define the instructive role of WT1 *in vivo* and they will be a pivotal tool to study WT1 functions in embryonic development as well as in the maintenance of the adult tissues.

Concluding remarks

Although the full understanding of the instructive role of WT1 isoforms in development, adult tissue maintenance and disease is still obscure, my work has hopefully provided the Ariadne's thread to address this question and has proposed intriguing clues on the processes that WT1 could be sufficient to induce.

Appendix A

Supplementary data

A.1 Additional figures

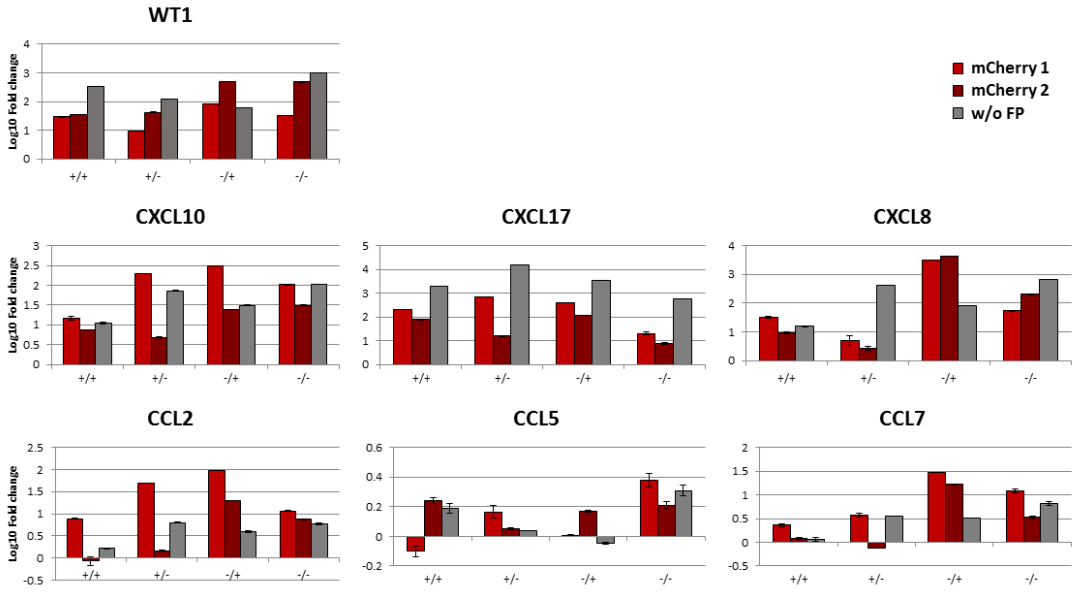

FIGURE A.1: Q-RT-PCR to determine the levels of expression of different chemokines in MDCK single clones induced for 96h. The gene levels in each sample were first normalized for the *GAPDH* expression levels. The column graphs represent the Log10 fold change of the mRNA expression in the +Dox samples relative to the levels in the -Dox and EV samples. SD of the mean of two technical replicates per clone.

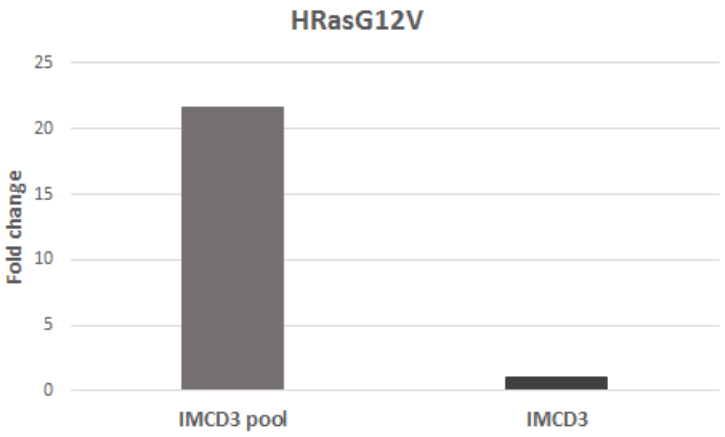

FIGURE A.2: Q-RT-PCR to assess the levels of upregulation of HRasG12V in the IMCD3 pool of clones stably transfected with the MSCV-HRasV12 construct. After normalising the HRasG12V levels for the levels of expression of the *Gapdh* gene, I calculated the fold change of expression by comparing the level in the pool of stable clones versus the one in the IMCD3 cells. The expression levels in the IMCD3 cells is therefore equal to 1.

A.2 List of genes differentially regulated in the microarray and RNA seq analysis

The genes are listed in alphabetical order.

List of genes differentially regulated in the microarray analysis of induced MDCK clones:

Upregulated genes:

Genes uniquely upregulated by +/+: ALOX5 CSF2 GJB1 GUCY1B3 NEIL1 SLC28A1 SPRY4 SYT13

Genes uniquely upregulated by +/-: ABCF1 ABHD3 ACACA ACLY ACOX1 ACSL1 ADCYAP1R1 AMPD3 ARL2BP ARMC2 ASAP2 ASPM BCHE BRI3BP C17H2orf56 C1H9orf64 C26H22orf39 C37H2orf47 C5H16orf55 CACYBP CDCA2 CDK2AP1 CDKN2C CENPP CEP89 CKAP2L CKAP4 CLASP1 CNGA1 CORO1C CP CTR9 CTSL2 CTSL2 CXADR CYP51A1 DHRS9 DHTKD1 DHX9 DLX1 DNAJA1 DNMT1 DROSHA DUT

E2F7 E2F8 ELOVL6 EXTL2 EZH2 FAM167A FAM83D FANCA FOXJ1 G3BP1 GIGYF2 GINS4 GLIPR1 HCAR3 HERC6 HLA-DMB HMGCR HNRNPA3 HNRNPAB HNRNPD HNRNPR HOXC5 HSPA8 ICMT IDH1 ITPKA IVL KIAA0494 KIAA1524 KIF18B KIF23 KIF24 KIF4A KPNA2 KPNB1 LIPT2 LOC100684663 LOC100684977 LOC100855560 LOC100855667 LOC100855736 LOC100855917 LOC100856058 LOC100856093 LOC100856162 LOC100856212 LOC100856353 LOC100856417 LOC100856636 LOC479820 LOC488258 LOC609233 LOC610335 LOC610383 LOR LRRC1 LUC7L LUC7L2 MCM4 MED14 MELK METTL13 MNS1 MORF4L2 MTMR4 MXD3 NEURL1B NOD2 NSF NUSAP1 NXPE3 OSTC PANX1 PAPSS1 PAXIP1 PIK3AP1 PIK3R5 PITPNA PLA2G12A POLA1 POLQ POLQ PSMD1 PSMD5 PSMD5 PTPLB RACGAP1 RAD54B RHPN2 RPA3 RRBP1 RTF1 SEC23B SEC24D SETD6 SGOL1 SHCBP1 SLC16A3 SLC20A1 SLC25A13 SLC9A6 SLCO3A1 SLCO3A1 SMC4 SNAP29 SNRNP25 SPAG5 SPCS3 SRRM1 SRSF1 SRSF6 SRSF7 STARD6 TACC3 TAF1 TARDBP TMC5 TMCO3 TOB1 TRIM35 TRIM50 TRPM6 TSPAN5 TTC19 TTLL5 TXNRD1 TYMS TYMS UHRF1 VCL XKR6 ZAK

Genes uniquely upregulated by -/+: A3GALT2 A4GALT ABCA3 ABCA4 ABHD14A ABHD6 ABLIM2 ABLIM3 ABR ABRACL ACE ACHE ACP2 ACSF2 ACSL4 ACSS2 ACTA2 ACTN1 ADA ADAM28 ADAM33 ADAMDEC1 ADAMTS2 ADAMTS7 ADAR ADD1 ADPGK AFAP1 AGFG2 AIM1L AK1 ALAS1 ALPK2 ALS2CL AMACR AMOTL1 ANAPC13 ANKRD1 ANKRD23 ANKRD52 AP2M1 AP4S1 APBB2 APC2 APOA5 APOBR APOE APOL6 AQP7 ARHGAP1 ARHGEF37 ARHGEF40 ARHGEF7 ARL2 ARRDC2 ARSA ASAP3 ASL ATHL1 ATOX1 ATP2B4 ATP5S ATP6AP1 B3GALT4 B3GALT5 B3GNT7 B3GNT8 B4GALT6 BAI2 BCAM BCAR3 BCL2L15 BDKRB2 BIN1 BIRC3 BST1 BTG2 BTG3 C11orf34 C11orf9 C17H2orf65 C18H11orf41 C18orf8 C19orf66 C1QL1 C1QL4 C1QTNF1 C1QTNF2 C26H22orf13 C27H12orf57 C28H10orf76 C2CD2 C2H1orf130 C2H5orf46 C30H15orf62 C32H4orf26 C34H3orf70 C4H1orf198 C5H16orf74 C6H16orf93 C6H7orf43 C7H18orf32 C8H14orf1 C9H17orf96 CAB39L CABP7 CACNG4 CAMK2A CAMTA1 CAPN14 CAPN2 CARD6 CARD6 CARHSP1 CASP12 CASP4 CBLN3 CBY3 CC2D1B CCBL1 CCDC134 CCDC159 CCDC64B CCHCR1 CCL17 CCL4 CCPG1 CD101 CD151 CD164 CD81 CD82 CD99L2 CDC37 CDC42 CDC42EP2

CDC42EP3 CDH17 CDH22 CDH6 CDK5R1 CDKL4 CDR2 CELF6 CENPB CERCAM CERS4 CFB CFL2 CHI3L1 CHRNB1 CHST11 CHST15 CHST3 CHTF18 CIB2 CIITA CISD3 CLDN1 CLDN23 CLDN6 CLDN9 CLEC16A CLIC3 CLN5 CLOCK CLTCL1 CLUL1 CNIH2 CNN2 CNPY4 CNRIP1 COBRA1 COL12A1 COL17A1 COL1A1 COL4A2 cOR52X3 CORO2A CPNE2 CPVL CRADD CRB2 CREB3L2 CREB5 CRIP1 CRIP2 CRLF1 CRYBA4 CRYBB1 CRYGA CSRNP2 CSRP1 CTNND1 CTSA CTSH CTTNBP2 CTTNBP2 CX3CL1 CXCL16 CXCR4 CXXC5 CYB561D1 CYB5R1 CYLD CYP26B1 CYP27C1 CYP2D15 CYP4B1 CYTH1 DAB2 DACT1 DAK DBN1 DCXR DDAH2 DEDD2 DEGS1 DENND2A DENND2D DENND5A DENND5B DEPDC7 DERL3 DES DIAPH1 DIXDC1 DKK3 DLA-12 DLA-64 DLA-79 DLA88 DLEC1 DLGAP4 DLX5 DMBX1 DMGDH DMKN DNAJB5 DNAJB9 DNAJC22 DNASE1L1 DNM3 DNPEP DOCK6 DOK1 DPP4 DPYSL3 DSTN DTNB DUSP3 DUSP4 DUSP7 DUSP8 DYSF EBF4 ECE1 ECHDC3 ECI1 EDEM2 EDN1 EFHD1 EFNA5 EFR3B EGFR ELF4 ELFN1 ELK4 ELMO2 EMC10 ENOSF1 ENSA EP300 EPB41L4B EPHA1 EPHA2 EPHB2 EPHX3 EPS8L1 EPS8L3 ERGIC1 ERO1L ESYT1 EVI2B EVPL FADS1 FADS3 FAM101B FAM118A FAM171A1 FAM173B FAM174A FAM176A FAM176C FAM189B FAM18A FAM20C FAM212A FAM3A FAM53A FAM65A FAM70A FAM71E1 FAM89A FAM89B FANK1 FARP1 FARP2 FARSA FASN FBLIM1 FBLN5 FBXL16 FBXL8 FBXO10 FGF1 FGFR3 FGFRL1 FGL1 FIBP FICD FLNA FLNB FLT1 FLT4 FLVCR2 FNDC3B FNDC4 FOXP4 FOXS1 FRMD4A FRMD6 FSCN1 FSTL1 FSTL3 FTH1 FUNDC2 FXN FXYD4 GAA GAL3ST2 GALNS GALNT10 GALNT3 GALNTL1 GAS2 GAS2L1 GATA2 GATSL3 GBGT1 GBP1 GCH1 GDI1 GDPD5 GGCT GIPC1 GJB4 GLB1 GLCCI1 GMIP GNAI2 GNAO1 GNAZ GNS GPC4 GPCPD1 GPI GPR115 GPR137B GPR143 GPR153 GPR176 GPR4 GPR68 GPR87 GPX1 GRAMD1B GRK5 GRM4 GSG1 GSTA4 GTF2IRD2 GXYLT1 H1FOO H6PD HAUS7 HAVCR1 HBEGF HDAC7 HEBP1 HECW1 HEXB HEYL HGFAC HGS HIVEP1 HIVEP3 HK1 HLA-DMA HLA-DOB HLA-DQB1 HLA-DRB1 HN1 HOGA1 HOMER2 HPS1 HR HSD17B14 HSPA12A HTR1D HTRA1 IAPP ICAM1 IER3 IFIT2 IFNGR2 IGDCC4 IKBIP IL13RA1 IL17RD IL1A IL1RAP IL34 IL6R ILK INF2 INHBA INO80C IQSEC1 IRF9 ISM2 ITGA3 ITGA5 ITGA6 ITGAV ITGB4 ITGB6 ITM2C ITPR3 IZUMO4

JAG2 JMY JUP KANK2 KBTBD4 KCND1 KCNIP2 KCNJ16 KCNK2 KDM4B KDSR KIAA0664 KIAA0895L KIAA0930 KIAA1107 KIAA1539 KIAA1755 KIF17 KIF25 KIF3C KIF5A KIRREL KLF7 KLHL29 KLHL5 KLK6 KMO KREMEN1 KRTCAP3 KXD1 L3MBTL1 LAMC2 LAMTOR1 LASP1 LCTL LDB1 LDLR LDLRAD1 LEPREL1 LEPROTL1 LFNG LGALS3BP LGI3 LIMK2 LIMS2 LLGL1 LMF2 LOXL3 LPAR3 LPGAT1 LPIN3 LRCH3 LRCH4 LRP1 LRRC20 LRRC48 LRRC8A LRRN4 LUZP1 LXN LYN MAGED1 MAP1B MAP1LC3A MAP3K5 MAP4 MAP7D2 MAPK1IP1L MAPK7 MAPKAPK3 MARCH2 MARK1 MAT1A MBNL2 MCCD1 MCFD2 MCM9 MCOLN1 MCRS1 MDGA1 MED15 MEI1 MESDC2 MFAP5 MFHAS1 MFNG MFSD12 MFSD2A MGAT4C MGAT5 MGAT5B MGST1 MICAL3 MICAL3 MICALL1 MIEN1 MLXIPL MME MMP13 MMP28 MOB3C MOSPD3 MPRIP MPZL1 MPZL2 MRPL14 MSTO1 MSX1 MUC1 MXRA8 MYBPC2 MYCL1 MYH14 MYH9 MYL12A MYL3 MYL4 MYL5 MYL9 MYLK3 MYO9B N4BP1 NAGLU NAV1 NAV3 NBL1 NCOR2 NCR3 NDRG4 NEBL NEBL NECAB3 NEU1 NFAT5 NFKB2 NFKBIE NHEJ1 NHLH1 NICN1 NINJ2 NIT2 NKAIN1 NKIRAS1 NMUR2 NOD1 NOTCH2 NPR3 NR2F2 NRBP2 NUDT18 NXN NXN NXPH3 NYNRIN OLFM3 OLFML2B OPN3 OPRD1 OPTN OTUD1 OTUD7B P2RX2 P2RX4 P2RY11 PAK3 PAM PAQR4 PAQR6 PARP11 PARP12 PARP3 PARVA PARVB PCBP4 PCDH18 PCDHB2 PCGF5 PCMTD1 PCNXL2 PCSK4 PCTP PDE2A PDGFB PDGFRA PDIA5 PDIA6 PDLIM2 PDLIM4 PDLIM7 PDZD11 PDZD3 PEA15 PECAM1 PEMT PGAP2 PGK1 PGP PHACTR2 PHF11 PHF17 PHTF2 PI3 PIAS3 PIEZO1 PIWIL4 PKD1 PKP3 PLAUR PLCD1 PLCD3 PLCG1 PLCXD1 PLEKHA7 PLEKHG2 PLEKHG4B PLEKHN1 PLEKHS1 PLIN3 PLP2 PLXDC2 PLXNA1 PLXNA3 PLXNB1 PLXNB3 PLXND1 PMAIP1 PMEPA1 PMP22 PNKD PNLIPRP2 PNPLA3 PODXL POLD4 POU2F3 PPAP2A PPARGC1B PPM1N PPP1R13L PPP1R16B PPP1R18 PPP1R36 PPP2R3A PRADC1 PRELP PRICKLE2 PRKAR1B PRKCD PRMT2 PRODH PRUNE PSEN1 PSMB9 PSMD3 PSME1 PTGDS PTGER3 PTGES PTGFRN PTMS PTPN12 PTPN23 PTPN6 PTPRCAP PTPRM PTPRM PTPRU PVRL4 PWWP2A PXN PYCRL PYGO2 QSOX1 RAB13 RAB17 RAB19 RAB25 RAB2B RAB31 RAB3D RAB4B RABGGTA RAI14 RALA RALGDS RALGPS2 RANBP9 RAPGEF3 RAPGEF4 RAPH1 RASGEF1A

RASGRP1 RASL10B RASSF7 RBKS RBP5 RBPMS2 RCBTB2 RCN2 REEP6 RELT RENBP REPS2 RGL1 RGS12 RGS12 RHBDF1 RHBDF2 RHOC RHOD RILP RLBP1 RNASE10 RNF11 RNF149 RNF181 RNF5 RNPEP ROCK2 ROGDI RPL28 RRM2B RTN2 RUNX2 S100A12 S100A16 S100A6 SAA1 SAMD4A SCAMP3 SCAND1 SCHIP1 SCN1B SCNN1B SCPEP1 SDC1 SDC3 SDR9C7 SEC14L2 SEC14L4 SEC62 SELRC1 SEMA3B SEMA3E SEMA4F SEPT5 SEPT8 SEPW1 SERINC5 SERP2 SERPING1 SERTAD3 SFN SGCA SGSH SH2D3A SH2D6 SH3BGRL3 SH3D21 SH3GL3 SHISA5 SHROOM1 SIK1 SIPA1 SLC10A6 SLC12A4 SLC12A7 SLC15A2 SLC16A2 SLC1A7 SLC20A2 SLC22A3 SLC25A1 SLC30A4 SLC30A7 SLC36A1 SLC38A10 SLC39A13 SLC39A4 SLC45A2 SLC45A4 SLC46A2 SLC46A3 SLC4A7 SLC5A3 SLC9A4 SLC9A8 SLCO2B1 SLIT3 SLTM SMAD7 SMAD9 SMARCC2 SMOC1 SMTN SNAI1 SNAI2 SNRNP35 SNX21 SNX22 SNX25 SNX30 SOCS2 SOD2 SOD3 SOGA1 SORBS1 SORCS1 SOX7 SP100 SPATS1 SPHK1 SPHK2 SPRYD3 SRCIN1 SRD5A1 SRPX SRRD SSBP3 SSPN SSSCA1 ST14 ST5 ST6GALNAC1 ST6GALNAC4 STARD8 STAT2 STIM1 STRA6 STS STUB1 SUFU SULF1 SULF2 SULT2B1 SUMF2 SUSD2 SVIL SYN2 SYNC SYNGR2 SYNM SYNPO SYT17 SYT7 SYTL1 TACC1 TACSTD2 TAGLN TAGLN2 TAPBP TAS1R2 TBC1D10C TBC1D12 TBC1D2 TBC1D22B TBCB TCF7L1 TCF7L1 TCF7L2 TCIRG1 TCP11 TCTA TEAD3 TESK1 TESK2 TFCP2L1 TGFB2 TGFB3 TGFBR2 THAP8 THBS1 THNSL2 THY1 TICAM1 TLE4 TM4SF4 TM7SF2 TMED1 TMEM109 TMEM127 TMEM14C TMEM150B TMEM151B TMEM154 TMEM173 TMEM184B TMEM201 TMEM245 TMEM63A TMEM63B TMEM80 TMEM86A TMEM92 TMEM98 TMOD4 TNFAIP1 TNFAIP8 TNFRSF12A TNFRSF1A TNIP1 TNKS1BP1 TNNI2 TNNT1 TNS1 TNS4 TNXB TOR4A TP53INP1 TP53INP2 TPCN2 TPI1 TPPP TPR TPRN TPST2 TRADD TRAF5 TRAFD1 TRAK1 TRAM2 TRIM21 TRIM29 TRIM56 TRIOBP TRIP10 TRPC4AP TRPT1 TRPV2 TSC22D1 TSC22D2 TSKU TSPAN14 TSPAN17 TSPAN8 TSPAN9 TSPYL2 TTC12 TTC21A TTC39C TTI2 TTLL3 TTPAL TUBA4A TUBB2A TUBB2B TUBB6 TUFT1 UBA6 UBA7 UBE2E2 UBE2QL1 UBE2V1 UBL5 UBTD2 UNC45B UNC5A UPB1 USF1 USP2 USP35 USP46 VASH1 VASH2 VASN VEGFB VHL VIL1 VPS25 VSIG10 VSIG2 VTN VWA1 VWA2 WBP1 WBP1L WBP2 WDR45 WDR6 WFDC2 WFDC5 WISP3

WNT11 WNT6 WNT7A WSB1 XG XYLB XYLT2 YPEL2 YPEL3 ZBTB4 ZBTB46 ZC3H12C ZFP36 ZFYVE21 ZNF407 ZNF469 ZNF618 ZNF821 ZNFX1 ZNRF3

Genes uniquely upregulated by -/-: AQP6 BAIAP2L2 C10orf54 CCR7 CDC25A CTRL DEFB1 DUSP5 FOSL1 GDF15 GRWD1 IFIT1 ISG20 LOC100855488 LOC100856190 LOC486404 MMP9 MST1R NPPC PLCG2 PSORS1C2 SAMD15 SLC13A2 SLC23A1 SLC2A5 SLC39A14 TEX14 TMEM41A UNC5B WDR37

Genes commonly upregulated by +/+ and +/-: ABCC5 CYP1A1 LOC100855982 SLC4A11

Genes commonly upregulated by +/+ and -/+: C1R CA12 GSTM4 HSPB1 IDO1 IL8 LBH MAP3K8 SLC4A11

Genes commonly upregulated by +/+ and -/-: FGFBP1 HSPB1 SLC4A11

Genes commonly upregulated by +/- and -/+: ACAT2 ALDOC ANKRD35 ARHGAP28 ARSB AVEN B4GALT5 BMP4 BNIP3 BST2 C2orf55 CABYR CCDC64 CCND1 CD300C CD40 CD55 CDSN CEP41 CHD4 CREB3L4 CSDC2 CSF1 CYP4A38 DAG1 DAPK2 DCLK1 DHCR7 DHX58 DLA-DRA DMBT1 DPYSL2 DSP DST DTX3L DUSP10 EHD2 EPB41L1 F3 FHDC1 FST FXYD6 HEXIM1 HINT2 HLA-DQA1 HLCS HSD17B7 HSPA2 IFI44 IFIH1 IGFL3 IL10RB IL4I1 IMPA1 KIAA0922 KIF20A LBP LGALS9 LRRC59 LSS MARCKSL1 ME3 MLEC MMP14 MON1B MSMO1 MSN N4BP3 NCALD NEDD9 NFKBIA NKX3-1 NPC1L1 NPR1 OST4 PALLD PARP14 PARP15 PARP9 PCSK6 PCYT1B PCYT2 PHLPP2 PLEKHG1 PLXNC1 PQLC3 PRKCDBP PRSS23 PVR QRFP RARRES2 RNF183 RTP4 S100A3 SAMHD1 SCUBE3 SEMA7A SEPT6 SEPT7 SESN1 SESN3 SH3KBP1 SHMT1 SLC11A1 SLC22A2 SLC40A1 SMARCAL1 SNN SNX6 SPSB1 SQLE SRD5A3 TAF15 TAOK2 TAP1 TEX2 TIMP2 TLCD1 TLR3 TRANK1 TTC9 TUBA1B TUBB USP18 VCP ZNF704

Genes commonly upregulated by +/- and -/-: ACSL1 DHRS9 LOC100684663 LOC100855560 LOC100855667 LOC100856058 LOC100856448 NEURL1B PIGR SRRM1 TBX2 TNFAIP3 TRIM35

Genes commonly upregulated by -/+ and -/-: ACOT11 ACPP ADORA2A BGN BPIFA1 C17H1orf56 CNN1 DDX60 DHRS2 DHX33 DOCK4 DRAM1 EFNB2 FLCN FOLR1 GAS2L2 GBP7 GCNT1 GJA5 GNG3 GPR111 GPR157 GPX3 GRAMD2 IL15RA IRGM IRGM ITGA10 KCNN3 KRT17 LCAT LGALS2 LYPD1 MATN3 MTMR11 NAV2 OLFML2A P2RX7 PLEKHB1 PSMB10 RCN1 S100A2 SEPT4 SFXN5 SLC22A4 STXBP1 TGM1 TMPRSS13 TRIM8 VWF

Genes commonly upregulated by +/+, +/- and -/+: C1S CEACAM1 CXCL17 CYP17A1 FDFT1 GLT1D1 HMGCS1 INSIG1 MAB21L3 PLAT RAP1GAP2 RBP4 RHOJ TBC1D8 TNFRSF14

Genes commonly upregulated by +/+, +/- and -/-: MYO7B LOC484468

Genes commonly upregulated by +/+, -/+ and -/-: MX2

Genes commonly upregulated by +/-, -/+ and -/-: ACYP2 ALOX15B APOA2 ATP10A CCL7 CTSK CXCL10 CXCR7 DTX4 ECM1 EHD4 EPAS1 EPHB3 FA2H FABP3 FXYD3 GNG2 GYS1 HMOX1 HSP70 HSP70 HSPB1 IDNK IFI35 IGSF23 LIPG LOX LRP8 MLLT11 MTSS1 NFIX OAS1 OAS2 OAS3 PFKFB3 PLA2G3 RNF213 RNF213 S100A4 SELM SLC43A2 SLC4A11 TAPBPL TGM2 TIMP3 TIMP4 TM4SF1 TMEM106A UNC5C XDH

Genes commonly upregulated by all isoforms: AQP3 BNIPL C3 CCL2 CCL5 CDH3 FOXN1 GPX2 IFI44L QPCT RARRES3 RSAD2 SLC6A12 TTC22 UPK3BL WT1

Downregulated genes:

Genes uniquely downregulated by +/+: EGFLAM EGR1 EGR2 EOMES ESYT3 FNDC5 HOXC13 LGALS1LRP3 SYT12

Genes uniquely downregulated by +/-: ABHD4 ACCS AGAP2 AGPAT2 ALOXE3 ANAPC11 ARHGEF2 ATG13 ATP8B2 BCAS3 BCAS3 BSDC1 C18H7orf10 C1H9orf3 C24H20orf96 C30H15orf48 C4H5orf4 C5H17orf103 CAND2 CBD118 CBY1 CCDC135 CCDC92 CES5A CIRBP CPAMD8 CUEDC1 CUL7 CXXC11 CYP27B1 DAPK3 DDB2 DFNA5 DHRS1 DNAJC5 ECT2L ELL ENO3 EPHX1 ERCC1 ERN1 EXT1 FAM211A FBXL12 FHIT

FKBP6 FTSJD2 GABRB1 GADD45G GCKR GJB5 GPR156 GTPBP2 HARS2 HHAT INPP5A IRAK2 ITPKC KDM6B KIAA0513 KIFC3 KLF10 KLF6 LAMB3 LATS2 LGMN LIF LOC100682773 LOC100682931 LOC100686332 LOC100687917 LOC100855818 LOC100855833 LOC100856113 LOC100856207 LOC100856391 LOC100856443 LOC100856457 LOC100856543 LOC100856683 LOC483802 LOC491550 LOC607305 LOC608437 LOC608857 LOC609535 LOC610293 LOXL2 LRRC8E LYPD6B MAML1 MAN2B1 MAPK8IP3 MAPT MEIS3 METRNL MFSD3 MIB2 MICAL2 MOB2 MORN4 MUS81 NEK8 NFKBIZ NOTCH3 OSBPL5 PCGF2 PCYOX1L PHC2 PIGV PLA2G16 PLA2G6 PLEKHA4 PLK3 POU6F1 PPM1J PRKAB1 PSD4 PTK2B PTPRS RAB24 RECQL5 RECQL5 RHBDL1 RNF122 RNF220 RNF39 RNF44 RXRB SDC4 SEMA6B SEPN1 SERPINF2 SGPL1 SH3BP2 SMAD6 SMG5 SMG9 SOCS3 SRPX2 ST6GAL1 STAT3 STK25 STK33 SZT2 SZT2 TENC1 TMC4 TMEM150A TMEM196 TMEM51 TMEM59L TMEM86B TMUB2 TPD52L1 UCKL1 UPP1 VPS39 WTIP YPEL5 ZDHHC14 ZNF837

Genes uniquely downregulated by -/+: AARS2 AARSD1 AASS ABCB4 ABCC3 ABHD10 ACAA2 ACAD8 ACADSB ACBD6 ACN9 ACOT13 ACOX3 ACPL2 ACVR1B ACYP1 ADAM32 ADAMTS9 ADAMTS9 ADAT2 ADCK4 ADCY9 ADM2 ADRA2A ADRBK2 ADSL AEN AGPAT9 AGR2 AHCY AHCYL2 AHRR AIM1 AK2 AK4 AKT3 ALDH18A1 ALDH1A1 ALDH5A1 ALG11 ALG5 ALG8 ALG9 ALKBH8 ALMS1 ALMS1 ALX1 AMMECR1 AMN1 AMZ2 ANAPC1 ANAPC16 ANAPC5 ANGPTL6 ANKRD11 ANKRD33B ANKRD40 ANKRD45 ANKRD46 ANKS4B ANO4 ANP32A ANXA10 ANXA13 ANXA3 AP3M2 APCDD1 APIP APOBEC1 ARF6 ARFGEF2 ARG2 ARHGAP10 ARHGAP24 ARHGAP35 ARHGAP9 ARHGEF26 ARHGEF38 ARID5B ARRB2 AS3MT ASB6 ASB7 ASCC1 ASF1A ASH1L ASH2L ATAD1 ATG4A ATG5 ATIC ATP1A1 ATP1B1 ATP2C2 ATP5A1 ATP5J ATP5O ATP5SL ATP6V1G2 ATP7B ATP8A1 ATP8A1 ATRNL1 ATXN10 B3GALNT1 B4GALNT4 B9D1 BACE1 BANP BATF3 BBS1 BBS2 BBS9 BCAS1 BCAT1 BCCIP BCL2 BCL2L1 BCL2L2 BCL7A BCOR BCORL1 BEND6 BEX4 BICD1 BLMH BMI1 BNIP1 BOD1 BOP1 BPHL BRD7 BRF2 BRP44 BRP44L BRP44L BRP44L BTBD1 BTF3 BTN1A1 BTN2A2 BTRC BUB3 BUD13 BUD31 C10H2orf29 C12H6orf108 C14orf164 C14orf79 C15H1orf210 C15orf61 C19orf44 C1H9orf85 C1orf116 C1QL3 C20H19orf53 C20orf20 C23H20orf3 C28H10orf88 C2H10orf47 C2H16orf80

C30H15orf44 C31H21orf62 C33H3orf26 C38H1orf192 C3H15orf42 C3H4orf48 C4H10orf57 C4H5orf42 C4H5orf62 C4orf21 C4orf29 C6H16orf62 C6H1orf194 C7H1orf189 C8H14orf105 C8H14orf126 C8orf33 C9H17orf75 C9H9orf9 CA13 CA2 CA4 CA7 CACFD1 CAMK1 CASK CASP10 CAT CBR3 CBS CBX5 CCDC106 CCDC117 CCDC149 CCDC151 CCDC164 CCDC28A CCDC36 CCDC50 CCL27 CCNB2 CCNK CCT5 CD38 CD44 CDC123 CDC16 CDC25C CDC26 CDC6 CDCA5 CDCA7 CDCA7L CDK11A CDK18 CDK5RAP2 CDKAL1 CEBPG CECR5 CEP104 CEP72 CEPT1 CFDP1 CHAF1A CHCHD2 CHCHD3 CHCHD5 CHD1L CHD3 CHEK2 CHKA CIDEC CIRH1A CISH CLCN4 CLDN2 CLEC1A CLIP2 CLPB CLUAP1 CMBL CMC1 CMTM4 CNBP CNNM2 CNNM2 CNNM4 CNO CNOT1 CNOT6L COA5 COBL COPA COQ5 COQ9 COX10 COX11 COX7B2 CPNE7 CPT2 CRCP CREBL2 CREBZF CREG1 CRX CRY2 CRYZ CSRP2BP CST6 CTBS CTDSPL CTH CTNNBL1 CTPS2 CTSC CTSE CWC15 CWF19L1 CYP2R1 CYP4A11 DALRD3 DAO DAPK1 DBF4B DBP DCAF4 DCAF5 DCTN5 DDX1 DDX10 DDX11 DDX19A DDX25 DDX26B DDX27 DDX31 DDX49 DENND1B DEPTOR DFFB DGAT1 DHODH DHRS3 DHX16 DHX35 DIEXF DIS3L2 DISC1 DKC1 DLG3 DLL1 DMPK DNAH10 DNAH10 DNAJA3 DNAJB13 DNAJC12 DNAJC16 DNAJC17 DNAJC7 DNAL4 DNALI1 DNMBP DNMT3B DOCK3 DOCK8 DPAGT1 DPCD DPH5 DPYD DSCR6 DUS1L DUSP18 DYDC2 DYM DYNLRB2 DYRK2 DYX1C1-CCPG1 E2F4 E2F5 EAPP ECD ECHDC1 ECI2 EED EEF1B2 EEF2 EFCAB1 EFCAB11 EFCAB6 EFEMP1 EGF EHBP1 EHF EHHADH EID2 EIF2A EIF2B3 EIF2D EIF2S3 EIF3C EIF3D EIF3H EIF3I EIF3K EIF3L EIF3M EIF4B EIF4H ELAC2 ELF3 ELP3 EMC7 EMC9 EMG1 EML1 EML6 ENC1 ENGASE ENTPD3 ERI3 ERLIN1 ERLIN2 ERP29 ERRFI1 ESRP1 ESRRA ETFA ETV1 ETV4 ETV5 ETV6 EXD1 EXD2 EXOC2 EXOC6 EXOSC1 EXOSC2 EXOSC7 EXOSC8 EXTL3 EYA3 FADS6 FAF1 FAHD1 FAM118B FAM125A FAM13A FAM13A FAM149A FAM155B FAM160A2 FAM168A FAM171B FAM188B FAM190A FAM211B FAM3C FAM40B FAM78B FAM81A FAM92A1 FAM96B FAN1 FANCC FAR2 FARSB FASTKD2 FASTKD3 FBL FBLN1 FBLN7 FBP1 FBXO18 FCGRT FCHSD2 FGD4 FGF9 FKBP4 FKBP7 FKBPL FKTN FLOT1 FLRT2 FNBP1 FNIP2 FOSB FOXA2 FOXK1 FOXN3 FOXN3 FOXP1 FRMD3 FRMD3 FRY FTO FTSJ1 FTSJ3 FUBP3 FUT10 FUT2 FUZ FXYD2

FYCO1 FZD4 GABRA3 GALC GAR1 GAS8 GATA3 GCA GCAT GCGR GCLC GDAP2 GDI2 GDPD1 GEMIN5 GEMIN6 GEMIN8 GFM1 GGA2 GINS2 GK GLRX GLTSCR2 GLUL GMEB1 GNA14 GNB2L1 GNB5 GNG4 GNL3 GPAM GPATCH4 GPHA2 GPHN GPLD1 GPNMB GPR89A GPR98 GPT2 GRB14 GRHL2 GRHL3 GRIP1 GSR GSTCD GTDC1 GTDC1 GTF2F2 GTF2F2 GTF3C3 GTPBP3 GTPBP4 H1FX H2AFY H3F3B HACL1 HAX1 HCCS HCFC1R1 HDAC8 HDDC2 HEATR6 HEMK1 HENMT1 HERC1 HEXIM2 HIBADH HIBCH HIRIP3 HJURP HMGA1 HNF4A HNRNPH3 HOXA2 HOXA4 HOXA6 HOXA9 HOXB8 HOXD3 HOXD8 HPCAL1 HPSE HS6ST1 HSPA1L HSPA9 HSPH1 HUS1 IARS ICA1 ICA1L ICOSLG ICT1 IDO2 IER3IP1 IFRD2 IFT172 IFT88 IGF1R IGF2BP2 IGF2BP3 IGHM IGSF3 IGSF5 IL1RL1 IMMP2L IMMT IMP4 IMPDH2 INIP INO80 INTS9 IPO5 IQCD IREB2 IRF2 IRF2BP2 IRX3 IRX5 ISCU ISOC1 ITGA7 ITIH2 ITPR1 ITPR1 ITPRIP JARID2 JPH1 KANSL1L KARS KAT2B KAT8 KCMF1 KCNJ2 KCNK6 KCNQ1 KCTD1 KCTD2 KCTD3 KCTD4 KDM1B KIAA0141 KIAA0240 KIAA0368 KIAA0564 KIAA0564 KIAA1147 KIAA1370 KIAA1407 KIAA1614 KIAA1671 KIAA1671 KIAA1704 KIF12 KIF1A KIF5C KITLG KLF11 KLF12 KLF13 KLF15 KLF5 KLHL12 KLHL20 KRBA2 KSR2 LAMB1 LARGE LARP1 LARS LARS2 LCMT1 LDHB LDLRAD3 LEO1 LETM2 LGALS4 LGR4 LHFPL4 LIAS LIFR LIG3 LMBR1L LMO4 LMO7 LNX1 LONP1 LRIF1 LRIG2 LRRC49 LSAMP LSAMP LSAMP LTA4H LTBP2 LTBP4 LURAP1L LZTFL1 MADD MALL MAP1A MAP2 MAPK13 MAPK15 MAPK4 MARS MARS2 MCAT MCCC2 MCEE MCTS1 MCU MDH1 MDN1 ME2 MECOM MED11 MED18 MED23 MEF2B METAP1 METTL17 METTL3 METTL7A MFAP3L MFSD6 MIOX MKNK2 MLF1 MLF2 MLH1 MLLT10 MLLT6 MMP26 MMS19 MOB3B MOCOS MOCS1 MOCS2 MOK MPP2 MPP6 MRPL10 MRPL11 MRPL21 MRPL21 MRPL37 MRPL39 MRPL46 MRPL48 MRPL48 MRPL55 MRPL9 MRPS15 MRPS22 MRPS27 MRPS30 MRPS35 MRPS5 MRPS9 MSLN MSRB2 MSRB3 MST4 MTA1 MTHFD1 MTHFD1L MTHFD2L MTMR1 MTMR2 MTO1 MTPAP MTR MUT MXI1 MYB MYC MYO10 MYO1B MYO5C NAA20 NAA40 NAB1 NAB2 NAP1L1 NAPB NARS NARS2 NBAS NCAPD2 NCAPH NCOA1 NCS1 NDRG1 NDRG3 NDUFAF2 NDUFS6 NDUFV1 NDUFV2 NEK2 NEK6 NEK9 NEO1 NETO2 NFATC1 NFATC2 NFATC3 NFKBIL1 NFU1

NFYA NGDN NGF NGRN NIPSNAP3B NLE1 NME7 NMI NMNAT2 NMRAL1 NOB1 NOL10 NOLC1 NOMO2 NOP14 NOS1AP NOTCH1 NOTUM NOVA1 NPHP1 NPM1 NPNT NPRL3 NQO2 NR2F6 NR4A1 NR5A2 NRP2 NSD1 NSMCE1 NSUN4 NSUN5 NUBPL NUDT15 NUDT2 NUDT21 NUDT3 NUP160 NUP37 OAT ODC1 OGFRL1 ONECUT1 OPLAH ORAOV1 OSCP1 OSGIN1 OSR1 OVGP1 OXA1L OXNAD1 P2RY1 PABPC1 PABPC4 PAFAH1B1 PAIP1 PAIP2 PAIP2B PAK1 PALM3 PARD3 PARL PARP1 PARP16 PARP6 PARP8 PAX6 PCBP2 PCCB PCMTD2 PCOLCE2 PCP4L1 PCSK5 PDAP1 PDCD1 PDCD11 PDCD2 PDCD2L PDCD4 PDCD5 PDCD6 PDE4B PDE4C PDE7B PDGFC PDGFRL PDSS2 PDZK1 PEBP1 PEG10 PER1 PES1 PET112 PEX26 PFAS PFKM PFKP PHB2 PHF1 PHF20 PHF21A PHLDA1 PHYHIPL PIAS1 PIGU PIM2 PIR PITPNM2 PITX2 PKD1L3 PKHD1 PKIG PKP4 PLA2G4A PLA2G7 PLAGL2 PLEKHA8 PLEKHB2 PLEKHG6 PLEKHH1 PLEKHM3 PLSCR1 PLXNA2 PLXNA4 PM20D1 PNPO POLA2 POLI POLR1A POLR1C POLR1D POLR1E POLR2H POLR3C PORCN POU2AF1 PPAP2B PPAP2B PPCDC PPFIBP2 PPIC PPIF PPIP5K1 PPL PPM1G PPM1H PPME1 PPOX PPP1R12B PPP1R1B PPP1R9A PPP1R9A PPP2R2D PPP6C PPPDE1 PPT2 PRDM1 PRDM16 PRKAA2 PRKAR2B PRKCA PRKCA PRKCG PRKCH PROSC PRPF19 PRPF38A PRPF4 PRPF8 PRPS1 PRPSAP2 PRR14 PRR15L PRSS12 PRTFDC1 PSAT1 PSD3 PSMA4 PSMB7 PSMC3IP PSMC5 PTCD2 PTCD3 PTER PTGER2 PTGES2 PTGR1 PTPLAD1 PTPMT1 PTPRB PTTG1 PUS1 PUS3 PWP1 PXK QARS QDPR QRSL1 QSOX2 QTRTD1 R3HCC1L RAB14 RAB15 RAB27B RAB28 RAB3GAP1 RAB7L1 RABGAP1L RABL5 RAD51AP1 RANBP17 RAP1GDS1 RARB RARS2 RASA3 RASA4 RASAL1 RASGEF1B RASIP1 RBM22 RBM48 RBM4B RCE1 RCL1 RCOR3 RDH10 REC8 REEP5 REM1 REM2 REPS1 RERE RERG RFC3 RFC5 RFT1 RGS2 RHEBL1 RHOU RIMKLB RIPK2 RIPK3 RNASE4 RNASEH2B RNF130 RNF144B RNF214 RNF43 RNMTL1 RORA RP9 RPL11 RPL13 RPL14 RPL15 RPL21 RPL21 RPL22 RPL24 RPL26 RPL27A RPL3 RPL30 RPL35A RPL4 RPL5 RPL7A RPL8 RPLP1 RPP14 RPP40 RPRD1B RPS12 RPS13 RPS16 RPS17 RPS18 RPS19 RPS3 RPS4X RPS5 RPS7 RPS8 RPS9 RPSA RPUSD2 RRM2 RRP8 RSG1 RSPH3 RTN4IP1 RTTN RUNDC3B RUVBL1 RXRA S1PR1 S1PR2 SALL1 SAMM50 SARNP SART1 SART3 SATB1 SBF2 SBF2

SBF2 SCARA3 SCARB2 SCG5 SCLY SCN8A SCNN1A SDCBP SDHA SDR16C5 SDR42E1 SEC11A SEMA3C SENP2 SERGEF SERHL2 SERPINB8 SERPINB9 SERPINE2 SERTAD4 SETD9 SETMAR SF3A3 SFI1 SFTPD SFXN4 SGCE SGK1 SH2B1 SH3BP4 SH3PXD2A SH3RF2 SHMT2 SHOX2 SIAE SIGIRR SIM2 SIRT4 SIRT5 SIRT6 SIVA1 SLAIN1 SLC10A7 SLC16A10 SLC16A5 SLC19A1 SLC22A15 SLC22A18 SLC22A23 SLC23A2 SLC25A15 SLC25A26 SLC25A33 SLC25A42 SLC25A5 SLC25A6 SLC26A11 SLC35C1 SLC38A3 SLC38A5 SLC5A9 SLC7A11 SLC9A2 SLC9A5 SLC9A7 SLIRP SLIT2 SMAP2 SMG7 SMN SMPD1 SMU1 SMYD2 SNRNP200 SNRPB SNRPD1 SNRPD3 SNRPN SNX24 SORBS2 SOX12 SOX2 SP1 SPAG6 SPATA13 SPATA17 SPATA6 SPATA6L SPC24 SPRY1 SPTLC3 SQSTM1 SRBD1 SREK1IP1 SRSF9 SRXN1 SS18L2 SSBP1 SSBP2 SSNA1 SSR4 SSRP1 SSTR1 ST3GAL4 ST3GAL5 ST3GAL6 ST7 STC2 STEAP1 STIL STK39 STOML2 STT3A STX10 STX11 SUPT4H1 SUV420H2 SYNGAP1 SYNRG SYT1 SYTL2 SYTL5 TADA2A TAF1B TAF3 TAF4B TAF5 TAMM41 TANC2 TARBP1 TARS2 TBC1D1 TBC1D19 TBC1D2B TBC1D30 TBC1D4 TBC1D4 TBC1D5 TBCE TBL1X TBPL1 TCEA3 TCF7 TCHP TCN2 TCTEX1D2 TCTN1 TCTN3 TDP1 TEC TEKT1 TEX26 TFAP2A TFB1M TFPI2 TFPT TGFBR3 TGFBRAP1 THADA THEM4 THG1L THOC6 THSD1 THYN1 TIAM1 TIMM17A TIMM44 TIMM9 TJP3 TLE3 TMCC3 TMCO4 TMEFF2 TMEFF2 TMEM106C TMEM107 TMEM132A TMEM144 TMEM160 TMEM164 TMEM194A TMEM2 TMEM205 TMEM218 TMEM229A TMEM38A TMEM39A TMEM39B TMEM42 TMEM56 TMIE TMPRSS4 TMTC2 TMTC3 TMX4 TNFRSF1B TNIK TNNT2 TNPO3 TOMM7 TP53I11 TP73 TPPP3 TRABD TRAPPC2 TRIB2 TRIM4 TRIP4 TRMT11 TRMU TRPA1 TSEN54 TSHZ1 TSHZ2 TSPAN4 TSTD2 TTC27 TTC39A TTC8 TTI1 TTLL10 TTLL12 TTYH2 TULP2 TULP3 TXNL4A TXNRD3 UBAC1 UBE2F UBE2T UBN1 UBXN1 UBXN10 UCHL1 UFM1 UGT1A6 ULK4 UNC13B UNC93B1 UQCRC2 UQCRH USE1 USP13 USP3 USP30 USP39 USP4 USP49 USP7 UTP14A UTP3 UXT VAMP1 VANGL1 VEGFC VNN1 VNN1 VPRBP VPS36 VSIG10L WARS2 WDFY1 WDR12 WDR3 WDR31 WDR34 WDR5 WDR59 WDR7 WDR74 WDTC1 WDYHV1 WHSC1 WNK4 WRAP73 WWC1 WWTR1 XPNPEP3 XPO4 XPO7 XRCC2 XRCC3 XRCC5 XRCC6BP1

YDJC YIF1B YWHAQ ZADH2 ZBTB17 ZBTB37 ZBTB5 ZCCHC17 ZCCHC3 ZCCHC4 ZDHHC1 ZDHHC4 ZFAND2A ZFAND5 ZFP64 ZIC2 ZIC5 ZMYND19 ZMYND8 ZNF131 ZNF167 ZNF202 ZNF212 ZNF304 ZNF395 ZNF45 ZNF496 ZNF503 ZNF512 ZNF605 ZNF606 ZNF609 ZNF652 ZNF655 ZNF687 ZNF740 ZNF774 ZNF777 ZNF786 ZNF827 ZNRD1 ZSWIM5 ZSWIM7 ZXDB

Genes uniquely downregulated by -/-: ACP5 ADARB1 C14H7orf41 C25H8orf42 CADPS2 CCDC80 CFI CLCN2 CLDN8 CPE ELOVL2 FBXL20 FBXO32 HOMEZ JAZF1 KLHL24 LOC100855524 LOC100856311 N4BP2L1 NTN4 SLC25A45 SYT11 SYTL4

Genes commonly downregulated by +/+ and +/-: AMOTL2 IL22RA1 LOC485002 SERPINE1

Genes commonly downregulated by +/+ and -/+: CAPN13 GSTA3 MFSD4

Genes commonly downregulated by +/+ and -/-: BNIPL LBH

Genes commonly downregulated by +/- and -/+: AARS ABCC2 ACAD10 ADRA1B AGAP1 AKAP7 AKAP8L AKIRIN2 ALDH1L1 ALDH1L2 ALDH3B1 ALKBH3 AMIGO1 ANKH AP3S2 ARMC12 ARRDC4 ARRDC5 ARV1 B3GNTL1 BAX C10H22orf23 C11H9orf91 C18H11orf49 C1H19orf12 C1QTNF4 C21H11orf75 C24H20orf43 C28H10orf2 C3orf52 C4H10orf35 C8H14orf93 CAP2 CARS CBX4 CCDC103 CCDC51 CDC20B CDKN2AIPNL CDYL2 CENPV CES2 CHTOP CMTM3 COL18A1 COQ7 COX14 CPT1A CTIF DACH1 DCST1 DEF8 DEM1 DGUOK EBPL EIF4EBP1 EPB49 ESAM FAM160B2 FARS2 FBLN2 FBP2 FGGY FGGY FRAS1 FRK GAB2 GABBR1 GADD45B GFRA1 GLI1 GMDS GRIK4 GRIN2C GSTZ1 GYG1 H19 HDAC11 HEPH HEPH HOXB9 HSD17B8 IL28RA INPP1 INPP5B IRF2BPL IZUMO1 JAG1 KALRN KALRN KCTD15 KDM4A KIAA0247 LACE1 LETMD1 MACROD1 MAP2K5 MBP MED8 METTL21B METTL24 MFSD2B MRC2 MRPL2 MRPS18B MTHFD2 NFS1 NPEPL1 NR3C2 NRF1 NUP210 ODZ4 OLFM1 OTUB2 PAN2 PARK2 PARK2 PARK2 PCBP3 PEBP4 PEX12 PHF21B PIGP PKDCC PNPLA4 PPP1R26 PRRC2B PSPH RAB39B RAD51B RAD51B RCC2 RFX3 RHBDD1 RNASEH1 RND1 RNF144A RNF186 RPAIN RPS6KA2 RPTOR RSAD1 RTDR1 RUSC2 SARS SCRN1 SEMA4D SLC1A5 SLC22A11

SLC25A37 SLC25A38 SLC3A2 SLC6A9 SLC7A1 SLC7A5 SLC7A7 SORL1 SPRY2 ST3GAL1 STAMBPL1 TCTEX1D4 TET3 TGIF2 TINAGL1 TK2 TMEM200A TMEM8B TOM1L1 TRIM41 TRPM3 TSPAN33 TST TTC25 TXNIP TXNL4B UBE2CBP UBTD1 USH1C USP43 VRK3 WBSCR27 WDR53 YARS ZFAND3

Genes commonly downregulated by +/- and -/-: ACCS ACE2 C18H7orf10 C18H7orf10 C18H7orf10 DFNA5 GADD45G GPR97 GRB7 LOC491550 LOC609535 PCYOX1L PLA2G16 PODN RNF122 SLC41A3 SRPX2 WIPI1 WLS

Genes commonly downregulated by -/+ and -/-: ABCB1 ABI2 BCL2L14 CGNL1 CLEC7A CST7 GCNT2 H1F0 HBP1 KIF21B LRRC42 PBX2 PLA2G2C PLSCR4 PPA2 RAB6B SLC13A1 STAU2 TLE2 TMEM231 TP53BP2 UCP1 WWC2 ZNF396

Genes commonly downregulated by +/+, +/- and -/+: BCAS4 CCDC165 DDIT3 HERPUD1 RAB37

Genes commonly downregulated by +/+, +/- and -/-: CYR61 LOC100855454 LOC100855456 LOC100855987 LOC476202 SLC1A4

Genes commonly downregulated by +/+, -/+ and -/-: ID1 LARP6

Genes commonly downregulated by +/-, -/+ and -/-: ABTB1 ACSS1 AGPAT3 ALPL ASNS BMF C10H12orf66 C32H4orf36 CERK CHN1 CHN1 CHRNB4 DDR2 DLG2 DLGAP1 ETS2 EXOC4 FAM131B FBXL2 FGFR2 FOS FUT1 GABARAPL1 H2AFY2 HABP2 HVCN1 JAM3 LMCD1 MAVS PAPSS2 PCK2 PDE9A PYGL RNLS RNLS SFMBT2 SLC9A9 SMAD3 SUMO4 TBCEL TFDP2 THSD4 TMEM63C UBE2E3 VEPH1 VLDLR XBP1 YBX2 ZFYVE1 ZHX2

Genes commonly downregulated by all isoforms: ADD2 ANKRD55 ATF3 CHAC1 DDIT4 DGAT2 FGF21 FUS JDP2 NUAK2 PPP1R15A SESN2 TRIB3 TSC22D3

List of genes differentially regulated in the RNA Seq analysis of induced IMCD3 clones:

Upregulated genes:

Genes uniquely upregulated by +/+: 11:119785604- 119785886 11:20642477- 20642672 12:111396072- 111396295 13:47625728-47626151 13:47627601-47628360 13:47629428-47630048 13:47630570-47631604 13:47632378-47634740 13:47634966-47635292 13:47635415-47636246 13:47636520-47637090 13:47637309-47637697 13:47638149-47639247 13:47639302-47639662 13:47651473-47652123 13:47656375-47656781 13:47661807-47662183 13:47669499-47669828 13:47670802-47671125 13:47675069-47675648 13:47686833-47687134 13:47687821-47688166 13:47688284-47689150 13:47689718-47690418 13:47691831-47692845 13:47692974-47693417 13:47693467-47693833 13:47694263-47695003 13:47700880-47701415 13:47701520-47702669 13:47703335-47703939 13:47704002-47704335 13:47705075-47706185 13:47706412-47706646 13:47707368-47707999 13:47708299-47709043 13:47709353-47712697 13:47712795-47714340 13:47718549-47719076 13:47723074-47724344 13:47724473-47725223 13:47725316-47736751 13:47725316-47736751 13:47725316-47736751 13:47725316-47736751 13:47749094-47749783 13:47750890-47751398 13:47753004-47753953 13:47754367-47756004 13:47756675-47757213 13:47757270-47757627 15:102925903-102926734 15:97867943-97868153 16:78541785-78542179 19:39002212-39002771 2:74505383-74505724 4:88643958-88644321 6:130378191-130379081 6:130380450-130380922 6:130386821-130387415 6:130418691-130419361 6:130425717-130426064 6:130426997-130427378 6:130429583-130429936 6:130431974-130453012 6:130453416-130454715 7:107826685-107827064 8:74658683-74658828 9:24600005-24600335 AL626784.1,Glis1 Bche Ccdc40 Egr2 Fos Gbp2 Gm11611,Srcin1 Gm20467 Gm6097 Hmgcll1 Kcnd1 Lass3 Lingo4,Rorc Lsamp Mir155 Mir23a,Mir24-2,Mir27a Mir34a Msx1 Naprt1 Nr4a1 Pdk4 Ptprm Rab17 Slc44a4 Spry2 Ttc18

Genes uniquely upregulated by +/-: 1:79597910-79599688 1:79693865-79694435 1:79694696-79695555 1:79906158-79906698 1:79929717-79930035 1:79930304-79930999 1:79931056-79931543 1:79931934-79933693 1:79933851-79933956 15:61294102-61342636 15:76901509-76901988 16:86764071-86764330 16:86770510-86806889 16:86770510-86806889 17:53962143-53965166 17:53965891-53966353 18:60468096-60468436 19:5059138-5059609 19:59698267-59698942 2:5155216-5155603 2010002N04Rik 2010111I01Rik 2210411K11Rik 3:104861388-104861922 3:104862739-104863326 3:32288087-32288415 3:69118887-69120526 3830406C13Rik

4933426M11Rik 4933427I04Rik 5:105924521-105924897 5:44249889-44250353 5:44250484-44250940 5:44251319-44251616 5430411K18Rik 6:87052205-87052755 7:30836112-30836364 8:109538760-109543416 8:36843394-36846336 8:86726525-86728604 9330161L09Rik,Ddx24 Acot5 Acsl3,Utp14b Adap1 Adar Adcy7 Add3 Adk Agpat5 Ahnak2 Akr1c14 Ano9 Arhgap9 Asap3 Atf5 Atp6v1c2 Atp8b1 Avpi1 AW011738 B230206F22Rik,Mir421 Baiap2 BC023105 BC034090 Bcat2 Bmp2k C2cd2l C530028O21Rik Calr4 Car5b Ccdc101 Ccdc90a Cd1d1 Cd209c Cd38 Cd74,Mir5107 Cebpg Chdh Churc1,Fntb Cilp2 Clic4 Clip1 Cln3 Commd7 Cox16,Gm20498,Synj2bp Cst6 Cstb D6Ertd527e Dapk2 Dcn Ddit4l Ddx58 Dhrs7 Dhrs9 Dlk2 Eea1 Eif2ak2,Gm6548 Emb Emp2 Ephx1 Erbb2ip Espn Ethe1 F830016B08Rik Fa2h Fam120c Fam131c Fam55d Fam65c Fig4 Fmnl1 Fstl1 Galr2 Gcat Gem Gfpt1 Gm11538 Gm11543 Gm12993 Gm13086 Gm13988 Gm3880 Gm6410 Gm9750 Gng7 Gpr126 H47 Hap1 Hdac5 Hdac6 Herpud1 Hpse Hspa1b Il17rb Il17re Il6ra Inpp5j Irgm1 Irgm2 Ispd Itm2b Klf2 Klf3 Klhl5 Krt4 Lphn1 Ltv1 Ly6g6d Mbnl1 Mir345 Mpv17l Mpzl3 Mrpl44 Mtap Mxra8 Ndrg1 Nrbp2 Nrtn Nudt4 Oas1g Oas1h Ociad2 Oxct1 P4ha3 Parp9 Pde4a Pdxk Pik3r1 Pkm2 Plekhf1 Plekhg6 Ppm1h Ppm1l Ppp1r14c Ppp3ca Prkch Prom1 Prox2 Ptgds Rarg Rasa3 Rcan1 Rhbdl2 Rilp Rnh1 S100a1 S100a13 Sdhd Sec24d Sema3c Sema4a Sephs2 Sgpp1 Sh2b1 Shisa5 Shmt2 Slc16a1 Slc22a17 Slc22a18 Slc25a39 Slc29a1 Slc30a4 Slc36a4 Slc6a9 Slfn9 Sphk1 Sqrdl St3gal4 Ston2 Syn3 Sypl Tap1 Tenc1 Tert Timp2 Tle6 Tlr3 Tlr6 Tmco4 Tmem40 Tmem8 Tnfsf15 Tob1 Trim2 Trim21 Trim30a Tspan5 Tspo Ttc9 Twist1 Ubxn2b Usp18 Vat1 Wdfy1 Xdh Xk Y:2190378-2190659 Y:2866059-2866215 Zfp109,Zfp111 Zfp14

Genes uniquely upregulated by -/+: 0610009D07Rik 1:176305430-176306020 1:176393770-176394180 1:31783687-31784418 1:31796381-31796918 1:50876018-50876599 1:51520576-51520966 1:7045882-7046293 1:82910050-82910263 1:89142778-89143298 10:3231763-3232151 10:32497352-32497722 10:59364054-59364399 10:79233859-79234166 11:121580706-121581050 11:16499938-16500145 11:54676861-54677367 1110057K04Rik 12:111009460-111009884

12:111010443-111010863 12:113180518-113180813 12:18069010-18069401 12:18069932-18070649 12:18071677-18072254 12:20648673-20649355 12:20654557-20655919 12:20663946-20664403 12:20666676-20667760 13:21830731-21831060 13:21831731-21833164 13:21833336-21836325 13:21836421-21839924 13:52075938-52076439 13:64458231-64458610 13:67107924-67108296 14:14583694-14584275 15:70241329-70242012 15:70242257-70243507 15:70243665-70245715 15:70245770-70246536 15:70246801-70247218 15:79820867-79821188 15:97309199-97310423 1500009L16Rik 16:17053482-17054057 16:36221554-36221787 16:77643296-77643592 16:7923089-7923521 16:7925285-7925631 16:7944697-7945885 16:86287608-86288004 16:8861590-8863138 17:18004667-18006331 17:23793978-23794312 17:23796671-23797108 17:42646873-42647313 17:42647704-42647898 17:69328576-69328889 17:69329260-69330065 17:87489645-87490021 1700007G11Rik 18:37400495-37401112 18:55042593-55042798 1810032O08Rik, Snord1a,Snord1b,Snord1c 19:27459286-27459740 19:59952141-59952498 2:173108483-173108815 2:174095331-174095795 2010005H15Rik 2310006M14Rik 2510009E07Rik 2810432L12Rik 3:114870565-114871243 3:119322345-119328357 3:119329321-119329810 3:119330207-119330554 3:119330760-119331176 3:119331796-119332316 3:119333542-119333834 3:119343411-119343719 3:19233528-19233953 3:39078546-39078998 3:57086958-57087067 3:57087163-57087508 3:87747374-87750447 37865 4:83912808-83916191 4:88647742-88648155 4930485B16Rik 5:105926406-105926606 5:107821757-107822171 5:108797837-108798470 5:30349248-30349544 5:31184494-31184850 5:31872170-31881641 5730559C18Rik 6:100654391-100654567 6:31029649-31029920 6330406I15Rik,BC028471,Gm20488 7:134650159-134650685 7:19927855-19928205 7:3301711-3303510 7:34813460-34814150 7:34815935-34816605 7:39000844-39001237 7:81185678-81186038 7:81210140-81210414 7:91729751-91730236 8:114224596-114224951 8:129337974-129338109 8:55600798-55601867 8:58046396-58046845 8:69889213-69889501 9:116310743-116311389 9:116316023-116316367 9:116316425-116316972 9930013L23Rik 9930111J21Rik2 A630095E13Rik,Gm17689 Acpl2 Adam19 Adamts17 Adamtsl1 Adarb1 Agpat4 Agphd1 AI464131 AI646023 Aldh1a3 Angptl2 Armc2 Asap2 Atad2b Atp10d Atp2a3 Atp2b4 B4galt1 BB287469,Gm2022,Gm8300 BC018507 Bgn Bhlhe40 Bmp4 Bmper C130021I20Rik Cacnb4 Camk4 Camkk1 Cbr3 Cdh18 Cdh5 Cdkl5 Cdr2 Chml,Opn3 Chsy1 Ckap4 Ckb Cldn15 Cldn23 Clgn Clip3 Col12a1 Col16a1 Col1a1 Col3a1 Cotl1 Crlf1 Csdc2 Csrnp1 Csrp2 Cux2 Cyp4b1 Daam2 Dclk1 Ddx43 Degs2 Dennd2a Dgat2 Dip2b Dlx2

Dnajc25,Gm20503,Gng10 Dnajc3 Dnmt3b Dpf1 Dpysl5 Dsel Dusp23 Dusp8 Dusp9 Dysf E030030I06Rik Efna2 Efr3b Ehd2 Ell2 Enpp1 Ephb6 Etnk2 Fam126a Fas Fbln2 Fhl3 Flt1 Fndc4 Foxj1,Rnf157 Frmd5 Gal3st4,Gpc2 Gjb4 Gli2 Gm11605 Gm12603 Gm13318 Gm15525,Shisa7 Gm2018 Gm20486 Gm2115 Gm6166 Gm7910 Gm8113 Gm9112 Gm9864 Gnaz Gpc1 Gpr123 Gpr124 Gpr135 Grin2d H2afx Hes1 Hist1h2ac Hist1h2bc Hist1h3g Hlf Hmga2 Hmgb1-ps2 Hs3st5 Hsph1 Ier3 Il3ra Irs1 Isoc2a Itga5 Itga9 Itgb3 Itm2a Itsn2 Izumo1,Rasip1 Jag2 Jam3 Kctd10 Kctd11 Kif26b Kng1 Krt13 Krt6a Krt6b L3mbtl3 Lbh Lce3c Lhx1 Lhx6 Lmtk3 Lpcat2 Lrfn1 Lrp1 Lrp12 Lynx1 Mapk4 Mast4 Matn3 Mcam Mdfi Metrnl Mir17,Mir17hg,Mir18,Mir19a,Mir19b-1,Mir20a,Mir92-1 Moxd1 Mras Myb Mycl1 Myo5a Myo7a Nav1 Ncs1 Nfe2l3 Nipsnap3b Npas3 Nppb Nsun7 Olfml2b Osmr Osr1 P4ha2 Pard3b Pard6g Pcdhb19 Pcdhb20 Pcdhb21,Pcdhb22 Pcsk6 Pde3b Pdia5 Perp Pgm2l1 Pla2g1b Plin2 Pmepa1 Ppp3cc Prdm8 Prkcc Prkd1 Prokr1 Pros1 Prss46 Rab32 Rcan2 Rdh10 Reep1 Rgs10 Rgs20 Rhobtb2 Rnf150 Rsph1 Rspo3 Rtn2 Rundc3b Runx1 S100a8 Sacs Sbno2 Sdc1 Sdc3 Sdf2l1 Sema3g Serpini1 Sgcb Sgk1 Sh3pxd2b Shisa4 Siglecg Sipa1l2 Sirpa Slc1a2 Slc2a4 Slc38a3 Slc38a5 Slc41a2 Slc45a3 Slc9a2 Slco5a1 Smarcd3 Smurf1 Snai1 Snx18 Snx7 Sp8 Speg Spink2 Sprr2b Spsb1 Stat2 Tac1 Thsd1 Tmcc3 Tmem158 Tmem169 Tmem56 Tmod2 Tmsb4x Tnfaip3 Tnfrsf23 Tnnt3 Tppp3 Trim36 Trim62 Trnp1 Trp53i11 Ttyh3 Tuba1a Tubb2a Tubb2b Uap1 Ugcg Vsig10l Vwa2 Vwa5b2 Wasf1 Zbtb7c Zfp419 Zfp521 Zfp647

Genes uniquely upregulated by -/-: 1:153089657- 153090145 1:184908671- 184910703 11:114679622- 114686141 11:117705019- 117705434 11:48636192- 48636724 11:83057322- 83057502 11:89783330- 89783930 11:89789238- 89789682 11:92430720- 92431125 1110067D22Rik 1200011M11Rik 13:12565266- 12565677 13:73484684- 73484824 14:100683748- 100683927 14:77047637- 77048169 14:84815531- 84815824 14:84822921- 84823389 14:84841917- 84842042 14:84842343- 84842707 14:85106329- 85106681 14:85106878- 85107236 15:37823460- 37823955 1500011K16Rik 16:15546981- 15547514 16:55419748- 55420057 16:55431472- 55431754 1700011H14Rik 18:53401033- 53401227 19:30639197- 30639521 19:30640485- 30641486 2:15624655- 15624854 2:167887377- 167887619 2:24212062- 24212661 2:80051020- 80051392 2210409E12Rik, Coil 2210416O15Rik, Cuedc1 2310043J07Rik 2410006H16Rik 2610035D17Rik 3110039M20Rik, Foxg1 3110043O21Rik 4:122643523- 122643990 4:132043988- 132044213

4:25728854- 25729439 5:103741663- 103742002 5:146019435- 146022388 5:150044139-150044508 5:16836184- 16838054 5:58523794- 58524339 5730588L14Rik 6:128973038-128973239 6:128974141- 128975163 6:128975275- 128975597 6:128975838- 128976828 7:6624929- 6625434 8:3645750- 3646117 9:102680160- 102680613 9:69735329- 69759711 9:69759767- 69760433 9:69903141- 69914924 9:69903141- 69914924 9:69915813- 69916601 9:69918709- 69919206 9330188P03Rik Aaas Abce1 Acsl4 Acss3 Adam22 Adssl1 Ahcyl1 AI662270 Akap1 Aldh18a1 Ano1 Aplp1 Apobec1 Appbp2 Arhgap40 Arhgef3 Art3 Asns Aspa Atf4 Atf6 Atxn2l Bach2 Bmp3 Brip1 Btn1a1 Bzw2 C130026I21Rik C130074G19Rik C630004H02Rik Carkd Cbln2 Ccdc68 Ccdc85b Ccnd2 Cdh10 Cdv3 Cirh1a Ckmt1 Clca4 Cldn8 Clec2f-ps,Clec2g Ctps Ctsc D630013G24Rik Ddx20 Ddx21 Deptor Dhrs11,Mrm1 Dnajc22 Dph5 Dpyd Dpysl3 Dtx4 Dusp4 Ebf1 Eef1e1 Eif3a Eif3d Elfn1 Entpd5 Eomes Eprs Ern1 Esd Espnl Etv1 Etv5 Fam129a Fam135a Fam150a Fam40a Fam46b Fam49b Fam65b Fdxr Fign Flnc Fth1 Fut9 Gabrp Gadd45a Galk1 Gc Gcnt1 Gdpd1 Glrp1 Gm11019 Gm11818 Gm12860,Gm8439 Gm13310 Gm13364 Gm14027,Zc3h6 Gm15035 Gm15250 Gm17443 Gm5101 Gm684 Gm7592 Gm8292 Gm8399 Gmds Got1 Gpa33 Gpt2 Gsta4 Gsto1 Gtpbp2 Gtpbp4 Hand2 Havcr1 Heatr1 Hk2 Hmox1 Hpcal1 Hsd17b4 Hunk Ibtk Ide Igfbp4 Igfbp7 Il1rn Il24 Il34 Ipo5 Ipo7 Itga3 Kazn Kcnj15 Kctd13,Sez6l2 Kctd6 Kpna2 Krt18 Krt8 Ksr1 Lamb3 Lamc2 Lars Layn Ldha Lingo2 Loxl4 Ltbp2 Mab21l3 Maml3 Mapkapk3 Mef2c Mgst1 Mgst2 Mif Mir1907, Trps1 Mitf Mmp2 Mrpl38 Mrps23 Mtap1b Mum1l1 Myo1c Nle1 Nol11 Nova1 Nt5c Nupr1 Odz3 Olfm4 Pabpc1 Pcdh7 Pcsk9 Pctp Pdha1 Pgk1 Pgs1 Phf10 Phgdh Pik3c3 Pim1 Pla1a Pla2g7 Plk2 Pof1b Pold4 Ppm1j Prkca Prr11 Prrc1 Prss12 Prss22 Psat1 Ptpn22 Rab25 Rab34 Rabggta Rad51c Rasgrp2 Rasl11a Rassf9 Reep6 Rell1 Renbp Rgs16 Ripply1 Rnd1 Rpl3 Rpl38 Rplp1 Rps6 Rras2 Rrp12 S100a10 Sars Satb2 Scpep1 Sec14l1 Sema4g Sepp1 Sesn2 Shank2 Sil1 Slc3a2 Slc44a2 Slc6a15 Slc9a3r1 Slco4c1 Slfn5 Slitrk5 Slitrk6 Snhg5 Snrpa1 Sox5 Sox6 Spire1 Spred2 Srp68 Stox2 Syt5 Taf15 Tagln2 Tars Tbrg1 Tex13 Tfpi Tigit Tmem97 Tmprss6 Tnip3 Tom1l1 Trim25 Tspan11 Tubb4a U4 Uchl5 Upk1b Usp36 Wdr67 Xkr5 Ypel2 Ythdc2 Zbtb7b Zfp143 Zfp238 Zic2 Zim1

Genes commonly upregulated by +/+ and +/-: 18:60468563-60469151 2:28339420-28339924 2610318N02Rik 7SK,Gm7536 A430107O13Rik Artn Bend7 Bsnd Cxcl10

D14Ertd668e Fcgrt Gbp7 Gpd1 H2-K1 H2-Q4,H2-Q6 Irs2 Kitl Krt20 Nhsl2 Phf19 Pitpnm3 Qpct Rap1gap Serpinh1 Sgms2 Slc25a48 Slc39a8 Tchh Trim30d Ttll7 Xpot Zfp36

Genes commonly upregulated by +/+ and -/+: 12:20651813 -20652734 12:20658491 -20659148 3:10413523 -10413979 5:107819132 -107819512 C1s,Gm5077 Cacna1g Cebpd Dcp1b Dmrtc1b Egr3 Fosb Gm14446 Hoxc9 Jun Morn4 Nfkbiz Rassf2 Rgs2 Sh3gl2 St8sia2 Tm4sf1 Upk3b

Genes commonly upregulated by +/+ and -/-: 1:90651227 -90651641 14:77050696 -77051156 2:24213365 -24213995 2310007B03Rik 9930023K05Rik Aadat Acvrl1 Aim2 Car12 Ccnd1 Ddah1 Entpd3 Fam198b Fgf13 Gbp8 Ggta1 Hebp1 Inmt Lrfn3 Nrp2 Paqr5 Ppbp Serpinb9 Serpinb9b Slc39a10 Tbx20 Tgfb1i1 Tgfb2 Tle4 Tlr5 Ugt1a1, Ugt1a10, Ugt1a2, Ugt1a5, Ugt1a6a, Ugt1a6b, Ugt1a7c, Ugt1a8, Ugt1a9 Vegfa Vtcn1 Wnt6

Genes commonly upregulated by +/- and -/+: 1:172873592 -172873917 10:37779320 -37783142 12:107324573 -107324801 12:20653034 -20654069 12:92871476 -92873979 14:65811284 -65816175 15:12283842 -12284425 16:7933475 -7936198 16:7939964 -7941729 16:7947230 -7951784 3:114874949 -114875871 3:114876023 -114876591 3:96117821 -96124221 4:150099274 -150099688 5:151402500 -151405189 8:69889717 -69900723 9:35112957 -35113076 Abi3bp Adamts1 Adamts5 Antxr1 Apcdd1 Apol8 Arhgap44 Arid5b Arl4a Atg3 Bdkrb2 Brsk1 Cbr2 Chst7 Cldn3 Cldn9 Crct1 Cyp1b1 Dcc Dlc1 Dsg3 E130012A19Rik Eno2 Epas1 Fat4 Fgf1 Fgf5 Fgfr3 Fosl2 Galnt10 Gdf11 Gm10801 Gm11331 Gm16869 Gpr162 Grhl3 Gvin1 Hhipl1 Hsd11b2 Iffo2 Igfbp3 Igtp Kcnab3 Kcnj2 Kcnj4 Klf4 Krt17 Lancl3 Lfng Mpp3 Msra Mt1 Myl7 Nexn Nfix Nppc Nt5dc3 Ntn1 Nxph4 Oas1b Parvb Pcdh19 Pde8a Pdlim2 Plekho2 Plxna2 Podxl Prss23 Rem2 Rhob Scarb2 Slc29a4 Sox21 Sprr1b Stmn4 Syk Syne1 Tgfbr2 Tmem159 Tmem229b Tnc Tnfrsf1b Tspan15 Vash2 Vsnl1 Xaf1 Zfp287

Genes commonly upregulated by +/- and -/-: 1:93697275 -93697677 12:104667881 -104669627 5:146014115 -146019353 7:113647950 -113648262 A230050P20Rik Acox1 Ankrd35 Anxa3 Arhgef2 Bglap Bst2 Btn2a2 Ccdc109a Cdr2l Cpox Cyb5r1 Dap,Fam136b-ps Ddx60 Def6

Dlg4 Dusp18 Eif3c,U6 Eif4ebp1 Enpep Farsb Fbxo2 Frmd6 Fut1 Galc Ghitm Gm129 Hgfac Hmga1 Hspa9 Htatip2 Irf7 Krtcap2 Lgals9 Lonp1 Me3 Nars Notch1 Oas3 Palm3 Pck2 Pde4dip Plk3 Por Ppp1r13b Ppp1r15a Rrad S100a16 Sema3b Slc1a4 Slc25a33 Slc25a5 Slc35e4 Soat2 Tdrd7 Tex2 Tpd52l1 Trib3 Wars Zfp605

Genes commonly upregulated by -/+ and -/-: 1:174446717-174447233 1:4896834-4897315 12:17999623-17999809 12:89488631-89488855 13:70819517-70820208 2:24210521-24211714 3:63846826-63847175 4930461G14Rik 5730469M10Rik 6030419C18Rik 8:114226712-114227144 9:102669018-102669267 9:69917122-69917614 9130008F23Rik Acot7 Acta2 Adam12 Adamts16 Adamts4 Adamts6 Adprh Areg Armcx2 Arrdc4 Atp7b Basp1 Capsl Cav1 Ccbe1 Cd55 Celf4 Col5a2 Creb5 Daam1 Dach1 Dse Egln3 Elavl4 Epb4.9 Eya2 Fabp5 Fam107a Fhl2 Gata6 Gfra1 Ggt1 Glipr2 Gm9343 Gm9766 Gpm6a Grb14 Hs3st1 Hspa12a Hspb1 Htra1 Ier5 Il11 Il1rl1 Inhba Inhbb Irx1 Kif5c Klf9 Lifr Lphn3 Lrrfip1 Lsp1 Mapk6 Masp1 Megf6 Mgat3 Mical2 Mir700,Rcan3 Mmd Mpeg1 Nfia Ngf Nmnat3 Nrg1 Ntm Ogfrl1 Osbpl6 P2ry1 Palld Pcdh17 Pcdhb14 Pdia6 Pik3r5 Plat Plaur Plekha6 Ptprn Rab27b Rnasel Rnf19b Rorb S100a3,S100a4 Sema3d Sema5a Serpinf1 Slc1a3 Sned1 Sorcs2 Sparc Spcs3 St3gal1 Stag3 Syngr3 Tcf7l1 Tgm1 Tinagl1 Tmem37 Tram1l1 Trpa1 Tsku Tspan13 Tspan7 Upp1 Vegfc

Genes commonly upregulated by +/+, +/- and -/+: 12:19835842-19836055 14:65816236-65816970 14:65817260-65817760 16:25429610-25433592 18:37821399-37824062 18:37830843-37831197 8:48745588-48746022 Arxes2 B4galnt4 BC017612 Btbd11 Cables1 Casp12 Ccdc114 Cela1 Celsr1 Cmpk2 Cp Evl Eya4 Gbp3 Gbp4,Gbp9 Gdpd5 Gm10800 Gm11532 Gnb4 Hist1h1c Iigp1 Itga7 Mt2 Mt4 Mx1 Mx2 Nfkbie Nipal2 Pcbp3 Peg10 Plagl1 Prkaa2 Ptp4a3 Rtp4 Spata13 Srgap1 Tlr1 Tmem44 Tprg

Genes commonly upregulated by +/+, +/- and -/-: 1110002E22Rik 9:69873821-69873908 A630001G21Rik Abcc3 Acot2 Aebp1 Angptl6 Aqp1 Arhgap32 B4galnt2 Car6 Cbs Ccdc3 Ccl5 Cd14 Chchd10 Clic5 Crabp2 Dbt Foxred2 Gm13227,Gm13230 Gm4951 Gphn Gramd1b H2-T23 Ifi44 Kcnk6 Klf5 Leprotl1 Lgals3bp Mr1 Myo1d Nkx2-3 Npr1 Nr4a3 Pcdh11x Rin1 Rsad2 S100a6,S100a7a Scd1 Serpinb6b Slc25a30 Slc25a37 Slc6a18 Slc7a11 Slfn10-ps Sp100,n-R5s215 Sp110 St8sia1

Genes commonly upregulated by +/+, -/+ and -/-: 1:134168449-134181386 12:88817916-88818156 4931408A02Rik Ang,Rnase4 Asph C3 Cdk14 Col11a1 Cx3cl1 Cyfip2 Cyp2s1 Dusp5 Gcnt3 Has1 Il17rd Kif27 Klra4 Lef1 Lgr6 Ly6c1 Mei4 Ncam1 Nrg2 Pcdhb16 Pcdhb17 Pdgfc Plau Pparg Prex2 Ptgr1 Ptgs2 Rapgef3 Rasef Sel1l3 Serpine1 Sh3rf2 Smarca1 Spry4 Steap1 Tmcc2 Ubash3b Vgf Vgll3 Wnt4

Genes commonly upregulated by +/-, -/+ and -/-: 14:14581948-14582458 16:7917808-7918293 2:24209197-24210361 2010015L04Rik 6330512M04Rik,Ctsd 9130219A07Rik,Il22ra1 Abcb1b Ank2 B3galt1 Blnk Ccdc80 Ccl20 Cd109 Cd44 Cda Cdc42ep3 Cpeb2 Ctsl Dapk1 Dmkn Dnajc27 Emp3 Epb4.1l3 Epb4.1l4b Fam81a Fgfr1 Gm11194 Gm13832,Msi1 Gpc6 Grasp Gulp1 Id3 Igfbp2 Inf2 Itpr3 Klhdc7a Krt80 Lmo1 Lox Lpar1 Ly6a Lypd3 Mcc Mfge8 Mgp Mtap6 Mthfd1l Mtus1 Myh14 Notch3 Nt5e Nxn Oxr1 Pdlim4 Phlda2 Pkdcc Pmp22 Ppa1 Prkg2 Prom2 Prune2 Psca Ptpre Rab6b Sat1 Serpinb5 Slc12a2 Slc13a2 Sord Sprr1a Steap3 Sult2b1 Sytl2 Tacc1 Tanc2 Tcea3 Tnfrsf21 Ttc39c Twist2 Vim Wipf1 Zcchc24 Zeb1,Zeb1.1

Genes commonly upregulated by all isoforms: 1110012J17Rik 14:77049314- 77049849 1810011O10Rik 2310046K01Rik 9330182L06Rik A330023F24Rik, Mir29b-2, Mir29c Acox2 Ahi1 Ak4 Akna Aldh2 Angpt1 Ankrd6 Anxa2 Anxa8 Apol9a Apol9b Arhgef10l Ascc3 Atg9b Atp8a1 Axl Cdsn Chd7 Chn1 Cldn1 Clmn Clu Col18a1 Cth Cxcl5 Dagla Ddr2 Dock4 Dok7 Dtna Eml1 Emp1 Epdr1 Epha4 Eps8 Etv4 Fam171b Fam38b Fam49a Fgfbp1 Flt4 Foxn1 Fzd1 Gch1 Gdnf Gfod1 Gja1 Gjb2 Gjb3 Glns-ps1 Glul Gm1673 Gpnmb Gsn H19,Mir675 H2-Q7 Hapln4 Has2 Hectd2 Id2 Ifi203,Mndal Ifi204 Ifitm3 Igf2 Igf2r Igsf3 Il18 Isg15 Kcnh2 Kcnk10 Kif19a Krt14 Lama3 Ldlrad3 Lgals1 Lgals3 Lmna Man1a Map3k13 Mecom Mfsd2a Mmp15 Mnda Mpp2 Msln Mtap2 Naip2,Naip6 Ndrg2 Nedd9 Nes Neurl1b Nfil3 Nkain1 Oas1a Oas2 Oasl1 Oasl2 Odz4 Onecut2 Papln Parp14 Pax9 Pcdh1 Pdlim1 Pkp1 Plekhg4,Slc9a5 Pogk Pstpip2 Ramp3 Rbp4 Rcn3 Runx2 S100a14 Sfmbt2 Sgsm1 Sh3kbp1 Slc16a10 Slc4a7 Slc4a8 Slc6a17 Slc7a3 Slfn2 Slfn8 Slit2 Slpi Smpdl3b Snta1 Sox11 Sox9 Spp1 Stat1 Stbd1 Sult1c2 Sybu Syt8,Tnni2 Taf9b Tbkbp1 Tiam2 Tmed3 Tmem136 Trp63 Tspan17 Ttyh2 Uchl1 Unc5b Ust Vcam1 Zbp1 Zfp9 Zfpm2 Zswim5

Genes uniquely downregulated by +/+: 12:9609396- 9609720 15:101839107- 101839487 15:12953159- 12953580 15:12956715- 12957003 17:35098873- 35099301 2700094K13Rik 2810417H13Rik 3:121424344- 121424548 6:125269522- 125269779 8:98198241- 98198602 Ank Anxa6 Atp9a Ccdc64 Cdc42ep5 Dgka Dock8 Fbln5 Gm13523 Gm15507,Nr2e3 Gm15941,Ncald Hr Lrp2 Mgst3 Rab7l1 Rapgef1 Slc37a1 Zfp72

Genes uniquely downregulated by +/-: 1:137713029- 137713321 11:16650764- 16652035 1110059E24Rik 1190005F20Rik 15:101230306 -101232099 15:5194288 -5194534 17:4992822 -4993136 1700029F09Rik, Kdelc1 18:75138845 -75139230 1810009A15Rik, Ganab, Ints5 19:33468995- 33469829 2:126502473- 126504616 2:173108079- 173108408 2:177772633- 177772739 2010317E24Rik 2410127L17Rik 2610019F03Rik 2700078E11Rik 2810025M15Rik 2810408M09Rik 3:121347634- 121347970 3:121425062- 121425289 3:128926729- 128928224 37500 4921507P07Rik 4930426L09Rik 4930558J18Rik 5430417L22Rik 6:70765533 -70765711 6330578E17Rik 7:4990109- 4990428 8:53444441- 53445360 8:53445417- 53445819 9:81522369- 81522728 9230111E07Rik, Gm14321 9930021J03Rik A330040F15Rik Abi2 Abl2 Acadl Actr1a Acvr2b Adipor2 Adss Ahnak AI597479 AI846148 AI848100 AK129341 Akt3 Aldh9a1 Als2, Mpp4 Anubl1 Aplp2 Arhgap19 Arl2 Arl3 Asah2 Aspm Atf7ip2 Atic Atrnl1 Aurka B630005N14Rik Bag2 Bard1 BC016495 Bcl2l1 Bdnf Bmpr2 Bscl2, Hnrnpul2 Btrc Btrc Bub1 C030046E11Rik Cacybp Cadm1 Camsap2 Capn2 Casp2, Tmem139 Casp7 Casp8 Cblb Cbwd1 Ccdc86 Ccdc93 Ccng2 Ccnj Ccnyl1 Cd164 Cdca5, Gm550 Cdca7 Cdkn2b Cep170 Cep55 Cep78 Chchd6 Chn2 Cited1 Clcf1 Cnnm3 Cntf, Zfp91 Col27a1 Cpsf7 Cstf2t Ctnnd1 Cuedc2 Cysltr1 D030056L22Rik D19Bwg1357e D19Wsu162e Dak Dcaf8 Ddb1 Dnajc10 Dnpep Dtl Dtymk Dusp2 Dync1i2 Dyrk3 Eef1g Efhc1 Eid1 Eif3m Eif5b Eml3,Mta2 Emx2 Epb4.1l5 Exo1 Ext1 F2r Fads1 Fads2 Fam108b Fam115a Fam117b Fam122a Fam160b1 Fam178a Fam188b Fam190a Fam60a Fam83b Fau Fermt1 Fgd3 Fhl1 Fndc3b Frmd4b Fsd1l Fzd4 Fzd5 Fzd7 Galnt3 Gkap1 Glis2 Glis3 Gls Gm10425 Gm16854 Gm20419 Gm20538,Ndufb8,Sec31b Gm20544 Gm5465 Gpam Gtf3c3 Haus2 Hdac4 Hey1 Hif1an Hmcn2 Hnrnpd Hnrnpf Hoxd8 Hs6st1 Igf1r Igf2bp3 Igsf9 Ikzf2 Incenp Ing5 Inpp4a Isy1 Itga6 Itm2c Itpkb Ivns1abp Jak2 Kdm5b Kif11 Kif14 Kif18a Kif20b Kifap3 Kifc3 Klf11 Lad1,Tnnt2 Lamc1 Lbr Lekr1 Lipa Lmnb1 Lnp Lpgat1 Lpp Lrig3 Lsm3 Map4k4 Mcm3 Mcm8 Mdm4 Mdm4-ps Met Mex3c Mfap3l

Mgat4a Mgea5 Minpp1 Mlf1 Mlf2 Mob1a Mocs2 Mogs Mrpl16 Mtpn Mxi1 Mybl2 Myef2 Myo5b Naa40 Nav2 Ncapd2 Ncaph Nck2 Nop10 Nop58 Npy2r Nrk Nsd1 Nucks1 Nuf2 Nup205 Nvl Nxf1,Tmem223 Osbp Ostf1 P2ry2 Pak6 Parp1 Pask Patl1 Pawr Pcdh18 Pcgf6 Pdcl Pde4c Pdgfd Pdzd8 Per2 Pfn2 Pgam1 Pgap1 Phlda1 Pign Pik3c2b Pikfyve Pkig Pkp4 Plcb3 Plch1 Plekha5 Plekha8 Plod2 Pola2 Pot1a Ppapdc2 Ppcdc Ppp1r14b Ppp2r5b Prdx5 Prdx6 Prelid2 Prpf19 Prrc2c Ptp4a1 Ptpn13 Ptprf Purg Qser1 Qsox2 Rab11fip2 Rad18 Rarb Rbl1 Rbm17 Rcl1 Repin1 Rfwd2 Rgmb Rnd3 Rnf128 Rnls Rpa3 Rpl31 Rpl7 Rpp30 Rps6ka4 Rrp15 Rtkn2 Rtn3 Ruvbl1 Sccpdh Schip1 Sema4c Setd5 Sfr1 Sfxn3 Sfxn4 Sgol2 Shroom4 Skil Slc35b4 Slc35f5 Slc6a6 Smad7 Smarcad1 Smc3 Smc5 Snrpg Snrpn Spns2 Spns3 Srgap2 Ss18l1 Stard4 Stip1 Stk35 Stx3 Stx7 Suv39h2 Tcf7l2 Tctn3 Tdrd5 Tead4 Thnsl1 Tjp2 Tm9sf3 Tmem109 Tmem132a Tmem176b Tmem178 Tmem185b Tmem194b Tmem2 Tmem231 Tmem51 Tmem8b Tmf1 Tmsb10 Tpp2 Tra2a Tram2 Trove2 Tsc1 Tsc22d1 Ttc12 Tulp3 Tut1 Uba3 Ube2h Ube2t Ubn2 Ubtd1 Uhmk1 Usp44 Vps37c Vps37d Wdr5 Wfdc2 Zbed3 Zc3h11a Zfp189 Zfp281 Zfp334 Zfp362 Zfp449 Zfp568 Zfp637 Zfp697 Zfp746 Zfp783,Zfp956 Zfp931 Znhit2-ps Zswim6 Zxdc

Genes uniquely downregulated by -/+: 10:11211918- 11211988 14:41709070- 41709217 16:23100101- 23100323 19:4203547- 4203857 2:11475378- 11475577 2:30070176- 30070391 2410004B18Rik 2610307P16Rik 2700089E24Rik 3:104441781- 104442141 3:116512764- 116513264 3:121424630- 121424980 3:121585016- 121586274 3:121589140- 121589654 3:121603179- 121603526 3:122687628- 122687801 3:96267497- 96270442 3:96270522- 96270839 4930422G04Rik 5730419I09Rik 5730508B09Rik 6:134878992- 134903415 6:134903828- 134904888 6:146495292- 146495814 8:60140941- 60141259 A830007P12Rik Abcc4 Ablim1 Acadm Adh5 Adora1 Agk Aimp1 Ankrd13c Anxa4 Ap1ar Apc2 Apoa1bp Arhgef16 Arhgef37 Arhgef5 Arpc5l Atp1b1 Atp5c1 Atp5e Atp5s Atp6v0e2 AU021092 Avl9 Bcar3 Bckdha Bhlhe41 Bst1 C330021F23Rik Ccdc88c Ccna2 Ccs Cdcp1 Cdh1 Cenpe Chac1 Chchd5 Cib2 Crbn Crebl2 Cry2 Cryz Cul9 Cxadr Cyr61 Cys1 D6Wsu116e Dag1 Ddit4 Dennd1a Depdc1a Dnajb14 E130311K13Rik Ecscr Edem2 Egf Evc2 Fnbp1 Fnbp1l Fpgt Frem2 Gatm Gm5900 Gramd3 Grhl2 Gstm7 Hadh Hoxd9 Hs2st1 Igsf5,Pcp4 Il17d Impact Irx5 Itch Itpr2 Lamtor3 Larp7 Lmo4 Lphn2 Marveld3 Metap1 Mpped2 Mrpl9

Mrps35 Mtss1 Myo6 Nfe2l2 Nfkb1 Nr3c2 Odf2l Osbpl2 Pbxip1 Pcmtd2 Pdrg1 Phc3 Pigy Pim3 Pkn2 Ppa2 Ppp1r14d Prkacb Psrc1 Ptprg Pygb Rab19 Rap1gds1 Rbbp9 Rbm43 Rpl22l1 Rpl23 Rpl34 Rps27 Rps3a Sardh Sdr42e1 Sgce Sh2d4a Sh3tc1 Siva1 Slc2a8 Slc35f2 Smarca2 Snord64 Spint1 Spry1 Stambp Stap2 Sv2a Syde2 Tet2 Tgif2 Tsen54 Ttc38 Ube2d3 Urm1 Usp20 Usp8 Uvrag Vamp5 Vamp8 Vldlr Wdr34 Wdr76 Wls Wrn Zbtb44 Zfhx4 Zfp13 Zfp217 Znhit6

Genes uniquely downregulated by -/-: 1:23273748- 23274043 1:9525840- 9526323 1:9533780- 9534074 10:126497535- 126499225 12:17908988- 17910915 12:19869316- 19869597 12:19870896- 19873024 12:76914761- 76915258 12:86417588- 86417899 15:100881093- 100909148 15:32708853- 32724920 16:4880568- 4883421 16:4883571- 4885623 16:8625772- 8627593 18:32432286- 32432511 2:177788944- 177789285 2:30576171- 30576495 2410001C21Rik 2510012J08Rik 2810030E01Rik 3:19216108- 19216496 3:19219663- 19220685 3:19359749- 19360311 3:67354581- 67354936 3110001I22Rik, Bfar 39873 4:71773870- 71774226 4931428F04Rik, Exoc3l 5:106122843- 106124229 6:129494578- 129494892 6:129498039- 129498346 6:134851742- 134852346 6:22222520- 22223061 6:22225910- 22226191 6:3292520- 3292881 7:144085618- 144086075 9:124073247- 124073682 9630013D21Rik 9930038K12Rik, Hoxa10, Hoxa9 Aacs AC115005.1, Gm7541 Afap1 AI597468 Apaf1 Arhgap1 Arhgef12 Arhgef25 Atp6v1e1 AU041133 Bach1 Bend5 Brca1 Cables2 Cachd1 Cbx6,Npcd,Nptxr Cd24a Cdk12 Cdk2 Cdk4 Cdk5 Cdkn2c Cnn3 Cnpy2 Cpne2 Ctbp1 Cyp2j6 D330028D13Rik Dctn1 Dhx9 Dnajc14 Dnajc5 Dpm2 Elmo2 Ephb4 Errfi1 Ets1 Fam100a Fam109a Fam115c Fam134c Fmo1 Galnt12 Gas1 Gjc1 Gm5819 Gns H2afz Hsd17b11 Hspa14 Ier5l Itgb8 Kcnn1 Kif12 Klf6 Klhl14 Klhl21 Klhl24 Lcmt2 Lemd3 Lgr4 Lrrc33 Luc7l2 Mal2 Maz Mdm1 Meig1 Meis3 Mgmt Mkl2 Msrb3 Mzf1 Ndor1 Nfatc4 Pbx3 Pcna Pde7a Phactr2 Pip4k2c Pip5k1c Plcb1 Plcb4 Podn Polm Ppic Ptbp2 Ptms Rab5b Rc3h2 Rnf130 Rnf34 Rnpepl1 RP24-201C14.5.1 Rtf1 Samd14 Samd9l Scarf2 Sim1 Slc25a10 Slc35e3 Slc37a3 Snn Sorl1 Spc25 Srrm4 Srsf6 Tbc1d23 Tbc1d9 Tcf4 Tmpo Tprn Ttc39a Twsg1 Txndc16 Uap1l1 Ulk1 Wdfy3 Zdhhc8 Zer1 Zfml Zfp282 Zfp316 Zfp324 Zfp444 Zfp612

Genes commonly downregulated by +/+ and +/-: Abcg2 Akr1b3 Arhgap11a Btbd3 Csf2ra D4Bwg0951e Dusp10 F2rl1 Fkbp9 Gng2 H6pd Il1r1 Jag1 Lbp Lrp11 Lrp8 Mtap9

Myadm Mycn Pdgfb Plxna1 Ppdpf Rai14 Sfn Spg11 Svip Tacstd2 Thbd Tspan18 Ttc7b Tubb4b Ube2c

Genes commonly downregulated by +/+ and -/+: 9830147E19Rik BC029722 Cdh16 Kcnk5 Rgl3 Stard8

Genes commonly downregulated by +/+ and -/-: Akr1c12 Bend4 Ccdc149 Cenpb,Spef1 Cmtm3 Cyp7b1 Elmod1 Eya1 Fam20c Fam43a Fzd8 Kcnj16 Limch1 Naaa Sfrp2 Slc27a4 Snx8 Tnc Ttl Zfp398

Genes commonly downregulated by +/- and -/+: 0610030E20Rik 11:20855913- 20857649 11:20868534- 20870392 11:20872350- 20875952 11:20876094- 20877283 11:20877358- 20886197 17:21611494- 21613313 17:21613455- 21617363 3:121291328- 121309628 8430419L09Rik AA986860 Acaa2 Adm AI661453 Akap12 Aldh1a2 Ankrd1 Ankrd26 Baiap2l2 Capn5 Ccdc79 Celf2 Ckap2l Cpm Csf1r D2Ertd750e Dclk3 Depdc7 Dhrs3 Dnajc4,Nudt22,Vegfb Dnmbp Ehf Ermp1 Fbxl14 Gm10925 Gm11492, Sept4 Gm12494, Gstm3, Gstm6 Gm13394 Gpr160 Gprc5c Hibadh Ifit3 Itga2 Itpk1 Itpr1 Kif16b Llgl2 Lpxn Ltb Ltbp3 Ltk Ms4a2 Nap1l3 Nedd4l Ngef Pabpc4l Pard6b Pdk1 Phf15 Pkhd1 Plac8 Prss16 Rbpms Rnf125 Rpl32 Rpl35 Rpl37a Rps21 Scarna17 Scg5 Sorbs1 Srgap3 Stard8 Tbc1d30 Tinag Tmem180 Tnfaip2 Trim8 Trpm6 Ubxn1 Ugt8a Wnt7b Xpc Zbtb26,Zbtb6

Genes commonly downregulated by +/- and -/-: 2410066E13Rik 9130019O22Rik Adcy1 Alms1 Apbb1 Arc Atg13 Atl3 Atrn Bcl7a Bicc1 Btg2 Cited2 Cxxc5 Dennd5b Dido1 E2f7 Fam125b Frat2 Gadd45g Gp1bb,Sept5 Gpc4 Gxylt2 Klhdc8a Magi1 Mid1 Mir30c-2 Pde4b Pds5b Plekhg3 Rnf103 Rnf19a Rybp Sertad4 Smad6 Smo Sox4 St5 Tfrc Tmem127 Tpm1 Trib2 Tspan12 Vps18 Zcwpw1

Genes commonly downregulated by -/+ and -/-: 16:16606479- 16610601 16:16618872- 16619934 16:5007342- 5008512 Arrdc3 Calcoco1 Cand2 Cdkl1 Chpt1 Dnajb4 Elovl6 Erbb3 Fam102a Gabarapl1 Gm13321 H13 Hdac11 Hist2h2be Icosl Ifit2 Klhdc5 Lpar5 Lrp6 Ndst1 Papss1 Plk1s1 Rab43 Rasgef1b Ror1 Sec62 Slc25a13 Tmprss2 Ttc30b Txnip Usp33 Zfp395

Genes commonly downregulated by +/+, +/- and -/+: 2610316D01Rik 4930556M19Rik Ahr Akr1b8 Bex1 Car2 Cd82 Cobll1 Dcdc2a Dnm3 Dsc2 Dsg2 Dsp Dusp16 Fam83d Fam84a Fst Gm13807 Gstp1 Mavs Nfatc2 Nmt2 Phyhipl Prps2 Sema3e Sh3tc2 Slc22a23 Slc4a11 Slco2a1 Tbc1d4 Wwc2 Zdhhc14

Genes commonly downregulated by +/+, +/- and -/-: 1810058I24Rik 2:164701401-164703316 AC117577.2,Ccnf Akr1c13 Arhgap28 BC005624 Cldn4 Cnksr3 Col4a3 Col4a4 Cpt1a Csrp1 D0H4S114 Efnb1 Fbxo21 Foxq1 Hspg2 Ildr1 Lrig1 Marcks Ms4a3 Nanos1 Nqo1 Nrip3 ORF63 Pitx2 Ppp1r26 Rnf144a Scnn1g Scube3 Six5 Slc4a3 Stxbp1 Tlr2 Zyx

Genes commonly downregulated by +/+, -/+ and -/-: Dll1 Fam73a Irx3 Mdfic Ndrg4 Npr3 Samd1 Syt14 Trpv4 Zcchc3

Genes commonly downregulated by +/-, -/+ and -/-: 16:16620008- 16622322 1600027N09Rik 1700020I14Rik 2:126507568- 126509781 2010300F17Rik 7:6683292- 6722847 9130017N09Rik Acrbp,Ing4 Arhgap29 Bex4 Cald1 Carns1 Cdk18 Cdkn1b Ctgf Dstn Eif2ak3 Epn3 Evc Fem1c Fgd4 Gm14391 Gm4631 Gm7292 Gstm2 Gyltl1b Hoxd3, Hoxd4, Mir10b Irak2 Kank1 Kdm3a Kif13b Lta Lzts2 Mapk8ip1 Mme Mtmr14 Nagk Npnt Ntn4 Nuak2 Ogdhl Peg3 Pex26 Pik3cg Ppm1k Rab11fip4 Ranbp3l Rassf3 Rmnd5a Tspan33 Uty Vgll4 Wbp5 Wbscr27

Genes commonly downregulated by all isoforms: 11:20857735- 20868271 16:16610663- 16618808 4933415A04Rik, Ccnjl 5430407P10Rik 9230102O04Rik, Gata3 9830001H06Rik Abtb1 Afap1l1 Akr1b10 Alcam Amot Ankrd44 Apln App Arhgap24 Arhgap31 Ass1 B230120H23Rik Bok Brd3 Cd40 Cdh6 Chst14 Ddx3y Edn1 Eif2s3y Enc1 Epb4.1l4a Erc1 F3 Fam171a1 Fgf18 Fhod3 Fras1 Gdf15 Gpr56 Gstm1 Hsd17b12 Id4 Kcnk1 Kdm5d Lcn2 Lcp1 Lipg Lrp5 Mal Mrps2 Ngfrap1 Pappa Pcdh10 Postn Ptges2 Ptprj Rasl11b Scin Serinc3 Slc16a12 Slc31a2 Slco4a1 Smpd1 Sox12 Spna2 Tanc1 Tet3 Tgfa Tgfbr3 Thbs1 Tln2 Tns1 Tpcn1 Trim7 Tusc1 Ube2e3 Vav2 Veph1 Wnt16 Wnt7a Zc3hav1l Zfp608 Zfp704

Bibliography

[1] Daniel A Haber, Alan J Buckler, Tom Glaser, Katherine M Call, Jerry Pelletier, Robert L Sohn, Edwin C Douglass, and David E Housman. An internal deletion within an 11p13 zinc finger gene contributes to the development of wilms' tumor. *Cell*, 61(7):1257–1269, 1990.

[2] Peter Hohenstein and Nicholas D Hastie. The many facets of the wilms' tumour gene, wt1. *Human molecular genetics*, 15(suppl 2):R196–R201, 2006.

[3] Jordan A Kreidberg, Hannu Sariola, Janet M Loring, Masahiro Maeda, Jerry Pelletier, David Housman, and Rudolf Jaenisch. Wt-1 is required for early kidney development. *Cell*, 74(4):679–691, 1993.

[4] Adrian W Moore, Andreas Schedl, Lesley McInnes, Michael Doyle, Jacob Hecksher-Sorensen, and Nicholas D Hastie. Yac transgenic analysis reveals wilms' tumour 1 gene activity in the proliferating coelomic epithelium, developing diaphragm and limb. *Mechanisms of development*, 79(1):169–184, 1998.

[5] Adrian W Moore, Lesley McInnes, Jordan Kreidberg, Nicholas D Hastie, and Andreas Schedl. Yac complementation shows a requirement for wt1 in the development of epicardium, adrenal gland and throughout nephrogenesis. *Development*, 126(9):1845–1857, 1999.

[6] Ute Herzer, Alexander Crocoll, Debra Barton, Norma Howells, and Christoph Englert. The wilms tumor suppressor gene wt1 is required for development of the spleen. *Current biology*, 9(15):837–S1, 1999.

[7] Kay-Dietrich Wagner, Nicole Wagner, Valerie PI Vidal, Gunnar Schley, Dagmar Wilhelm, Andreas Schedl, Christoph Englert, and Holger Scholz. The wilms' tumor gene wt1 is required for normal development of the retina. *The EMBO journal*, 21(6):1398–1405, 2002.

[8] Nicole Wagner, Kay-Dietrich Wagner, Annette Hammes, Karin M Kirschner, Valerie P Vidal, Andreas Schedl, and Holger Scholz. A splice variant of the wilms' tumour suppressor wt1 is required for normal development of the olfactory system. *Development*, 132(6):1327–1336, 2005.

[9] A Ijpenberg, JM Perez-Pomares, JA Guadix, R Carmona, V Portillo-Sanchez, D Macias, P Hohenstein, CM Miles, ND Hastie, and R Munoz-Chapuli. Wt1 and retinoic acid signaling are essential for stellate cell development and liver morphogenesis. *Developmental biology*, 312(1):157–170, 2007.

[10] Nicholas D Hastie. Life, sex, and wt1 isoformsthree amino acids can make all the difference. *Cell*, 106(4):391–394, 2001.

[11] J Kent, AM Coriat, PT Sharpe, ND Hastie, and V Van Heyningen. The evolution of wt1 sequence and expression pattern in the vertebrates. *Oncogene*, 11(9):1781–1792, 1995.

[12] Daniel A Haber, Robert L Sohn, Alan J Buckler, Jerry Pelletier, Katherine M Call, and David E Housman. Alternative splicing and genomic structure of the wilms tumor gene wt1. *Proceedings of the National Academy of Sciences*, 88(21): 9618–9622, 1991.

[13] Annette Hammes, Jian-Kan Guo, Gudrun Lutsch, Joerg-Robert Leheste, Danilo Landrock, Ulrike Ziegler, Marie-Claire Gubler, and Andreas Schedl. Two splice variants of the wilms' tumor 1 gene have distinct functions during sex determination and nephron formation. *Cell*, 106(3):319–329, 2001.

[14] Thomas A Natoli, Alice McDonald, Julia A Alberta, Mary E Taglienti, David E Housman, and Jordan A Kreidberg. A mammal-specific exon of wt1 is not required for development or fertility. *Molecular and cellular biology*, 22(12):4433–4438, 2002.

[15] Chavaboon Dechsukhum, Joy L Ware, Andrea Ferreira-Gonzalez, David S Wilkinson, and Carleton T Garrett. Detection of a novel truncated wt1 transcript in human neoplasia. *Molecular Diagnosis*, 5(2):117–128, 2000.

[16] Anthony R Dallosso, Anne L Hancock, Keith W Brown, Ann C Williams, Sally Jackson, and Karim Malik. Genomic imprinting at the wt1 gene involves a novel coding transcript (awt1) that shows deregulation in wilms' tumours. *Human molecular genetics*, 13(4):405–415, 2004.

[17] Christoph Englert. Wt1more than a transcription factor? *Trends in biochemical sciences*, 23(10):389–393, 1998.

[18] Colin G Miles, Joan Slight, Lee Spraggon, Maureen O'Sullivan, Charles Patek, and Nicholas D Hastie. Mice lacking the 68-amino-acid, mammal-specific n-terminal extension of wt1 develop normally and are fertile. *Molecular and cellular biology*, 23(7):2608–2613, 2003.

[19] Stephen L Madden, Donna M Cook, and FJ Rauscher 3rd. A structure-function analysis of transcriptional repression mediated by the wt1, wilms' tumor suppressor protein. *Oncogene*, 8(7):1713–1720, 1993.

[20] Zhao-Yi Wang, QING-QING Qiu, Kevin T Enger, and Thomas F Deuel. A second transcriptionally active dna-binding site for the wilms tumor gene product, wt1. *Proceedings of the National Academy of Sciences*, 90(19):8896–8900, 1993.

[21] Greg Holmes, Sima Boterashvili, Milton English, Brandon Wainwright, Jonathan Licht, and Melissa Little. Two n-terminal self-association domains are required for the dominant negative transcriptional activity of wt1 denys-drash mutant proteins. *Biochemical and biophysical research communications*, 233(3):723–728, 1997.

[22] Josina C Reddy, John C Morris, Jing Wang, Milton A English, Daniel A Haber, Yang Shi, and Jonathan D Licht. Wt1-mediated transcriptional activation is inhibited by dominant negative mutant proteins. *Journal of Biological Chemistry*, 270(18):10878–10884, 1995.

[23] Michael Ladomery, John Sommerville, Sarah Woolner, Joan Slight, and Nick Hastie. Expression in xenopus oocytes shows that wt1 binds transcripts in vivo, with a central role for zinc finger one. *Journal of cell science*, 116(8):1539–1549, 2003.

[24] Lynn M McKay, Brian Carpenter, and Stefan GE Roberts. Regulation of the wilms' tumour suppressor protein transcriptional activation domain. *Oncogene*, 18(47):6546–6554, 1999.

[25] Brian Carpenter, Kathryn J Hill, Marika Charalambous, Kate J Wagner, Diya Lahiri, Dominic I James, Jens S Andersen, Valérie Schumacher, Brigitte Royer-Pokora, Matthias Mann, et al. Basp1 is a transcriptional cosuppressor for the wilms' tumor suppressor protein wt1. *Molecular and cellular biology*, 24(2):537–549, 2004.

[26] Weihong Wang, Sean Bong Lee, Rachel Palmer, Leif W Ellisen, and Daniel A Haber. A functional interaction with cbp contributes to transcriptional activation by the wilms tumor suppressor wt1. *Journal of Biological Chemistry*, 276(20): 16810–16816, 2001.

[27] Reinhard Depping, Susann G Schindler, Charlotte Jacobi, Karin M Kirschner, and Holger Scholz. Nuclear transport of wilms tumour protein wt1 involves importins α and β. *Cellular Physiology and Biochemistry*, 29(1-2):223–232, 2012.

[28] PR Vajjhala, E Macmillan, T Gonda, and M Little. The wilms tumour suppressor protein, wt1, undergoes crm1-independent nucleocytoplasmic shuttling. *FEBS letters*, 554(1):143–148, 2003.

[29] Martina Niksic, Joan Slight, Jeremy R Sanford, Javier F Caceres, and Nicholas D Hastie. The wilms' tumour protein (wt1) shuttles between nucleus and cytoplasm

and is present in functional polysomes. *Human molecular genetics*, 13(4):463–471, 2004.

[30] T Dudnakova, L Spraggon, J Slight, and N Hastie. Actin: a novel interaction partner of wt1 influencing its cell dynamic properties. *Oncogene*, 29(7):1085–1092, 2010.

[31] Stefan H Larsson, Jean-Paul Charlieu, Kiyoshi Miyagawa, Dieter Engelkamp, Minoo Rassoulzadegan, Allyson Ross, François Cuzin, Veronica van Heyningen, and Nicholas D Hastie. Subnuclear localization of wt1 in splicing or transcription factor domains is regulated by alternative splicing. *Cell*, 81(3):391–401, 1995.

[32] Ute Herzer, Bertram Lutz, Kristina Hartmann, and Christoph Englert. The speckling domain of the wilms tumor suppressor wt1 overlaps with the transcriptional repression domain. *FEBS letters*, 494(1):69–73, 2001.

[33] Toska Eneda and Stefan GE Roberts. Mechanisms of transcriptional regulation by wt1 (wilms' tumour 1). *Biochemical Journal*, 461(1):15–32, 2014.

[34] John H Laity, H Jane Dyson, and Peter E Wright. Molecular basis for modulation of biological function by alternate splicing of the wilms' tumor suppressor protein. *Proceedings of the National Academy of Sciences*, 97(22):11932–11935, 2000.

[35] Gary Zhai, Maya Iskandar, Kathleen Barilla, and Paul J Romaniuk. Characterization of rna aptamer binding by the wilms' tumor suppressor protein wt1. *Biochemistry*, 40(7):2032–2040, 2001.

[36] Michael R Ladomery, Joan Slight, Sharon Mc Ghee, and Nicholas D Hastie. Presence of wt1, the wilm's tumor suppressor gene product, in nuclear poly (a)+ ribonucleoprotein. *Journal of Biological Chemistry*, 274(51):36520–36526, 1999.

[37] Rachel C Davies, Cinzia Calvio, Eva Bratt, Stefan H Larsson, Angus I Lamond, and Nicholas D Hastie. Wt1 interacts with the splicing factor u2af65 in an isoform-dependent manner and can be incorporated into spliceosomes. *Genes & development*, 12(20):3217–3225, 1998.

[38] Natalie A Little, Nicholas D Hastie, and Rachel C Davies. Identification of wtap, a novel wilms tumour 1-associating protein. *Human molecular genetics*, 9(15): 2231–2239, 2000.

[39] Angeles Ortega, Martina Niksic, Angela Bachi, Matthias Wilm, Lucas Sánchez, Nicholas Hastie, and Juan Valcárcel. Biochemical function of female-lethal (2) d/wilms' tumor suppressor-1-associated proteins in alternative pre-mrna splicing. *Journal of Biological Chemistry*, 278(5):3040–3047, 2003.

[40] Andrea Caricasole, Antonio Duarte, Stefan H Larsson, Nicholas D Hastie, Melissa Little, Gregory Holmes, Ivan Todorov, and Andrew Ward. Rna binding by the wilms tumor suppressor zinc finger proteins. *Proceedings of the National Academy of Sciences*, 93(15):7562–7566, 1996.

[41] AA Morrison, JP Venables, G Dellaire, and MR Ladomery. The wilms tumour suppressor protein wt1 (+ kts isoform) binds alpha-actinin 1 mrna via its zinc-finger domain. *Biochemistry and cell biology*, 84(5):789–798, 2006.

[42] Harald D Rupprecht, Iain A Drummond, Stephen L Madden, FJ Rauscher, and Vikas P Sukhatme. The wilms' tumor suppressor gene wt1 is negatively autoregulated. *Journal of Biological Chemistry*, 269(8):6198–6206, 1994.

[43] Julie Wells, Miguel N Rivera, Woo Jae Kim, Kristen Starbuck, and Daniel A Haber. The predominant wt1 isoform (+ kts) encodes a dna-binding protein targeting the planar cell polarity gene scribble in renal podocytes. *Molecular Cancer Research*, 8(7):975–985, 2010.

[44] Fariba Jian Motamedi, Danielle A Badro, Michael Clarkson, M Rita Lecca, Stephen T Bradford, Fabian A Buske, Kathrin Saar, Norbert Hübner, André W Brändli, and Andreas Schedl. Wt1 controls antagonistic fgf and bmp-psmad pathways in early renal progenitors. *Nature communications*, 5, 2014.

[45] WA Bickmore, K Oghene, MH Little, A Seawright, V Van Heyningen, and ND Hastie. Modulation of dna binding specificity by alternative splicing of the wilms tumor wt1 gene transcript. *Science*, 257(5067):235–237, 1992.

[46] Yeou Bor, Jennifer Swartz, Avril Morrison, David Rekosh, Michael Ladomery, and Marie-Louise Hammarskjöld. The wilms tumor 1 (wt1) gene (+ kts isoform) functions with a cte to enhance translation from an unspliced rna with a retained intron. *Genes & development*, 20(12):1597–1608, 2006.

[47] Jayasha Shandilya, Eneda Toska, Derek J Richard, Kathryn F Medler, and Stefan GE Roberts. Wt1 interacts with mad2 and regulates mitotic checkpoint function. *Nature communications*, 5, 2014.

[48] Jane F Armstrong, Kathryn Pritchard-Jones, Wendy A Bickmore, Nicholas D Hastie, and Jonathan BL Bard. The expression of the wilms' tumour gene, wt1, in the developing mammalian embryo. *Mechanisms of development*, 40(1):85–97, 1993.

[49] You-Ying Chau and Nicholas D Hastie. The role of wt1 in regulating mesenchyme in cancer, development, and tissue homeostasis. *Trends in Genetics*, 28(10):515–524, 2012.

[50] You-Ying Chau, David Brownstein, Heidi Mjoseng, Wen-Chin Lee, Natalija Buza-Vidas, Claus Nerlov, Sten Eirik Jacobsen, Paul Perry, Rachel Berry, Anna Thornburn, et al. Acute multiple organ failure in adult mice deleted for the developmental regulator wt1. *PLoS Genet*, 7(12):e1002404–e1002404, 2011.

[51] Rosalba Parenti, Roberto Perris, Giada Maria Vecchio, Lucia Salvatorelli, Antonietta Torrisi, Lucia Gravina, and Gaetano Magro. Immunohistochemical expression of wilms tumor protein (wt1) in developing human epithelial and mesenchymal tissues. *Acta histochemica*, 115(1):70–75, 2013.

[52] Eve Miller-Hodges and Peter Hohenstein. Wt1 in disease: shifting the epithelial–mesenchymal balance. *The Journal of pathology*, 226(2):229–240, 2012.

[53] Ofelia M Martínez-Estrada, Laura A Lettice, Abdelkader Essafi, Juan Antonio Guadix, Joan Slight, Víctor Velecela, Emma Hall, Judith Reichmann, Paul S Devenney, Peter Hohenstein, et al. Wt1 is required for cardiovascular progenitor

cell formation through transcriptional control of snail and e-cadherin. *Nature genetics*, 42(1):89–93, 2010.

[54] Jamie A Davies, Michael Ladomery, Peter Hohenstein, Lydia Michael, Anna Shafe, Lee Spraggon, and Nick Hastie. Development of an sirna-based method for repressing specific genes in renal organ culture and its use to show that the wt1 tumour suppressor is required for nephron differentiation. *Human molecular genetics*, 13(2):235–246, 2004.

[55] Abdelkader Essafi, Anna Webb, Rachel L Berry, Joan Slight, Sally F Burn, Lee Spraggon, Victor Velecela, Ofelia M Martinez-Estrada, John H Wiltshire, Stefan GE Roberts, et al. A wt1-controlled chromatin switching mechanism underpins tissue-specific wnt4 activation and repression. *Developmental cell*, 21(3): 559–574, 2011.

[56] Kinji Asahina, Bin Zhou, William T Pu, and Hidekazu Tsukamoto. Septum transversum-derived mesothelium gives rise to hepatic stellate cells and perivascular mesenchymal cells in developing mouse liver. *Hepatology*, 53(3):983–995, 2011.

[57] Bettina Wilm, Annemieke Ipenberg, Nicholas D Hastie, John BE Burch, and David M Bader. The serosal mesothelium is a major source of smooth muscle cells of the gut vasculature. *Development*, 132(23):5317–5328, 2005.

[58] Jianwen Que, Bettina Wilm, Hiroshi Hasegawa, Fan Wang, David Bader, and Brigid LM Hogan. Mesothelium contributes to vascular smooth muscle and mesenchyme during lung development. *Proceedings of the National Academy of Sciences*, 105(43):16626–16630, 2008.

[59] You-Ying Chau, Roberto Bandiera, Alan Serrels, Ofelia M Martínez-Estrada, Wei Qing, Martin Lee, Joan Slight, Anna Thornburn, Rachel Berry, Sophie McHaffie, et al. Visceral and subcutaneous fat have different origins and evidence supports a mesothelial source. *Nature cell biology*, 16(4):367–375, 2014.

[60] Ruby Yun-Ju Huang, Parry Guilford, and Jean Paul Thiery. Early events in cell adhesion and polarity during epithelial-mesenchymal transition. *Journal of cell science*, 125(19):4417–4422, 2012.

[61] Raghu Kalluri and Robert A Weinberg. The basics of epithelial-mesenchymal transition. *The Journal of clinical investigation*, 119(6):1420, 2009.

[62] Samy Lamouille, Jian Xu, and Rik Derynck. Molecular mechanisms of epithelial–mesenchymal transition. *Nature reviews Molecular cell biology*, 15(3):178–196, 2014.

[63] Jean Paul Thiery and Jonathan P Sleeman. Complex networks orchestrate epithelial–mesenchymal transitions. *Nature reviews Molecular cell biology*, 7(2): 131–142, 2006.

[64] Glauben Landskron, Marjorie De la Fuente, Peti Thuwajit, Chanitra Thuwajit, and Marcela A Hermoso. Chronic inflammation and cytokines in the tumor microenvironment. *Journal of immunology research*, 2014, 2014.

[65] Claudia Palena, Duane H Hamilton, and Romaine I Fernando. Influence of il-8 on the epithelial-mesenchymal transition and the tumor microenvironment. *Future oncology*, 8(6):713–722, 2012.

[66] Irina M Shapiro, Albert W Cheng, Nicholas C Flytzanis, Michele Balsamo, John S Condeelis, Maja H Oktay, Christopher B Burge, and Frank B Gertler. An emt-driven alternative splicing program occurs in human breast cancer and modulates cellular phenotype. *PLoS Genet*, 7(8):e1002218–e1002218, 2011.

[67] Samy Lamouille, Deepa Subramanyam, Robert Blelloch, and Rik Derynck. Regulation of epithelial–mesenchymal and mesenchymal–epithelial transitions by micrornas. *Current opinion in cell biology*, 25(2):200–207, 2013.

[68] Jennifer Haynes, Jyoti Srivastava, Nikki Madson, Torsten Wittmann, and Diane L Barber. Dynamic actin remodeling during epithelial–mesenchymal transition depends on increased moesin expression. *Molecular biology of the cell*, 22 (24):4750–4764, 2011.

[69] Anne J Ridley. Life at the leading edge. *Cell*, 145(7):1012–1022, 2011.

[70] Michael Z Gilcrease. Integrin signaling in epithelial cells. *Cancer letters*, 247(1): 1–25, 2007.

[71] Paola Nisticò, Mina J Bissell, and Derek C Radisky. Epithelial-mesenchymal transition: general principles and pathological relevance with special emphasis on the role of matrix metalloproteinases. *Cold Spring Harbor perspectives in biology*, 4(2):a011908, 2012.

[72] Henry M Kronenberg. Developmental regulation of the growth plate. *Nature*, 423 (6937):332–336, 2003.

[73] Elazar Zelzer and Bjorn R Olsen. The genetic basis for skeletal diseases. *Nature*, 423(6937):343–348, 2003.

[74] Mark F Pittenger, Alastair M Mackay, Stephen C Beck, Rama K Jaiswal, Robin Douglas, Joseph D Mosca, Mark A Moorman, Donald W Simonetti, Stewart Craig, and Daniel R Marshak. Multilineage potential of adult human mesenchymal stem cells. *science*, 284(5411):143–147, 1999.

[75] Arnold I Caplan and Scott P Bruder. Mesenchymal stem cells: building blocks for molecular medicine in the 21st century. *Trends in molecular medicine*, 7(6): 259–264, 2001.

[76] Florian Otto, Anders P Thornell, Tessa Crompton, Angela Denzel, Kimberly C Gilmour, Ian R Rosewell, Gordon WH Stamp, Rosa SP Beddington, Stefan Mundlos, Bjorn R Olsen, et al. Cbfa1, a candidate gene for cleidocranial dysplasia syndrome, is essential for osteoblast differentiation and bone development. *Cell*, 89(5):765–771, 1997.

[77] Patricia Ducy, Rui Zhang, Valérie Geoffroy, Amy L Ridall, and Gérard Karsenty. Osf2/cbfa1: a transcriptional activator of osteoblast differentiation. *cell*, 89(5): 747–754, 1997.

[78] Chisato Ueta, Masahiro Iwamoto, Naoko Kanatani, Carolina Yoshida, Yang Liu, Motomi Enomoto-Iwamoto, Tomoharu Ohmori, Hirayuki Enomoto, Ken Nakata, Kenji Takada, et al. Skeletal malformations caused by overexpression of cbfa1 or its dominant negative form in chondrocytes. *The Journal of cell biology*, 153(1): 87–100, 2001.

[79] Wei Huang, Shuying Yang, Jianzhong Shao, and Yi-Ping Li. Signaling and transcriptional regulation in osteoblast commitment and differentiation. *Frontiers in bioscience: a journal and virtual library*, 12:3068, 2007.

[80] Mary B Goldring. Chondrogenesis, chondrocyte differentiation, and articular cartilage metabolism in health and osteoarthritis. *Therapeutic advances in musculoskeletal disease*, page 1759720X12448454, 2012.

[81] Peter Dy, Weihuan Wang, Pallavi Bhattaram, Qiuqing Wang, Lai Wang, R Tracy Ballock, and Véronique Lefebvre. Sox9 directs hypertrophic maturation and blocks osteoblast differentiation of growth plate chondrocytes. *Developmental cell*, 22(3):597–609, 2012.

[82] Nathalie Billon and Christian Dani. Developmental origins of the adipocyte lineage: new insights from genetics and genomics studies. *Stem Cell Reviews and Reports*, 8(1):55–66, 2012.

[83] Evan D Rosen and Ormond A MacDougald. Adipocyte differentiation from the inside out. *Nature reviews Molecular cell biology*, 7(12):885–896, 2006.

[84] Yaacov Barak, Michael C Nelson, Estelita S Ong, Ying Z Jones, Pilar Ruiz-Lozano, Kenneth R Chien, Alan Koder, and Ronald M Evans. Pparγ is required for placental, cardiac, and adipose tissue development. *Molecular cell*, 4(4):585–595, 1999.

[85] Evan D Rosen, Pasha Sarraf, Amy E Troy, Gary Bradwin, Kathryn Moore, David S Milstone, Bruce M Spiegelman, and Richard M Mortensen. Pparγ is required for the differentiation of adipose tissue in vivo and in vitro. *Molecular cell*, 4(4):611–617, 1999.

[86] Min Jae Jeon, Jeong Ah Kim, Sung Hee Kwon, Sang Wan Kim, Kyong Soo Park, Sung-Woo Park, Seong Yeon Kim, and Chan Soo Shin. Activation of peroxisome proliferator-activated receptor-γ inhibits the runx2-mediated transcription of osteocalcin in osteoblasts. *Journal of Biological Chemistry*, 278(26):23270–23277, 2003.

[87] Jeong-Ho Hong, Eun Sook Hwang, Michael T McManus, Adam Amsterdam, Yu Tian, Ralitsa Kalmukova, Elisabetta Mueller, Thomas Benjamin, Bruce M Spiegelman, Phillip A Sharp, et al. Taz, a transcriptional modulator of mesenchymal stem cell differentiation. *Science*, 309(5737):1074–1078, 2005.

[88] Volkher Scharnhorst, Alex J van der Eb, and Aart G Jochemsen. Wt1 proteins: functions in growth and differentiation. *Gene*, 273(2):141–161, 2001.

[89] Jean Paul Thiery. Epithelial–mesenchymal transitions in tumour progression. *Nature Reviews Cancer*, 2(6):442–454, 2002.

[90] Sendurai A Mani, Wenjun Guo, Mai-Jing Liao, Elinor Ng Eaton, Ayyakkannu Ayyanan, Alicia Y Zhou, Mary Brooks, Ferenc Reinhard, Cheng Cheng Zhang, Michail Shipitsin, et al. The epithelial-mesenchymal transition generates cells with properties of stem cells. *Cell*, 133(4):704–715, 2008.

[91] Makiko Takeichi, Keisuke Nimura, Masaki Mori, Hironori Nakagami, and Yasufumi Kaneda. The transcription factors tbx18 and wt1 control the epicardial epithelial-mesenchymal transition through bi-directional regulation of slug in murine primary epicardial cells. *PloS one*, 8(2):e57829, 2013.

[92] L1 Yang, Y Han, F Saurez Saiz, and MD Minden. A tumor suppressor and oncogene: the wt1 story. *Leukemia*, 21(5):868–876, 2007.

[93] Qianghua Hu, Fei Gao, Weihua Tian, E Cristy Ruteshouser, Yaqing Wang, Alexander Lazar, John Stewart, Louise C Strong, Richard R Behringer, and Vicki Huff. Wt1 ablation and igf2 upregulation in mice result in wilms tumors with elevated erk1/2 phosphorylation. *The Journal of clinical investigation*, 121(1): 174, 2011.

[94] Daniel A Haber, Seon Park, Shyamala Maheswaran, Christoph Englert, Gian G Re, Debra J Hazen-Martin, Donald A Sens, and A Julian Garvin. Wt1-mediated growth suppression of wilms tumor cells expressing a wt1 splicing variant. *Science*, 262(5142):2057–2059, 1993.

[95] Christoph Englert, Shyamala Maheswaran, A Julian Garvin, Jordan Kreidberg, and Daniel A Haber. Induction of p21 by the wilms' tumor suppressor gene wt1. *Cancer research*, 57(8):1429–1434, 1997.

[96] Leif W Ellisen, Nadia Carlesso, Tao Cheng, David T Scadden, and Daniel A Haber. The wilms tumor suppressor wt1 directs stage-specific quiescence and differentiation of human hematopoietic progenitor cells. *The EMBO journal*, 20 (8):1897–1909, 2001.

[97] Helena Svedberg, Johan Richter, and Urban Gullberg. Forced expression of the wilms tumor 1 (wt1) gene inhibits proliferation of human hematopoietic cd34 (+) progenitor cells. *Leukemia*, 15(12):1914–1922, 2001.

[98] Yoji Murata, Tetsuhiro Kudoh, Haruo Sugiyama, Kumao Toyoshima, and Tetsu Akiyama. The wilms tumor suppressor gene wt1 induces g1 arrest and apoptosis in myeloblastic leukemia m1 cells. *FEBS letters*, 409(1):41–45, 1997.

[99] Haim Werner, Zila Shen-Orr, FJ Rauscher, Jennifer F Morris, CT Roberts, and Derek LeRoith. Inhibition of cellular proliferation by the wilms' tumor suppressor wt1 is associated with suppression of insulin-like growth factor i receptor gene expression. *Molecular and cellular biology*, 15(7):3516–3522, 1995.

[100] Shirley I Smith, Michelle Down, Andrew W Boyd, and Chung L Li. Expression of the wilms tumor suppressor gene, wt1, reduces the tumorigenicity of the leukemic cell line m1 in cb-17 scid/scid mice. *Cancer research*, 60(4):808–814, 2000.

[101] Teng-Fei Zhang, Shui-Qing Yu, Li-Shuang Guan, and Zhao-Yi Wang. Inhibition of breast cancer cell growth by the wilms' tumor suppressor wt1 is associated with a destabilization of beta-catenin. *Anticancer research*, 23(5A):3575–3584, 2002.

[102] Debra J Morrison, Marianne KH Kim, Windy Berkofsky-Fessler, and Jonathan D Licht. Wt1 induction of mitogen-activated protein kinase phosphatase 3 represents a novel mechanism of growth suppression. *Molecular Cancer Research*, 6(7):1225–1231, 2008.

[103] Aswin L Menke, Avi Shvarts, Nicole Riteco, Reinier CA van Ham, Alex J van der Eb, and Aart G Jochemsen. Wilms' tumor 1-kts isoforms induce p53-independent apoptosis that can be partially rescued by expression of the epidermal growth factor receptor or the insulin receptor. *Cancer research*, 57(7):1353–1363, 1997.

[104] Debra J Morrison, Milton A English, and Jonathan D Licht. Wt1 induces apoptosis through transcriptional regulation of the proapoptotic bcl-2 family member bak. *Cancer research*, 65(18):8174–8182, 2005.

[105] Mary L McMaster, Manfred Gessler, Eric J Stanbridge, and Bernard E Weissman. Wt1 expression alters tumorigenicity of the g401 kidney-derived cell line. *Cell growth & differentiation: the molecular biology journal of the American Association for Cancer Research*, 6(12):1609–1617, 1995.

[106] Lei Wang and Zhao-Yi Wang. The wilms' tumor suppressor wt1 inhibits malignant progression of neoplastigenic mammary epithelial cells. *Anticancer research*, 28(4B):2155–2160, 2008.

[107] H Miwa, M Beran, and GF Saunders. Expression of the wilms' tumor gene (wt1) in human leukemias. *Leukemia*, 6(5):405–409, 1992.

[108] Robert Koesters, Michael Linnebacher, Johannes F Coy, Anja Germann, Yvette Schwitalle, Peter Findeisen, and Magnus von Knebel Doeberitz. Wt1 is a tumor-associated antigen in colon cancer that can be recognized by in vitro stimulated cytotoxic t cells. *International journal of cancer*, 109(3):385–392, 2004.

[109] Yasuo Miyoshi, Akiko Ando, Chiyomi Egawa, Tetsuya Taguchi, Yasuhiro Tamaki, Hiroya Tamaki, Haruo Sugiyama, and Shinzaburo Noguchi. High expression of wilms tumor suppressor gene predicts poor prognosis in breast cancer patients. *Clinical Cancer Research*, 8(5):1167–1171, 2002.

[110] Yusuke Oji, Shinichiro Miyoshi, Hajime Maeda, Seiji Hayashi, Hiroya Tamaki, Shin-Ichi Nakatsuka, Masayuki Yao, Eigo Takahashi, Yoko Nakano, Hirohisa Hirabayashi, et al. Overexpression of the wilms' tumor gene wt1 in de novo lung cancers. *International Journal of Cancer*, 100(3):297–303, 2002.

[111] Saeid Amini Nik, Peter Hohenstein, Ali Jadidizadeh, Kim Van Dam, Adriana Bastidas, Rachel L Berry, Charles E Patek, Bernadette Van der Schueren, Jean-Jacques Cassiman, and Sabine Tejpar. Upregulation of wilms' tumor gene 1 (wt1) in desmoid tumors. *International journal of cancer*, 114(2):202–208, 2005.

[112] Elizabeth Devilard, Franck Bladou, Olivier Ramuz, Gilles Karsenty, Jean-Philippe Dalès, Gwenaëlle Gravis, Catherine Nguyen, François Bertucci, Luc Xerri, and Daniel Birnbaum. Fgfr1 and wt1 are markers of human prostate cancer progression. *BMC cancer*, 6(1):272, 2006.

[113] Yusuke Oji, Tsuyoshi Suzuki, Yoko Nakano, Motohiko Maruno, Shin-ichi Nakatsuka, Tanyarat Jomgeow, Sakie Abeno, Naoya Tatsumi, Asumi Yokota, Sayaka Aoyagi, et al. Overexpression of the wilms' tumor gene wt1 in primary astrocytic tumors. *Cancer science*, 95(10):822–827, 2004.

[114] Bonnie Hylander, Elizabeth Repasky, Protul Shrikant, Marilyn Intengan, Amy Beck, Deborah Driscoll, Pankaj Singhal, Shashikant Lele, and Kunle Odunsi. Expression of wilms tumor gene (wt1) in epithelial ovarian cancer. *Gynecologic oncology*, 101(1):12–17, 2006.

[115] Saketh R Guntupalli, DengFeng Cao, Rupal Shroff, Feng Gao, Christine Menias, L Stewart Massad, Matthew A Powell, David G Mutch, and Premal H Thaker. Wilms tumor 1 protein and estrogen receptor beta expression are associated with poor outcomes in uterine carcinosarcoma. *Annals of surgical oncology*, 20(7): 2373–2379, 2013.

[116] Tsukasa Sotobori, Takafumi Ueda, Yusuke Oji, Norifumi Naka, Nobuhito Araki, Akira Myoui, Haruo Sugiyama, and Hideki Yoshikawa. Prognostic significance of wilms tumor gene (wt1) mrna expression in soft tissue sarcoma. *Cancer*, 106(10): 2233–2240, 2006.

[117] Kazushi Inoue, Haruo Sugiyama, Hiroyasu Ogawa, Masashi Nakagawa, Tamotsu Yamagami, Hiroshi Miwa, K Kita, A Hiraoka, T Masaoka, and K Nasu. Wt1 as a new prognostic factor and a new marker for the detection of minimal residual disease in acute leukemia. *Blood*, 84(9):3071–3079, 1994.

[118] Vicki Huff. Wilms' tumours: about tumour suppressor genes, an oncogene and a chameleon gene. *Nature Reviews Cancer*, 11(2):111–121, 2011.

[119] Raajit Rampal, Altuna Alkalin, Jozef Madzo, Aparna Vasanthakumar, Elodie Pronier, Jay Patel, Yushan Li, Jihae Ahn, Omar Abdel-Wahab, Alan Shih, et al. Dna hydroxymethylation profiling reveals that wt1 mutations result in loss of tet2 function in acute myeloid leukemia. *Cell reports*, 9(5):1841–1855, 2014.

[120] Yiping Wang, Mengtao Xiao, Xiufei Chen, Leilei Chen, Yanping Xu, Lei Lv, Pu Wang, Hui Yang, Shenghong Ma, Huaipeng Lin, et al. Wt1 recruits tet2 to regulate its target gene expression and suppress leukemia cell proliferation. *Molecular cell*, 57(4):662–673, 2015.

[121] Stefan Mundlos, Jerry Pelletier, André Darveau, Michael Bachmann, Andreas Winterpacht, and Bernhard Zabel. Nuclear localization of the protein encoded by the wilms' tumor gene wt1 in embryonic and adult tissues. *Development*, 119 (4):1329–1341, 1993.

[122] Shin-ichi Nakatsuka, Yusuke Oji, Tetsuya Horiuchi, Takayoshi Kanda, Michio Kitagawa, Tamotsu Takeuchi, Kiyoshi Kawano, Yuko Kuwae, Akira Yamauchi, Meinoshin Okumura, et al. Immunohistochemical detection of wt1 protein in a variety of cancer cells. *Modern pathology*, 19(6):804–814, 2006.

[123] Jörg Hartkamp, Brian Carpenter, and Stefan GE Roberts. The wilms' tumor suppressor protein wt1 is processed by the serine protease htra2/omi. *Molecular cell*, 37(2):159–171, 2010.

[124] Silvestre Vicent, Ron Chen, Leanne C Sayles, Chenwei Lin, Randal G Walker, Anna K Gillespie, Aravind Subramanian, Gregory Hinkle, Xiaoping Yang, Sakina Saif, et al. Wilms tumor 1 (wt1) regulates kras-driven oncogenesis and senescence in mouse and human models. *The Journal of clinical investigation*, 120(11):3940, 2010.

[125] EM Algar, T Khromykh, SI Smith, DM Blackburn, GJ Bryson, and PJ Smith. A wt1 antisense oligonucleotide inhibits proliferation and induces apoptosis in myeloid leukaemia cell lines. *Oncogene*, 12(5):1005–1014, 1996.

[126] Rosalba Parenti, Venera Cardile, Adriana Carol Eleonora Graziano, Carmela Parenti, Assunta Venuti, Maria Paola Bertuccio, Debora Lo Furno, and Gaetano Magro. Wilms tumor gene 1 (wt1) silencing inhibits proliferation of malignant peripheral nerve sheath tumor snf96. 2 cell line. *PloS one*, 9(12):e114333, 2014.

[127] Diana E Zamora-Avila, Moises A Franco-Molina, Laura M Trejo-Avila, Cristina Rodríguez-Padilla, Diana Resendez-Perez, and Pablo Zapata-Benavides. Rnai silencing of the wt1 gene inhibits cell proliferation and induces apoptosis in the b16f10 murine melanoma cell line. *Melanoma research*, 17(6):341–348, 2007.

[128] Kay-Dietrich Wagner, Nicole Wagner, Sven Wellmann, Gunnar Schley, Anja Bondke, Heinz Theres, and Holger Scholz. Oxygen-regulated expression of the wilms tumor suppressor wt1 involves hypoxia-inducible factor-1 (hif-1). *The FASEB journal*, 17(10):1364–1366, 2003.

[129] N Wagner, JF Michiels, A Schedl, and KD Wagner. The wilms' tumour suppressor wt1 is involved in endothelial cell proliferation and migration: expression in tumour vessels in vivo. *Oncogene*, 27(26):3662–3672, 2008.

[130] Varalakshmi Katuri, Stephanie Gerber, Xiaofei Qiu, Gregory McCarty, Seth D Goldstein, Hans Hammers, Elizabeth Montgomery, Allen R Chen, and David M Loeb. Wt1 regulates angiogenesis in ewing sarcoma. *Oncotarget*, 5(9):2436, 2014.

[131] K Ito, Y Oji, N Tatsumi, S Shimizu, Y Kanai, T Nakazawa, M Asada, T Jomgeow, S Aoyagi, Y Nakano, et al. Antiapoptotic function of 17aa (+) wt1 (wilms' tumor gene) isoforms on the intrinsic apoptosis pathway. *Oncogene*, 25(30):4217–4229, 2006.

[132] Jane Renshaw, Rosanne M Orr, Michael I Walton, Robert te Poele, Richard D Williams, Edward V Wancewicz, Brett P Monia, Paul Workman, and Kathryn Pritchard-Jones. Disruption of wt1 gene expression and exon 5 splicing following cytotoxic drug treatment: antisense down-regulation of exon 5 alters target gene expression and inhibits cell survival. *Molecular cancer therapeutics*, 3(11):1467–1484, 2004.

[133] Weiying Gu, Shaoyan Hu, Zixing Chen, Guoqiang Qiu, Jiannong Cen, Bai He, Jun He, and Wei Wu. High expression of wt1 gene in acute myeloid leukemias with more predominant wt1+ 17aa isoforms at relapse. *Leukemia research*, 34(1): 46–49, 2010.

[134] Naoya Tatsumi, Yusuke Oji, Naoko Tsuji, Asako Tsuda, Mari Higashio, Sayaka Aoyagi, Ikuyo Fukuda, Ken Ito, Junya Nakamura, Satoshi Takashima, et al. Wilms' tumor gene wt1-shrna as a potent apoptosis-inducing agent for solid tumors. *International journal of oncology*, 32(3):701–711, 2008.

[135] Marty W Mayo, Cun-Yu Wang, S Scott Drouin, Lee V Madrid, Allen F Marshall, John C Reed, Bernard E Weissman, and Albert S Baldwin. Wt1 modulates apoptosis by transcriptionally upregulating the bcl-2 proto-oncogene. *The EMBO journal*, 18(14):3990–4003, 1999.

[136] Irene Luna, Esperanza Such, Jose Cervera, Eva Barragán, Mariam Ibañez, Inés Gómez-Seguí, María López-Pavía, Marta Llop, Oscar Fuster, Sandra Dolz, et al. Wt1 isoform expression pattern in acute myeloid leukemia. *Leukemia research*, 37(12):1744–1749, 2013.

[137] Xi Wang, Ping Gao, Fang Lin, Min Long, Yuanyuan Weng, Yongri Ouyang, Li Liu, Junxia Wei, Xi Chen, Ting He, et al. Wilms tumour suppressor gene 1 (wt1) is involved in the carcinogenesis of lung cancer through interaction with pi3k/akt pathway. *Cancer Cell Int*, 13(1):114, 2013.

[138] Caitlin M Braitsch, Onur Kanisicak, Jop H van Berlo, Jeffery D Molkentin, and Katherine E Yutzey. Differential expression of embryonic epicardial progenitor markers and localization of cardiac fibrosis in adult ischemic injury and hypertensive heart disease. *Journal of molecular and cellular cardiology*, 65:108–119, 2013.

[139] Bin Huang, Lei Pi, Cha Chen, Fei Yuan, Qingsong Zhou, Junqi Teng, and Tang Jiang. Wt1 and pax2 re-expression is required for epithelial-mesenchymal transition in 5/6 nephrectomized rats and cultured kidney tubular epithelial cells. *Cells Tissues Organs*, 195(4):296–312, 2012.

[140] Ingmar Mederacke, Christine C Hsu, Juliane S Troeger, Peter Huebener, Xueru Mu, Dianne H Dapito, Jean-Philippe Pradere, and Robert F Schwabe. Fate tracing reveals hepatic stellate cells as dominant contributors to liver fibrosis independent of its aetiology. *Nature communications*, 4, 2013.

[141] Hacer Sahin and Hermann E Wasmuth. Chemokines in tissue fibrosis. *Biochimica et Biophysica Acta (BBA)-Molecular Basis of Disease*, 1832(7):1041–1048, 2013.

[142] TA Wynn. Cellular and molecular mechanisms of fibrosis. *The Journal of pathology*, 214(2):199–210, 2008.

[143] Steven Eugene Mutsaers, Kimberly Birnie, Sally Lansley, Sarah E Herrick, C Lim, and Cecilia M Prêle. Mesothelial cells in tissue repair and fibrosis. *Name: Frontiers in Pharmacology*, 6:113, 2015.

[144] Masayuki Iwano, David Plieth, Theodore M Danoff, Chengsen Xue, Hirokazu Okada, Eric G Neilson, et al. Evidence that fibroblasts derive from epithelium during tissue fibrosis. *The Journal of clinical investigation*, 110(110 (3)):341–350, 2002.

[145] Youhua Liu. New insights into epithelial-mesenchymal transition in kidney fibrosis. *Journal of the American Society of Nephrology*, 21(2):212–222, 2010.

[146] Benjamin D Humphreys, Shuei-Liong Lin, Akio Kobayashi, Thomas E Hudson, Brian T Nowlin, Joseph V Bonventre, M Todd Valerius, Andrew P McMahon, and Jeremy S Duffield. Fate tracing reveals the pericyte and not epithelial origin of myofibroblasts in kidney fibrosis. *The American journal of pathology*, 176(1): 85–97, 2010.

[147] Moin A Saleem, Jiri Zavadil, Maryse Bailly, Karen McGee, Ian R Witherden, Hermann Pavenstadt, Hsianghao Hsu, Julia Sanday, Simon C Satchell, Rachel Lennon, et al. The molecular and functional phenotype of glomerular podocytes reveals key features of contractile smooth muscle cells. *American Journal of Physiology-Renal Physiology*, 295(4):F959–F970, 2008.

[148] Michael Zeisberg, Changqing Yang, Margot Martino, Michael B Duncan, Florian Rieder, Harikrishna Tanjore, and Raghu Kalluri. Fibroblasts derive from hepatocytes in liver fibrosis via epithelial to mesenchymal transition. *Journal of Biological Chemistry*, 282(32):23337–23347, 2007.

[149] Kevin K Kim, Matthias C Kugler, Paul J Wolters, Liliane Robillard, Michael G Galvez, Alexis N Brumwell, Dean Sheppard, and Harold A Chapman. Alveolar epithelial cell mesenchymal transition develops in vivo during pulmonary fibrosis and is regulated by the extracellular matrix. *Proceedings of the National Academy of Sciences*, 103(35):13180–13185, 2006.

[150] Brigham C Willis, Roland M duBois, and Zea Borok. Epithelial origin of myofibroblasts during fibrosis in the lung. *Proceedings of the American Thoracic Society*, 3(4):377–382, 2006.

[151] Elisabeth M Zeisberg, Scott E Potenta, Hikaru Sugimoto, Michael Zeisberg, and Raghu Kalluri. Fibroblasts in kidney fibrosis emerge via endothelial-to-mesenchymal transition. *Journal of the American Society of Nephrology*, 19(12): 2282–2287, 2008.

[152] Yuchang Li, Jiaohong Wang, and Kinji Asahina. Mesothelial cells give rise to hepatic stellate cells and myofibroblasts via mesothelial–mesenchymal transition in liver injury. *Proceedings of the National Academy of Sciences*, 110(6):2324–2329, 2013.

[153] Jason S Zolak, Rajesh Jagirdar, Ranu Surolia, Suman Karki, Octavio Oliva, Thomas Hock, Purushotham Guroji, Qiang Ding, Riu-Ming Liu, Subhashini Bolisetty, et al. Pleural mesothelial cell differentiation and invasion in fibrogenic lung injury. *The American journal of pathology*, 182(4):1239–1247, 2013.

[154] Suman Karki, Ranu Surolia, Thomas David Hock, Purusotham Guroji, Jason S Zolak, Ryan Duggal, Tong Ye, Victor J Thannickal, and Veena B Antony. Wilms' tumor 1 (wt1) regulates pleural mesothelial cell plasticity and transition into myofibroblasts in idiopathic pulmonary fibrosis. *The FASEB Journal*, 28(3):1122–1131, 2014.

[155] Laurent Gautier, Leslie Cope, Benjamin M Bolstad, and Rafael A Irizarry. affy-analysis of affymetrix genechip data at the probe level. *Bioinformatics*, 20(3): 307–315, 2004.

[156] Matthew E Ritchie, Belinda Phipson, Di Wu, Yifang Hu, Charity W Law, Wei Shi, and Gordon K Smyth. limma powers differential expression analyses for rna-sequencing and microarray studies. *Nucleic acids research*, page gkv007, 2015.

[157] Cole Trapnell, Adam Roberts, Loyal Goff, Geo Pertea, Daehwan Kim, David R Kelley, Harold Pimentel, Steven L Salzberg, John L Rinn, and Lior Pachter. Differential gene and transcript expression analysis of rna-seq experiments with tophat and cufflinks. *Nature protocols*, 7(3):562–578, 2012.

[158] Kurtis Eisermann, Sunpreet Tandon, Anton Bazarov, Adina Brett, Gail Fraizer, and Helen Piontkivska. Evolutionary conservation of zinc finger transcription factor binding sites in promoters of genes co-expressed with wt1 in prostate cancer. *BMC genomics*, 9(1):337, 2008.

[159] Larissa Ivanova, Michael J Butt, and Douglas G Matsell. Mesenchymal transition in kidney collecting duct epithelial cells. *American Journal of Physiology-Renal Physiology*, 294(5):F1238–F1248, 2008.

[160] Philip A Gregory, Andrew G Bert, Emily L Paterson, Simon C Barry, Anna Tsykin, Gelareh Farshid, Mathew A Vadas, Yeesim Khew-Goodall, and Gregory J Goodall. The mir-200 family and mir-205 regulate epithelial to mesenchymal transition by targeting zeb1 and sip1. *Nature cell biology*, 10(5):593–601, 2008.

[161] Robert D Fagerlund, Poh Ling Ooi, and Sigurd M Wilbanks. Soluble expression and purification of tumor suppressor wt1 and its zinc finger domain. *Protein expression and purification*, 85(2):165–172, 2012.

[162] Chen Cm, J Krohn, S Bhattacharya, and B Davies. A comparison of exogenous promoter activity at the rosa26 locus using a phic31 integrase mediated cassette exchange approach in mouse es cells. *PloS one*, 6(8):e23376, 2011.

[163] Daniela Meilinger, Karin Fellinger, Sebastian Bultmann, Ulrich Rothbauer, Ian Marc Bonapace, Wolfgang EF Klinkert, Fabio Spada, and Heinrich Leonhardt. Np95 interacts with de novo dna methyltransferases, dnmt3a and dnmt3b, and mediates epigenetic silencing of the viral cmv promoter in embryonic stem cells. *EMBO reports*, 10(11):1259–1264, 2009.

[164] Arun Venkatesan and Asim Dasgupta. Novel fluorescence-based screen to identify small synthetic internal ribosome entry site elements. *Molecular and cellular biology*, 21(8):2826–2837, 2001.

[165] Jin Hee Kim, Sang-Rok Lee, Li-Hua Li, Hye-Jeong Park, Jeong-Hoh Park, Kwang Youl Lee, Myeong-Kyu Kim, Boo Ahn Shin, and Seok-Yong Choi. High

cleavage efficiency of a 2a peptide derived from porcine teschovirus-1 in human cell lines, zebrafish and mice. 2011.

[166] Pablo Perez-Pinera, David G Ousterout, Matthew T Brown, and Charles A Gersbach. Gene targeting to the rosa26 locus directed by engineered zinc finger nucleases. *Nucleic acids research*, page gkr1214, 2011.

[167] Thomas GM Schmidt, Lilia Batz, Lidia Bonet, Uwe Carl, Gerd Holzapfel, Klaus Kiem, Kamila Matulewicz, Dennis Niermeier, Isabel Schuchardt, and Kristian Stanar. Development of the twin-strep-tag® and its application for purification of recombinant proteins from cell culture supernatants. *Protein expression and purification*, 92(1):54–61, 2013.

[168] Tim Grotjohann, Ilaria Testa, Marcel Leutenegger, Hannes Bock, Nicolai T Urban, Flavie Lavoie-Cardinal, Katrin I Willig, Christian Eggeling, Stefan Jakobs, and Stefan W Hell. Diffraction-unlimited all-optical imaging and writing with a photochromic gfp. *Nature*, 478(7368):204–208, 2011.

[169] Pita Enriquez-Harris, Nicola Levitt, Diana Briggs, and Nick J Proudfoot. A pause site for rna polymerase ii is associated with termination of transcription. *The EMBO journal*, 10(7):1833, 1991.

[170] Sari Tojkander, Gergana Gateva, and Pekka Lappalainen. Actin stress fibers–assembly, dynamics and biological roles. *Journal of cell science*, 125(8):1855–1864, 2012.

[171] Eran Eden, Roy Navon, Israel Steinfeld, Doron Lipson, and Zohar Yakhini. Gorilla: a tool for discovery and visualization of enriched go terms in ranked gene lists. *BMC bioinformatics*, 10(1):48, 2009.

[172] Mette M Rosenkilde and Thue W Schwartz. The chemokine system–a major regulator of angiogenesis in health and disease. *Apmis*, 112(7-8):481–495, 2004.

[173] Albert Zlotnik and Osamu Yoshie. Chemokines: a new classification system and their role in immunity. *Immunity*, 12(2):121–127, 2000.

[174] Juan Carlos Acosta, Ana Banito, Torsten Wuestefeld, Athena Georgilis, Peggy Janich, Jennifer P Morton, Dimitris Athineos, Tae-Won Kang, Felix Lasitschka, Mindaugas Andrulis, et al. A complex secretory program orchestrated by the inflammasome controls paracrine senescence. *Nature cell biology*, 15(8):978–990, 2013.

[175] Victor Velecela, Laura A Lettice, You-Ying Chau, Joan Slight, Rachel L Berry, Anna Thornburn, Quinn D Gunst, Maurice van den Hoff, Manuel Reina, Fernando O Martínez, et al. Wt1 regulates the expression of inhibitory chemokines during heart development. *Human molecular genetics*, 22(25):5083–5095, 2013.

[176] Valérie Gouon-Evans, Elaine Y Lin, and Jeffrey W Pollard. Requirement of macrophages and eosinophils and their cytokines/chemokines for mammary gland development. *Breast Cancer Research*, 4(4):155, 2002.

[177] Maria Doitsidou, Michal Reichman-Fried, Juürg Stebler, Marion Köprunner, Julia Dörries, Dirk Meyer, Camila V Esguerra, TinChung Leung, and Erez Raz. Guidance of primordial germ cell migration by the chemokine sdf-1. *Cell*, 111(5): 647–659, 2002.

[178] Sreelaja Nair and Thomas F Schilling. Chemokine signaling controls endodermal migration during zebrafish gastrulation. *Science*, 322(5898):89–92, 2008.

[179] Abdelhak Belmadani, Phuong B Tran, Dongjun Ren, Stavroula Assimacopoulos, Elizabeth A Grove, and Richard J Miller. The chemokine stromal cell-derived factor-1 regulates the migration of sensory neuron progenitors. *The Journal of neuroscience*, 25(16):3995–4003, 2005.

[180] Christine A Griffin, Luciano H Apponi, Kimberly K Long, and Grace K Pavlath. Chemokine expression and control of muscle cell migration during myogenesis. *Journal of cell science*, 123(18):3052–3060, 2010.

[181] Juliana Croitoru-Lamoury, Francois MJ Lamoury, John J Zaunders, Laura A Veas, and Bruce J Brew. Human mesenchymal stem cells constitutively express

chemokines and chemokine receptors that can be upregulated by cytokines, ifn-β, and copaxone. *Journal of Interferon & Cytokine Research*, 27(1):53–64, 2007.

[182] Wei-Yu Lee, Chun-Jen Wang, Ting-Yu Lin, Chih-Lun Hsiao, and Ching-Wei Luo. Cxcl17, an orphan chemokine, acts as a novel angiogenic and anti-inflammatory factor. *American Journal of Physiology-Endocrinology and Metabolism*, 304(1): E32–E40, 2013.

[183] Xingru Li, Sofia Ottosson, Sihan Wang, Emma Jernberg, Linda Boldrup, Xiaolian Gu, Karin Nylander, and Aihong Li. Wilms tumor gene 1 regulates p63 and promotes cell proliferation in squamous cell carcinoma of the head and neck. *BMC cancer*, 15(1):342, 2015.

[184] Xiaoyan Li, Yan Li, Tian Yuan, Qing Zhang, Yujiao Jia, Qihui Li, Lei Huai, Pei Yu, Zheng Tian, Kejing Tang, et al. Exogenous expression of wt1 gene influences u937 cell biological behaviors and activates mapk and jak-stat signaling pathways. *Leukemia research*, 38(8):931–939, 2014.

[185] Hiroaki Asai, Hiroshi Fujiwara, Jun An, Toshiki Ochi, Yukihiro Miyazaki, Kozo Nagai, Sachiko Okamoto, Junichi Mineno, Kiyotaka Kuzushima, Hiroshi Shiku, et al. Co-introduced functional ccr2 potentiates in vivo anti-lung cancer functionality mediated by t cells double gene-modified to express wt1-specific t-cell receptor. *PloS one*, 8(2):e56820, 2013.

[186] Youqi Han, Serban San-Marina, Jian Liu, and Mark D Minden. Transcriptional activation of c-myc proto-oncogene by wt1 protein. *Oncogene*, 23(41):6933–6941, 2004.

[187] Chen Wu, Sihan Wang, Caihua Xu, Andreas Tyler, Xingru Li, Charlotta Andersson, Yusuke Oji, Haruo Sugiyama, Yijiang Chen, and Aihong Li. Wt1 enhances proliferation and impedes apoptosis in kras mutant nsclc via targeting cmyc. *Cellular Physiology and Biochemistry*, 35(2):647–662, 2015.

[188] Stephen M Hewitt, Shinshichi Hamada, Timothy J McDonnell, Frank J Rauscher, and Grady F Saunders. Regulation of the proto-oncogenes bcl-2 and c-myc by the wilms' tumor suppressor gene wt1. *Cancer research*, 55(22):5386–5389, 1995.

[189] Tetsuhiro Kudoh, Takao Ishidate, Masatsugu Moriyama, Kumao Toyoshima, and Tetsu Akiyama. G1 phase arrest induced by wilms tumor protein wt1 is abrogated by cyclin/cdk complexes. *Proceedings of the National Academy of Sciences*, 92 (10):4517–4521, 1995.

[190] Michael C Heymann, Sabrina Rabe, Susanne Ruß, Franz Kapplusch, Felix Schulze, Robert Stein, Stefan Winkler, Christian M Hedrich, Angela Rösen-Wolff, and Sigrun R Hofmann. Fluorescent tags influence the enzymatic activity and subcellular localization of procaspase-1. *Clinical Immunology*, 2015.

[191] Chen Wu, Weiyou Zhu, Jing Qian, Shaohua He, Changping Wu, Yijiang Chen, and Yongqian Shu. Wt1 promotes invasion of nsclc via suppression of cdh1. *Journal of Thoracic Oncology*, 8(9):1163–1169, 2013.

[192] Adina Brett, Sony Pandey, and Gail Fraizer. The wilms tumor gene (wt1) regulates e-cadherin expression and migration of prostate cancer cells. *Mol Cancer*, 12(3), 2013.

[193] Maria V Barbolina, Brian P Adley, Lonnie D Shea, and M Sharon Stack. Wilms tumor gene protein 1 is associated with ovarian cancer metastasis and modulates cell invasion. *Cancer*, 112(7):1632–1641, 2008.

[194] Tanyarat Jomgeow, Yusuke Oji, Naoko Tsuji, Yoko Ikeda, Ken Ito, Asako Tsuda, Tsutomu Nakazawa, Naoya Tatsumi, Nao Sakaguchi, Satoshi Takashima, et al. Wilms tumor gene wt1 17aa (–)/kts (–) isoform induces morphological changes and promotes cell migration and invasion in vitro. *Cancer science*, 97(4):259–270, 2006.

[195] Romelda L Omeir, Belete Teferedegne, Gideon S Foseh, Joel J Beren, Philip J Snoy, Lauren R Brinster, James L Cook, Keith Peden, and Andrew M Lewis Jr.

Heterogeneity of the tumorigenic phenotype expressed by madin–darby canine kidney cells. *Comparative medicine*, 61(3):243, 2011.

[196] Mariana Hiromi Massaoka, Alisson Leonardo Matsuo, Felipe Valença Pereira, Carlos Rogerio Figueiredo, Jorge Augusto Scutti, Natália Girola, and Luiz Rodolpho Travassos. A novel wt1-derived peptide induces cellular senescence and inhibits tumor growth in a human melanoma cell line and xenograft model. *Cancer Research*, 72(8 Supplement):2867–2867, 2012.

[197] Dolly J Holt and David W Grainger. Multinucleated giant cells from fibroblast cultures. *Biomaterials*, 32(16):3977–3987, 2011.

[198] Thomas Kuilman and Daniel S Peeper. Senescence-messaging secretome: Sms-ing cellular stress. *Nature Reviews Cancer*, 9(2):81–94, 2009.

[199] Joseph Severino, RG Allen, Samuel Balin, Arthur Balin, and Vincent J Cristofalo. Is β-galactosidase staining a marker of senescence in vitro and in vivo? *Experimental cell research*, 257(1):162–171, 2000.

[200] Francis Rodier and Judith Campisi. Four faces of cellular senescence. *The Journal of cell biology*, 192(4):547–556, 2011.

[201] Linda J Kuo and Li-Xi Yang. γ-h2ax-a novel biomarker for dna double-strand breaks. *In Vivo*, 22(3):305–309, 2008.

[202] Sari Tojkander, Gergana Gateva, and Pekka Lappalainen. Actin stress fibers–assembly, dynamics and biological roles. *Journal of cell science*, 125(8):1855–1864, 2012.

[203] Stéphanie Pellegrin and Harry Mellor. Actin stress fibres. *Journal of cell science*, 120(20):3491–3499, 2007.

[204] Oliver Thompson, Jeelan S Moghraby, Kathryn R Ayscough, and Steve J Winder. Depletion of the actin bundling protein sm22/transgelin increases actin dynamics and enhances the tumourigenic phenotypes of cells. *BMC cell biology*, 13(1):1, 2012.

[205] Patrick Dumont, Maggi Burton, Qin M Chen, Efstathios S Gonos, Christophe Frippiat, Jean-Baptiste Mazarati, François Eliaers, José Remacle, and Olivier Toussaint. Induction of replicative senescence biomarkers by sublethal oxidative stresses in normal human fibroblast. *Free Radical Biology and Medicine*, 28(3): 361–373, 2000.

[206] Christian Frantz, Kathleen M Stewart, and Valerie M Weaver. The extracellular matrix at a glance. *Journal of cell science*, 123(24):4195–4200, 2010.

[207] Matthew Giannandrea and William C Parks. Diverse functions of matrix metalloproteinases during fibrosis. *Disease models & mechanisms*, 7(2):193–203, 2014.

[208] Anne M Manicone and John K McGuire. Matrix metalloproteinases as modulators of inflammation. In *Seminars in cell & developmental biology*, volume 19, pages 34–41. Elsevier, 2008.

[209] Yusuke Oji, Hirofumi Yamamoto, Masaya Nomura, Yoko Nakano, Ai Ikeba, Shinichi Nakatsuka, Sakie Abeno, Eiji Kiyotoh, Tanyarat Jomgeow, Mitsugu Sekimoto, et al. Overexpression of the wilms' tumor gene wt1 in colorectal adenocarcinoma. *Cancer science*, 94(8):712–717, 2003.

[210] C Rosenfeld, MA Cheever, and A Gaiger. Wt1 in acute leukemia, chronic myelogenous leukemia and myelodysplastic syndrome: therapeutic potential of wt1 targeted therapies. *Leukemia*, 17(7):1301–1312, 2003.

[211] Chen Wu, Sihan Wang, Caihua Xu, Andreas Tyler, Xingru Li, Charlotta Andersson, Yusuke Oji, Haruo Sugiyama, Yijiang Chen, and Aihong Li. Wt1 enhances proliferation and impedes apoptosis in kras mutant nsclc via targeting cmyc. *Cellular Physiology and Biochemistry*, 35(2):647–662, 2015.

[212] Christoph Englert, XIANYU Hou, SHYAMALA Maheswaran, P Bennett, CHIDI Ngwu, GG Re, AJ Garvin, MR Rosner, and DA Haber. Wt1 suppresses synthesis of the epidermal growth factor receptor and induces apoptosis. *The EMBO Journal*, 14(19):4662, 1995.

[213] Xiao-wei Qi, Fan Zhang, Hong Wu, Jun-lan Liu, Bei-ge Zong, Chuan Xu, and Jun Jiang. Wilms' tumor 1 (wt1) expression and prognosis in solid cancer patients: a systematic review and meta-analysis. *Scientific reports*, 5, 2015.

[214] Jason B Brayer and Javier Pinilla-Ibarz. Developing strategies in the immunotherapy of leukemias. *Cancer Control*, 20(1):49–59, 2013.

[215] Lu Huang and Christopher M Counter. Reduced hras g12v-driven tumorigenesis of cell lines expressing kras c118s. 2015.

[216] Ingrid W Caras, Michael A Davitz, Lucy Rhee, Greg Weddell, David W Martin, and Victor Nussenzweig. Cloning of decay-accelerating factor suggests novel use of splicing to generate two proteins. 1987.

[217] M Andrea Markus, Bettina Heinrich, Oleg Raitskin, David J Adams, Helena Mangs, Christine Goy, Michael Ladomery, Ruth Sperling, Stefan Stamm, and Brian J Morris. Wt1 interacts with the splicing protein rbm4 and regulates its ability to modulate alternative splicing in vivo. *Experimental cell research*, 312 (17):3379–3388, 2006.

[218] Seiyu Hosono, Xiangnong Luo, Deborah P Hyink, Lynn M Schnapp, Patricia D Wilson, Christopher R Burrow, Josina C Reddy, George F Atweh, and Jonathan D Licht. Wt1 expression induces features of renal epithelial differentiation in mesenchymal fibroblasts. *Oncogene*, 18(2):417–427, 1999.

[219] Su-Ren Chen, Min Chen, Xiao-Na Wang, Jun Zhang, Qing Wen, Shao-Yang Ji, Qiao-Song Zheng, Fei Gao, and Yi-Xun Liu. The wilms tumor gene, wt1, maintains testicular cord integrity by regulating the expression of col4a1 and col4a2. *Biology of reproduction*, 88(3):56, 2013.

[220] Karin M Kirschner, Nicole Wagner, Kay-Dietrich Wagner, Sven Wellmann, and Holger Scholz. The wilms tumor suppressor wt1 promotes cell adhesion through transcriptional activation of the α4integrin gene. *Journal of Biological Chemistry*, 281(42):31930–31939, 2006.

[221] Jane Sottile and Jennifer Chandler. Fibronectin matrix turnover occurs through a caveolin-1–dependent process. *Molecular biology of the cell*, 16(2):757–768, 2005.

[222] Marianne K-H Kim, Thomas J McGarry, Pilib Ó Broin, Jared M Flatow, Aaron A-J Golden, and Jonathan D Licht. An integrated genome screen identifies the wnt signaling pathway as a major target of wt1. *Proceedings of the National Academy of Sciences*, 106(27):11154–11159, 2009.

[223] Daniela Cilloni, Enrico Bracco, Ilaria Defilippi, Francesca Messa, Sonia Carturan, Daniela Di Giovanni, Francesca Arruga, Valentina Rosso, Renata Catalano, Emanuela Messa, et al. Absence of spred1, a negative regulator of ras/mapk pathway, as a mechanism responsible for the constitutive activation of rtk mediated signalling in acute leukemias. In *ASH Annual Meeting Abstracts*, volume 106, page 2287, 2005.

[224] Debra J Birn-Morrison, Jacqueline M Mason, Milton A English, Windy Berkofsky-Fessler, and Jonathan D Licht. The wilms tumor suppressor protein1 activates anti-proliferative and apoptotic pathways resulting in growth arrest and apoptosis in a cellular system. *Cancer Research*, 64(7 Supplement):410–411, 2004.

[225] Rive Sarfstein and Haim Werner. The wt1 wilms' tumor suppressor gene is a downstream target for insulin-like growth factor-i (igf-i) action in pc12 cells. *Journal of neurochemistry*, 99(3):818–826, 2006.

[226] Musaffe Tuna, Arturo Chavez-Reyes, and Ana M Tari. Her2/neu increases the expression of wilms' tumor 1 (wt1) protein to stimulate s-phase proliferation and inhibit apoptosis in breast cancer cells. *Oncogene*, 24(9):1648–1652, 2005.

[227] Emelie Svensson, Karina Vidovic, Carin Lassen, Johan Richter, Tor Olofsson, Thoas Fioretos, and Urban Gullberg. Deregulation of the wilms' tumour gene 1 protein (wt1) by bcr/abl1 mediates resistance to imatinib in human leukaemia cells. *Leukemia*, 21(12):2485–2494, 2007.

[228] Yusuke Tanaka, Fumiko Sekiguchi, Hao Hong, and Atsufumi Kawabata. Par2 triggers il-8 release via mek/erk and pi3-kinase/akt pathways in gi epithelial cells. *Biochemical and biophysical research communications*, 377(2):622–626, 2008.

[229] Xin-Jian Li, Li-Xia Peng, Jian-Yong Shao, Wen-Hua Lu, Jia-Xing Zhang, Shi Chen, Zhi-Yuan Chen, Yan-Qun Xiang, Ying-Na Bao, Fang-Jing Zheng, et al. As an independent unfavorable prognostic factor, il-8 promotes metastasis of nasopharyngeal carcinoma through induction of epithelial-mesenchymal transition and activation of akt signaling. *Carcinogenesis*, page bgs181, 2012.

[230] Philippe E Van den Steen, Anja Wuyts, Steven J Husson, Paul Proost, JO Van Damme, and Ghislain Opdenakker. Gelatinase b/mmp-9 and neutrophil collagenase/mmp-8 process the chemokines human gcp-2/cxcl6, ena-78/cxcl5 and mouse gcp-2/lix and modulate their physiological activities. *European Journal of Biochemistry*, 270(18):3739–3749, 2003.

[231] SF Gabby Krens, Herman P Spaink, and B Ewa Snaar-Jagalska. Functions of the mapk family in vertebrate-development. *FEBS letters*, 580(21):4984–4990, 2006.

[232] Alexander Aulehla and Olivier Pourquié. Signaling gradients during paraxial mesoderm development. *Cold Spring Harbor perspectives in biology*, 2(2):a000869, 2010.

[233] Lionel Larue and Alfonso Bellacosa. Epithelial–mesenchymal transition in development and cancer: role of phosphatidylinositol 3 kinase/akt pathways. *Oncogene*, 24(50):7443–7454, 2005.

[234] Lindsey N Kent, Shigeki Ohboshi, and Michael J Soares. Akt1 and insulin-like growth factor 2 (igf2) regulate placentation and fetal/postnatal development. *The International journal of developmental biology*, 56(4):255, 2012.

[235] Liliana Soroceanu, Samir Kharbanda, Ruihuan Chen, Robert H Soriano, Ken Aldape, Anjan Misra, Jiping Zha, William F Forrest, Janice M Nigro, Zora Modrusan, et al. Identification of igf2 signaling through phosphoinositide-3-kinase

regulatory subunit 3 as a growth-promoting axis in glioblastoma. *Proceedings of the National Academy of Sciences*, 104(9):3466–3471, 2007.

[236] Olivier G Morali, Alice Jouneau, K John McLaughlin, Jean Paul Thiery, and Lionel Larue. Igf-ii promotes mesoderm formation. *Developmental biology*, 227 (1):133–145, 2000.

[237] Masayuki Haruta, Yasuhito Arai, Waka Sugawara, Naoki Watanabe, Shohei Honda, Junjiro Ohshima, Hidenobu Soejima, Hisaya Nakadate, Hajime Okita, Jun-ichi Hata, et al. Duplication of paternal igf2 or loss of maternal igf2 imprinting occurs in half of wilms tumors with various structural wt1 abnormalities. *Genes, Chromosomes and Cancer*, 47(8):712–727, 2008.

[238] Kim E Nichols, Gian G Re, Yu Xin Yan, A Julian Garvin, and Daniel A Haber. Wt1 induces expression of insulin-like growth factor 2 in wilms' tumor cells. *Cancer research*, 55(20):4540–4543, 1995.

[239] IA Drummond, Stephen L Madden, Patricia Rohwer-Nutter, Graeme I Bell, Vikas P Sukhatme, and FJ d Rauscher. Repression of the insulin-like growth factor ii gene by the wilms tumor suppressor wt1. *Science*, 257(5070):674–678, 1992.

[240] Mutsumi Kanamori-Katayama, Ai Kaiho, Yuri Ishizu, Yuko Okamura-Oho, Okio Hino, Masaaki Abe, Takumi Kishimoto, Hisahiko Sekihara, Yukio Nakamura, Harukazu Suzuki, et al. Lrrn4 and upk3b are markers of primary mesothelial cells. *PloS one*, 6(10):e25391, 2011.

[241] RL Attanoos, R Webb, SD Dojcinov, and AR Gibbs. Value of mesothelial and epithelial antibodies in distinguishing diffuse peritoneal mesothelioma in females from serous papillary carcinoma of the ovary and peritoneum. *Histopathology*, 40 (3):237–244, 2002.

[242] Robert T Pu, Yijun Pang, and Claire W Michael. Utility of wt-1, p63, moc31, mesothelin, and cytokeratin (k903 and ck5/6) immunostains in differentiating adenocarcinoma, squamous cell carcinoma, and malignant mesothelioma in effusions. *Diagnostic cytopathology*, 36(1):20–25, 2008.

[243] Nelson G Ordóñez and Aysegul A Sahin. Diagnostic utility of immunohistochemistry in distinguishing between epithelioid pleural mesotheliomas and breast carcinomas: a comparative study. *Human pathology*, 45(7):1529–1540, 2014.

[244] Zahia Hamidouche, Olivia Fromigué, Jochen Ringe, Thomas Häupl, and Pierre J Marie. Crosstalks between integrin alpha 5 and igf2/igfbp2 signalling trigger human bone marrow-derived mesenchymal stromal osteogenic differentiation. *BMC cell biology*, 11(1):44, 2010.

[245] Carla M Kaneto, Patrícia SP Lima, Dalila L Zanette, Karen L Prata, João M Pina Neto, Francisco JA de Paula, and Wilson A Silva. Col1a1 and mir-29b show lower expression levels during osteoblast differentiation of bone marrow stromal cells from osteogenesis imperfecta patients. *BMC medical genetics*, 15(1):45, 2014.

[246] Tsuyoshi Takagi, Hiroki Moribe, Hisato Kondoh, and Yujiro Higashi. Deltaef1, a zinc finger and homeodomain transcription factor, is required for skeleton patterning in multiple lineages. *Development*, 125(1):21–31, 1998.

[247] Antonio A Postigo. Opposing functions of zeb proteins in the regulation of the tgfβ/bmp signaling pathway. *The EMBO journal*, 22(10):2443–2452, 2003.

[248] ARGIRIS Efstratiadis. Genetics of mouse growth. *International Journal of Developmental Biology*, 42:955–976, 1998.

[249] Hoin Kang, Young-Dan Jeong, Paul Verma, and Sangho Roh. Induced chondrogenic differentiation of parthenogenetic murine embryonic stem cells by insulin-like growth factor 2 treatment in a three-dimensional culture environment. *Tissue Engineering and Regenerative Medicine*, 10(6):380–387, 2013.

[250] Hoin Kang, Jihye Sung, Hong-Moon Jung, Kyung Mi Woo, Seong-Doo Hong, and Sangho Roh. Insulin-like growth factor 2 promotes osteogenic cell differentiation in the parthenogenetic murine embryonic stem cells. *Tissue Engineering Part A*, 18(3-4):331–341, 2011.

[251] Daniel J Dumont, Lotta Jussila, Jussi Taipale, Athina Lymboussaki, Tuija Mustonen, Katri Pajusola, Martin Breitman, and Kari Alitalo. Cardiovascular failure in mouse embryos deficient in vegf receptor-3. *Science*, 282(5390):946–949, 1998.

[252] Lia Kwee, H Scott Baldwin, H Min Shen, Colin L Stewart, Catherine Buck, Clayton A Buck, and Mark A Labow. Defective development of the embryonic and extraembryonic circulatory systems in vascular cell adhesion molecule (vcam-1) deficient mice. *Development*, 121(2):489–503, 1995.

[253] Barbara Garmy-Susini, Hui Jin, Yuhong Zhu, Rou-Jia Sung, Rosa Hwang, and Judy Varner. Integrin $\alpha 4\beta 1$–vcam-1–mediated adhesion between endothelial and mural cells is required for blood vessel maturation. *Journal of Clinical Investigation*, 115(6):1542, 2005.

[254] Fan Zhang, Zhongshu Tang, Xu Hou, Johan Lennartsson, Yang Li, Alexander W Koch, Pierre Scotney, Chunsik Lee, Pachiappan Arjunan, Lijin Dong, et al. Vegf-b is dispensable for blood vessel growth but critical for their survival, and vegf-b targeting inhibits pathological angiogenesis. *Proceedings of the National Academy of Sciences*, 106(15):6152–6157, 2009.

[255] Jessica N Saykally, Soner Dogan, Margot P Cleary, Michel M Sanders, et al. The zeb1 transcription factor is a novel repressor of adiposity in female mice. *PloS one*, 4(12):e8460, 2009.

[256] Ajaya Kumar Reka, Himabindu Kurapati, Venkata R Narala, Guido Bommer, Jun Chen, Theodore J Standiford, and Venkateshwar G Keshamouni. Peroxisome proliferator-activated receptor-γ activation inhibits tumor metastasis by antagonizing smad3-mediated epithelial-mesenchymal transition. *Molecular cancer therapeutics*, 9(12):3221–3232, 2010.

[257] Kiyoshi Miyagawa, Jill Kent, Andreas Schedl, Veronica van Heyningen, and Nicholas D Hastie. Wilms tumour-a case of disrupted development. *Journal of Cell Science*, 1994(Supplement 18):1–5, 1994.

[258] Patrick Niaudet and Marie-Claire Gubler. Wt1 and glomerular diseases. *Pediatric nephrology*, 21(11):1653–1660, 2006.

[259] Mohnish Suri, Peter Kelehan, David O'Neill, Shantala Vadeyar, Judith Grant, S Faisal Ahmed, John Tolmie, Emma McCann, Wayne Lam, Shirley Smith, et al. Wt1 mutations in meacham syndrome suggest a coelomic mesothelial origin of the cardiac and diaphragmatic malformations. *American Journal of Medical Genetics Part A*, 143(19):2312–2320, 2007.

[260] Jian-Kan Guo, Aswin L Menke, Marie-Claire Gubler, Alan R Clarke, David Harrison, Annette Hammes, Nicholas D Hastie, and Andreas Schedl. Wt1 is a key regulator of podocyte function: reduced expression levels cause crescentic glomerulonephritis and mesangial sclerosis. *Human Molecular Genetics*, 11(6):651–659, 2002.

[261] Fei Gao, Sourindra Maiti, Nargis Alam, Zhen Zhang, Jian Min Deng, Richard R Behringer, Charlotte Lécureuil, Florian Guillou, and Vicki Huff. The wilms tumor gene, wt1, is required for sox9 expression and maintenance of tubular architecture in the developing testis. *Proceedings of the National Academy of Sciences*, 103 (32):11987–11992, 2006.

[262] Barbara Klamt, Ania Koziell, Francis Poulat, Peter Wieacker, Peter Scambler, Philippe Berta, and Manfred Gessler. Frasier syndrome is caused by defective alternative splicing of wt1 leading to an altered ratio of wt1+/- kts splice isoforms. *Human molecular genetics*, 7(4):709–714, 1998.

[263] Dominique Baudry, Marine Faussillon, Marie-Odile Cabanis, Muriel Rigolet, Jean-Michel Zucker, Catherine Patte, Sabine Sarnacki, Liliane Boccon-Gibod, Claudine Junien, and Cecile Jeanpierre. Changes in wt1 splicing are associated

with a specific gene expression profile in wilms' tumour. *Oncogene*, 21(36):5566–5573, 2002.

[264] K Kramarzova, J Stuchly, A Willasch, B Gruhn, J Schwarz, J Cermak, K Machova-Polakova, O Fuchs, J Stary, J Trka, et al. Real-time pcr quantification of major wilms tumor gene 1 (wt1) isoforms in acute myeloid leukemia, their characteristic expression patterns and possible functional consequences. *Leukemia*, 26 (9):2086–2095, 2012.

[265] Soo-Hyun Kim, Jeremy Turnbull, and Scott Guimond. Extracellular matrix and cell signalling: the dynamic cooperation of integrin, proteoglycan and growth factor receptor. *Journal of Endocrinology*, 209(2):139–151, 2011.

[266] Caroline Bonnans, Jonathan Chou, and Zena Werb. Remodelling the extracellular matrix in development and disease. *Nature Reviews Molecular Cell Biology*, 15 (12):786–801, 2014.

[267] Ryan T Kendall and Carol A Feghali-Bostwick. Fibroblasts in fibrosis: novel roles and mediators. *Frontiers in pharmacology*, 5, 2014.

[268] Joon-Il Jun and Lester F Lau. Cellular senescence controls fibrosis in wound healing. *Aging (Albany NY)*, 2(9):627, 2010.